DOCTOR OF PHILOSOPHY

Design and manufacturing of a (PEMFC) proton exchange membrane fuel cell

Mustafa, Mohamad Y F A

Award date:
2009

Awarding institution:
Coventry University

Design and Manufacturing of a (PEMFC) Proton Exchange Membrane Fuel Cell

Mohamad Y. F. A. Mustafa

A thesis submitted in partial fulfilment of the University's requirements for the Degree of

Doctor of Philosophy

May 2009

Coventry University

Allah (The God) is the Light of the heavens and the earth. The similitude of His light is as a niche wherein is a lamp. The lamp is in a glass. The glass is as it were a shining star. (This lamp is) kindled from a blessed tree, an olive neither of the East nor of the West, whose oil would almost glow forth (of itself) though no fire touched it. Light upon light. Allah guideth unto His light whom He will. And Allah setteth forth for mankind similitudes, for Allah is Knower of all things.

The Holy Quran (24-35)

Acknowledgments

I would like to thank my research advisor Professor F. S. Bhinder for his patience, guidance and endless supervision. I am very much impressed and inspired by his knowledge, stamina and determination. Without his support, this work could not have been possible.

I am deeply indebted to my supervisor and director of studies Professor Arne Erik Holdø (Now Vice Chancellor of Narvik University College, Norway) whose encouragement, support and stimulating discussions helped me so much through the hard times of this research.

Special thanks must go to Dr Mohammad H. Kailani (Faculty of science at Jordan University), for his precious time and guidance. His knowledge, sincere supervision and love of chemistry and polymers are most inspiring.

I owe more thanks to my co-supervisors: Dr. Munzer Ebaid (formerly head of the research unit at KADDB) and Dr William Hall (Coventry University) for their guidance and advice and to all my colleagues at the Engineering and Environmental Technologies Applied Research Group (EETARG) at Coventry University for their stimulating discussions and mutual contributions.

This research has been supported by the Royal Jordanian Air Force (RJAF), King Abdullah II Design and Development Bureau (KADDB), King Abdullah II Fund for Development (KAFD) and The Higher Council for Science and technology, Jordan (HCST). Special thanks are due to those establishments that work persistently for the prosperity of Jordan.

Many thanks to my parents, my wife and children, and everyone who helped me with this research.

All your help and guidance have been invaluable.

Table of Contents

Table of Figures

List of Tables

Nomenclature

P,p	Electrical power, Pressure
V	Voltage of the system/ Volume/ Atomic diffusion volume
I	Current drawn by the electrical load
i	Current density in *Amperes per squared centimeter*; (A/cm^2)
i_o	Exchange current density
A	Cross sectional area/ Active area of the fuel cell in (cm^2)
n, c	Number of cells in a fuel cell stack/ Number of electrons transferred per Molecule in the reaction/ Constant parameter
V_{cell}	Single cell voltage
F	Faraday's constant = 96485 (*Coulomb/mole*)
n_{e^-}	The amount of electron transfer (*kmol*)
t	Time in (*seconds*)
m	Mass of fuel (*kg*)/ Constant parameter
$\dot{m}$	Mass flow rate
M	Molar mass of fuel *(kg/kmol)*
z	Number of electrons transferred per molecule in the reaction
ΔG_r	Gibbs free energy *(J/g. mole H_2)*.
E_o	The electrode potential at equilibrium (also called the reversible potential or theoretical Open Circuit Potential or Open Circuit Voltage, i.e. OCP or OCV)
E_o^o	Standard equilibrium potential
Δg	Gibbs free energy change for the reaction defined on a per mole basis of one of the reactants
Δg^o	Standard Gibbs free energy change for the reaction defined on a per mole basis of one of the reactants
T	Temperature (K)
ΔT	Temperature difference
Δh	Change in enthalpy
l	Length (of membrane)
S, s	Entropy, specific entropy
H, h	Enthalpy, specific enthalpy
E_{ocv}	Open circuit voltage
b	Parametric value in Tafel equation
$\bar{m}$	Molar flow rate of fuel

j	Local transfer current densities
x	Thickness of the medium/ Mole fraction
k	Thermal conductivity of the medium.
e^-	Charge of an electron=1.602×10^{-19} (Coulomb)
N_a	Avogadro's number= 6.022×10^{23}
Q,q	Amount of heat
L	Latent heat
Δs	Change in entropy
Δg_f	Gibbs free energy of formation
a	Activity
P^*	Partial pressure of a reactant gas(es)
R	Universal gas constant (8.314 kJ/kmol.K), Resistance
Pr	Prandtl number
U_o	Overall heat transfer coefficient
$Q^{"}$	Heat flux in the fuel cell
c_p	Specific heat capacity
D	Diffusion coefficient (m^2/s)/ Constant parameter
R_{cat}	Volumetric current density, (Am^{-3})
EW	Equivalent molecular weight
S	Source or sink term/ Entropy
W,w	Work (Joule)
h_p	Heat transfer coefficient of the plate
Nu	Nusselt number
Re	Reynold's number
T_o	Overall temperature difference
q	Amount of heat per second
u	Velocity vector ($m\ s^{-1}$), ‘
w	Mass fraction
n_d	Drag coefficient
C	Concentration

U	Internal energy of a system
$c^*_{O_2}$	Effective concentration of oxygen at the cathode catalyst sites
E_{Nernst}	Thermodynamic potential
C_i	Reactant concentrations
CV_{H_2}	Calorific value (Hydrogen)

Subscripts

a	Anodic/ air
c	Cathodic
o	Equilibrium state
act	Voltage Losses Due to Activation
Ohmic	Voltage Losses Due to Ohmic Resistances
conc	Voltage Losses Due to Concentration Losses
int	Voltage Losses Due to Internal Currents
M,m	Membrane
electronic	Electronic portion of the total resistance
protonic	Protonic portion of the total resistance
i	Internal Current Resistance
l	The Limiting Current Density
wr	Water Removal
w	Water
ss	Stainless Steel
p	Plate
o	Overall Temperature Difference
r	Reversible
i	Denotes Oxygen at the Cathode and Hydrogen at the Anode Sides
j	Denotes Water Vapour at the Cathode and Anode Sides
H_2O	Water
O_2	Oxygen
λ	Pertaining to Water Content of the Membrane
s	Gas Distribution Along the Electrode

OC, OCV	Open Circuit, Open Circuit Voltage
cell	Cell
rev	Reversible
f	Free Energy of Formation
remain	Remaining heat in the fuel cell

Superscripts

avg	Average
hum	Humidified
o	Standard State
electronic	Electronic Portion of the Total Resistance
protonic	Protonic Portion of the Total Resistance
i	Internal
eff	Effective
ref	Reference

Greek symbols

α	Charge transfer coefficient
η_{actc}	Activation overvoltage at the cathode
η_{acta}	Activation overvoltage at the anode
η_{ohmic}	Ohmic overvoltage
η_{conc}	Concentration overvoltage
ρ	Specific resistivity ($ohm \cdot cm$)
λ	Effective water content of the membrane per sulphonic group (H_2O / SO_3^-)
β_1	Constant coefficient
β_2	Constant coefficient
φ	Constant coefficient/ potential (Volt)
ε_{th}	Thermal efficiency of the fuel cell
ϑ	Polytropic index

γ	Ratio between the specific heat capacities ($\gamma = {c_p}/{c_v}$)
μ	Viscosity (kg m^{-1} s^{-1})
σ	Effective conductivity
ξ	Constant parametric coefficients
ρ	Density (kg/m^3)
ε	Porosity of the GDL
μ_i	Chemical potential

Abbreviations

PEM	Proton electrolyte membrane (or) Proton exchange membrane
MEA	Membrane electrode assembly
GDL	Gas diffusion layer
CL	Catalyst layer
FC	Fuel cell
SS	Stainless Steel
PTFE	Polytetrafluorethylene
PFSA	Per-fluorinated Sulfonic Acid
PFICMs	Per-fluorinated ionomer composite membranes.
ICR	Interfacial Contact Resistance
ORR	Oxygen Reduction Reaction
OCV	Open Circuit Voltage
OCP	Open Circuit Potential

Abstract

This research addresses the manufacturing problems of the fuel cell in an applied industrial approach with the aim of investigating the technology of manufacturing of Proton Exchange Membrane (PEM) fuel cells, and using this technology in reducing the cost of manufacturing through simplifying the design and using less exotic materials.

The first chapter of this thesis briefly discusses possible energy alternatives to fossil fuels, arriving at the importance of hydrogen energy and fuel cells. The chapter is concluded with the main aims of this study.

A review of the relevant literature is presented in chapter 2 aiming to learn from the experience of previous researchers, and to avoid the duplication in the current work.

Understanding the proper working principles and the mechanisms causing performance losses in fuel cells is very important in order to devise techniques for reducing these losses and their cost. This is covered in the third chapter of this thesis which discusses the theoretical background of the fuel cell science.

The design of the fuel cell module is detailed in chapter 4, supported with detailed engineering drawings and a full description of the design methodology.

So as to operate the fuel cell; the reactant gases had to be prepared and the performance and operating conditions of the fuel cell tested, this required a test facility and gas conditioning unit which has been designed and built for this research. The details of this unit are presented in chapter 5.

In addition to the experimental testing of the fuel cell under various geometric arrangements, a three dimensional 3D fully coupled numerical model was used to model the performances of the fuel cell. A full analysis of the experimental and computational results is presented in chapter 6. Finally, the conclusions of this work and recommendations for further investigations are presented in chapter 7 of this thesis.

In this work, an understanding of voltage loss mechanism in the fuel cell based on thermodynamic irreversibility is introduced for the first time and a comprehensive formula for efficiency based on the actual operating temperature is presented.

Furthermore, a novel design of a 100W (PEMFC) module which is apt to reduce the cost of manufacturing and improve water and thermal management of the fuel cell is presented. The work also included the design and manufacturing of a test facility and gas conditioning unit for PEM fuel cells which will be useful in performing further experiments on fuel cells in future research work.

Taking into consideration that fuel cell technology is not properly revealed in the open literature, where most of the work on fuel cells does not offer sufficient information on the design details and calculations, this thesis is expected to be useful in the manifestation of fuel cell technology.

It is also hoped that the work achieved in this study is useful for the advancement of fuel cell science and technology.

Chapter 1 INTRODUCTION

1.1. ENERGY OPTIONS

Our primary source of energy is fossil fuel in the form of coal, oil and natural gas. Other sources of energy such as solar, wind and wave energy may make a significant contribution to our needs, but this contribution would be very limited and is not expected to exceed 10% of the total demand for energy as projected by the Energy Information Administration, the official energy review from the U.S. Government figure (1-1):

Figure 1-1 World Primary Energy Consumption by Fuel Type, 1970-2025 [1]

Although these predictions are not necessarily very accurate, and the trend of oil consumption could change due to social and political reasons, the fact remains that fossil fuels are running out at a considerable rate. Views that they will finish in a specific number of years may differ, but there is no disagreement that they will be exhausted one day. In contrast, the demand for energy is growing due to the rapidly increasing population, rising standards of living and the emergence of new industrial economies [2].

Finite fossil fuel resources are not the only problem. The use of fossil fuels has created other difficulties, mainly environmental pollution and global warming. Nevertheless, there have been some remedial efforts to reduce the impact of environmental pollution, such as the *Kyoto Protocol in 1997*, which compels industrial societies to gradually reduce the levels of production of harmful emissions, particularly carbon dioxide, in an effort to reduce the green house emissions causing global warming dilemma and its predictable tragic consequences.

This, however, creates further problems, such as the increasingly stringent legislations directed to the control of harmful emissions. Yet, it fosters the efforts for exploring cleaner sources of energy.

In the light of these circumstances, it is very important to find a clean and reliable substitute for fossil fuels. Fuels produced from biological waste (bio-fuels) for instance, are becoming very popular; but considering the demand for energy in a typical power plant, such as a 500 MW power station, and considering the average efficiency of a power plant which is in the range of 40%, the necessary power supply for such a station is 1,250 MW, which means a consumption of nearly 32 kg/s of natural gas (the calorific value of natural gas is 10.83 kWh/kg) or nearly 62.5 kg/s of biofuels (taking the calorific value of sunflower oil; 5.56 kWh/kg, as an average value for biofuels) [3]. And considering an average yield of 1200 kg/acre of biofuel crops, it is obvious that enormous land area is needed to run a station of that moderate size.

Although plants grown for the production of biofuels may not be human food plants, increased plantation of biofuel plants occupies part of the agricultural land used for growing crops in addition to consuming water resources and affecting the wild life,

not to mention the green house gases that will be emitted in the process as a result of using fuels containing carbon. Furthermore, the biofuel solution would not be acceptable when the world is running out of food and, in terms of priority; agricultural land and water cannot be sacrificed for running cars when the majority of people are suffering from scarcity of food supplies.

The most abundant source of energy on planet earth is hydrogen; it is available in almost infinite quantities in water, which covers two thirds of the surface of earth, in hydrocarbons and it is part of every organic material, but it is not freely available as a substance due to its high reactivity with other materials. Hydrogen is distinguished by its high energy density and its clean reaction with oxygen in a combustion or oxidation process where the only by-product is water, which renews the cycle of hydrogen production.

Energy is required to extract hydrogen from hydrogen-rich materials such as the electrolysis of water or thermal cracking of hydrocarbons and, as such, the economy of hydrogen extraction has a direct impact on the energy efficiency of the system where it is used. However, the same argument applies to hydrocarbon fuels, and the comparison between the two should involve a well-to-wheels analysis.

Hydrogen is the smallest atom, and it is fairly easy, using the appropriate type of catalyst, to divide it to an electron and a proton, which can be utilised in a fuel cell to generate electrical energy.

1.2. Fuel Cells and Heat Engines

The fuel cell, which is the subject matter of this research, is an electrochemical energy conversion device that converts the chemical energy of its inputs to electrical energy in a chemical reaction without the need for combustion, thus eliminating the high energy losses and harmful emissions which are usually combined with the combustion process.

The energy waste in the combustion process is an important factor that renders the efficiency of the process low (28 - 45%) although this can be higher value in the

case of heat recovery in a combined heat and power plant (CHP) or combined cycle gas turbine (CCGT).

The efficiency of a heat engine is limited by the rise in temperature which is limited by the Carnot efficiency. This implies that in order to achieve high values of efficiency, the heat engine has to be operated at very high temperatures which places severe demands on the material and equipment used and wastes energy. High temperatures have another disadvantage which is the production of Nitrogen oxides, which are likely to form at elevated temperatures.

Nevertheless, heat engines and particularly the internal combustion engine, are credited with being the workhorses of our modern-day civilization, however their main problems can be summarised as follows:

1. Whether they are operated on Hydrogen or hydrocarbon fuels, harmful exhaust emissions which pollute the environment will be produced. In the case of hydrocarbons, carbon monoxide, carbon dioxide and Nitrogen oxides will be produced together with water vapour. In the case of pure Hydrogen, Nitrogen Oxides will be produced at high temperatures together with water vapour. In both cases the harmful emissions cannot be avoided.
2. They are limited by the Carnot efficiency and have to be operated at high temperatures; hence a lot of the energy used in them is wasted. The pressure volume diagram below; Figure (1-2), shows the heat losses combined with the combustion cycle and Carnot efficiency.
3. The use of Hydrogen in a combustion process creates more technical problems. For instance, the blow-by gases containing water vapour will condense in the engine compartment and cause deterioration of the lubricating oil which will reduce the life-time of the engine.

Heat engines are severely criticised for their detrimental effect on the environment, added to this is the fact that they are dependant on the rapidly depleting resources of energy, which are not being utilized properly due to the poor efficiency of heat engines.

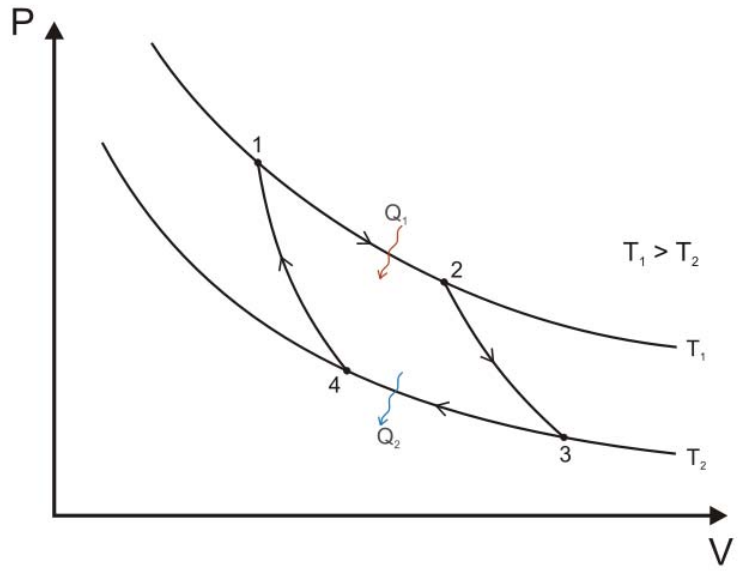

Figure 1-2 Pressure-Volume diagram of a combustion cycle and Carnot efficiency, T_1 and T_2 are isotherm lines, Q_1 and Q_2 refer to input heat and rejected heat respectively

The low temperature direct conversion process, in which hydrogen is chemically oxidized, is the best alternative to heat engines. In this process, the heat emitted to the surroundings, or in driving the reaction, is kept to a minimum.

This method would meet the pressing need of humanity to find replacement methods of power generation and utilization, that can both reduce the amount of energy needed per unit time, i.e. power in terms of kWh, so as to conserve energy resources, and at the same time, protect the environment by reducing the amount of harmful emissions, and thermal loading i.e. greenhouse effects.

In fact, fuel cell technology can overcome those difficulties; and pave the way for utilizing different sources of energy. However, the major challenge that scientists, particularly engineers, face with fuel cell technology is the cost of manufacturing, and this is the major issue that will be tackled in this research.

1.3. TYPES OF FUEL CELLS

There are different types of fuel cells and different approaches in their classification. Fuel cells are classified according to the type of electrolyte used in them, fuel type, temperature of operation and physical nature of the electrolyte whether solid or liquid. Almost all types of fuel cells run on hydrogen as a fuel, but other types of ions can also be used in some fuel cells. Table (1-1) represents the major types of fuel cells:

Table 1-1 Major types of fuel cells and their main features.

Proton Exchange Membrane Fuel Cell (PEMFC)	**Electrolyte**	*Solid Polymer*
	Operating Temp. °C	*20 - 180*
	Anode Reaction	$H_2 \rightarrow 2H^+ + 2e^-$
	Cathode Reaction	$½\ O_2 + 2H^+ + 2e^- \rightarrow H_2O$
	Mobile ion	H^+
Alkaline Fuel Cell (AFC)	**Electrolyte**	*(KOH) solution*
	Operating Temp. °C	*60 – 120*
	Anode Reaction	$H_2 + 2(OH)^- \rightarrow H_2O + 2e^-$
	Cathode Reaction	$½\ O_2 + H_2O + 2e^- \rightarrow 2(OH)^-$
	Mobile ion	$(OH)^-$
Phosphoric Acid Fuel Cell (FAFC)	**Electrolyte**	*Phosphoric Acid*
	Operating Temp. °C	*160 – 200*
	Anode Reaction	$H_2 \rightarrow 2H^+ + 2e^-$
	Cathode Reaction	$½\ O_2 + 2H^+ + 2e^- \rightarrow H_2O$
	Mobile ion	H^+
Molten Carbonate Fuel Cell (MCFC)	**Electrolyte**	*Molten Carbonate*
	Operating Temp. °C	*500 – 650*
	Anode Reactions	$H_2 + CO_3^{-2} \rightarrow H_2O + CO_2 + 2e^-$ $CO + CO_3^{-2} \rightarrow 2\ CO_2 + 2e^-$
	Cathode Reaction	$½\ O_2 + 2H^+ + 2e^- \rightarrow H_2O$
	Mobile ion	CO_3^{-2}
Solid Oxide Fuel Cell (SOFC)	**Electrolyte**	*Ceramic Compound*
	Operating Temp. °C	*600 - 1000*
	Anode Reactions	$H_2 + O^{-2} \rightarrow H_2O + 2e^-$ $CO + O^{-2} \rightarrow CO_2 + 2e^-$ $CH_4 + 4O^{-2} \rightarrow 2H_2O + CO_2 + 8e^-$
	Cathode Reaction	$½\ O_2 + CO_2 + 2e^- \rightarrow CO_3^{-2}$
	Mobile ion	O^{-2}

1.4. AIMS OF THIS RESEARCH

In view of the energy scenario given earlier in this chapter, the aims of this research can be stated as follows:

1. To carry out a comprehensive critical review of the relevant literature with focus on issues pertaining to the design of the fuel cell and theoretical models of fuel cells available in the open literature.
2. To analyze current fuel cell designs in order to expose the areas of these designs which can be developed to reduce the manufacturing cost of a Proton Exchange Membrane Fuel Cell (PEMFC).
3. To design and produce selected components of the (PEMFC), such as the electrode plates, gas distributors and their geometry.
4. To put forward the design details of a 100W fuel cell module based on the design methodology adopted in this research with the aim of reducing the cost of manufacturing.
5. To design and manufacture a fuel cell with variable configurations for carrying out experimentation of the fuel cell in order to validate the design methodology.
6. To develop a numerical model of the proposed fuel cell design so as to perform parametric and optimisation studies on the fuel cell using computational techniques, and to use the obtained experimental results for validating the numerical model.
7. To design and build a test rig for operating the necessary experiments on the manufactured fuel cell under various operating conditions, and to obtain experimental results to validated the proposed design and mathematical model.
8. To summarise the experience gained in this exercise and disseminate this knowledge through reporting this research.

Chapter 2 LITERATURE REVIEW

2.1. INTRODUCTION

In today's world, the need for more energy seems to be ever-increasing. Both households and industries require large amounts of power. At the same time, the existing means of energy production face new problems. International treaties aim to limit the levels of pollution, global warming prompts action to reduce the output of carbon dioxide and several countries have decided to decommission old nuclear power plants and not build new ones. In addition, the unprecedented global increase in energy demand has meant that the price of conventional energy sources has risen dramatically and that the dependence of national economies on a continuous and undistorted supply of such sources has become critical. Such development brings about the need to replace old energy production methods with new ones. These new sources of energy have some indisputable advantages over the older methods. At the same time, they present new challenges [4].

Essentially, energy from these sources must come from a sustainable supply of energy or else it will be exhausted, and must not involve combustion. The reason for this is that the combustion process has a limited efficiency and produces unsafe gases. These undesirable effects are apt to increase as demand increases, humanity must go for direct conversion of energy which is combustion free. These criteria are met by hydrogen when used in an electrochemical direct conversion process to produce electrical energy.

Hydrogen has a major advantage over fossil and biological fuels. It can be used in a direct conversion device to produce electricity with efficiency higher than that of the combustion process, and it has the potential to reduce the harmful emissions as the only by product of the reaction of hydrogen with pure oxygen is water.

The conversion device which avoids combustion and uses hydrogen to directly produce work is the fuel cell. Ever since its discovery in 1839 at the hands of the welsh

barrister William Grove, fuel cells lay dormant until the early fifties when a clean, reliable and a highly efficient energy converter was needed for space missions.

In today's measures, fuel cells are still too expensive for commercial applications and a lot of effort is spent by the research community to bring their price down. Thus any efforts to achieve these goals would be a significant contribution to the technology of the fuel cell.

The price of any product depends on materials, labour and the manufacturing processes. Dealing with materials and labour costs are outside the scope of this research, but the manufacturing processes, including design, are the areas where this research is focused to achieve the desired objective of reducing prices.

The research presented in this thesis focuses on investigating the design and manufacturing with the aim of simplifying the design, which may be helpful in lowering the cost of the fuel cell. Because of the oil crisis, energy prices have gone up to unprecedented levels and energy research is being taken very seriously almost everywhere. Industrial countries, who are the major consumers of oil, are spending considerable amounts of money to deal with energy related research, where most of the investment is spent on energy itself and not the energy conversion systems and, very often, reference is made to solar and wind energies as if they are the solutions to our energy and environmental problems. Under these circumstances, engineering has a key role to play to present a solution to the current problems. It is the only discipline which can deal with the technical aspects of the energy problem, while other disciplines are dealing with the science of energy.

Tracking the general trends of publications in the field of energy, it is greatly noticeable that the fuel cell has attracted a great deal of interest; however, design data information is very rare and in many cases has not been validated.

Industrial applications of the fuel cells were stimulated by the fuel crisis of the seventies. Since then there has been a flurry of research in new sources of energy, and because of the multidisciplinary nature of the fuel cell, there has been a lot of input from a vast range of disciplines, without a unifying force to bring them together. For these reasons, it is impossible to review all that literature in this brief attempt.

The present research is concerned with the design of a PEM fuel cell, an area which is not very well disclosed in the open literature. Mainly the publications which are directly relevant to this area are picked up and reviewed very carefully; papers that are partially relevant are reviewed briefly, while papers and publications that provide useful reading are included in the bibliography. Another purpose of this literature review is to find the current state of the art and to explore the areas where the effort should be focused in order to simplify the design and manufacturing process.

Current researches are mainly concerned with bringing the prices of fuel cells from space levels down to earth levels. Despite this, the cost is still a stumbling block in accepting fuel cells for commercial use. These researches are mainly concerned with developing new manufacturing techniques [5], reducing the amount of noble materials needed for fuel cell operation, mainly the Platinum catalyst, through the implementation of nano-technology and other techniques [6, 7], and investigating new types of polymer membranes that can withstand temperatures higher than $100^{o}C$ and that are cheaper to produce than the currently used perfluorinated membranes [8, 9].

Throughout the published literature on fuel cells, a lot of research has been done on small scale fuel cells; but papers that plainly deal with the technology of construction of the various components of fuel cell stacks are scarce. Most of the published investigations concentrate on modelling and simulating the effects of varying operating conditions on the performance of the fuel cell. The majority of these are published by researchers who attempt to investigate these performances analytically, and then try to verify their findings on a ready made fuel cell.

While such investigations are very useful in simulating and predicting the performance of the fuel cell, they are not the main focus of this study. The aim of this research, in addition to investigating the technology of construction of various fuel cell components, is to study the influence of *principal design variables* on the performance of the (PEM) fuel cells by means of parametric and numerical modelling and simulation studies. The observations from these studies would serve as a graphical tool for design optimization.

2.2. BRIEF HISTORY OF FUEL CELLS

As early as 1839; William R. Grove, a welsh barrister and amateur scientist, performed his first experiments in Swansea, and reported the effects of electrochemical reactions; where electric current was produced by the chemical reaction of hydrogen and oxygen (reverse electrolysis); that were produced on two different electrodes by the electrolysis of water. In his account of this experiment he reported that: "*A shock was given which could be felt by five persons joining hands, and which, when taken by one person was painful*" [10]. He called it: "*The Gaseous Battery*".

In 1841 and 1842 Christian Friedrich Schoenbein of Switzerland, published experiments of his own that were similar in subject, and had results closely connected to those of Grove. Schoenbein had been trying to prove that currents were not the result of two substances coming into "mere contact" with each other, but were caused by chemical reaction.

In 1882 a new form of "*Gas Battery*" was developed by Lord Rayleigh, and was an attempt to improve the efficiency of the platinum electrodes by increasing the surface of action between the solid electrode, the gas and the liquid [11].

In 1889 another improved form of the "*Gas Battery*" was described by Mond and Carl Langer, this was more than an improvement; it was the prototype for the practical fuel cell, in which they used a matrix, basically a porous, non-conducting diaphragm, to hold the sulphuric acid; thus solving the problem of electrode flooding caused by the electrolyte.

In response to the demonstration of Mond and Langer's Gas Battery, Alder Wright and Thompson (1889) brought attention to their "*Double Action Plate Cells*" which was claimed to have been developed earlier [12].

In (1896) William W. Jacques reported his experiments to produce electricity from coal. A few years after that Haber and Bruner (1904) worked on direct coal fuel cells, which were called: "*The Jacques Element*" [12].

In the 1920s the gas diffusion electrode was recognized as the key for successful low temperature operation of the fuel cell. A. Schmidt was one of the pioneers, followed

by F. K. Bacon, who worked on an alkaline fuel cell system with porous metal electrodes; his fuel cell system was the first prototype of the later NASA Space Fuel Cell, which enabled men to fly to the moon in 1968 [12].

Ever since their success in space missions, fuel cells have been gaining more interest and more success, though slow, in bringing them down to earthly prices and applications. To achieve this, many new companies and research groups have been set up around the world.

The Clean Urban Transport for Europe (CUTE), which is a European Union project initiative; to test three fuel cell buses each in nine cities in Europe, is an example of fuel cell applications on a wider scale. The project started in 2003 with the aim of demonstrating the feasibility of an innovative, high energy efficient, clean urban public transport system [13].

Recently, Boeing Research & Technology Europe (BR&TE), based in Madrid, successfully trialled a manned fuel-cell hybrid electric plane under their project: "*Fuel Cell Demonstrator Airplane*" (FCDA), which had been under development since 2001. The sole goal of the programme was to demonstrate for the first time that a manned airplane can maintain a straight level flight with fuel cells as the only power source [14].

Due to the industrial nature of this research, focus is centred mainly on issues pertaining to the design and operation of (PEM) Fuel cells. This entails the areas which are dealing mainly with the fuel cell hardware. Literature pertaining to other types of fuel cells is excluded at first hand.

It is worth mentioning at this stage; that some aspects of this technology have been treated in a confidential manner by their authors, and some procedures and techniques are referred to as *proprietary* [15-17]. Hence, information revealed in some publications is incomplete, and cannot be considered useful.

In this chapter, a review of the studies relevant mainly to the materials and design of the fuel cell components are presented. The operational issues will be covered briefly.

Publications on modelling and simulation will be covered and used in the formulation of a numerical model representing the design approach proposed in this study, which will be used for testing and optimising the proposed fuel cell design. A summary of the main observations from the literature is included in the last section of this chapter.

2.3. REVIEW OF THE RELEVANT PUBLISHED LITERATURE

Review of the relevant published papers related to the design, manufacturing and testing of a working (PEM) fuel cell would entail the following areas:

1. Materials and design of the fuel cell components:

    (a) The Proton Exchange membrane.
    (b) The membrane electrode assembly (MEA).
    (c) Flow Structure and Electrode plates.

2. Operational issues.
3. Modelling and simulation.

2.3.1. Materials and Design of Fuel Cell Components.

Figure (2-1) below shows an exploded view of a conventional Proton Exchange Membrane (PEM) fuel cell where the electrode plates (denoted as bipolar plates and end plates on the diagram) are made of graphite with machined channels for the flow of the gases. The membrane, catalyst layers and gas diffusion layers are treated as one unit and denoted the membrane electrode assembly (MEA).

Figure 2-1 Exploded View of a PEM fuel cell stack [18]

The issues of materials and design of the fuel cell components will be tackled, as far as literature review is concerned, in a systematic manner; starting with the membrane, which is the heart of the fuel cell, by reviewing publications on the various types of proton exchange membranes, and their production techniques, then moving on to the other components of the fuel cell.

- ***The Proton Exchange Membrane***

The Proton Exchange Membrane is the heart of the fuel cell where electrochemical reactions take place. It has two main functions; it works as a gas separator, preventing the reactant gases from directly reacting with each other, and it is the media through which the protons flow from the anode side to the cathode side. Thus, it has to be physically impermeable to gas; meanwhile it has to be a protonic conductor and an electronic insulator so as to prevent the electrons from flowing through it; as they are required to flow through the external load.

It is necessary for the membrane to retain a certain amount of water content under various operating and load conditions, so as to maintain its ability to transfer protons. This depends on two phenomena; the first one is the chemical affinity for water in the hydrophilic regions of the membrane that enables the membrane to absorb water, and the second one is the electro-osmotic drag phenomenon, where each hydrogen ion

will travel accompanied with at least one molecule of water, hence causing a drag of water molecules from the anode to the cathode [19].

The first phenomenon is a desirable one as it retains the water needed for proton mobility in the membrane, while the second one causes a transfer of water molecules from anode to cathode and hence reduces the protonic conductivity, and might lead to a complete dry up of the anode side and flooding of the cathode side of the membrane. Nevertheless, there is another problem affecting the water content of the membrane, which is the evaporation of water. This is the main reason for operating the fuel cell at temperatures below 100^{o}C. If the membrane could be developed in such a way that enables it to retain water or to retain its protonic conductivity at temperatures above 100^{o}C, in the range of 100-200^{o}C for instance, the performance of the fuel cell will be improved substantially due to the following reasons:

1. Higher temperatures reduce the water management problem as the water produced by the fuel cell will come out as vapour, which is easier to remove from the fuel cell, as it can be driven out of the flow field channels by the stream of gases.
2. Higher temperatures promote the chemical reaction in the fuel cell and improve its output voltage.
3. The diffusivity of the hydrogen protons through the membrane electrolyte is enhanced due to higher temperatures, thereby reducing membrane resistance [20].
4. Catalyst tolerance to carbon monoxide and other impurities is enhanced at higher temperature; they also promote the catalytic activity, hence reducing the required amount of catalyst, which reduces the cost of the fuel cell.

The state of the art in the fuel cell technology membranes is the Nafion® membrane (a registered trade mark of Du Pont™ Co.), which is a perfluorinated sulfonic acid (PFSA) membrane, however, there are other variants based on the same type of membrane such as Flemion® and Aciplex® membranes, which are also well known in the fuel cell industry [21].

Up to now, these membranes have been the best choice for commercial low temperature (<80°C) polymer electrolyte membranes. The advantages of (PFSA) membranes are:

1. Their strong stability in oxidative and reduction media due to the structure of the polytetrafluorethylene backbone.
2. Their proton conductivity, which can be as high as 0.2 $S.cm^{-1}$ (Siemens per centimetre)[1] [22] in polymer electrolyte fuel cells.

When these membranes are used in (PEM) fuel cells at elevated temperatures (higher than 80°C), the performance of the fuel cells decreases. This decrease is related to the following reasons [23]:

1. Dehydration of the membrane.
2. Reduction of the ionic conductivity of the membrane.
3. Decrease in affinity with water.
4. Loss of mechanical strength through a softening of the polymer backbone.
5. Parasitic losses (the high level of gas crossover).

The work presented by Savadogo [23] was an exhaustive review of the various aspects of works done recently on the developments of composite membranes for polymer electrolyte fuel cell (PEMFC) applications. Research on alternative proton conducting membranes to the per-fluorinated membranes for high temperature PEMFC applications is shown. The following aspects of the researches on proton conducting proton membranes were discussed:

---

[1] Siemens per centimetre (S/cm) is a unit in the category of *Electric conductivity and* has a dimension of '$M^{-1}L^{-3}t^{3}I^{2}$,where '*M'* is mass, '*L'* is length, '*t'* is time, and '*I'* is electric current.

1. Macro- and Nano-composites per-fluorinated ionomer composite membranes (PFICMs).
2. Partially per-fluorinated composite membranes.
3. Non-perfluorinated composite membranes.

Results based on the original works of the author were also presented. It was concluded that two main characteristics of the current membranes were the causes of high cost and operation intricacy; namely:

1. The perfluorination step, which is a costly process.
2. The low temperature operation (<80 $^{\circ}$C), which is necessary so as to maintain humidity of the membrane, and hence the proton transfer.

Genies *et al.* [8] presented a preparation method for soluble sulfonate naphthalenic polyimides by polycondensation in *m*-cresol, using aromatic diamines containing phenyl- ether bonds and / or bulky groups. The paper described the synthesis procedures and related properties of new naphthalenic copolyimides. This was supported later on by U.S Patent: 6,245,881 [24] by the same authors. It was claimed in the publication that the proposed polymer was cheaper than Nafion®, but with similar properties; especially durability and proton conduction. The originality of the author's approach stems from the introduction of ionic groups on to the polyimide backbone, using a sulfonated monomer.

Despite the laborious work undertaken by the authors, it was concluded that the ionic conductivity values were in the order of few $mS.cm^{-1}$ at room temperature; these values remain quite low compared to 0.1 $S.cm^{-1}$ required for fuel cell application. However, the methodology presented is worth following in the process of synthesizing polyimide membranes for fuel cell applications. A similar approach can be followed by introducing different ionic groups onto the same, or an alternative, polyimide backbone.

- ***The Catalyst Layer and Fabrication of the MEA.***

A thin film of highly intermixed ionomer and catalyst (which is mainly Platinum, Pt) is applied to the electrolyte membrane; the ionomer serves as a protonic

conductor, while the catalyst, and another electrically conducting material like Carbon, serve as an electronic conductor, thus making this film conductive for both protons and electrons.

The focus of researchers in the context of catalysts for PEM fuel cells was focused on two main issues:

1. Reducing the cost of catalyst per kW, either by the economic use of Platinum (or its alloys), or by finding other cheaper catalyst materials [11].
2. Tolerance to Carbon Monoxide (CO), particularly when the hydrogen fuel is produced from Hydrocarbons such as Methanol. This only applies to the anode where the catalyst material can get poisoned when reacted with carbon monoxide, while the cathode catalysts do not have to be CO tolerant. Mehta et al. [25] classified the anode catalyst materials into three categories:

   - Single metal catalyst, based on a single element which is Platinum (Pt).
   - Binary catalysts, based on platinum and another material.
   - Tertiary catalysts, those are based on two elements added to Platinum, but in these catalysts, Ruthenium (Ru) plays an important role. The authors listed 26 possible anode catalyst alloys.

However, for the cathode of the fuel cell, catalysts that can stimulate oxygen reduction are needed. The authors pointed out that little information was available on cathode catalysts for PEM fuel cells. Nevertheless, Pt/C is the main catalyst, although non-platinum catalysts are being researched.

Two modes for the preparation of the (MEA) are reported in the work of Mehta *et al*.[25]:

- Application of the catalyst layer to the Gas Diffusion Layer (GDL) followed by membrane addition.
- Application of the catalyst layer to the membrane followed by (GDL) addition.

However, several manufacturing options exist within these two modes of (MEA) manufacturing.

As far as the application of the catalyst layers are concerned, there are various methods published in the literature. Wilson *et al.* [7] presented two methods for the application of catalyst and the preparation of the (MEA) for the perfluorinated type of membranes. The technique presented was based on the preparation of a solubilised form of the thermoplastic ionomer by simply converting the perfluorinated ionomer into the thermoplastic form by the ion exchange inclusion of large, "hydrophobic" counter-ions such as Tetrabutylammonium (TBA^+). In this way, a solubilised thermoplastic form of the ionomer was made available. Thus, thin-film catalyst layers are cast from inks that consist of supported platinum catalyst and solubilised ionomer in the (TBA^+) form. The catalyst can then be applied to the membrane either directly; or via a decal transfer process.

The work presented by Wilson *et al.* [7] is claimed to offer two advantages:

- The performance of the cells is claimed to be very good.
- The (TBA^+) processed cells have a distinct advantage over the other low platinum loading cells in the long-term performance.

Another method for the preparation of the catalyst layer was presented by Shukla *et al.* [26], Pt/C (Platinum on Carbon) was prepared for the cathode and PtRu/C (Platinum-Ruthenium on Carbon) for the anode. The Pt content in both cathode and anode was maintained at about 5 mg cm^{-2}. When applied to Nafion® 117 by compacting under a pressure of 50 kg cm^{-2} at 125^{o}C for 3 minutes, the (MEA) thus obtained was about 1 mm in thickness. The paper presents a systematic approach to manufacturing MEAs which is useful.

Atonolini *et al.* [27] aimed to evaluate the effect of Ruthenium (Ru) content on carbon-supported PtRu (Platinum-Ruthenium) alloys, with respect to phase composition, crystallinity, particle size, surface area of the alloy and metal-carbon interaction, and to correlate them to fuel cell performance with H_2 and H_2+CO.

The catalyst was prepared using a deposition and reduction process of Pt and Ru precursors**.** The powders were fabricated by a spray technique into three-layer electrodes for PEM fuel cells.

It was shown in this study that PtRu/C catalyst showed a better CO tolerance than Pt/C, which is useful in the case when fuels with high content of carbon-monoxide are used in the fuel cell such as reformed hydrocarbon fuel.

A promising technique for the application of the catalyst to the (PEM) is through the syntheses of hexachloroplatinate ($PtCl_6$) through chemical reaction where aqueous ($PtCl_6$) ions are transferred to non-polar organic solvents by phase-transfer molecules, Mandal *et al.* [28] described a single step method for the synthesis of catalytically active, hydrophobic (Pt) nanoparticles by the spontaneous reduction of aqueous ($PtCl_6$) ions at a liquid–liquid interface.

Zhang *et al.* [29] described another technique for the production and application of the catalyst based on hexachloroplatinate, where Platinum–ruthenium catalysts were prepared by incipient wetness co-impregnation of the carbon support with solutions of $RuCl_3 \cdot xH_2O$ and $H_2PtCl_6 \cdot 6H_2O$ in a benzene and ethanol mixture (4:1 in volume) with the appropriate concentrations to obtain different loadings. The authors were mainly concerned with the characterization of highly dispersed (Pt/Ru) alloyed catalysts with different Pt:Ru atomic ratios and uniform particle sizes. However, the main concern here is the preparation technique of the catalyst for which this paper is useful.

- ***Gas Diffusion Media***

In polymer electrolyte membrane fuel cell (PEMFC) electrodes, an effective mass transport of reactants as well as products to/from the reaction zones is of utmost importance to achieve high reaction rates with minimal efficiency losses. Accordingly,

such electrodes include a porous Gas Diffusion Layer (GDL) between the flow field of the bipolar plate and the reaction zone (the catalyst layer), to ensure a homogeneous and efficient mass transport over the whole active area of the cell [30]. In most cases, the Gas diffusion layer (GDL) consists of an anisotropic[2] [31] fibrous structure, either in the form of paper or woven cloth that allows the distribution of reactant gases through the porous structure and the collection of current through the fibres. Figure (2-2) is a microscopic view of Toray® paper GDL [32]:

[2] **Anisotropy** is the property of being directionally dependent, as opposed to isotropy, which means homogeneity in all directions. It can be defined as a difference in a physical property (absorbance, refractive index, density, etc.) for some material when measured along different axes. An example is the light coming through a polarizing lens.

Figure 2-2 Microscopic image depicting the random fibre structure of a GDL formed of Toray® carbon paper [32]

The (GDL) has several specific functions [33]:

• *Reactant permeability*: provides reactant gas access from the flow-field channels to the catalyst layers including the in-plane permeability to regions adjacent to lands.

• *Product permeability*: provides passages for the removal of product water from catalyst-layer area to flow-field channels including in-plane permeability from regions adjacent to lands.

• *Electronic conductivity*: provides electronic conductivity from the bipolar plates to the catalyst layers including in-plane conductivity to regions adjacent to channels.

• *Heat conductivity*: provides for efficient heat removal from the membrane electrode assembly (MEA) to the bipolar plates where coolant channels are located; and

• *Mechanical strength*: provides mechanical support to the MEA in case of reactant pressure difference between the anode and cathode gas channels; thus maintaining good contact (i.e. good electrical and thermal conductivity) with the catalyst layer, and preventing the MEA from compressing into the channels and resulting in blockage to flow and consequently high channel pressure drops.

Most of the published scientific work on PEMFC gas-diffusion media, which is very little, is of an applied nature. This reflects the fact that current diffusion media is typically not a major source of voltage loss within the state-of-the-art PEMFCs. However, this component is expected to receive additional attention as focus shifts from steady-state performance to cold-start and stability, issues that will require tailoring of the diffusion media to more efficiently deal with liquid water under a variety of conditions. Durability and cost considerations also increase focus on the gas diffusion media [33].

Conventional GDLs have arbitrary micro-structure and small pore size, especially under compression, which can require larger capillary pressures to drive liquid water through. Consequently, the GDL and catalyst layer in practical PEM fuel cells undergo flooding. The key issues of flooding and mass transport limitation under steady-state and transient (e.g., start-up) conditions will benefit significantly from GDLs with carefully designed architectures and controlled pore-size distribution [34].

Moreira *et al.* [35] studied the influence of the type and combination of gas diffusers on the performance of the MEA. As gas diffusers, carbon cloth and carbon paper were used in different combinations. In their experimental procedure they gave a detailed account of the preparation of the GDL and the test procedures which can be very useful. It was concluded that the carbon cloth has better characteristics as the gas diffusion electrode in a PEM fuel cell than the carbon paper.

Zhang *et al*. [34] fabricated a novel porous medium from copper foil using nanotechnology and investigated its performance as replacement for a conventional GDL in an operational fuel cell. They demonstrated that if the pores were straight and not interconnected, the liquid water would freely drain out of the GDL once the water flow was initiated. Such a careful optimization of pore morphology and pore-size distribution is difficult to achieve in conventional GDLs due to the random distribution of carbon fibres. Furthermore, conventional GDLs are typically made hydrophobic by treating them with PTFE, which increases their weight by 5 to 30% and also reduces their electronic and thermal conductivities. In addition, GDLs made from carbon cloth or carbon paper are subjected to compressive stresses which reduce their thickness, and

decrease their porosity and permeability by up to 50%. These conditions also limit the durability of the GDL and consequently the fuel cell. The small thickness and straight pore feature of the proposed material provided improved water management even at low flow rate which was an improvement from the conventional GDL; however, they showed lower performance indicated by the sharp decline of the polarisation curve at low flow rates. The developed copper GDL only had straight pores which restricted its in-plane transport. As a result, the reaction could occur only under the flow channel area, but not under the land area. The authors attempted to overcome this problem by inserting a carbon paper GDL between the bipolar plate and the copper GDL for the purpose of demonstration which improved the performance, but using GDLs again in the fuel cell.

Other scopes of improvement were proposed by the authors which included increasing the porosity of the GDL and changing the pore morphology and dimensions for better water removal. The study presented an empirical study on the production techniques and design of a metallic GDL. It also pointed out various avenues of development in terms of the materials applicability to fuel cells and design optimization. However, the justification presented for the declined performance did not take into consideration the chemical behaviour of the metallic GDL.

- ***Flow Structure and Electrode Plates.***

In this research it is intended to explore new approaches to design through which the cost of the fuel cell can be reduced. The electrode plates contribute largely to the high cost of the fuel cell and there is ample scope for reducing this cost through the use of new materials and production and machining techniques. Hence, it is very important to understand the main functions of the electrode plates and to study the various trends in their design and manufacture as presented in literature.

Research in the area of Bipolar Plates (BPP) is focused on two main issues that facilitate the functions of the bipolar plates: *Materials and Topologies of the electrode plates*.

It is important to point out at this stage that the terminology used to describe the electrode plates and flow field plates is ambiguous and sometimes confusing. The word

electrode is used to describe many components of the fuel cell that include the catalyst layer, the gas diffusion layer (GDL) and the bipolar plates. It is almost customary in the literature to describe the electrode plates as Bi-polar or Uni-polar plates. It should be noted here that the terms (Bi-polar or Uni-polar plates) apply only to plates that incorporate flow fields for the flow of gases in a fuel cell where the cells are in series and in direct contact with each other.

A comprehensive overview of the state of the art technology of the Electrode Plates in a PEM fuel cell stack was presented by Xianguo *et al.* [36]. A variety of flow channel configurations have been proposed in different designs, including pins, straight channels, interdigitated channels and channels formed from sheet metals.

Mehta *et al.* [25] presented a review and analysis of bipolar plate design and manufacturing. The plate materials were classified into three categories: Non-porous graphite plates, coated metallic plates and composite plates. Graphite has been traditionally used in fuel cells due to its chemical stability. The acidic environment of the fuel cell, enhanced with high temperatures will cause metallic plates to corrode or dissolve, consequently, metal ions will diffuse into the membrane; and they will get trapped at the ion exchange sites, hence lowering the ionic conductivity of the membrane. In addition, a corrosion layer on the surface of the bipolar plate increases the electrical resistance in the corroded portion and decreases the output of the cell.

Because of these issues, metallic bipolar plates are designed with protective coating layers. The authors presented an overview of plate materials and possible coating materials for metallic plates. Figure (2-3) below summarizes the information presented:

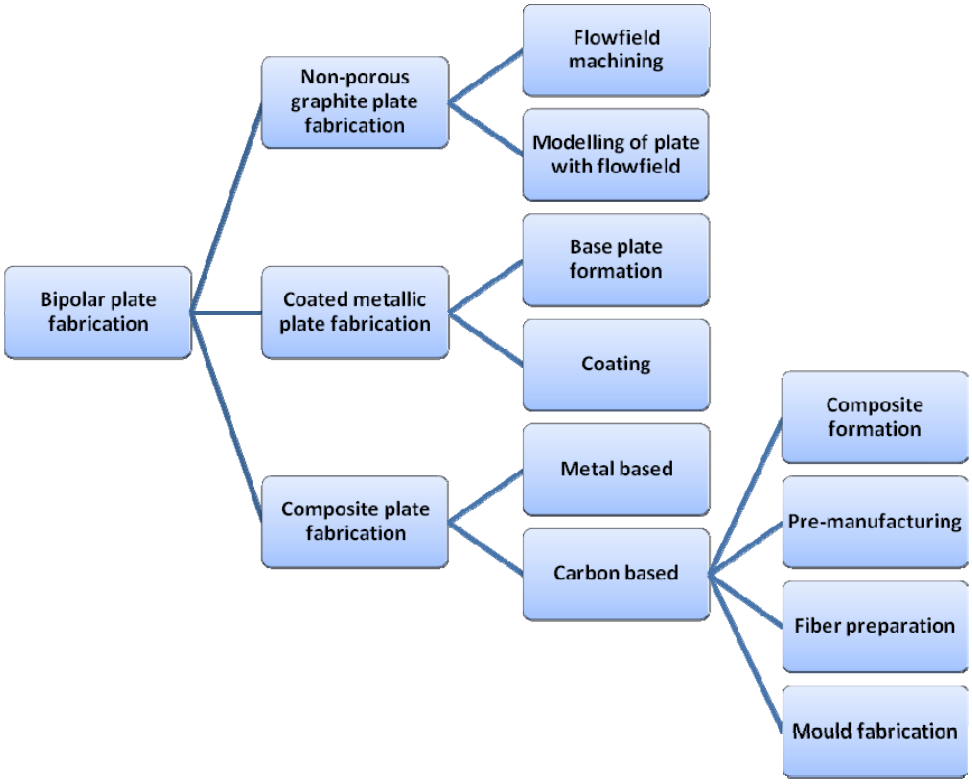

Figure 2-3 Classification of Bipolar plate materials and manufacturing alternatives

An approach based on the use of porous material in the gas flow field of the bipolar/end plates was proposed by Kumar *et al.* [37]. The idea behind this was the reduction in the effective permeability of the gas flow-field which improved the distribution and residence time of the gases. Through experiments in fuel cell stack; it was found that metal foam performed better than the conventional channel design flow-field. Furthermore, it was seen that; with a decrease in the permeability of the metal foam, the cell performance increased. This could be related to the improved current collection and reduced resistance of the electrode plates.

Tawfik *et al*. [38] presented a comprehensive review of the research work conducted on metal bipolar plates to prevent corrosion while maintaining a low contact resistance. A comprehensive coverage of their findings is summarised here due to its importance to the current research.

The authors stated that the ideal characteristics of a bipolar plate's material are: high corrosion resistance and low surface contact resistance, like graphite, and high mechanical strength, no permeability to reactant gases and no brittleness like metals such as stainless steel, aluminium, titanium, etc. The main challenge, however; is that corrosion-resistant metals develop a passivating oxide layer on the surface that protects the bulk metal from the progression of corrosion, but also causes the undesirable effect of a high surface contact resistance. This causes the dissipation of some electric energy into heat and a reduction in the overall efficiency of the fuel cell power stack. The authors also presented a review of the different approaches in using non-coated and coated metals, metal foams and non-metal graphite composites for potential application in PEM fuel cells. The following chart; Figure (2-4), summarises the various approaches described in this paper:

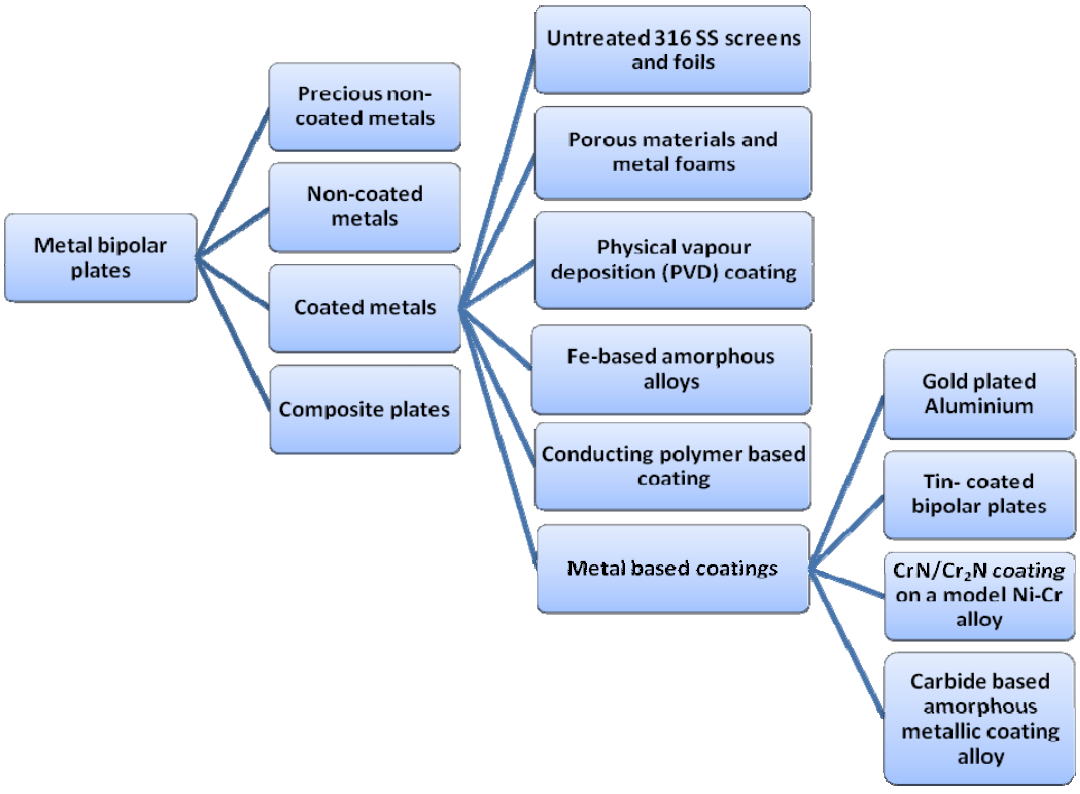

Figure 2-4 Metal-based materials for potential application in PEM fuel cells

The authors reported that aluminium, stainless steel, titanium, and nickel BPP when exposed to an operating environment similar to that of a fuel cell with a pH of (2–3) at temperatures around 80 ^{o}C were prone to corrosion or dissolution (Dissolution is most likely in the case of Aluminium). Moreover, a corrosion layer on the surface of a BPP increases the electrical resistance and decreases the output of the cell. While this surface oxide layer protects the metal and stops the corrosion from progressing further through the lower layers (beneath the surface), it forms an electrically insulating interfacial layer. As the thickness of the oxide layer increases the electrical surface contact resistance also increases and accordingly causes a decrease in the electric power output.

Furthermore, the authors reported that both austenitic 349TM and ferritic AISI446 stainless steel with high Cr (Chromium) content showed good corrosion resistance and could be suitable for fuel cell application as electrode plates; though AISI446 requires some improvement in contact resistance due to the formation of a surface passive layer of Cr_2O_3.

It was additionally verified by the same authors that (Cr) in the alloy forms a passive film on the surface of stainless steel. Consequently, as the (Cr) content in stainless steel increased, the corrosion-resistance improved, however; a thick non-conductive surface passive layer of Cr_2O_3 will produce an undesirable low surface contact resistance. Moreover, uncoated metal ions and oxides could directly foul the electrolyte and tarnish the catalyst in the MEA which results in considerable adverse effects on the cell performance. They also found that metal dissolution will occur as the non-protected metal bipolar plates are exposed to the harsh operating environment inside the fuel cell, which is very conducive to corrosion with relative humidity of more than 90%, high acidity (pH 2–3) and temperature range of 60-80°C. The dissolved metal ions diffuse into the membrane and then get trapped in the ion exchange sites inside the ionomer, resulting in lowered ionic conductivity as described by Mehta *et al*. [25]. A highly conductive corrosion resistance coating with high bonding strength at the interfacial layer between base metal substrate and coating layer is required to minimize this problem.

As far as coatings for stainless steel are concerned, the authors reported that the use of appropriate corrosion-resistant coatings on metallic components offers an avenue to minimize material degradation and extend their lifetime. The results revealed that (Tin) coating can offer SS316 stainless steel higher corrosion resistance and electric conductivity than uncoated SS316. Further efforts to improve the coating quality and evaluation of the long-term stability of SS316/Tin coating system under simulated conditions are required. It was also indicated that Au-coated SS316 stainless steel clearly demonstrated no difference between the metal-based and graphite plates. An important speculation by the authors in a previous publication and reported here states that a smoother surface finish may further reduce and/or improve the following bipolar plate characteristics:

- The interfacial resistance.
- The micro potential difference between the (MEA) and the metallic bipolar plates; which may further reduce localized corrosion of the metallic bipolar plates.
- The surface characteristics became hydrophobic; which may improve the two-phase flow of the reactant gases and water.

Another interesting piece of information regarding porous metals and metal foam was presented in this work; in which it was indicated that metal foams performed better than the conventional channel design flow-field. Furthermore, it was seen that with a decrease in permeability of the metal foam, the cell performance increased (but of course to a certain limit; after which the performance is expected to decline due to transport limitations of the reactant species). The performance could be further improved by carefully tailoring the size, shape and distribution of pores in the metal foam. This agrees with the concept proposed by Kumar *et al.* [37] mentioned earlier in this report. The authors confirm that an additional advantage will accrue as these metal foams could possibly be used for catalyst support in the electrochemical reactions within the fuel cell, thereby eliminating the need to use carbon electrodes.

As regards uncoated stainless steel, it was pointed out by the same authors that many types of alloys have been developed for applications where common stainless steels such as SS304 or SS 316 did not provide adequate corrosion resistance.

In general, the compositions of these alloys are similar to their stainless steel or nickel-base counterparts except that certain stabilizing elements, such as Ni, Cr, and Mo are added or are present in much higher concentrations in order to obtain desirable corrosion properties. However, in neutral to oxidizing media, a high Chromium (Cr) content, which is often accompanied by the addition of Molybdenum (Mo), is necessary.

In the same context, Wang and Turner [39] investigated various samples of ferrite stainless steel in a simulated PEM fuel cell bipolar plate environment. The results suggest that AISI446 could be considered as a candidate bipolar plate material in polymer electrolyte membrane fuel cell anode and cathode environments, (AISI446) steel underwent passivation and the passive films were very stable. An increase in the *interfacial contact resistance* (ICR) between the steel and the carbon backing material due to the passive film formation was noted, which agreed with results reported by Tawfik et al. [38]. The passive film formed on the cathode side was found to be thicker than that on the anode side, and both had a deteriorating effect on the interfacial resistance between the plates and the gas diffusion material [40]. Further investigation of the passive film on the AIS446 indicated that they were mainly chromium oxides and the iron oxides played only a minor role.

Although the study showed that the performance of the AIS446 stainless steel was superior to the other series AIS stainless steel investigated in this study under a simulated chemical environment of the fuel cell, it should be noted that the simulated environment takes into account only the chemical nature of the fuel cell environment, which could vary due to the electrochemical reaction and fluid flow taking place in the fuel cell.

2.3.2. PEM Fuel Cell Operational Issues

Fuel cell systems are influenced by many issues and parameters that affect their performance, amongst the most significant issues that influence the proper operation of the fuel cell are the water management problem, gas distribution, temperature and pressure variations, membrane conductivity and mass transport through the membrane and gas diffusion layers.

Fuel cell performance can be adversely affected by the formation of water, the dilution of reactant gases by water vapour, or by the dehydration of the solid polymer membrane.

Fuel cell water management can be accomplished by a number of approaches which include:

- System design, such as utilizing the interdigitated flow-field design with sequential exhausting of each cell in a PEM fuel cell stack, so as to ensure that the gas will flow to each cell equally and provide the water management necessary to achieve good performance [41].

- Stack operating conditions, such as increasing the operating temperature and reactants flow rate [42].

- Stack hardware, such as; the use of interdigitated flow field design in conjunction with direct liquid water injection to the anode [18].

- Membrane electrode assembly design, such as; water transfer coefficient, water permeability, specific conductivity and contamination by foreign impurities [43].

Performance loss is mainly on the cathode and at high current densities, typically greater than 0.8 Acm^{-2}, where mass transport effects dominate. The low concentration of oxygen in air, the reaction kinetics associated with oxygen reduction, the formation of liquid water resulting in water flooding of active sites and restriction of

oxygen transport to the active electrocatalyst layer, all result in substantial cathode loss of voltage particularly at high current densities [44].

Voss *et al.* [45] reported a technique for water removal based on modifying the water concentration profile (or gradient) of the solid polymer electrolyte membrane to increase the back diffusion rate of water from the cathode to the anode, such that water at the cathode electrocatalyst layer diffuses through the membrane and is removed via the anode reactant gas stream. This was achieved by using a fuel flow rate which resulted in an optimum pressure drop in the fuel flow channels and hence induced water transport through the membrane from cathode to anode and into the fuel stream. The pressure drop between the inlet and outlet of the anode flow field significantly increased as the hydraulic radius of the flow channel decreased. This approach could be applicable but will impose further complications and control effort on the fuel cell design.

Mennola *et al.* [46] performed experiments on a free breathing PEM fuel cell to study the water balance in the fuel cell, focusing on the effect of anode conditions. The methods used were current distribution measurements, water collection from the anode outlet, and the measurement of cell polarization and resistance. The fraction of product water exiting through the anode outlet was found to increase with increasing temperature and hydrogen flow rate, which is expected due to the increased water carrying capacity of the gas with temperature as well as the increased amount of water available in a greater rate of flow. When the general direction of hydrogen flow was against the direction of air flow, the percentage of water removal through the anode was smaller and the current distributions were more even than in the cases where the direction was the same as that of the air flow. This point is worth taking into consideration when designing a fuel cell, whether air-fed or free air-breathing.

Santarelli and Torchio [47] performed experimental studies on a single cell PEM fuel cell to observe the effects of varying the temperatures of the fuel cell, anode and cathode flow temperatures in saturation and dry conditions; and reactants pressure on the behaviour of a commercial single fuel cell. As expected, it was observed that a higher cell temperature increased the membrane conductivity and exchange current density with an improvement of cell behaviour. Of course the conductivity of the

membrane and the exchange current density are geometric variables which cannot be changed in operation, but the effect of temperature on these variables can be examined.

The protonic resistance in the fuel cell is inversely proportional to the ionic conductivity of the membrane; the latter is a function of cell temperature, current density, reactants temperature and humidification. The degree of humidification of the membrane is linked to: the water produced by the reaction taking place at the cathode, the inlet water content of the reactant gases and the mass transport phenomena occurring in the membrane. Therefore, an improvement in the ionic conductivity is expected at higher temperatures.

Moreover, a decrease in the activation overpotential can be observed at higher temperatures. This could be due to the positive effect of the temperature increase on the exchange current density at the electrodes, which, as a consequence, decreases the activation overpotential and improves fuel cell performance.

The anode and cathode exchange currents are functions of several variables such as: materials and porosity of the electrodes; concentration, distribution and dimensions of the catalyst particles; and operating temperature. Among these variables, the temperature is the only one that can be modified during cell operation. However, it is concluded from this work that a balance between the temperature of the fuel cell and the temperature and humidity of the inlet gases is very important. it is also shown that it is difficult to evacuate the water product of the fuel cell with the exhaust cathode flow for a fuel cell operating at 323K (50^{o}C) fed with a fully humidified reactant flow at 353K (80^{o}C); because water production at the cathode at high currents is high and the effect is that the diffusion layer could become flooded on the cathode side [47].

Regarding the effects of pressure on the performance of the single PEM fuel cell under consideration, the authors noted that the increase of operating pressure did not offer a significant improvement when the reactants were dry, while leading to significant improvements when both anode and cathode reactants were humidified. It was observed that there were good improvements up to 2.5 bar and slight improvements between 2.5 and 3.1 bar, in particular with high current densities. This finding confirms the theoretical study which will be presented in chapter 3 of this thesis.

The decreased improvement at high current densities is again referred to the accumulation of water product at the cathode, which increases at high pressures because the cathode exhaust flow reduces its water absorption potential that hinders flooding. They also observed another interesting effect of the operating pressure; which was a better stability of cell voltage (that is, a lower standard deviation) at high current densities when the pressure was increased. This observation was presented by the authors without further explanation and it needs to be investigated at a larger scale fuel cell stack for validation.

The authors also offered an impartial comparison between their work and that of other authors, which showed that the performance of fuel cells reported by other authors had better performance compared to the commercial cell analyzed in their work. This, of course, is a respectable attitude, but it is observed that the information presented in most publications on fuel cell performances do not sufficiently cover the interactions between the different variables affecting the fuel cell behaviour, nor offer satisfactory information on the design of the fuel cell.

It is also worth mentioning that most of the published work covers results on single cells which are taken as representative for fuel cell stacks, while the behaviour of a single cell is expected to be better than that of a stack because of the simplified flow, water and thermal management problems.

Lin *et al.* [48] presented a method for the fabrication and testing of a miniature PEM fuel cell using a novel manufacturing process for creating carbon bipolar plates by treating a pre-patterned organic structure at high temperatures in an inert or reducing environment. The fuel cell was tested under different operating temperatures and pressures, and a voltage gain was observed with increased temperature; however, a performance drop occurred at 353K (80°C), most likely due to dehydration of the membrane. Another significant observation was that the pressure effect was not as significant as the temperature effect.

From the polarization curve of the fuel cell stack and single cells presented by the authors; figure (2-5), the three-cell stack showed a much steeper slope reaching the concentration polarization region earlier than that of the single cells. This could be

mainly due to water accumulation in the gas channels which prevented the gas from reaching the membrane. Increasing the mass flow rate of air or oxygen in the fuel cell can overcome this problem to a certain limit.

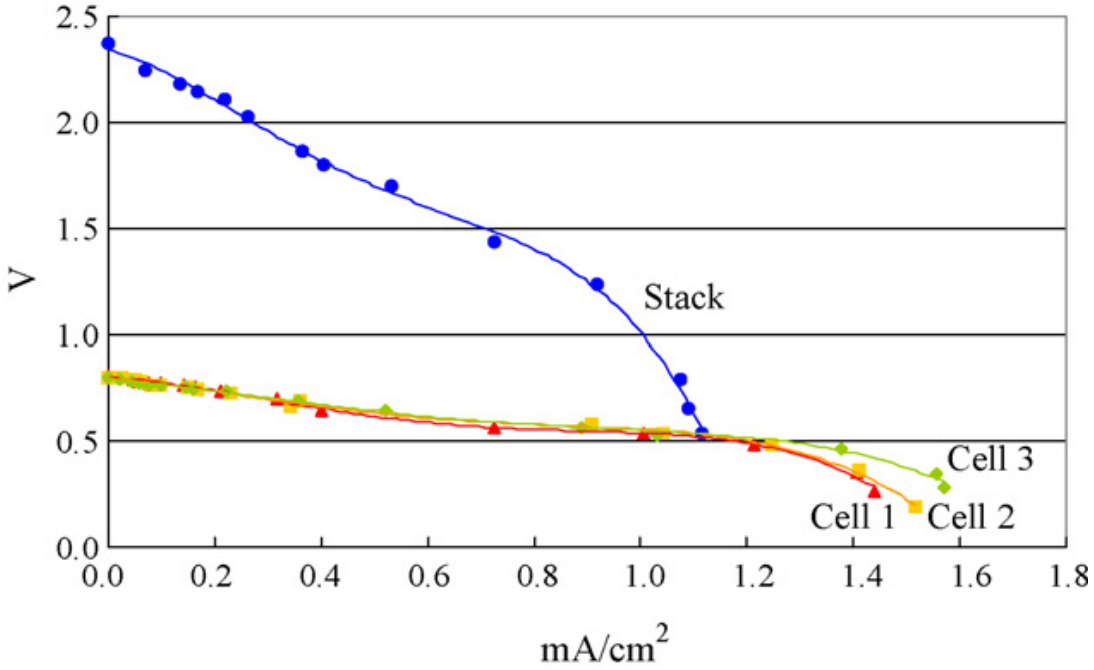

Figure 2-5 Polarization curve of the fuel cell stack and single cells as reported by Lin *et al.* [48]

This study indicated very clearly that the issues pertaining to the stack were very much different from those pertaining to a single cell. In the case of the stack, special consideration has to be paid to more complex challenges such as gas distribution problems, humidification, water management, sealing and thermal management problems.

Tori *et al.* [49] presented their results on designing and testing a 3-cell fuel cell based on 112 Nafion® membranes and 0.4 mg/cm^2 platinum loading on both sides, which is relatively a high loading of catalyst. They used serpentine channels on graphite plates, the dimensions of the channels and the type and specifications of the graphite plates were not disclosed, the active area of the cell was 9 cm^2. The authors used a home-made data acquisition system for testing, but the calibration of various instruments used was not given.

The heat generated by the fuel cell was not enough to raise its temperature to the desired limit; which was 335K (62°C), because of the small size of the fuel cell compared to the bulky end plates, and because of the short running time which would not allow the fuel cell to reach the operating temperature, consequently, the authors used heaters and thermocouples to maintain and control fuel cell temperature.

The authors presented characteristic curves for a single cell, 2 cells, 3 cells and 4 cells stacks; and observed that the overall potential depended on current drain from the fuel cell stack with 2, 3 and 4 cells in series respectively. At current values larger than 1A, the current – voltage characteristics of the multi-cell stack also showed that the voltage varied with current in a linear manner over most of the operating range, which indicates that Ohmic losses in the MEAs play a major role in the intermediate to high current range.

The overall Ohmic resistance, which mainly includes Ohmic resistance within the electrodes, at the electrode/membrane interfaces and in the membrane, as derived from the slopes of the plots obtained for the characteristic curves increased from 0.13 Ω for the 2-cell stack up to 0.20 Ω for the 4-cell stack which was not a linear increase, indicating that stacking of the fuel cells reduced the overall Ohmic losses. This interesting conclusion could be better represented by plotting the average voltage per cell in a stack against the current, as shown in figure (2-6) below.

It was noted that as the number of cells in a stack increased, the losses decreased and the characteristic curve became less sloping, which improved the overall performance of the fuel cell stack and lead to a more stable voltage. This could be attributed to the decrease of Ohmic losses due to the relative reduction of the number of components through which the current had to flow, although these results contradict with the results reported by Lin *et al.* [48] who reported a decrease in performance due to stacking which was attributed to gas distribution problems, humidification, water management, sealing and thermal management problems.

The authors, Tori *et al.* [49], presented only three test points in their experiments which do not give a full idea about the behaviour of the fuel cell and indicated only a trend line of the Ohmic area of the polarization curve. It would have been much better

to define five points in each experiment to make sure the results reflected the actual behaviour of the fuel cell and to reduce errors in the experiments.

Figure 2-6 Characteristic curves for three fuel cell stacks[49]

2.3.3. Modelling and Simulation

In order to understand the processes occurring within a PEM fuel cell and to optimise its performance, models that predict PEM fuel cell performance based on input parameters are required. Such models are advantageous because experimentation is costly and time consuming. Furthermore, experimentation is limited to designs which already exist, thus does not facilitate innovative designs [50].

Several models are available in the published literature, and can be classified as either empirical (or semi-empirical) or mathematical (known as "mechanistic models"). Empirical models calculate the cell voltage by using curve fitting schemes based on experimental data, but these models are limited in that they are specific to a particular fuel cell and operating conditions and many parameters that affect the performance of PEM fuel cells; such as catalyst layer structure are not included in the model; hence

parametric studies cannot be performed using these models. Therefore, mathematical models have been developed which apply fundamental laws to describe the processes occurring within the PEM fuel cell with mathematical equations, these equations are solved to find either cell voltage or power density. The main limitations of this type of models are that model development takes time and validation of the fuel cell stack details can be difficult to achieve [51].

- ***Empirical and Semi Empirical Models***

Publications on modelling and simulations of the fuel cell performance cover a great deal of the published literature. The work of Amphlett *et al.* [52] stands out as one of the most important and pioneering works in this field. They presented the activation losses taking place in the fuel cell in parametric form, deduced from the Tafel equation and empirical data as follows:

$$\eta_{act} = \xi_1 + \xi_2 T + \xi_3 T[\ln(c^*_{O_2})] + \xi_4 T[\ln(i)] \qquad \textbf{2-1}$$

Where 'i' is the fuel cell operating current density (Acm^{-2}), the 'ξ' terms are constant parametric coefficients and '$c^*_{O_2}$' is the effective concentration of oxygen at the cathode catalyst sites and was defined as follows, where '$P^*_{O_2}$' is the partial pressure of oxygen [52, 53]:

$$c^*_{O_2} = \frac{P^*_{O_2}}{5.08 \times 10^6 \times e^{(-498/T)}} \qquad \textbf{2-2}$$

The expression for the activation overpotential presented in their work was based on data that is specifically obtained from Nafion® PEM fuel cells and cannot be implemented to fuel cells using other types of membranes. It is worth noting that the expression is semi-empirical, which means that some functions serve as curve fitting tools, but the authors present reasonable physical justification for the terms involved.

In their following work, [53] the same group developed a generalised steady-state electrochemical model for a PEM fuel cell (GSSEM) which was largely mechanistic, with most terms being derived from theory or including coefficients that have a theoretical basis. This type of modelling differs from the empirical or non-

mechanistic models which are based on empirical data. The model adopted the following expression for the voltage of a single cell:

$$V_{cell} = E_{Nernst} + \eta_{act,a} + \eta_{act,c} + \eta_{ohmic} \qquad \textbf{2-3}$$

where: 'E_{Nernst}'is the thermodynamic potential, '$\eta_{act,a}$' is the anode activation overvoltage, a measure of the voltage loss associated with the anode, '$\eta_{act,c}$' is the cathode activation overvoltage, a measure of the voltage loss associated with the cathode, and 'η_{ohmic}' is the Ohmic overvoltage, a measure of the resistive losses associated with the proton conductivity of the solid polymer electrolyte and electronic internal resistances.

All quantities in the equation are in units of volts, the three overvoltage terms are all negative in the above expression and represent reductions from 'E_{Nernst}' to give the useful cell voltage, 'V_{cell}'. The model assumed an isothermal stack, and that the excess water was totally removed due to gas flow rate and the design of the fuel cell. It was also assumed that liquid phase concentration of hydrogen at the anode/gas interface (mol/cm^3) and water concentration at the cathode membrane/gas interface (mol/cm^3) were constant.

The aim of the work under consideration was to modify and generalise the terms in their previous model, which were specific to the Ballard® Mark IV fuel cells, to introduce cell dimensions and characteristics such as temperature, pressure and reactant concentration as input parameters and to extend the useful range of the model to higher current densities above about 0.5 A/cm^2.

Fuel cell characteristic curves obtained using the two models are plotted in figure (2-7) below for comparison. It is noted that the pressure effects in the (GSSEM) are more significant compared to the previous model. This however indicates that there is not a satisfying model that represents the behaviour of a range of fuel cells, and each fuel cell design has to be characterised experimentally to verify its behaviour.

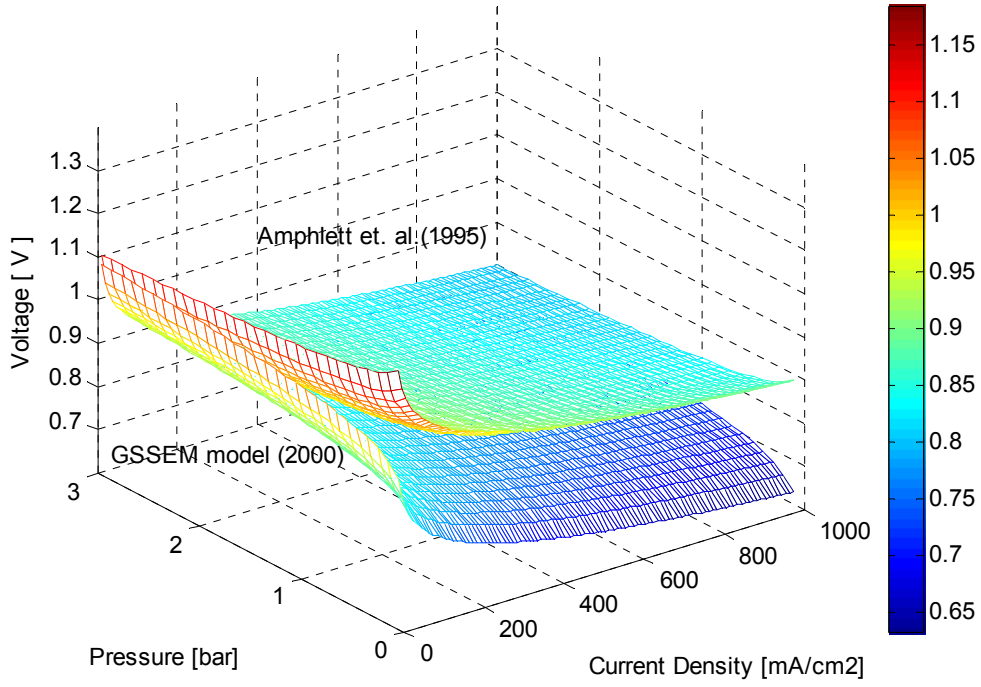

Figure 2-7 Effects of pressure and gas concentration on the performance of the PEM fuel cell, based on the work of Amphlett et al.

However, as the (GSSEM) model was largely built on mechanistic bases; giving it flexibility in application to a wide range of operating conditions, it should suffice in modelling all cells using Nafion® membranes to current densities below 1 A/cm^2. Conversely, the model could not accurately predict the effect of temperature for a fuel cell using Nafion® 117 membrane. Nevertheless, the authors stated the simplifications and weaknesses of their model which is useful for understanding the model and its applicability to different fuel cell configurations. Bearing in mind the complexity of the processes that must be modelled to accurately predict fuel cell performance, the approach and model presented by the authors is admirable.

Al-Baghdadi and Al-Janabi [54] presented a simplified mathematical model for investigating the performance optimization of a PEM fuel cell containing some semi-empirical equations based on the chemical-physical knowledge of the phenomena occurring inside the cell. The model was compared to the experimental data given by

another researcher and presented a good fit to the experimental data for the operation of the fuel cell at various operating temperatures. The authors discussed the possible mechanisms of the parameter effects and their interrelationships.

The authors related losses in output voltage at high current densities to the use of part of the available reaction energy to drive the mass transfer due to diffusion limitations which is a reasonable physical interpretation of the concentration losses.

The effects of pressure on the fuel cell performance were studied on the basis of their model, however, no experimental data was presented to validate those results, and the effects of humidity were not presented at all.

An interesting argument on the efficiency of the fuel cell was presented in this paper to illustrate that the efficiency of a fuel cell may be "*bought*" by adding more cells, driven by economic factors, such as the cost of individual cells, cost of hydrogen and the resulting cost of generated power. However, this argument was based on the characteristic curve of a single cell and should not be applied to a stack of multiple fuel cells, without further consideration of the characteristics of the stack which are expected to be different from those of a single cell.

In another publication by Al-Baghdadi [55]; a semi-empirical equation of the performance of the fuel cell was presented. The model took into account not only the current density; but also the process variations, such as gas pressure, temperature, humidity, and fuel utilization to cover the operating processes. The modelling results compared well with known experimental results, however, the paper did not focus much on the relative humidity of the reactants and did not indicate the assumptions upon which the model was based. Nevertheless, physical interpretations of the various causes of losses in the fuel cell were presented. The empirical equation for the fuel cell potential presented in the paper referred to the condition where the product water of the fuel cell was in vapour form and, though not clearly indicated in the paper, ideal gas behaviour for all the reactants and products was assumed. The paper is helpful in understanding the behaviour of the fuel cell but does not add much to the work of previous researchers.

- ***Mechanistic Models***

It is observed that mechanistic modelling has received most attention in the published literature. In mechanistic modelling, differential and algebraic equations are derived based on the physics and electrochemistry governing the phenomena internal to the cell. These equations are solved using some sort of computational method [50].

Common issues with many computational models are the uncertainties associated with values of various parameters that impact the transport processes in the fuel cell. Rational models based on the fundamentals of chemical processes together with experimental observations are used as essential tools to gain better understanding of the operation of the fuel cell.

Initial efforts towards the development of numerical models were focused on simply single phase 2D computational models with a lot of assumptions. But recent developments in computational technology and improved transport models have made it possible to simulate more accurate two phase computational models of the fuel cell accounting for fluid, thermal and electrical transport. Models by Bernardi and Vebrunge [56] and Springer and Gottesfeld [57] were based upon fundamental studies towards the understanding of PEM fuel cell. They developed an isothermal one dimensional model of a membrane electrode assembly, which considered mass continuity through the flow channels, gas diffusion in the GDL, water transport through the membrane and proton conduction in the membrane.

Bernardi and Vebrunge [56] were able to couple a greater set of phenomena than Springer and Gottesfeld [57]. They also implemented the Butler-Volmer equation to model the electro-chemistry and Schlogl's equation[3] [58] for transport in the membrane.

The model presented by Springer and Gottesfeld [57] studied the net water flux through the membrane and showed that the convective transport of water in the membrane was limited to drag force on the water molecules due to proton flux.

Braden *et al*. [59] employed a novel method of reducing the computational effort required to achieve a pseudo three dimensional solution by implementing a hybrid numerical model. They resolved a two dimensional cross section of the fuel cell perpendicular to the flow channel using finite difference method. In their model; the membrane and the anode were not considered and the catalyst layer was modelled as a boundary condition with flux determined from a first order reaction expression. Although the model is very useful for setting up a two dimensional model of the fuel cell and for reducing the computational effort required, it does not cover all the phenomena taking place in the fuel cell.

Gurau *et al.* [60] developed the first real two dimensional model of a fuel cell with flow channels and membrane, in which they studied the effect of composition changes of the reactants within the fuel cell on fuel cell performance. They realised that the governing differential equations in the gas flow channels and the gas diffusion

[3] Schlogl's model of the second order (or continuous) phase transition between the active phase and the absorbing phase is frequently used to model phase transition-like phenomena in chemical reactions, which are similar to the ferromagnetic phase transition observed in materials such as iron, where global magnetization increases continuously from zero as the temperature is lowered below the critical (Curie) temperature.

electrodes were similar, and hence combined both regions into one domain. Consequently, no internal boundary conditions or continuity equations needed be defined. The only difference was that material properties and source terms assumed different values for the two regions. This formed the basis of the single-domain approach.

Instead of combining two regions into one domain, the single-domain approach combines all the regions of interest into one domain. Conservation equations are defined which govern the entire domain of interest, typically the entire fuel cell (gas flow regions and membrane electrode assembly). In each region, the differences are accounted for by source and sink terms. All equations are written in the form of generic convection-diffusion equations, and all terms, which do not fit that format, are dumped into the source or sink terms. This formulation allows for solution using known computational fluid dynamics (CFD) methods [50].

Coppo *et al.* [61] developed a three dimensional computational model to describe liquid water removal from the GDL surface by advection due to the interaction of water droplets and gas stream in the gas flow channel. The model was validated for a wide range of temperatures to study the effect of temperature dependant parameter variation on cell performance and concluded that both liquid water transport within the GDL and liquid water removal from the surface of the GDL played a critical role in determining variations in cell performance with temperature. They used a simple mechanical model to evaluate the interaction between gas stream and liquid water droplets at the GDL/Gas Channel interface, where the flow surrounding the droplet is assumed laminar and water droplets move along the GDL surface as a result of forces acting on the droplets due to the viscous drag and surface tension. These forces can be expressed in terms of droplet diameter, drag coefficient, gas-liquid velocity, surface tension and contact angle. The model is useful for optimising the fuel cell design to assist the removal of water droplets from the flow field, but should give more consideration to the capillary action in the GDL which tends to restrain water droplets within the GDL.

Jung *et al.* [62] put forward a steady state, isothermal, two phase computational model, in which key transport and electrochemical reactions inside the PEM and catalyst layer were investigated. The results from this model showed that membrane thickness was one of the crucial parameters for water transport between anode and cathode, which severely affected the cell performance. For thin membranes such as Nafion® 111 or Gore® membranes, water exchange between anode and cathode via diffusion was so effective that both sides achieved equilibrium sufficiently downstream, however, thick membranes such as Nafion® 112 made the water concentration on both sides of the membrane diverge further. Detailed analysis showed that both anode and cathode will be flooded by liquid water condensed from the gas for thin membranes, while for thick membranes only the cathode was susceptible to flooding [63].

Most of these numerical models of PEMFC do not include the description of two phase flow that actually takes place in the gas distribution channels. A comprehensive flow transport electrochemical coupled model is still necessary to faithfully capture the water transport characteristics of PEMFC. Wang and his co-workers [63] developed a unified water transport model applicable throughout the PEMFC including the membrane region. The model recognises that there are different phases of water existing in various regions of the fuel cell. As a result; phase equilibrium is considered and various modes of water transport, diffusion, convection and electro-osmotic drag are incorporated in the unified water transport equation. Nevertheless, it is difficult for one model to cover all the physical phenomena taking place in the fuel cell, and most of the models reviewed in this study are good enough to give a clear idea about the interactions of all the physical parameters in the fuel cell.

2.4. SUMMARY OF MAIN OBSERVATIONS FROM PREVIOUS WORK

In the published literature on fuel cells, the input of researchers of various disciplines can be found; where they try to find ways to advance fuel cell technologies and make them compete with other power conversion devices. Throughout this literature review, the following observations can be summarised:

- The perfluorinated polytetrafluorethylene sulfonic acid (PFSA) polymer membranes have been the best choice for (PEM) fuel cells due to their significant stability in oxidative and reduction media owing to the structure of the polytetrafluorethylene backbone and their fairly high protonic conductivity, but they tend to lose their conductivity when used in the fuel cell at elevated temperatures higher than 353K (>80°C) due to dehydration and loss of mechanical stability. A breakthrough is needed in fuel cell technology to find new materials which can serve as protonic conductors in the fuel cell at temperatures higher than 373K (100°C).

- The catalyst material is one important component of the (PEM) fuel cell which affects its performance and cost. More research is needed in this area to reduce the cost of catalyst per kW either by the economic use of Platinum (through nano technology for instance) or by finding other materials that can replace Platinum.

- Research interests in fuel cell technology need to shift to more practical issues such as cold start, transient performance, the investigation of new materials for high temperature operation, novel designs and production technologies and the solution of major problems such as water management through design and tolerance to Carbon Monoxide .

- The terminology used to describe fuel cell components is ambiguous and sometimes confusing. For example, the word electrode is used to describe many components of the fuel cell that include the catalyst layer, the gas diffusion layer (GDL) and the bipolar plates. The term used to describe voltage losses are lent

from many disciplines, such as the words voltage losses, polarisation and overvoltage, which are all used to describe the same phenomenon. A unified terminology has to evolve so that fuel cell science can advance more rapidly.

- Performance losses, heat generation and product water generation all occur at the cathode side of the fuel cell which should receive most attention in design and modelling work.

- Most of the experimental work published on fuel cells presents results obtained from a single fuel cell; the results are then applied to a fuel cell stack. Different conclusions are reported by researchers about the effect of stacking on fuel cell performance. Therefore, long term testing of fuel cell stacks needs to be performed and reported before a solid conclusion on the best configuration of fuel cells can be reached.

- Several empirical and mathematical models of (PEM) fuel cell are reported in the published literature. Empirical models calculate cell voltage by using curve fitting techniques based on experimental data, which limits those models to a particular fuel cell and operating conditions, and cannot include many parameters that affect the performance of the fuel cell especially geometric conditions. On the other hand, there are many mathematical models which take into consideration various phenomena occurring in the fuel cell and many geometric conditions, but these models are based on many simplifying assumptions which are usually not certain and in most cases they overlook certain components or characteristics of the fuel cell. Although these models are mathematically very elegant, the accuracy of these models needs to be validated against some sort of experimental testing of actual fuel cells.

Chapter 3 THEORETICAL BACKGROUND AND DEVELOPMENT

3.1. INTRODUCTION

In the first chapter of this thesis, the aims of this programme of research were stated and, in chapter two, a review of recently published literature, particularly pertaining to the design issues of the fuel cell has been presented. It became clear from the literature study that fuel cell research was multidisciplinary and required a good understanding of many topics, therefore, to help the reader understand fuel cell research literature, it would be necessary to have a good grounding of the basics of a range of subjects including electrochemistry, and thermodynamics.

The fuel cell, as a system, comprises a large number of variables which, for the sake of analysis, maybe grouped into three groups [64]: design, operating conditions and performance variables. The design specifications define the design variables; while the operating variables define the prevailing ambient conditions; finally, the geometrical quantities are grouped together as the design variables that would satisfy the specified performance requirements. These three groups are shown in table (3.1) below:

Table 3-1 Fuel cell performance variables

Operating conditions	***Design variables***	***Performance variables***
1. Inlet temperature 2. Operating pressure 3. Flow rate of reactants 4. Humidity	1. Active area of the membrane 2. Thickness of the membrane 3. Catalyst loading 4. Number of cells 5. Equivalent weight of the membrane (EW)	1. Current 2. Voltage 3. Efficiency

It should be noted that several combinations of operating conditions and design variables can meet the design requirements, but in order to select a correct combination of variables it is necessary to perform some form of optimisation.

For the purpose of analysis; it is necessary to develop equations relating the three groups of variables. The graphical representations of the solutions of those equations would help in finding the optimum combination of the design variables for changing operating conditions. They can also be used to formulate a more complex numerical model of the system which can be resolved using computational methods to simulate the fuel cell performance and find avenues for optimisation. The said equations are derived in the following sections.

3.2. THE WORKING PRINCIPLES OF THE (PEM) FUEL CELL

The principle of operation of fuel cells simply depends on the oxidation of hydrogen to produce water. In this process, hydrogen, which is the simplest atom composed of one proton and one electron only, and does not include any neutrons, is split, with the help of a catalyst material, into its elementary constituents; the positive proton ion and the negatively charged electron.

If this reaction is carried out through the direct mixing of hydrogen and oxygen in the presence of a catalyst or ignition, the products will be water and heat only because the process is exothermic; i.e. heat is produced rather than absorbed, by the reaction. However, in the fuel cell this reaction needs to be controlled so that the two flows of electrons and protons are separated to create a stream of electrons through an external circuit; that will produce a current of electrical energy as required by the load.

To achieve this, hydrogen and oxygen are not allowed to mix directly in the fuel cell. Instead, they are confined in two separate compartments, separated by a proton conducting electrolyte membrane. This electrolyte membrane is not permeable, but it allows protons to go through it through a transfer process similar to electrical conductivity, and this is why it is called the proton exchange membrane (or solid polymer electrolyte because it is a solid material).

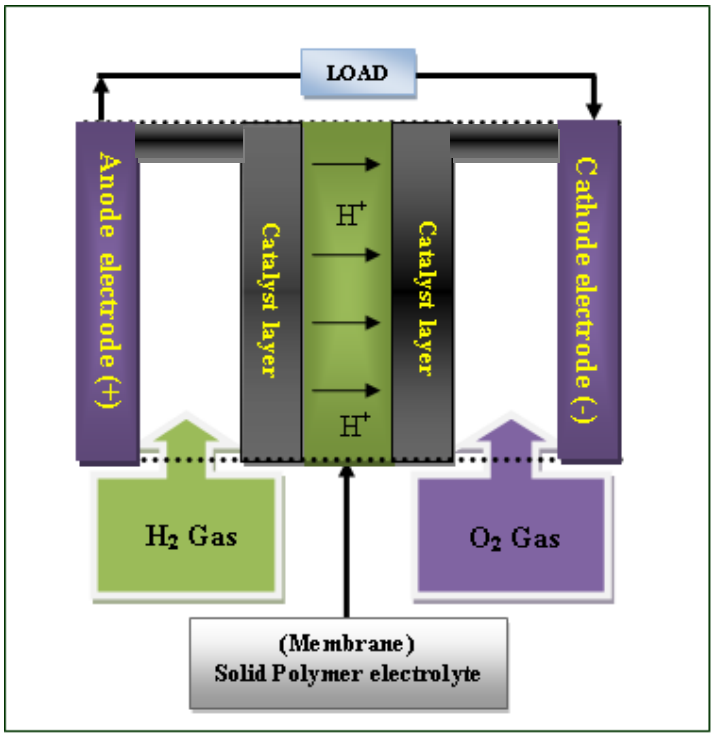

Figure 3-1 Schematic representation of a Proton exchange membrane fuel cell (PEMFC), not to scale

Figure (3-1) above is a schematic representation of a Proton exchange membrane fuel cell (PEMFC) which represents this basic principle, briefly described as follows:

Hydrogen is fed to the anode side of the fuel cell, this is the case in the Proton Exchange Membrane Fuel Cells (PEMFC) where it is oxidized (loses electrons) by the aid of a catalyst, mainly Platinum (Pt); one of the expensive materials used in the construction of fuel cells. The advances in technology are in the area of applying the thinnest layer of platinum in order to reduce the cost per unit area of the membrane.

Oxygen, taken from air or from an oxygen source such as a pressurised oxygen or air cylinder, is fed to the other side of the fuel cell, which is the cathode, where it is reduced (gains electrons); which are available from the external circuit. The electrolyte, which is the membrane, constitutes a physical barrier between the two reactants, (Oxygen and Hydrogen), that are fed to the fuel cell. Protons can pass through the electrolyte due to the fact that it is a protonic conductor, but an electronic insulator,

while the electrons will be compelled to travel through an external circuit to supply the load. This way; electrical energy is generated which can drive the load, at the same time the result of combining hydrogen and oxygen produces water.

The reaction also produces some amount of heat; because it is an exothermic reaction (releases heat), but this heat is much less than the heat produced in a direct combustion of oxygen and hydrogen; because some of the energy of the reaction has been released as electrical energy.

The fuel cell described above produces a voltage less than one volt under practical conditions, and a current which depends on the active area of the membrane; because the current depends on the amount of the protons and electrons transferred during the reaction and the number of protons depends on the active area of the membrane.

So as to achieve practical values of voltage, a certain number of fuel cells are connected together in series; connection can be achieved internally, as is the case with bipolar plates which provide internal connection of the cells, or externally. A group of cells connected together is usually called a fuel cell *stack*. Stacks can also be connected together in parallel to achieve higher values of current.

We have two options for increasing the current; either connect the fuel cells in parallel, or increase the active area of a single cell. However, current and voltage can be conditioned to the desired output values using power conditioning devices, which are electronic equipment that can manipulate the output voltage and current values.

3.3. DESIGN SPECIFICATIONS

In order to carry out the task of designing a fuel cell, the chemical and mathematical backgrounds of this research have to be understood. In this chapter; the theoretical foundation for the design is established on the basis of the required specifications.

This research aims at reducing the cost of manufacturing PEM fuel cells through simplifying the design and reducing machining and assembling costs. As a

demonstration of the design approach, the design specifications of a *100W fuel cell module as the basic unit for a 5 kW fuel cell for stationary applications* are put forward.

Where '*P'* is the electrical power, '*V'* is the voltage of the system and '*I'* is the current drawn by the electrical load, the electrical power output is given by Ohm's law as follows:

$$P = I \times V \qquad \textbf{3-1}$$

For the fuel cell, we have to decide the values of the voltage, current, number of cells and area of the single fuel cell that would give us the required output.

The current in a single fuel cell is given by:

$$I = iA \qquad \textbf{3-2}$$

Where '*i'* is the current density in *Amperes per squared centimetre*; (A/cm^2) and '*A'* is the active area of the fuel cell in (cm^2).

For a stack of '*n'* number of cells, the voltage of the fuel cell stack, where the cells are connected in series, is given by:

$$V = nV_{cell} \qquad \textbf{3-3}$$

Where 'V_{cell}' is the single cell voltage which will be discussed later on in this chapter.

Combining the equations for voltage and current, the total power output of the fuel cell can be written as:

$$P = iA \times nV_{cell} \qquad \textbf{3-4}$$

Under specific operating conditions, the cell voltage is a function of current density, and the operating point on the characteristic curve has to be determined in the light of the application for which the fuel cell is designed, as this will reflect on the power density and efficiency of the fuel cell.

The number of cells and the active area of the fuel cell are also important parameters that decide the power of the fuel cell and reflect on the power density.

3.3.1. Fuel Cell Current

The current in the fuel cell depends mainly on two factors:

1. The number of electrons produced.
2. The number of protons transferred.

The first one depends on the efficiency of the catalyst, while the second one depends on the protonic conductivity and the number of functional groups in the membrane. The proton exchange capacity (usually known as the Ion Exchange Capacity, IEC) or acidity of a polymer is measured by its Equivalent Weight; (*EW*), which is the mass of polymer per active sulfonic acid group as measured by titration[4]. For a given ion exchange polymer; a lower EW results in higher conductivity of the polymer, and it is; therefore, important to be able to control the exact stoichiometry of the polymer produced. For instance; Nafion® membranes, which are state-of-the-art membranes for PEM fuel cells, are available with EWs ranging between approximately 900 and 1100 (g/mmol) and thicknesses between 1 and 7 mil (1 mil = 10^{-3} inch or 25.4 μm). These materials are particularly suitable for fuel cell applications, and they have been shown to have a lifetime of more than 60,000 hours when operating in a fuel cell stack at 80°C and with appropriate humidification. Nafion® 117 (the first two digits denote a hundredth of the equivalent weight; here EW=1100 (g/mmol), and the last digit denotes the thickness in mils; here 7 *mil* = 178 μm thickness) exhibits high ionic conductivity at approximately 0.17 Scm^{-1} [11].

[4] Titration is a technique where a solution of known concentration is used to determine the concentration of an unknown solution. Typically, the *titrant* (the know solution) is added from a burette to a known quantity of the *analyte* (the unknown solution) until the reaction is complete. Knowing the volume of titrant added allows the determination of the concentration of the unknown. Often, an indicator is used to usually signal the end of the reaction, the endpoint.

The number of electrons and protons available in the fuel cell depend on the *amount of fuel supplied*, namely hydrogen in the case of PEM fuel cell. The relationship between current, which is the amount of flow of charge, and flow rate can be written using the basic definition of current as follows:

$$I = F\frac{dn_{e^-}}{dt} \qquad \textbf{3-5}$$

Where '*I'* is current (*Amperes*), '*F'* is Faraday's constant = 96473 (*Coulomb/mole*), 'n_{e^-}' is the amount of electron transfer (*kmol*) and '*t*' is time in (*seconds*).

The fuel consumption is related to the current drawn from the circuit during operation through the following equation:

$$\frac{dm}{dt} = M\frac{1}{n}\cdot\frac{dn_{e^-}}{dt} = M\frac{1}{n}\cdot\frac{I}{F} \qquad \textbf{3-6}$$

Where '*M'* is molar mass of fuel *(kg/kmol)* and '*n'* is the number of electrons transferred per molecule in the reaction.

Rearranging this equation yields an expression for current in terms of fuel usage as follows, using 'm' for the mass of fuel *(kg)*:

$$I = \frac{nF}{M}\cdot\frac{dm}{dt} \qquad \textbf{3-7}$$

This equation can be used to calculate the flow rate of fuel and oxidant in the fuel cell.

3.3.2. Fuel Cell Voltage

On each side of the fuel cell there is a potential difference between the electrode and the electrolyte due to the electrochemical reaction taking place, the voltage of the fuel cell is the resultant of these two potential differences. However, this voltage goes through many losses and influences that determine the final voltage of the fuel cell.

- ***Open Circuit Voltage***

Considering the half cell reaction in which two hydrogen atoms are split into two electrons and two protons, *the total energy change, at equilibrium*, for taking an infinitesimal amount (that would not disturb the system) of H_2 to $2H^+ + 2e^-$ must be *zero* [65]. Also when an infinitesimal amount of H_2 at a fixed pressure is converted to a fixed concentration of H^+, a precise change in chemical free energy occurs, ΔG, which is the change in the free energy of the reaction known as Gibb's free energy and its units are *(J/g. mole* H_2*)*.

The total free energy consists of two parts: the chemical free energy and the effect of potential on the components. When a potential difference exists between the electrode and the electrolyte, the reaction produces an electron on the electrode at one potential and a positive ion, H^+ in the electrolyte at another potential.

Separation of charge at two potentials requires energy; this energy is FE_o for 1 equivalent of electrons, where 'E_o'is the potential difference. Putting energy on a *per g-mole* H_2 basis, the total free energy change at equilibrium is:

$$\Delta g + nFE_o = 0 \qquad \textbf{3-8}$$

And more generally:

$$\Delta g = -nFE_o \qquad \textbf{3-9}$$

Where 'Δg' is Gibbs free energy change for the reaction defined on a per mole basis of one of the reactants, '*n'* is the number of electrons participating in the reaction of interest per molecule and '*F'* is Faraday's Constant.

For a change at constant '*T'* and '*P'*, Gibbs free energy change is defined as:

$$\Delta g_{T,P} = \Delta h - T\Delta s \qquad \textbf{3-10}$$

Where 'Δh' is the change in enthalpy; 'Δs' is the change in entropy and '*T'* is the temperature in *Kelvin*.

It is important to emphasize that several forms of the Gibbs free energy for a given species exist, however, the most commonly used form is the Gibbs free energy of formation, 'Δg_f'. As long as a consistent form of Gibbs free energy and the reference state are used, the numerical value of 'Δg' will be the same. The derivation of the thermodynamic relationships is presented in Appendix A.

E_o in equation (3-8) is often referred to as: *The electrode potential at equilibrium or Equilibrium potential* (also called *the Reversible Potential or Theoretical Open Circuit Potential or Theoretical Open Circuit Voltage*), where it is understood to be a difference in potential between electrode and electrolyte [65]. This represents the maximum electrical work obtained in the reaction. These relationships will be used later on to derive the expressions for the efficiency of the fuel cell.

- ***The Nernstian Voltage***

Fuel cell reactions involve the movement of electrons from the oxidised species to the reduced species. It is a reduction-oxidation reaction (known as redox reactions) where hydrogen is oxidised at the anode (loses electrons) and oxygen is reduced at the cathode (gains electrons). Nernst derived an equation correlating the electrode potential E of the electrode and activities of the species involved in the reaction. For a general reaction of the form:

$$jJ + kK \rightarrow mM \qquad \textbf{3-11}$$

Where 'j' moles of 'J' species react with 'k' moles of 'K' species, to produce 'm' moles of 'M' product. Nernst's equation can be generalised as follows:

$$E = E_o + \frac{RT}{nF}\ln\left(\frac{a_J^j . a_K^k}{a_M^m}\right) \qquad \textbf{3-12}$$

In this equation, 'a_J' and 'a_K' being the activities[5] [65] of the reactants, and 'a_M' the activity of the product. In the special case when the reactants and products exist in the standard states of unit activity at a given temperature, potential in this case is equal to equilibrium potential, i.e. $E = E_o$, and in this case the equilibrium potential is referred to as standard equilibrium potential, denoted as (E_o^o) and related to standard Gibbs free change for the reaction as follows [17, 66]:

$$\Delta g^o = -nFE_o^o \qquad \textbf{3-13}$$

Δg^o, the standard free energy change for the reaction, must be expressed in J/mole for E_o^o[6] to be in volts.

Some authors prefer to write the Nernst equation (3-12) in the form:

$$E = E_o + \frac{2.3RT}{nF}\log_{10}\left(\frac{a_J^j.a_K^k}{a_M^m}\right) \qquad \textbf{3-14}$$

Using '$\log_{10}$' instead of '*ln*'*;* which makes it easier to interpret the departure from the standard electrode potential. As an example; if the number of electrons *'n'* is 2, the value of $2.3RT/nF = 0.03$ Volt, therefore, the Nernst equation predicts about 30

---

[5] Activities are defined by $a = \gamma_A c_A / c_0$ where c_A is the concentration of A, c_0 is the concentration used for the standard state and γ_A is the activity coefficient of A at a constant concentration of c_A. $\gamma_A = 1$ at standard state; it is a variable which makes the equation above applicable even for non-ideal systems. Since c_A and c_0 are in the same units, a and γ_A are dimensionless. c_0 maybe taken as 1 *atmosphere* when a gas is involved, as *1 g-mole / litre* when a solute is involved or as *1 g-mole / cm*^{3} when a surface concentration is involved.

[6] Upper note denotes standard conditions and lower note denotes the equilibrium state.

millivolts departure from 'E_o' for each tenfold change from unit activity of the reactants or products [65].

The Nernst equation shows precisely how raising the activity of the reactants *increases* the voltage. On the other hand, raising the activity of the products *decreases* the voltage.

For simplicity, it is safe to assume that water is produced as steam at atmospheric pressure in the fuel cell, i.e. water has unity activity, and hence the value of the fuel cell voltage relies mainly on the partial pressures of the reactants.

The value of 'E_o' can be calculated from free energy data, and it is found that in any cell comprising an oxygen electrode and a hydrogen electrode, both operating reversibly, with the gases at one atmospheric pressure; 'E_o' *will have a voltage of 1.229Volt*. This voltage will be independent of the hydrogen ion concentration of the medium, provided the activity of water remains at unity [66].

By applying equation (3.12) at the cathode side (oxygen side) at two oxygen pressures and constant temperature *T*, it is easily shown that:

$$\Delta E = E_2 - E_1 = \frac{RT}{4F} \ln\left(\frac{P_2}{P_1}\right) \qquad \textbf{3-15}$$

Where 'E' is the potential difference between the electrode and electrolyte and the subscripts *1* and *2* define the states of operation at pressures 'P_1' and 'P_2' respectively. It is clear that 'ΔE' remains small because it is proportional to the log of a ratio of 'P_2'and 'P_1'.

For a fuel cell of a fixed geometry, to supply air instead of oxygen at the cathode means to reduce the pressure by a factor of 5, because the partial pressure of oxygen in air is (0.21), in this case, the fuel cell will have a theoretical potential only a few millivolts lower than a pure oxygen electrode (pure oxygen supplied at the same pressure), the same argument applies to the hydrogen electrode in the case of supplying pure hydrogen or diluted hydrogen.

The change in equilibrium voltage with pressure is plotted in figure (3-2) below. It shows that the effect of pressure changes the equilibrium potential in the order of millivolts. The effect of pressure is higher at pressures below 3 bar., but this effect reduces at higher pressures. This means that, with a hydrogen-oxygen fuel cell *where the reactants are gases*, the change of volume due to pressure changes will be large, and the effect of pressure can be observed. This has to be balanced with the gains achieved from pressurising and the design changes that have to be made.

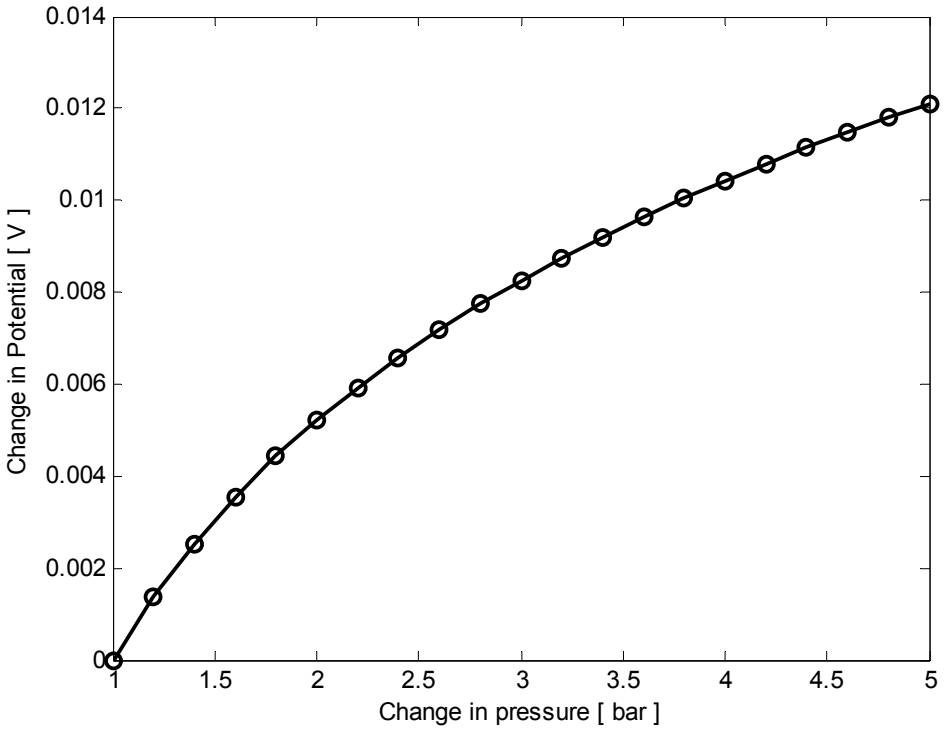

Figure 3-2 Change in equilibrium voltage with pressure

The effects of temperature and pressure on cell voltage have been quoted by many authors [17, 55]. The basic Nernst equation includes a term of temperature indicating that cell potential is directly proportional to temperature, this is in conformation with the kinetic theory of gases; which anticipates higher reaction rates at higher temperatures due to the increased kinetic energy of the molecules; however the following thermodynamic argument aims at studying the effect of raising the temperature of the reaction.

Assuming a chemical reaction where variations in temperature are not too high and the electron transfer is slow so that the reaction is not disturbed. From the equation of state and using the relationship for a polytropic process; for a change of pressure from 'P_1' to 'P_2' and temperature changes from 'T_1' to 'T_2':

$$\left(\frac{P_2}{P_1}\right)=\left(\frac{T_2}{T_1}\right)^{\frac{\vartheta}{\vartheta-1}} \qquad \textbf{3-16}$$

Where 'ϑ' is the polytropic index. Assuming 'P^o' is a standard unity pressure, and substituting the pressure values at state 1 and 2, the Nernst equation becomes:

$$E_1 = E_o + \frac{RT_1}{nF}\ln\left(\frac{P_1}{P^o}\right) \qquad \textbf{3-17}$$

$$E_2 = E_o + \frac{RT_2}{nF}\ln\left(\frac{P_2}{P^o}\right) \qquad \textbf{3-18}$$

$$\Delta E = E_2 - E_1 = \frac{R(T_2 - T_1)}{nF}\ln\left(\frac{P_2}{P_1}\right) \qquad \textbf{3-19}$$

Substituting for the pressure ratio using the temperature ratio in a polytropic process from equation (3-16); equation (3-19) above yields:

$$\Delta E = \frac{R(T_2 - T_1)}{nF}\ln\left(\frac{T_2}{T_1}\right)^{\frac{\vartheta}{\vartheta-1}} \qquad \textbf{3-20}$$

This equation is used to plot the variation of 'ΔE' with temperature over the range of operation of a (PEM) fuel cell using different values for the polytropic index ranging from 1.5 to 1.6; Figure (3-3) below :

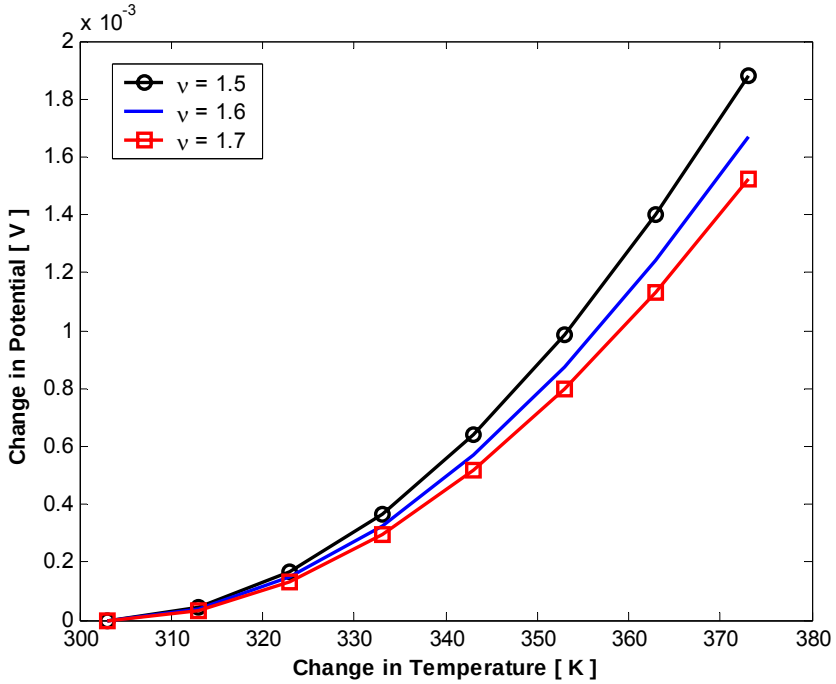

Figure 3-3 Variation of ΔE with temperature using different values for the polytropic index

Where 'γ' is the ratio between the specific heat capacities ($\gamma = {c_p}/{c_v}$), the poly tropic index can take one of the following values:

$\upsilon = 1$ The process is isothermal

$\upsilon = \gamma$ The process is isentropic

$\upsilon > \gamma$ The process is a real process

$\upsilon < \gamma$ Cannot be realistic as the system is losing heat and entropy is negative

The graph shows that there is a slight gain in potential due to the increase in temperature, but this gain decreases as the polytropic index increases. This is due to the fact that as the polytropic index increases, the system departs further from reversibility.

Now, considering the case where water is in the form of vapour at atmospheric pressure with unit activity, equation (3-12) reduces to the form:

$$E = E_o + \frac{RT}{nF}\ln\left\{P_{H_2}^{*}\left(P_{O_2}^{*}\right)^{1/2}\right\} \qquad \textbf{3-21}$$

Where P^{*} represents the partial pressures of the reactant gases denoted by the respective subscript.

As mentioned elsewhere, the standard state (298.15*K*, and 1 *atm*.) defines a standard state reference potential E_o^o=1.229 *V* and the equilibrium potential; 'E_o' will vary from the standard state reference in accordance with temperature as follows [52]:

$$E_o = E_o^o + (T - T^o)\left(\frac{\Delta S^o}{nF}\right) \qquad \textbf{3-22}$$

Where 'T^o' is the standard state temperature (298.15 K). The entropy change of a given reaction is approximately constant (assuming that the variation in specific heat with the expected change in temperature is negligible) and can be set to the standard state value. Rearranging equation (3-22) above and using standard values for temperature and standard state equilibrium potential, the reference potential varies directly with temperature as follows:

$$E_o = \beta_1 + \beta_2 T \qquad \textbf{3-23}$$

Where:

$$\beta_1 = 1.229 - \frac{T^o \Delta S^o}{nF} \qquad \textbf{3-24}$$

And,

$$\beta_2 = \frac{\Delta S^o}{nF} \qquad \textbf{3-25}$$

Using literature values for the standard-state entropy change, the value of β_2 in this equation can be calculated to be (0.85×10^{-3}) *V/K* [52], with further expansion; equation (3-21) can now be written as:

$$E = 1.229 - \beta_2\left(T - T^o\right) + \varphi T\left\{\ln\left(P_{H_2}^{*}\right) + \frac{1}{2}\ln\left(P_{O_2}^{*}\right)\right\} \qquad \textbf{3-26}$$

Where $\varphi = 4.3085 \times 10^{-5}\,[VK^{-1}]$. This general expression gives *the thermodynamic potential for a hydrogen/oxygen fuel cell on the basis of the Nernst equation*, which indicates the importance of this equation.

Evaluation of the two partial pressures for oxygen and hydrogen as per equation (3-26) typically involves mass transfer calculations and requires averaging over the cell surface or along the direction of gas flow to account for significant changes in the partial pressures of the gaseous reactants due to reaction in the cell. Amphlett *et al.* [52] assumed that the partial pressures of hydrogen and oxygen will decline exponentially with respect to their residence time in the flow channels due to their consumption at the electrodes. They assumed that the exponential decay will depend on the velocity of gas flow in the flow channels.

On the cathode side, where the consumed oxygen represents a small fraction of the total flow (the stoichiometric ratio of oxygen, which is the ratio of the actual quantity of gas supplied to the actual quantity needed, is generally > 1.75 using atmospheric air, which means that the excess flow is in the order of 733% due to the presence of nitrogen), velocity will be approximately constant. The effective oxygen partial pressure can then be approximated using a log-mean average of the inlet and outlet oxygen partial pressures, where subscripts '*avg'* and '*hum'* stand for average and humidified respectively:

$$P_{O_2}^{avg} = \frac{P_{O_2,out}^{hum} - P_{O_2,in}^{hum}}{\ln\left(\frac{P_{O_2,in}^{hum}}{P_{O_2,out}^{hum}}\right)} \qquad \textbf{3-27}$$

Along the anode flow channels, on the other hand, the decline in flow velocity due to consumption and absorption of hydrogen is a much more significant fraction of the total velocity, since the excess flow of fuel is typically quite small (Stoichiometric Ratio is in the range of 1.15 to 1.3) hence, an arithmetic mean is justifiable as a good first approximation of the effective hydrogen partial pressure which can be represented by the following equation:

$$P_{H_2}^{avg} = \frac{P_{H_2,in}^{hum} + P_{H_2,out}^{hum}}{2} \qquad \textbf{3-28}$$

3.4. FUEL CELL VOLTAGE LOSSES

The performance of a fuel cell can usually be described by a *Current Density vs. Voltage* curve, known as the *polarization curve*, where the voltage of the fuel cell is related to the current density, or by a power density curve, where the power output is related to the current density. Figure 3.4 is a schematic of a polarization curve.

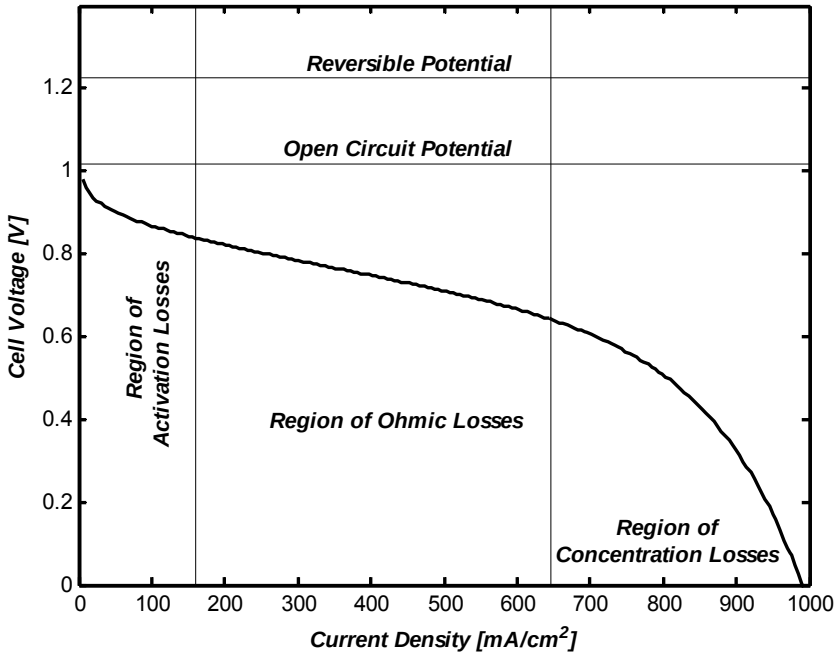

Figure 3-4 Schematic of a polarization curve, axis values and region limits are arbitrary

The polarisation curve, figure (3-4) indicates that the open circuit voltage (E_o) is less than the theoretical value of the reversible potential, E_o^o, which indicates that there is a loss in voltage even when no current is drawn from the fuel cell. This loss can be attributed to *fuel cross over and internal currents through the electrolyte*. The electrolyte should only transport ions, but a small amount of fuel, and even a lesser amount of electrons, will be conducted through the electrolyte, which will have a reducing effect on the open circuit voltage, as seen from the polarization curve [17].

As we move away from the zero current point, a rapid initial drop in voltage is noted, this can be referred to *activation losses* which are caused by the slowness of the

reaction taking place on the surface of the electrodes. A proportion of the voltage generated is lost in driving the chemical reaction that transfers the electrons to and from the electrode [17].

Moving to higher current densities, the voltage loss becomes more linear and falls less slowly, this loss is due to *Ohmic losses*, sometimes called "resistive losses", as they stem from the straightforward resistance to the flow of electrons in the various fuel cell components, as well as the resistance to the flow of ions in the electrolyte. This voltage drop is approximately linear and proportional to current density.

The final region of the polarization curve occurs at higher current density, where the voltage falls rapidly away due to mass transport limitations in the cell. These are usually termed "*Mass transport* or *concentration losses"*, and they result from the change in the concentration of the reactants at the surfaces of the electrodes, due to obstruction that prevents the gases from reaching the reaction sites on the membrane and most commonly due to the accumulation of product water blocking the flow channels in the bipolar plates or the GDL. This type of loss is sometimes called "Nernstian", because of its connection with concentration effects which are modelled by the Nernst equation [17]. So as to avoid the drastic decrease in power density in this region, the optimal operating regime for a fuel cell is up to the maximum power density.

It should be pointed out that the terms used for *losses* are variable from one discipline to another, they are called: losses, voltage drop or conversely; overvoltage, which gives the impression that voltage increases rather than decreases, but it is the term usually used in electrochemical literature. The terms losses and overvoltage will be used mostly in our analysis.

In the following sections we attempt to consider each one of these losses separately, and present, in mathematical and graphical forms, the effects of varying certain operating conditions such as: temperature and pressure on the performance of the fuel cell, as well as certain geometric dependant parameters such as the values of exchange current density and charge transfer coefficient which are dependant on the electrode material and catalyst loading of the fuel cell electrodes.

The following assumptions are applied throughout this analysis:

i. The fuel cell operates under steady state conditions.

ii. The gases are assumed to be ideal compressible gases.

iii. Due to the low velocity of the gases, their flow is laminar.

iv. The product water is assumed to be in liquid form.

v. The electronic resistance of the fuel cell components and the external circuit are constant over the range of operating temperatures.

vi. The pressures of the anode and cathode are assumed to be the same.

vii. The internal currents in the fuel cell are equal to fuel cross over.

3.4.1. Activation Overvoltage; η_{act}

There is a close similarity between electrochemical and chemical reactions in that both involve an activation barrier that must be overcome by the reacting species. In doing so, part of the electrode potential is lost in driving the electron transfer rate to the rate required by the current demand. The Butler-Volmer equation describes the reaction kinetics when mass transfer effects are negligible as follows [65]:

$$i = i_o[e^{-\alpha nF\eta_{actc}/RT} - e^{-(1-\alpha)nF\eta_{acta}/RT}] \qquad \textbf{3-29}$$

Where '*R'* is the universal gas constant (*8.314 kJ/kmol.K*), '*T'* is the temperature of operation in *Kelvin*, '*n'* is the number of electrons involved per mole of electrolysed component, 'α' is the *charge transfer coefficient*, which is the portion of the electrical energy assisting the forward reaction, the remaining portion $(1-\alpha)$ hinders the reverse process. The value of 'α' depends on the reaction involved and the material the

electrode is made from, but it must be in the range of (0< α <1), '*F'* is Faradays constant (96485 C/mole), 'η_{actc}' and 'η_{acta}' are the activation overvoltages on the cathode and anode respectively, '*i'* is the current density (A/cm^2) and 'i_o' is the exchange current density[7], which is the rate of flow of electrons from and to the electrolyte [65].

In equation (3-29) above, the first exponential represents the forward reaction potential (the reduction reaction on the cathode), while the second exponential represents the backward reaction potential (the oxidation reaction on the anode). Writing the equation in the logarithmic form yields:

$$\ln\left(\frac{i}{i_o}\right) = \frac{-\alpha nF\eta_{actc}}{RT} + \frac{(1-\alpha)nF\eta_{acta}}{RT} \qquad \textbf{3-30}$$

When the activation overvoltage on the cathode is very much higher than the activation overvoltage on the anode, the first part of the equation which represents the forward oxidation reaction prevails and the second part can be ignored, and vice a versa in the case of prevailing anodic overvoltages.

These two expressions can be written separately for anode and cathode in the form known as Tafel's laws. For a net cathodic overvoltage, the backward activation overvoltage (anodic reaction) is negligible, and the equation becomes:

$$\eta_{actc} = -\frac{RT}{\alpha nF}\ln\left(\frac{i_c}{i_o}\right) \qquad \textbf{3-31}$$

[7] The exchange current density is defined as the current flowing equally in each direction at the reversible potential. Equilibrium in a chemical reaction is established when the forward and backward rates are equal. In the case of electrochemical reactions, rates of the reaction define the current, which at equilibrium would be the exchange current density.

On the other hand, for a net anodic overvoltage, the anodic reaction becomes the forward reaction and the cathodic reaction is neglected, equation (3-30) becomes:

$$\eta_{acta} = \frac{RT}{(1-\alpha)nF}\ln\left(\frac{i_a}{i_o}\right) \qquad \textbf{3-32}$$

Subscripts '*a*' and '*c*' are used in equations (3-31) and (3-32) to denote the anodic and cathodic current densities respectively. Both equations are in the form known as Tafel's Law which can be written in terms of current density as follows:

$$\eta_{actc} = x + y\ln i_c \qquad \textbf{3-33}$$

Where; for the cathode side:

$$x = \frac{RT}{\alpha nF}\ln i_o \quad \textbf{And} \quad y = -\frac{RT}{\alpha nF}$$

This equation can also be written in terms of both current density and exchange current in the following form which is used by many researchers:

$$\eta_{act} = b\log\left(\frac{i_c}{i_o}\right) \qquad \textbf{3-34}$$

Where '*b*' in this equation is equal to '*y*' as follows [20]:

$$b = -\frac{RT}{\alpha nF} \qquad \textbf{3-35}$$

Equation (3-35) is very important as it will be used again in the expression for the concentration overvoltage

Tafel's equation is applicable where the activities of the species involved in the reaction are not very much affected by the current flow. The equation can also be used to deduce the exchange current density which occurs at $\eta_{act} = 0$. Rearranging equation (3-31) to give '$\ln i_c$' in terms of 'η_{act}', considering the other terms constant gives:

$$\eta_{actc} = -\frac{RT}{\alpha nF}\ln i_c + \frac{RT}{\alpha nF}\ln i_o \qquad \textbf{3-36}$$

Rewriting the equation using the coefficient 'b':

$$\eta_{actc} = b\ln(i_0) - b\ln(i) \qquad \textbf{3-37}$$

Substituting the proper values for the constant terms in equation (3-35), and taking the value $n = 4$ for the cathode side, $\alpha = 0.5$ [17] and an operating temperature 'T' = 373 K, the value of coefficient 'b' is found to be = 0.0161. This equation is plotted below for various exchange current densities:

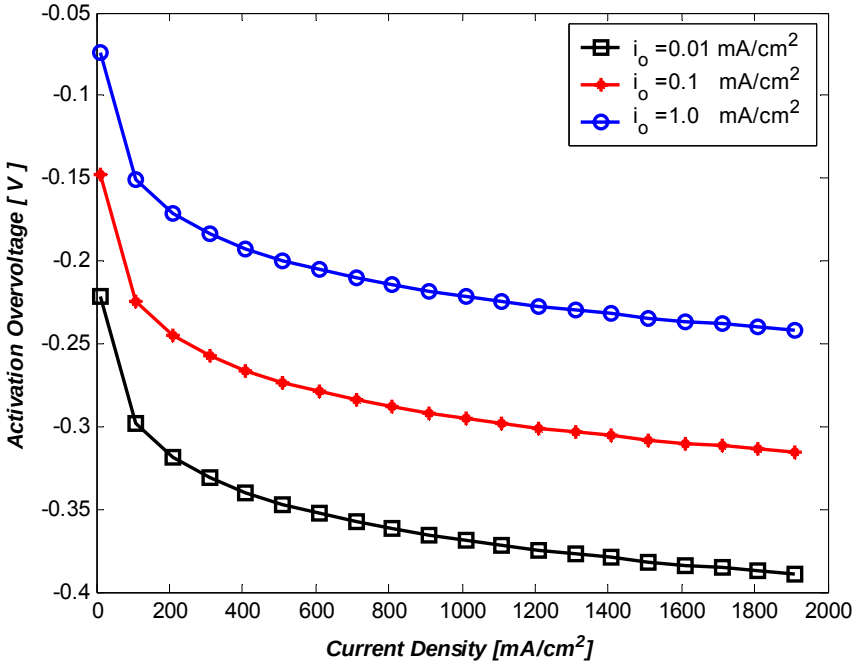

Figure 3-5 Variation of activation overvoltage as a function of exchange current density

From the graph it is seen that increasing the exchange current density leads to reducing the activation losses.

For a low temperature, hydrogen fuel cell running on air at ambient pressure, the cathode exchange current density is over 2000 times less than that on the anode, a typical value for the exchange current density, i_o ; would be about $0.1\,mAcm^{-2}$ at the cathode and about 200 $mAcm^{-2}$ at the anode [17], which makes losses due to activation much greater on the cathode side and hence requires more catalyst loading to improve the kinetics of the reaction.

It is also noted from the figure that the voltage drop increases exponentially as the current density increases. In situations where the polarization curve is obtained experimentally, it is possible to deduce the activation current density from this curve by extrapolation; in this case activation overpotential is plotted against $\ln(i)$.

It was reported by some researchers that the exchange current density; i_o also depends on the partial oxygen pressure. Parthasarathy *et al.* [67] conducted experiments on a PEM fuel cell at a temperature of 50 °C. The results are summarized in Fig. (3-6).

Figure 3-6 Dependence of the exchange current density of oxygen reduction reaction (ORR) on oxygen pressure [20].

A linear relationship was found between the logarithm of the exchange current density i_o and the logarithm of the oxygen partial pressure, according to:

$$i_o = x.\exp(yP_{O_2}^*) \qquad \textbf{3-38}$$

Where '$x = 1.27 \times 10^{-8}$' and '$y = 2.06$'. However, this relationship is only applicable to the particular conditions of the experiment performed by Parthasarathy *et al.* [67] and is not applicable to other fuel cells because, as mentioned earlier, the

exchange potential, particularly at the cathode side, is a mixed potential due to competing reactions. Furthermore, there are other geometric variables and operating conditions that contribute to the value of the exchange current density, however, the reported experiments indicate the oxygen partial pressure is also a factor in determining the value of 'i_o'.

To understand the effects of the charge transfer coefficient on the activation overvoltage; Tafel's equation is plotted for different values of the charge transfer coefficient (α) for a given value of exchange current density i_o = 0.01 and an operating temperature of $T = 373K$:

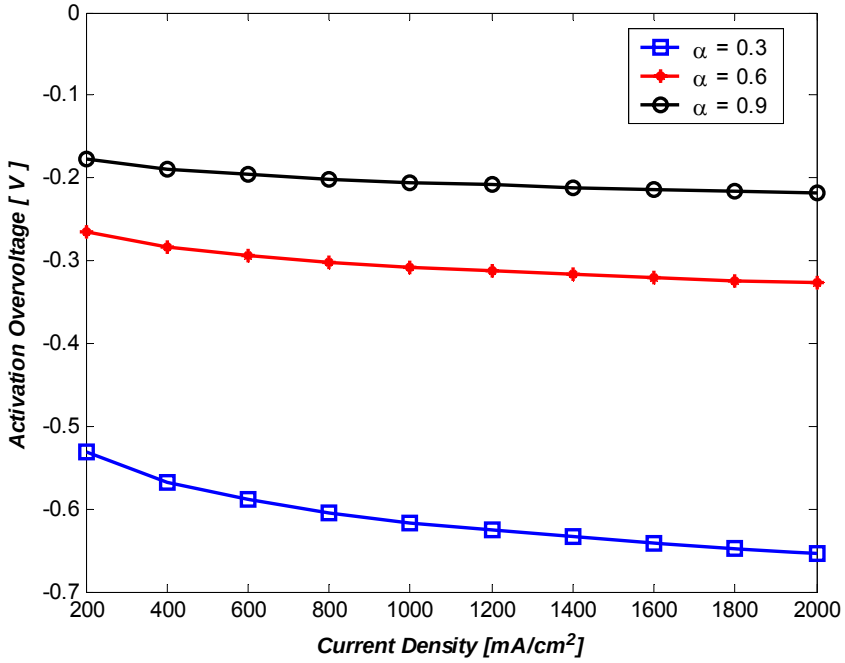

Figure 3-7 Effect of varying the values of the charge transfer coefficient (α) on the activation overvoltage, for exchange current density (i_o =0.01) and operating temperature *T*=373K

As the charge transfer coefficient decreases, figure (3-7) shows that the activation overvoltage increases exponentially. This indicates the importance of the charge transfer coefficient which depends on the type of the electrode material; consequently, the type of electrode material is an important factor in improving the power output of the fuel cell.

The same equation is plotted for various temperatures of operation and various current densities; the graph shows that at higher temperatures the activation losses increase. However, this is counterbalanced by the increased activities of the reactants due to higher temperatures, in accordance with the kinetic theory of gases.

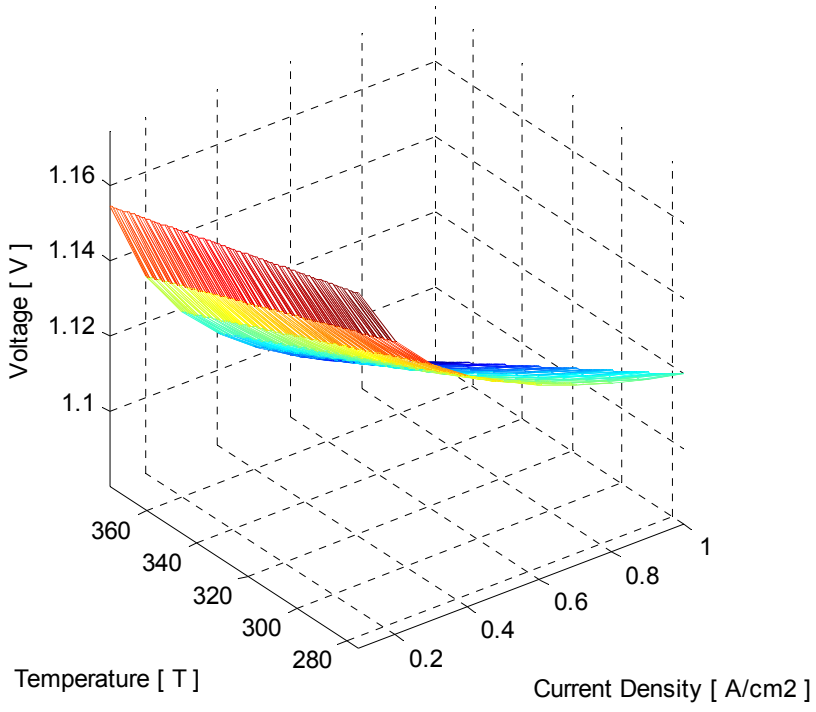

Figure 3-8 Changes of voltage due to activation overvoltage with respect to variations in temperatures of operation and variations of current densities

In the case of the PEM fuel cell, with effective catalyst action, the hydrogen electrode operates close to thermodynamic equilibrium conditions. The hydrogen oxidation reaction proceeds readily so that the anodic activation overvoltage; 'η_{acta}' is negligible.

In contrast, the rate of oxygen reduction in aqueous media at the thermodynamic equilibrium potential is about (10^{-5}) times slower than that of hydrogen, even with the best catalysts currently available [17]. Consequently, the voltage drop due to activation can be mainly attributed to the cathodic reaction.

Following from the previous discussion, the second exponential in equation (3-30) which represents the anodic part of the total activation overvoltage, is safely ignored in most of the published literature on PEM fuel cells; the equation is simplified to the form of Tafel's law.

However, this is not the case for other types of fuel cells, such as the Direct Methanol Fuel Cell (DMFC), which is similar to the PEM fuel cell in using the same type of membrane electrolyte with a different catalyst and basically the same construction, but the activation overvoltages on the anode are considerable and have to be accounted for in the equation.

3.4.2. Ohmic Overvoltage; η_{Ohmic}

The Ohmic voltage drop in the fuel cell is due to the resistances of the various components of the fuel cell to the flow of electrons, and the resistance of the membrane to the flow of protons. This can be divided into two components:

i. **Electronic resistance**; which is the resistance to the flow of the electrons in the various components of the fuel cell and the connected load. The resistance of all pure materials increases as temperature increases, whereas the resistances of carbon, electrolytes and electrically insulating materials decrease with temperature increase. For a moderate range of temperatures, up to 373K (100°C), the change of resistance is usually proportional to the change of temperature, however, in this analysis, it will be assumed constant. The electronic resistance of the fuel cell can be determined by simple measurement of the resistance of the various components of the fuel cell excluding the membrane at the required operating temperature.

ii. **Protonic resistance** to the flow of the protons, and this mainly occurs in the proton exchange membrane, and depends greatly on the structure of the membrane, the dimensions of the membrane, its water content, temperature and catalyst loading. Hence, the total Ohmic Overvoltage can be expressed as follows:

$$\eta_{ohmic} = -i(R^{electronic} + R^{protonic}) \qquad \textbf{3-39}$$

Considering the protonic portion of the total resistance, for a membrane of length 'l' in the direction of flow of protons, which is in this case the thickness of the membrane; 'A' is the active area of the membrane in (cm^2), the protonic resistance of the membrane; '*R',* can be defined as follows [68]:

$$R^{protonic} = \frac{\rho_M l}{A} \qquad \textbf{3-40}$$

Where 'ρ_M' is the membrane specific resistivity for the flow of protons measured in ($ohm \cdot cm$) and it is a function of the type and characteristics of the membrane, temperature, water content or degree of hydration of the membrane and current density.

An empirical expression for Nafion® membrane resistivity was proposed by Mann *et al.* [53] on the basis of published PEM Fuel cell performance curves. It was represented as a function of current, temperature, active area and the semi-empirical parameter (λ); representing the effective water content of the membrane per sulphonic group (H_2O / SO_3^-) as follows:

$$\rho_M = \frac{\varphi_1\left[1+\left(\frac{0.03i}{A}\right)+\varphi_2\left(\frac{T}{303}\right)^2\left(\frac{i}{A}\right)^{2.5}\right]}{\left[\lambda-\varphi_3-\left(\frac{3i}{A}\right)\right]\exp\left(\varphi_4\left[\frac{T-303}{T}\right]\right)} \qquad \textbf{3-41}$$

Where $\varphi_1 = 181.6$, $\varphi_2 = 0.062$, $\varphi_3 = 0.634$ and $\varphi_4 = 4.18$. The parameter (λ) depends on the preparation procedures of the membrane, the relative humidity and the stoichiometric ratio of the anode feed gas and the working life of the membrane. It can have a value as high as 14 under ideal, 100% relative humidity conditions, and has had reported values as high as 23 [53]. The value of 'λ' has to be determined on the basis of experimental results.

For simplicity, the two types of resistances can be grouped together in one term, and equation (3-39) can be written as:

$$\eta_{ohmic} = R_i i \qquad \textbf{3-42}$$

Where ' R_i 'is the internal current resistance which comprises both electronic and protonic resistances caused by membrane and contact losses [20].

3.4.3. Concentration Overvoltage; η_{conc}

Concentration overvoltage or "mass transport losses" result from the change in the concentration of one of the reactants at the surfaces of the electrolyte, which occurs when a chemical species participating in the reaction is in short supply due to obstruction in the pathway of this species. This type of loss is sometimes called "*Nernstian*" because of its connection with concentration effects which are modelled by the Nernst equation [17].

The reduction in the concentration of the reactants depends on the rate at which they are being consumed, which in turn depends on the current drawn from the fuel cell, and on the physical characteristics of the system. All these factors will eventually lead to variations in the pressures and concentrations of the gases, as well as the rate at which they are being transported from the flow channel to the surface of the membrane through the catalyst layer and the GDL. The effect of partial pressures was discussed earlier; however, a similar argument will be adopted in the analysis of the concentration overvoltages.

As pointed out earlier in the context of this chapter, the initial concentration of the reactant gases, represented by their partial pressures, has an influence on the open circuit voltage. The pressures of the gases will decrease in the fuel cell in the course of their consumption, until they reach a point where the amount of reactant gases reaching the electrolyte is equal to the rate of their consumption. At this point, the partial pressure of the reactant gas has reached zero, hence, it is impossible to increase the current output of the fuel cell beyond this point, which is the maximum current density attainable, from now on called the limiting current density, ' i_l '.

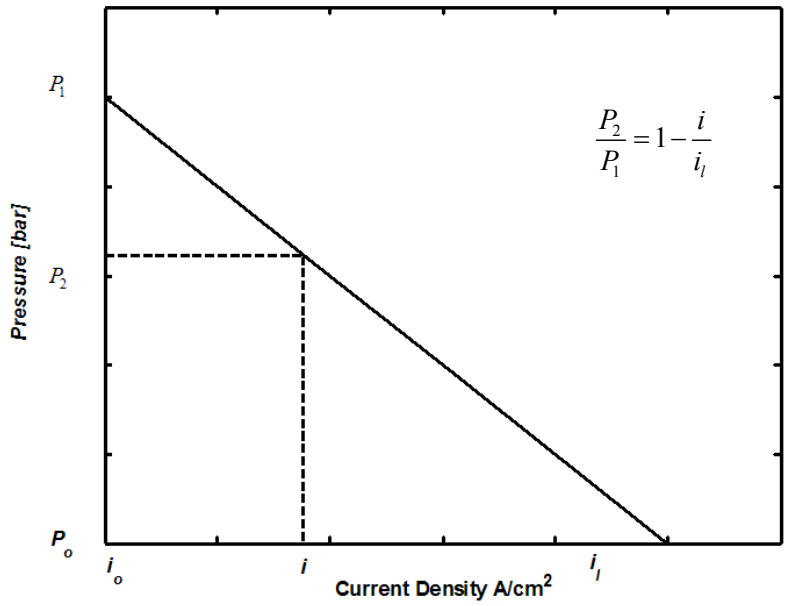

Figure 3-9 Assumed variation of current density with concentration pressure

Assuming that the pressure drops down to zero at the limiting current density 'i_l' in a linear manner due to mass transport, and that the initial pressure at zero current was 'P_1', then from the similarity of triangles in Figure (3-9), it can be shown that:

$$\frac{P_2}{P_1} = 1 - \frac{i}{i_l} \qquad \textbf{3-43}$$

Substituting this value in the Nernst equation (3-15), which explains the relationship between the voltage drop and partial pressures of the reactant gases, the following relationship is obtained:

$$\eta_{conc} = -\frac{RT}{nF} \ln\left\{1 - \frac{i}{i_l}\right\} \qquad \textbf{3-44}$$

Where 'n' is the number of electrons transferred per molecule in the reaction, in the case of Hydrogen-Oxygen Fuel cell n = 2 for Hydrogen, and n = 4 for Oxygen, 'R' is the universal gas constant (8.314 *KJ/kmol .K*), 'T' is the temperature of operation in Kelvin, and 'F' is Faraday's constant.

This can be compared to equations (3-36) where:

$$b = -\frac{RT}{\alpha nF} \qquad \textbf{3-36}$$

Hence equation (3-44) can be written as follows:

$$\eta_{conc} = \alpha b \ln\left\{1 - \frac{i}{i_l}\right\} \qquad \textbf{3-45}$$

This equation can now be used for plotting the concentration overvoltage for hydrogen and oxygen using the proper values of '*n*' at a temperature of 353K and *charge transfer coefficient* '$\alpha = 0.5$' [17], the plots are shown in figure (3-10). The open circuit voltage is taken as 1 Volt.

It is noted from the graph that the effect of the concentration overvoltage is more dominant at the Anode compared to the Cathode, this is due to the fact that the reaction kinetics are more rapid on the anode, consequently any effect that causes a delay to the reaction will be more noticeable on the anode.

It is also noted that the limiting current does not occur suddenly, and the curve drops down gradually at the anode side, while, in the case of the cathode, the drop-down of the curve is more gradual.

The two curves drop down to the limiting current value simultaneously, hence the final drop at the cathode side is more rapid and any attempt to draw more current from the fuel cell beyond this value will result in a sharp drop in cell voltage, hence decreasing the power output.

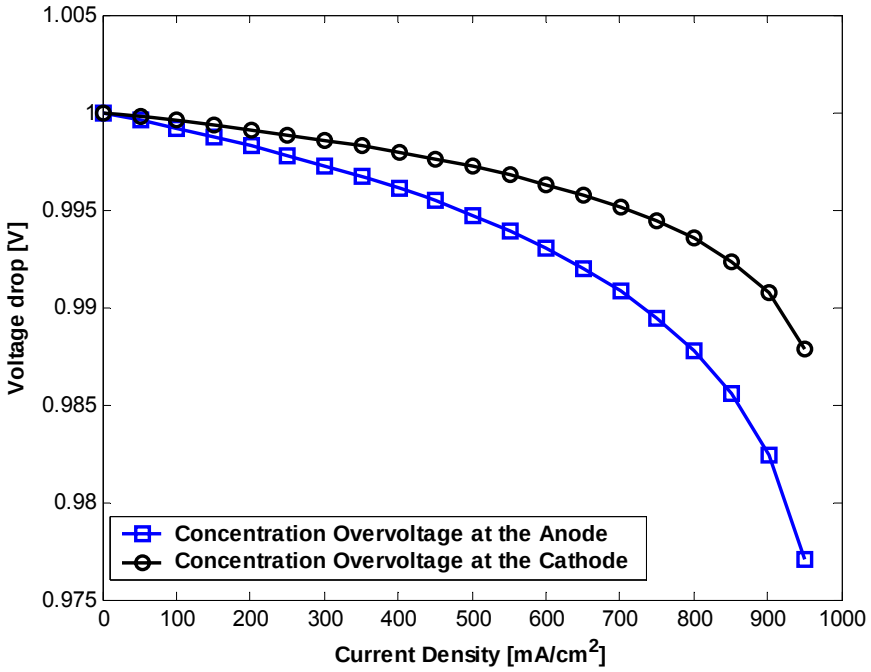

Figure 3-10 Concentration Overvoltage at the Anode and Cathode at 353 K, Open circuit voltage is taken as 1 Volt.

In order to study the effect of temperature on the concentration overvoltage, equation (3-45) is plotted for two values of temperature for the cathode; figure (3-11) below, it is noticed that the concentration losses increase slightly as temperature increases. This is in accordance with Nernst equation, but in reality this is counterbalanced by the increase in the kinetics of the chemical reaction as predicted by the kinetic theory of gases. However, the concentration losses behaviour in the fuel cell is a complex phenomenon and involves many factors. The main factor is the generation of water at the cathode due to the chemical reaction which increases at high current densities, at the same time, water evaporation increases at higher temperatures, which reduces the species transport limitations and thus the concentration losses, but at the same time could result in dehydration of the membrane and reduction in its protonic conductivity. Consequently, it is difficult to predict the voltage behaviour due to the variation of one parameter without considering the interactions of other parameters, which necessitates the implementation of more advanced analytical tools such as

computational fluid dynamic (CFD) modelling and simulations, which will be used to model the final design of the fuel cell proposed in this study.

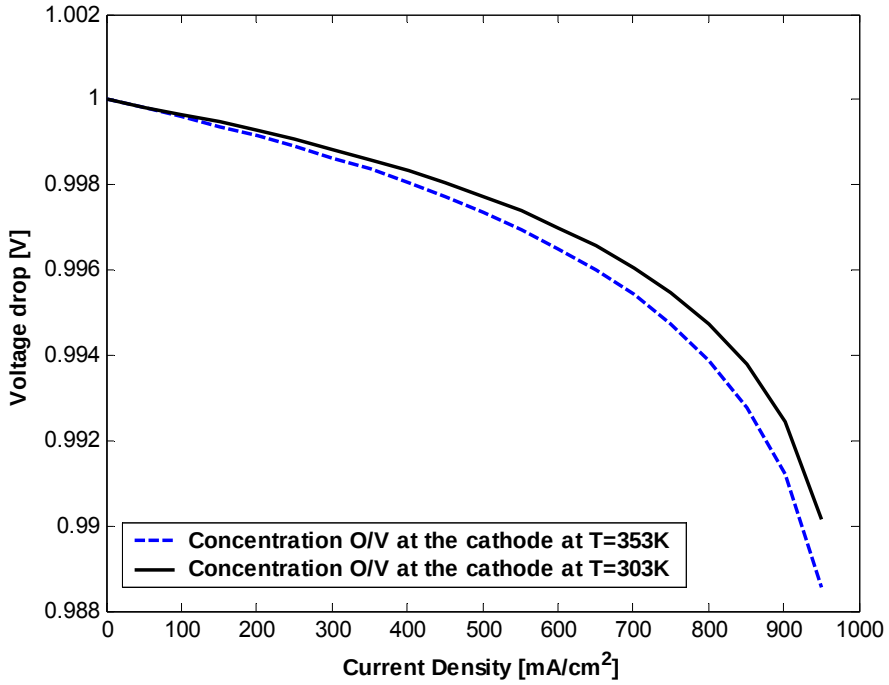

Figure 3-11 Concentration Overvoltage at the Cathode at various temperatures

A different approach in modelling the concentration overpotential was presented by Kim *et al.* [69], in which an empirical equation based on experimental data was presented as:

$$\eta_{conc} = m\exp(ni) \qquad \textbf{3-46}$$

A physical interpretation for the parameters '*m*' and '*n*' was not given, but Bevers et al. [70] found in their one-dimensional modelling study that '*m*' correlates to the electrolyte conductivity and '*n*' to the porosity of the gas diffusion layer. Following up on this we can speculate now that both '*m*' and '*n*' relate to water management issues: a partially dehydrated electrolyte membrane leads to a decrease in conductivity, which can be represented by '*m*', whereas an excess in liquid water leads to a reduction in porosity and hence to an early onset of mass transport limitations, which can be captured by the parameter '*n*' [65].

The equation is derived on the basis of curve fitting techniques and only applies to the fuel cell and operating parameters of the particular experiment of the authors. Typical values for '*m'* and '*n'* as suggested by [17] are m = 2.11E-5 and n = 0.008.

The Geometry of the fuel cell plays an important role in minimizing the concentration losses, and hence, increasing the value of the limiting current and improving the range of operation of the fuel cell. This can mainly be achieved through reducing pressure drop in the flow channels, increasing the active area of the membrane and improved water management which is capable of removing the water produced by the reaction at the cathode side in order to maintain access for the reactants to reach the active sites on the membrane.

3.4.4. Fuel Cross-Over and Internal Currents

Although the proton exchange membrane in the fuel cell is an electronic insulator, it will support very small amounts of electron cross-over. It will also allow some hydrogen to pass through diffusion from the anode to the cathode. This hydrogen will react with oxygen at the cathode in the presence of the catalyst to produce water and heat, but without producing electric current.

It is assumed here that the internal currents are equal to fuel cross-over. The amount of fuel wasted due to fuel cross over can be approximated using a relationship that relates this amount to current. This current value can then be added to the total current in the voltage-current relationship. The internal current in the fuel cell cannot be measured, but using the basic equation for current in terms of fuel usage derived earlier; equation (3-7), and measuring the fuel consumption at open circuit, the value of internal current can be estimated.

An empirical value for the internal currents suggested by [17] is *3.00 mA/cm*^{2}. Substituting this value in equation (3-7) above, gives a value of fuel consumption due to fuel crossover equal to: 0.314×10^{-10} *kg/s.cm*^{2} of hydrogen.

The value of internal current has to be added to the fuel cell current when measuring fuel cell performance.

3.5. OVERALL VOLTAGE

The four types of overvoltage discussed above, namely: Activation, Internal currents, Ohmic and Concentration Overvoltages act together throughout the range of operation of the fuel cell. They have a combined effect that will drive the performance curve of the fuel cell, commonly known as the polarization curve, away from linearity with respect to the amount of current required from the fuel cell.

To visualize the combined effect of these losses, a general equation that represents the summation of their basic equations is representative of their total effect. The basic equations are as follows:

$$V = E_o + \eta_{act+\text{int}} + \eta_{Ohmic+\text{int}} + \eta_{conc+\text{int}} \qquad \textbf{3-47}$$

Where V is the output voltage, and E_o is the reversible voltage of the fuel cell. For a fuel cell operated on hydrogen with the gases at one atmospheric pressure; and the activity of water remains at unity; E_o *will have a voltage of 1.229 volt* [66].

The three following terms represent the activation, Ohmic and concentration overvoltages; the '*int'* suffix denotes the voltage losses due to internal currents that will be included in the equation:

$$E_o = 1.229 - \beta_2 \left(T - T^o\right) + \varphi T \left\{ \ln\left(P^*_{H_2}\right) + \frac{1}{2}\ln\left(P^*_{O_2}\right) \right\} \qquad \textbf{3-26}$$

Where $\beta_2 = 0.85 \times 10^{-3}$ $[VK^{-1}]$ and $\varphi = 4.3085 \times 10^{-5}$ $[VK^{-1}]$.

$$\eta_{act} = b \log\left(\frac{i_c}{i_o}\right) \qquad \textbf{3-34}$$

Where:

$$b = -\frac{RT}{\alpha n F} \qquad \textbf{3-35}$$

$$\eta_{ohmic} = R_i i \qquad \textbf{3-42}$$

Where ' R_i 'is the internal current resistance which comprises both electronic and protonic resistances caused by the membrane together with the contact losses.

$$\eta_{conc} = \alpha b \ln\left\{1 - \frac{i}{i_l}\right\} \qquad \textbf{3-45}$$

Where 'α' is the *charge transfer coefficient* and *'b'* is taken from equation (3-35).

In all these equations, the internal current has been added to the total value of current, the following constants and parameter values (Table 3-2) have been used to plot the polarization curve for equation (3-47), the MatLab® code used for the plot is presented in Appendix B.

Table 3-2 Values of constant parameters used to plot the polarisation curve in figure (3-12)

PARAMETER	VALUE	UNITS
E_o	1.031	*Volt*
b	0.032	*kJ.mole/kg.°C*
R	$3x10^{-3}$	*Ohm*
i_o	50	A/cm^2
i_l	2000	A/cm^2
T	353	*Kelvin*

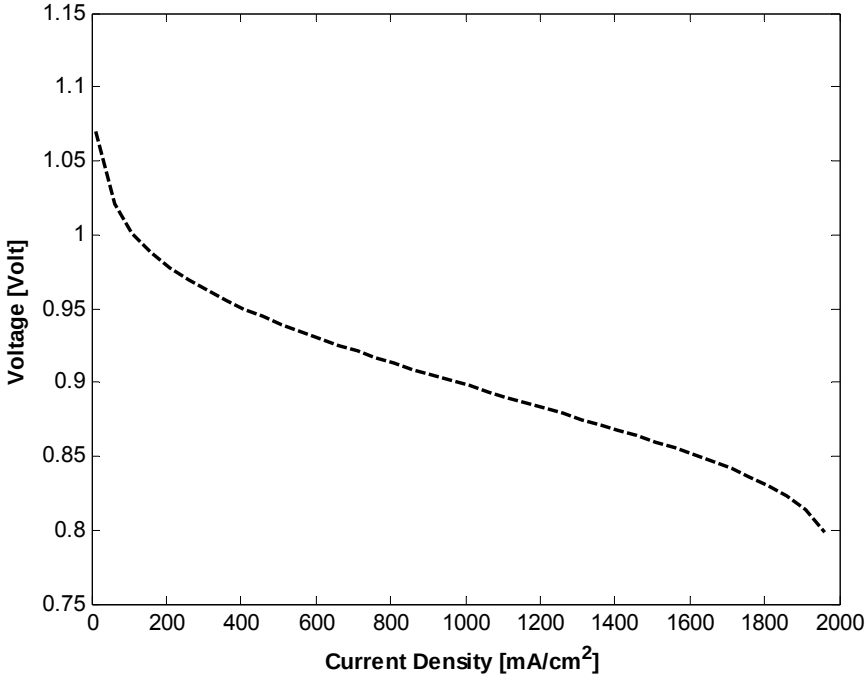

Figure 3-12 Polarisation curve as functions of the current density of the fuel cell

3.6. NOTES AND OBSERVATIONS ON THE POLARISATION CURVE

The following observations can be drawn from this graph:

1. The shape of the curve is typical of the fuel cell performance, but deviation from this curve under practical conditions is expected, as the theory behind this curve is based on idealistic assumptions and does not consider all the factors affecting the practical applications.
2. This study applies only to changes in pressure and temperature and their influence on the performance of the fuel cell, however, those changes will cause changes in the conductivity of the various components, viscosity of the fluids, and variations in certain parameters that have been assumed constant, such as the specific heat at constant pressure.
3. The geometry of the fuel cell plays a major role in its performance, but in this analysis, only the theoretical background of the analysis is considered as an exercise for establishing similar parameters under experimental

conditions. This however cannot be achieved until a practical fuel cell is constructed and its geometric parameters are established.

4. This analysis puts forward the theory of the fuel cell operation which will be used for optimization of the fuel cell design and components in a later stage.

3.7. EFFICIENCY AND HEAT OUTPUT

The basic definition of efficiency, where 'ε_{th}' the thermal efficiency of the fuel cell is:

$$\varepsilon_{th} = \frac{\text{Power 0utput}}{\text{Power input}} \times 100\% \qquad \textbf{3-48}$$

Efficiency can be the process efficiency or the system efficiency, where the process efficiency indicates how efficient a single process in the system is performing, but does not indicate the total system efficiency; such as the combustion process itself in a heat engine which could reach 95% while the system efficiency is in the range of 28%.

The efficiency of the thermodynamic process taking place in the fuel cell is the *theoretical maximum efficiency allowed by the second law of thermodynamics* and can be expressed as follows:

$$\varepsilon_{th} = \frac{\Delta G_T}{\Delta H^o} \qquad \textbf{3-49}$$

Where 'ΔG_T' is the Gibbs free energy at the cell operating at temperature 'T' [K], and 'ΔH^o' is the reaction enthalpy at the (STP) standard temperature and pressure 101.3 Pa, 298 K.

In the case of PEM fuel cells and other types of fuel cells running on hydrogen, it is important to take the proper value for enthalpy depending on the phase at which the product water is produced. Higher heating value HHV[8] [17] is used when the water product is liquid at 298K (25^{o}C) and lower heating value LHV is used when the water product is vapour at 423K (150^{o}C), as part of the enthalpy has been consumed in evaporating the water. It is worth noting that in the PEM fuel cell, the water product is produced at 353K (80^{o}C), and the calorific value of the fuel should be somewhere between the lower and higher heating value, according to the definitions of the heating values.

Table 3-3 Gibbs free energy, enthalpy and calorific value for hydrogen

Value	ΔG_T	ΔH^0	*Calorific Value*
Unit	*kJ/mole*	*kJ/mole*	*MJ/kg*
LHV	223.0	240.4	120.21
HHV	237.1	285.8	142.18
Interpolated value at 353K (80^{o}C)	230.5	264.6	132.0

From standard thermodynamic values, the values for the Gibbs free energy 'ΔG' for hydrogen and the enthalpy of the reaction 'ΔH' at 353K (80°C) are approximated by linear interpolation, table (3-2). Applying equation (3-49) for thermal efficiency

4 The lower heating value; LHV; (also known as net calorific value) of a fuel is defined as the amount of heat released by combusting a specified quantity (initially at 25°C) and returning the temperature of the combustion products to 150°C, which assumes the latent heat of vaporization of water in the reaction products is not recovered. The higher heating value; HHV (also known as gross calorific value or gross energy) of a fuel is defined as the amount of heat released by a specified quantity (initially at 25°C) once it is combusted and the products have returned to a temperature of 25°C, which takes into account the latent heat of vaporization of water in the combustion products.

above, using the interpolated values at 353K (80^oC) from table (3-3); it follows that the maximum thermal efficiency is approximately = ***0.87***.

Hence, from the equation for the thermodynamic efficiency above, it can be concluded that:

$$\Delta G_T = 0.87 \times \Delta H^0 \qquad \textbf{3-50}$$

Gibbs free energy represents the maximum thermodynamic output possible in an electrochemical process. However, in real operation, the actual power output derived from the fuel cell is:

$$\text{Actual electrical power output} = IV_{cell} \qquad \textbf{3-51}$$

To get a value for the electrical efficiency of the fuel cell, the actual output should be compared to the actual input which is the total enthalpy of the reaction, hence:

$$\varepsilon = \frac{\text{Actual electrical power output}}{\bar{m}\,\Delta H^o} = \frac{IV_{cell}}{\bar{m}\,\Delta H^o} \qquad \textbf{3-52}$$

But:

$$I = \bar{m}\,nF \qquad \textbf{3-53}$$

Where '$\bar{m}$' is the molar flow rate of fuel, 'n' is the number of electrons transferred per molecule in the reaction. 'V_{cell}' is the measured cell voltage, hence, from equation (3-50):

$$/\Delta H^o/ = \frac{/\Delta G_T/}{0.87} = \frac{/-nFE^o/}{0.87} \qquad \textbf{3-54}$$

Absolute values of the enthalpy and Gibbs free energy are taken because the negative sign indicates the direction of energy transfer, while absolute numerical values are considered for efficiency calculation.

Substituting equations (3-54) and (3-53) in (3-52) yields the electrical efficiency of the fuel cell:

$$\varepsilon = 0.87\frac{V_{cell}}{E^o} \qquad \textbf{3-55}$$

Where V_{cell} is the measured cell voltage; which is a function of current density, and E^o is the reversible voltage of the fuel cell.

The expression can be interpreted as the maximum theoretical efficiency multiplied by the electrical efficiency; i.e. ($\varepsilon = \varepsilon_{th} \times \varepsilon_e$).

Following the same lines, the electrical efficiency is the ratio of measured electrical output to actual electrical input, which can be written as:

$$\varepsilon_e = \frac{iV_{cell}}{(i + i_{\text{int}})E^o} \qquad \textbf{3-56}$$

Where 'i' is the current density, 'i_{int}' is the cross over current which is assumed to be equivalent to internal currents; both are considered as currents defining the input power together with the theoretical reversible voltage of the fuel cell. From equations (3-56) and the definition of maximum thermal efficiency:

$$\varepsilon = \frac{0.87 \times iV_{cell}}{(i + i_{\text{int}})E^o} \qquad \textbf{3-57}$$

This relationship is plotted in fig (3-13) below:

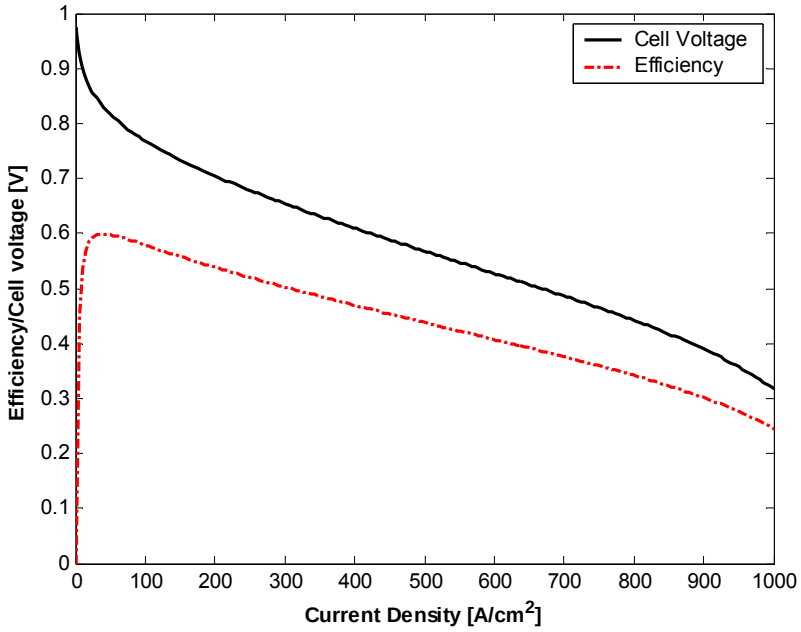

Figure 3-13 Efficiency and cell voltage as functions of current density

It is observed from the figure that, contrary to heat engines, the efficiency of the fuel cell is higher at low fuel flow rates corresponding to low current densities. The efficiency curve follows almost the same shape as the voltage curve; being a function of cell output voltage, hence, efforts should be focused on improving the fuel cell voltage and reducing voltage losses as this would improve the performance of the fuel cell.

Following the conventional definition of efficiency in thermodynamics, another approach for defining the efficiency of the fuel cell is to compare the actual output with the input calorific value, the system efficiency of the fuel cell can be written as:

$$\varepsilon_{fc} = \frac{V_{cell} \times I}{\dot{m}_{H_2} \times \text{Calorific value (LHV)}} \times 100\% \qquad \textbf{3-58}$$

Using the expression for current, for a hydrogen fuel cell:

$$I = \frac{\dot{m}_{H_2}}{M_{H_2}} \times 2F \qquad \textbf{3-59}$$

$$\varepsilon_{fc} = \frac{V_{cell} \times 2F}{M_{H_2} \times \text{Calorific value (LHV)}} \times 100\% \qquad \textbf{3-60}$$

Substituting the values for Faraday's constant, molar mass of hydrogen and the interpolated calorific value for hydrogen, the efficiency of the fuel cell becomes:

$$\varepsilon_{fc} = \frac{V_{cell}}{1.38} \times 100\% \qquad \textbf{3-61}$$

In this work the expression for efficiency based on the calorific value of hydrogen will be used.

Comparing the two expressions for efficiency; equations (3-61) and (3-55); which should be equal, the theoretical open circuit voltage of a pure hydrogen fuel cell can be found as follows:

$$\varepsilon_{fc} = \frac{V_{cell}}{1.38} \times 100\% = 0.87 \frac{V_{cell}}{E^o} \times 100\% \qquad \textbf{3-62}$$

Hence the reversible voltage of the fuel cell assuming the water product is steam at 80^{o}C is:

$$E^o = 0.87 \times 1.37 = 1.20 \text{ V} \qquad \textbf{3-63}$$

This value is close to the value of potential of equilibrium for hydrogen fuel cells which is 1.229 V, which verifies the above method for calculating the efficiency of the fuel cell.

3.8. Fuel Utilisation Efficiency

In actual operation, it is expected that some fuel will pass through the fuel cell and come out unused, this is a significant issue when the outlet end of the fuel cell is open and excess fuel is vented out of the fuel cell, however, if the fuel cell is operated dead ended or in the case where the excess fuel is recirculated or used in another process; such as an after burner for heat generation, fuel utilisation will not be an important issue for the fuel cell. In all cases the final efficiency of the fuel cell has to be multiplied by the fuel utilisation value to calculate the exact efficiency of the fuel cell.

Assuming fuel utilisation efficiency was given the term 'μ', the above expression of efficiency equation (3-57) becomes as follows:

$$\varepsilon = \mu \frac{0.87 \times iV_{cell}}{(i + i_{\text{int}})E^{o}} \qquad \textbf{3-64}$$

3.9. SUMMARY

In this chapter; the theoretical background to PEM fuel cell science is discussed starting with the working principles of PEM fuel cells. A thermodynamic analysis is followed to establish the relationship between current and voltage in relation to other operational and geometric parameters such as pressure, temperature, exchange current density, charge transfer coefficient and gas concentrations in the fuel cell.

For the first time, an analysis based on the polytropic index is used to study the effects of pressure and temperature on fuel cell performance which shows the effects of irreversibility on output voltage of the fuel cell.

A comprehensive expression for the efficiency of the fuel cell; which takes into consideration the actual operating conditions, internal currents, fuel utilisation efficiency and thermal and electrical efficiencies is derived and used to plot the complete curve of efficiency against current density. The equations derived in this chapter are useful in performing parametric studies on fuel cell performances. The graphical representations of the solutions of those equations would help in finding the optimum combination of the design variables for changing operating conditions. They can also be used to formulate a more complex numerical model of the system which can be resolved using computational methods to simulate the fuel cell performance and find avenues for optimisation.

This chapter was very useful in understanding the behaviour of PEM fuel cells under various operating and geometrical conditions. The knowledge and findings acquired in this study will be useful in designing the fuel cell and formulating the mathematical model which will be used for optimisation of the design. Those issues are presented in the following chapters.

Chapter 4 DESIGN OF THE (PEM) FUEL CELL

4.1. INTRODUCTION

The theoretical background necessary to understand the working of a PEM fuel cell was given in the previous chapter. This research aims to investigate the fuel cell technology through the actual making of a working fuel cell and at the same time attempts to reduce the cost of fuel cell manufacturing through simplifying the design and investigating new materials for the various components of the fuel cell.

More than half of the fuel cell cost goes to three major components: The gas distributors, constituting ≈30% of the total cost [71], the electrolyte, which is the protonic conducting membrane which constitutes ≈14% of the total cost and the catalyst layer which also constitutes ≈14% of the total cost. The estimated percentage cost of each of the major components of the fuel cell are shown in the following chart, figure (4-1) [72]:

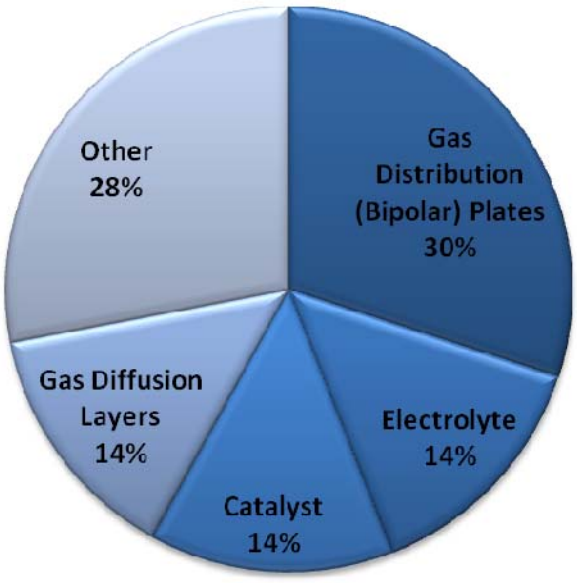

Figure 4-1 Estimated percentage cost of each of the major components of PEM fuel cells based on graphite bipolar plates

The design of the fuel cell plays a major role in determining their cost. It is not only the cost of materials that increases the cost of the fuel cell, but also the manufacturing techniques and the need for skilled technicians for assembling and testing the fuel cell.

The main aim of this research is to design and manufacture a fuel cell at low cost using conventional materials and production techniques, then testing the fuel cell to validate its performance. The following chart describes the design process leading to the production stage of the fuel cell:

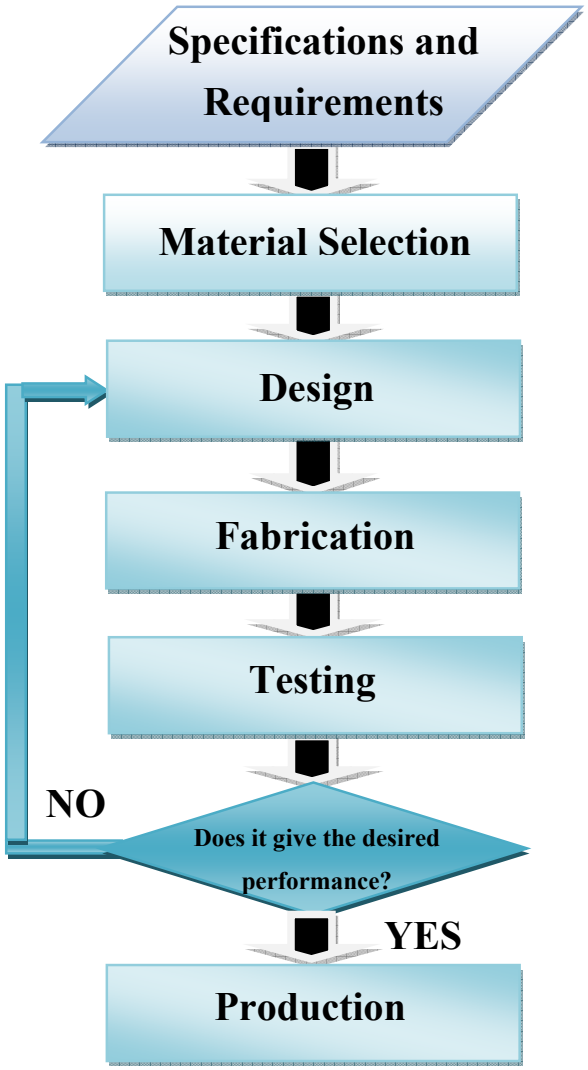

Figure 4-2 Fuel cell design and manufacturing process

4.2. MATERIAL SELECTION

Material selection is a very important step after the specifications have been put forward to meet the requirements of the end user. So as to select the proper materials, a proper understanding of the function and general requirements of the fuel cell components is necessary. A general description of the main components is briefly discussed.

4.2.1. The Electrolyte

The electrolyte is the media where chemical reactions in the fuel cell take place; it should have good proton conductivity because higher protonic conductivity means larger electron flow in the external circuit and hence more current output of the fuel cell. At the same time, the electrolyte should have good chemical and physical properties regarding its manufacturability, cost and fitness for fuel cell application.

One important feature which is desirable in the PEM is the operation at temperatures higher than 100°C. Operation at higher temperatures simplifies the water management problem as the by-product water will come out as vapour which is easy to remove, and the temperature output of the fuel cell will be of a higher grade, which can be better utilised, hence; improving the overall efficiency of the fuel cell.

The most important advantage of operation at a higher temperature is the improvement in the kinetics of the chemical reaction, particularly oxygen reduction at the cathode, which results in a reduction of the catalyst loading on the cathode and hence; a reasonable reduction in the cost of the fuel cell. Another advantage is the reduction of CO poisoning which is reduced at higher temperatures.

The electrolyte commonly used in PEM fuel cells is the poly (perfluorosulfonic acid) copolymer. Those copolymers are based on a sulfonated Teflon backbone. The state of the art is the Nafion® membrane produced by Du Pont plc. These polymers have good chemical and physical properties for use as PEM in fuel cells, however, they are recognized to have some significant technical deficiencies such as reduction in conductivity at low humidity or high temperatures and high cost [9].

In this research, it was attempted to investigate new materials for PEM through the synthesis of new polymer membranes based on Sulfonated Polyimides. However, the focus of the study was directed towards the design aspects of the fuel cell hardware, but understanding of the functions and properties of other components remains important.

4.2.2. The Catalyst Layer

The electrochemical reaction in the fuel cell takes place within the porous catalyst layer at the boundaries of three phases: the gases, the electrolyte and the catalyst surface. The performance of the fuel cell is limited by the electrochemical kinetics of these three components, where the catalyst determines the electrochemical kinetics of the reduction and oxidation reactions, the membrane determines the proton conduction and the gas phase is concerned with mass transport issues.

The catalyst layer has to cater for the three phases at the same time; it has to generate the protons by breaking the bonds between hydrogen particles and then transport them to the surface of the membrane; hence, it should have the same protonic conductivity of the membrane material. It has to transport the electrons to the electrodes; hence, it has to be an electronic conductor, and it has to allow the gases to diffuse through it to reach the active sites in the catalyst layer.

As the oxidation of hydrogen and reduction of oxygen take place on the surface of the catalyst, the catalyst layer should have a large surface area. This does not only improve the reaction, but also reduces the amount of catalyst material used, which is the precious platinum.

Usually the catalyst material is dispersed on the surface of a high surface area carbon material, which helps reduce the amount of platinum used, increases the surface area of the catalyst material and maintains its gas permeability and electronic conductivity. This platinum on carbon is then prepared in the form of an ink by mixing it with a solution of the membrane material, which enhances its bonding to the membrane and makes it protonically conductive, and then it is applied to the membrane surface by means of a brush, spray or a decal method.

4.2.3. Gas Distributors and Electrode Plates

Commonly known as bipolar plates (BPP) and end plates in fuel cell terminology, and are conventionally made of graphite. They constitute a considerable percentage; nearly (30%) of the total estimated cost of the fuel cell and nearly (80%) of the volume when made of graphite [71], this is due to the fact that graphite is fragile and has to have some thickness to provide for the depth of the flow channels and to withstand machining. The gas distributors serve two main tasks:

1. To distribute the gases over the surface of the membrane
2. To work as electrodes that transport the electrons from anode to cathode and connect individual fuel cells in series to form a fuel cell stack with required voltage output.

Conventionally, the plates' material is chosen, machined or treated to satisfy both requirements at the same time. It will generate a good saving in the fuel cell if the functions of the bipolar plates were separated and different materials used to satisfy each requirement separately. For instance, a composite material can be used for the gas distribution and a metallic material for the electrical connection and current transfer.

Furthermore, the cost can be reduced by reducing the number of components. This can be achieved by changing the configuration of the fuel cell.

The common approach is to connect the cells together internally in series using the bipolar plates, this is actually where the term bipolar plate comes from; the cathode of one cell is connected to the anode of the adjacent cell. The number of those plates can be reduced if one compartment was used to supply hydrogen or oxygen to two cells at the same time, in this case the configuration of the fuel cell is changed in such a way; that one gas distributor is used to supply the gas to two anodes or two cathodes at the same time, the configuration of the fuel cell in the conventional design is:(*Anode - Cathode – Anode … etc*.), the proposed configuration is :(*Anode – Anode – Cathode – Cathode ….etc*.).

Further details of this design will be presented in the fuel cell design section of this chapter including a proposed detailed design of a fuel cell module of *0.1 kW* output which constitutes a building block in a larger fuel cell for stationary applications.

The first step in the present design approach is to separate the two tasks of the bipolar plate, namely gas distribution and interconnection of the fuel cells. The second step is to change the internal configuration of the fuel cell to reduce the number of electrode plates and gas distributors used. The details of this design will be discussed in this section together with calculations for the fuel cell module.

The materials for the electrode plates must be selected to satisfy the following requirements:

1. High electric conductivity typically in excess of (100 *Siemens/cm*) [72] to reduce (Ohmic) resistive losses in the fuel cell
2. Low hydrogen permeability ($< 2\times10^{-6} cm^3/cm^2.s$) [72] to reduce power losses resulting from fuel cross-over. .
3. Satisfactory corrosion resistance ($< 16\mu A/cm^2$) [71, 72] (*Data in parentheses represent recent targets for future fuel cells published by the US Department of Energy; DOE*) [72]. Due to the fact that the fuel cell medium is weakly acidic and hence corrosive to most metals. Corrosion does not only lead to the destruction of the corroded material, but also leads to the blockage of active sites in the membrane due to the dissociation of the corroded material and could also lead to the poisoning of the catalyst.
4. Gas distributors and electrode plates are not designed to withstand high forces or to be used as moving components, hence low level of mechanical properties are needed such as: strength, stiffness anddurability.
5. Manufacturability, which contributes to the cost effectiveness of the system.
6. Low cost, so as to lower the cost of the system, which is a main challenge for fuel cell technology.

There are different approaches in the manufacture of electrode plates and gas distributors; the major types of materials used were discussed in the literature review. A brief discussion of the major types of materials used in their fabrication is presented in this chapter:

- ***Graphite Bipolar Plates***

Graphite is the commonly used material for fuel cell bipolar plates due to its high conductivity, corrosion resistance and chemical compatibility. The production of high density graphite plates is a complex process that involves high-temperature treatment which can cause defects in the material such as porosity and cracks. The material has then to be treated with certain resins to reduce its porosity, which causes a decrease in its electrical conductivity.

The flow channels in the graphite plates are usually made by machining with different configurations, which increases the cost depending on the complexity of the topology of the channels. Furthermore, another factor in increasing the cost of the graphite plates is the fact that they are fragile and prone to damage during manufacturing and handling. This compels the designer to select a material of larger thickness so that it can withstand machining stresses and tightening torque in the fuel cell. This also reduces the power density of the fuel cell in terms of kW/m^3. In the first design attempt for this research, graphite was chosen as the material for bipolar plates, figure (4-3).

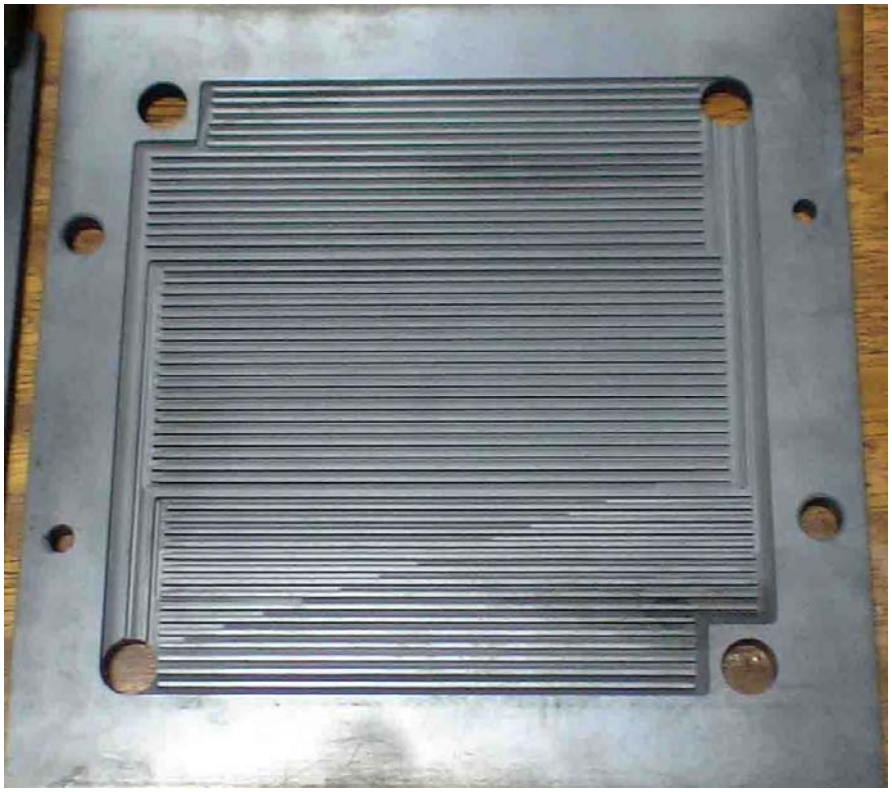

Figure 4-3 A machined graphite plate for use as a bipolar plate, the main four holes at the corners of the flow field are for the inlet and outlet of gases, the large side holes are for the cooling fluid, the small side holes are for guide pins.

Table (4-1) below shows a comparison between stainless steel and graphite for fuel cell applications [73]:

Table 4-1 Comparison of properties between Graphite and SS 316

Property	Graphite	SS-316
Cost ($\$\,kg^{-1}$)	75	7
Density ($g\,cc^{-1}$)	2.25	8.02
Thickness of bipolar plate for same weight (mm)	2.5–4	1
Modulus of elasticity (GPa)	10	193
Tensile strength (MPa)	15.85	515
Corrosion current ($mA\,cm^{-2}$)	<0.01	<0.1
Electrical resistivity ($\Omega\,cm \times 10^{-6}$)	6000	73
Thermal conductivity ($W\,(m\,K)^{-1}$)	23.9	16.3
Permeability ($cm^3\,cm^{-2}\,s$)	Porous 10^{-2} to 10^{-6}	$<10^{-12}$

The graphite material was replaced with stainless steel for the following reasons:

1. The high cost of graphite material, and the added high cost of machining
2. The graphite material is porous; although high density graphite was used it still needed treatment to block the tiny pores.
3. Graphite is bulky and has to be chosen with a certain thickness to withstand machining.

- ***Metallic Bipolar Plate.***

A variety of materials can be used as fuel cell electrodes as they meet the major requirement for good electrical conductivity, but they need to be treated to withstand the corrosive environment of the fuel cell. The treatment could be chemical such as alloying or surface treatment such as coating with a metallic or a non metallic compound; these issues were discussed in more details in chapter 2. It is worth pointing out that the treatment itself is an additional process that adds to the cost, and the material used for coating, be it gold or another material, is another added cost that renders them expensive. The main problem with corrosion is not only the distortion of the material, but because the dissociated metal will react with the catalyst and may block the active sites in the catalyst, it can also contaminate the membrane and reduce its protonic conductivity. Figure (4-4) below depicts a meshed stainless steel SS316 plate produced for this research. The plate was cut on a laser cutting machine from a prefabricated meshed stainless steel sheet acquired from RS Components. Laser cutting has many advantages over mechanical cutting. The heat affected zone in the case of laser cutting is very narrow, hence the probability of material deformation or property loss due to thermal stresses is minimised, furthermore, in laser cutting there is no physical contact between the cutting tool and the material, and hence the probability of contamination is also reduced. High precision and fast cutting control is usually obtained in the laser cutting technique, but the amount of energy consumed in the process is higher than conventional cutting techniques.

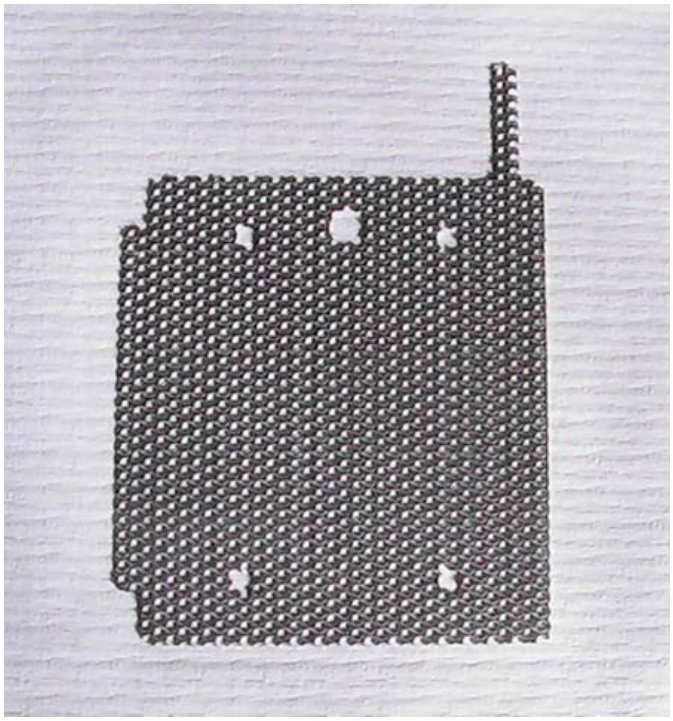

Figure 4-4 Electrode plate fabricated from 0.55 mm thick, 2.5 mm dia. circular hole meshed 316SS stainless steel, the large hole is for gas flow through the membrane, the smaller holes are for guide pins

- ***Composite Plates***

Those are normally plates or gas distributors that are made of polymer resins such as thermosetting and thermoplastic polymers. They are easy to manufacture in mass production by common moulding techniques and can be made electrically conductive using electrically conducting fillers such as graphite or metal powders. Their main advantage is their chemical stability in the fuel cell environment and their relatively low cost, but their electrical conductivity is not as good as metals or graphite, unless excessive conductive fillers are added which weakens their mechanical properties.

For the simplicity of the design and machining purposes, it seems logical to use stainless steel as the material for the electrode plates as they are readily available, they satisfy the conductivity, corrosion resistance, mechanical properties, machinability and cost. The use of stainless steel for fuel cell application has been discussed in more

details in chapter (2). It was reported by Tawfik *et al.* [38] that both austenitic 349TM and ferritic AISI446 stainless steel with high Chromium (Cr) content showed good corrosion resistance and could be suitable for fuel cell application as electrode plates; though AISI446 requires some improvement in contact resistance due to the formation of a surface passive layer of Cr_2O_3. The results revealed that (Tin) coating can offer SS316 stainless steel higher corrosion resistance and electric conductivity than uncoated SS316.

It has been reported by Nikam *et al.* [71] that Low Temperature Carburization (LTC)[9] [74] of stainless steels LTC SS316 exhibited excellent performance for polymer electrolyte membrane fuel cell PEMFC bipolar plate applications. It displayed excellent corrosion resistance in these conditions compared to SS316. The mechanism of anodic dissolution and general corrosion of LTC SS316 was observed to be similar to SS316; however the extent of corrosion in the LTC SS316 was less. The LTC SS 316 showed corrosion currents well below $16A/cm^2$ in anodic and cathodic atmospheres, it was also observed to form a thinner oxide layer as compared to SS316 after 24 hour of potentiostatic testing. Moreover, LTC SS316 lowered the interfacial contact resistance by approximately 24% as compared to SS316 after corrosion testing

For the purpose of this work, non treated SS316 stainless steel meshed plates of various mesh configurations with a thickness of 0.55 mm will be used. The meshed plates were acquired from (RS Components, UK). The use of stainless steel sheet metal offered the design of the fuel cell more advantages such as:

[9] Low-temperature carburization technology hardens the surface of austenitic stainless steels. The process involves activation of the surface followed by a gas-phase treatment, performed at temperatures low enough to avoid the formation of carbides, for a sufficient time to allow carbon diffusion to occur. The result is a hardened conformal case on the treated parts without distortion or change to dimension. The treated case remains austenite (with verified carbon concentrations over 12 atomic percent at the surface) and retains its ductility.

- The plates could be customised according to the design of the particular fuel cell and perforations could be restricted to the active area only.
- Series or parallel connection of the cells could be made externally, giving more flexibility to output customisation.
- Simple to assemble and does not require highly skilled technicians which reduces the cost of manpower.
- More compact than graphite based fuel cells.
- Easier to replace damaged or faulty cells (Maintainability) in the fuel cell stack, or easy replacement of a complete fuel cell module.

4.3. DESIGN SPECIFICATIONS

The first step in delivering a good product lies in putting forward a detailed design specification of the product and its application. A *product design specification* (PDS) is a statement of what the product is intended to do. It's aim is to ensure that the subsequent design and development of a product meets the needs of the user [75]. However, the new product should be as efficient as the conventional fuel cell, with the scope of using the new approach for the advancement of fuel cell science and technology. Following is a presentation of the main design specifications for the proposed experimental fuel cell:

The fuel cell stack is a group of single fuel cells connected in series, the connection can be achieved internally using bipolar plates, or externally by wiring each cell to the adjacent cells by means of electrical conductors.

A single cell is usually sufficient to resemble the behaviour of a fuel cell stack for research purposes, and in this research, a single cell will be used to test the cell configuration and its performance and to perform an experimental parametric study which will be used to optimise the design.

The ultimate target is to design a modular fuel cell that can be mass produced and used to set up a larger fuel cell stack for stationary applications which is capable of

powering a medium sized household. The fuel cell should have the following specifications:

1. The fuel source is pure hydrogen.
2. The oxidant is ambient air.
3. The fuel cell should be of a modular design that can be manipulated to change the current, voltage or power output of the fuel cell stack.
4. The fuel cell should be of a moderate size that can be assembled in different configurations to suit the user.

These specifications raise a number of important questions such as:

- *What should the size of membrane be for such a fuel cell? And what size and number of cells are needed for the stack to produce the desired voltage and power of the fuel cell?*

It was shown in chapter 3 that the power output is a function of the number of cells and active area of the membrane, since the active area determines current and the number of cells determines the Voltage.

It was also shown that fuel cells exhibit higher efficiency at low current densities, in other words, the efficiency is improved when the fuel cell has a larger area or when it is overdesigned in terms of active area. Hence, there should be a compromise between the cross sectional area of the fuel cell and the number of cells.

To produce a realistic working voltage; a large number of cells connected in series will be needed; while the area of the fuel cells is determined by the load. To switch between these two parameters; Voltage and Current, some sort of voltage conditioning will be needed, this dilemma can be resolved by using power conditioning units or voltage transformers, which inevitably add to the cost and complexity of the fuel cell system [76]. Figure (4-5) shows the profile lines for two power ratings of PEM fuel cells, the *x*-axis represents the power density, which reflects the active area of the cell, while the *y*-axis represents the voltage, which reflects the number of cells. A point

on the profile line has to be chosen to satisfy the required power output, and at the same time compromise efficiency and volume issues.

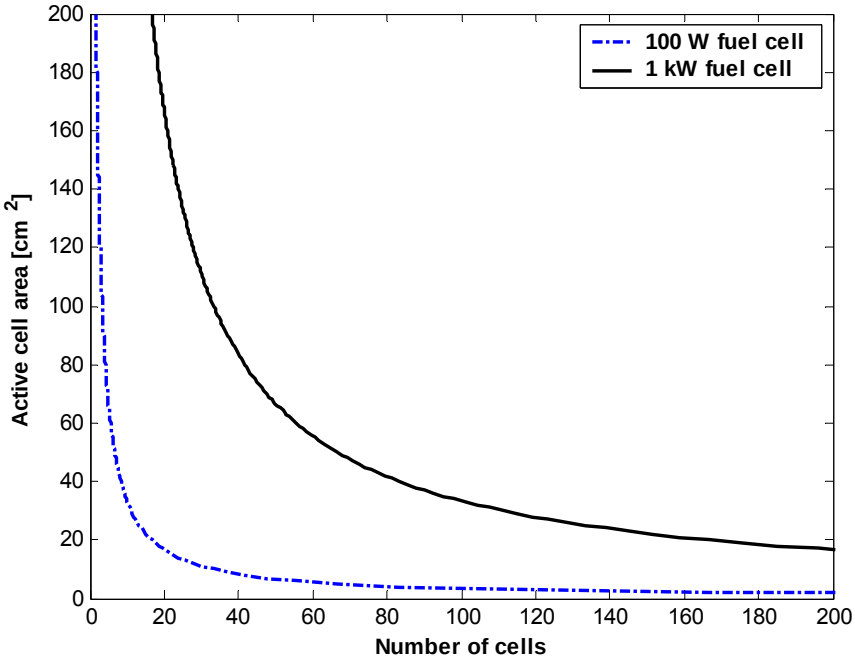

Figure 4-5 A graph of fuel cell area against the number of cells in a 0.1kW and 1 kW fuel cell stacks.

- *What is the heat output rejected by the fuel cell? How is it going to be removed? And what are the prospects of recovering this heat?*

The power output of the fuel cell is the outcome of the reaction between oxygen and hydrogen. This reaction is tamed by the fuel cell; otherwise it takes place in the form of a combustion resulting in all the energy of the reaction being released in the form of heat. Due to the function of the fuel cell, some of this energy is converted to electrical energy, while the rest of the energy is released in the form of heat. Available heat, available thermal and unavailable thermal energies are controlled by the 2nd law of thermodynamics. The grade of heat which is recoverable is a function of temperature. Not all heat can be converted to work, some low grade heat has to be rejected, and in the case of PEM fuel cell, the working temperature is quite low (<100°C), hence the heat

output is low grade heat and wasted energy due to heat output cannot be recovered efficiently, some of this heat is inevitably wasted.

- *How much fuel and oxidant are needed for the fuel cell operation? And how are they going to be supplied?*

Hydrogen fuel has to be supplied to the fuel cell under a specific temperature and pressure. Normally, excess amount of hydrogen is supplied to ensure that the fuel is available everywhere along the surface of the fuel cell. The excess fuel can either be recirculated to the intake line or wasted to the environment. In the first case, where the fuel is recirculated, it is very difficult to redirect the fuel to the supply tank as it is usually under high pressure, and the recirculated fuel has to be pressurised again, which is a costly and complex process. The other alternative, which is releasing the excess fuel to the environment, can cause further problems pertaining to pollution and harmful emissions. The best option is to supply the exact amount of fuel required by the fuel cell, but this option has its drawbacks as the output of the fuel cell will decrease due to concentration losses and gas distribution issues. The scope of this thesis is not concerned with fuelling issues of the fuel cell, but a calculation of the needed supply of fuel and oxidant will be presented as this is necessary for the operation of the fuel cell and for the calculations of the test rig.

- *How much water will be produced by the fuel cell? And how is it going to be managed?*

The only by-products of a fuel cell working on pure hydrogen are water and heat. Both of them can be utilised to increase the advantages of the fuel cell. In the case of fuel cells used in space ships, water by-product was used for drinking; however, there should be a way to remove the excess water from the fuel cell so that it does not cause flooding and blockage in the way of gases. State of the art fuel cells using Nafion® membranes or its derivatives operate at temperatures below 80°C, because operation at higher temperatures causes dehydration of the membrane and loss of protonic conductivity. Operation at such low temperatures causes the product water to be generated mostly as condensate, although some of the water will evaporate, but liquid water will accumulate at the cathode side, and will block the channels preventing the

gases from covering the whole active area of the membrane and also filling the holes of the membrane and gas diffusion electrodes, hence preventing the gases from reaching the active sites on the membrane and catalyst layer. Some of the available options for removing the excess water from the fuel cell will be discussed in due course.

4.3.1. Electrical Output

The most important thing when setting out to design the fuel cell is to decide on the voltage and current of the fuel cell, the main design options here are as follows:

- To design a fuel cell that gives an output voltage equal to the grid voltage (220V in the UK). In this case the area of the fuel cell will be fairly small and a large number of cells (400 cells connected in series as the output working voltage of a single cell is nearly 0.6 V) will be required.
- To design for a larger area (and a smaller number of fuel cells) so as to produce a current higher than the required maximum current. In this case power conditioning will be required to transform the voltage and current to match the requirements.
- To design a group of modular fuel cells of a smaller size, then connect the fuel cells in parallel or in series to obtain the desired output. This option offers additional advantages such as:
    - Flexibility in configuring the fuel cell to various load requirements.
    - Easier to manufacture as the total fuel cell size will be smaller.
    - Easier to replace a faulty fuel cell by replacing a single module instead of replacing or dismantling the complete fuel cell stack.
    - Reduced cost.

Due to the advantages offered by the modular design, the choice is made to design a fuel cell stack module of 0.1 kW. The fuel cell stack module can be used as a

building block to construct a larger fuel cell to match the load and voltage requirements. In the case of household applications, for instance, a group of 60 modules can be used to construct a fuel cell stack of 6kW power output. The output voltage in this case will be 216 V, so it is ideal to use 61 cells to obtain ≈ 220 V which is the grid voltage, otherwise; voltage conditioners can be used to adjust voltage to the required specifications. The fuel cell modules can be arranged in rows and can be accommodated within the wall structure to occupy a limited space.

In the proposed configuration, two adjacent fuel cells are designed to share one gas distributor; this means that the module has to comprise an even number of cells, the proposed number of cells is *6 cells*.

The aim here is to provide the answers for the above questions which are necessary to complete the design and manufacturing of the *fuel cell stack*.

4.3.2. Heat and Reactant Flow

Based on the above characteristics and specifications of the fuel cell stack and its components, the basic assumptions, and calculations of the design can be performed. For domestic applications; load, voltage and size are selected in the light of published results of fuel cell performance [20] and the following guide lines:

- The selected active area of the fuel cell is *7.5 x 7.5 cm^2 = 56.25 cm^2*
- The current density is assumed to be *0.5 A/cm^2 at the design point*.
- The total current output of the cell is *28.13 A (Area × current density)*.
- From Ohm's Law, as *Power = IV*, then the total voltage of the module is:

$$V = {}^{100}\!/_{28.13} = 3.6\ V\ . \qquad \textbf{4-1}$$

- At the design point, assuming the voltage of a single cell is 0.6 volts, hence the number of cells in a stack connected in series is = *3.6/0.6 = 6 cells*.

- Hence the module will be designed to have an active cross sectional area of (*7.5 x7.5 cm^2*) and *6 cells*. The total power output of the module at the design point is *100 W*.

Design parameters and calculations for a *100 W* fuel cell module are presented in table (4-2) below:

Table 4-2 Design parameters and calculations for 100 *W* fuel cell module

Design parameter	*Calculation*	*Value*	*Unit*	Explanation
Number of fuel cells in module	*6*	*6*		First assumption, the number of cells has to be even.
Voltage per cell	*0.6*	*0.6*	*V*	Selected Design Point
Module output voltage	*6 x 0.6*	*3.6*	*V*	
Module output current	*100/3.6*	*≈28.0*	*A*	Current density at the design point is nearly *0.5 A/cm^2* according to most published fuel cell results
Membrane active area	*28 /0.5*	*56*	*cm^2*	Current output divided by the current density (*A/Acm^{-2}*)
Dimensions of the active area	*√56*	*≈7.5*	*cm*	Assuming a square active area of the membrane
Membrane dimensions	*9.5 x 9.5*		*cm^2*	*2 cm* on each side to allow for sealing
Binding plate dimensions	*11.5x11.5*		*cm^2*	*2.0 cm* on each side for binding sealing
Gas distributor thickness	*4mm*			Selected to compromise between compactness and flow characteristics
Total cell area	*11.5 x 13.5*		*cm^2*	To allow for the electrodes and gas supply ports from the large end
Total cell thickness	*5.6*		*cm*	Average cell thickness = *0.5 cm*
Overall fuel cell module dimensions	*5.6* x *11.5*x*13.5*	*869*	*cm^3*	Volume of the module

- ***Oxygen and air flow rate calculations***

To find the amount of reactants needed for the operation of the fuel cell, a relationship that relates the amount of electrical energy transferred per unit substance should be used. This can be derived from Faraday's constant which gives the amount of charge per electron transferred, and Avogadro's number, that gives the number of elements per mole of the same element.

The basic chemical formula of the chemical reaction in the PEMFC gives the molar ratio of each of the reactants; this was stated earlier in chapter one of this report as follows:

$$2H_{2(g)} + O_{2(g)} \rightarrow 2H_2O_{(l)} \qquad \textbf{4-2}$$

In this formula, two moles of Hydrogen react with one mole of Oxygen to produce two moles of water. The electrons transferred per molecule are two electrons in the case of Hydrogen, and four electrons in the case of Oxygen. Based on this information, the amount of charge transferred per mole, and hence, electrical current, are calculated in the following section for the two reactants.

Assuming that 'n_{e^-}' is the number of electrons transferred per mole, hence:

$$\text{Charge} = N_a \times e^- \times n_{e^-} \times \text{ amount of reactant in } moles \qquad \textbf{4-3}$$

Where, 'N_a' is Avogadro's number, which represents the number of entities (molecules) in one mole, and 'e^-' is the charge of an electron in (Coulomb).

But;

$$N_a \times e^- = F \qquad \textbf{4-4}$$

Where: 'F' is Faraday's constant (coulomb/mole), that represents the charge on a mole of electrons, and its value is:

$$\boldsymbol{F} = N_a \times e^- = 6.022 \times 10^{23} \times 1.602 \times 10^{-19} = 96{,}473 \text{ (Coulomb/mole)} \qquad \textbf{4-5}$$

The molar flow rates of oxygen and hydrogen can be found by substituting the proper values of 'n_{e^-}' and multiplying by the number of cells '*c*' as follows:

$$Molar\ flow\ rate\ of\ Oxygen\ =\ \frac{cI}{4F} \qquad \textbf{4-6}$$

And; for hydrogen:

$$Molar\ flow\ rate\ of\ Hydrogen\ =\ \frac{cI}{2F} \qquad \textbf{4-7}$$

To transform the molar flow rate to mass flow rate, we have to divide by the molar mass of each gas, given the symbol '*M*' with the proper subscript, as follows:

$$Mass\ flow\ rate\ of\ Hydrogen\ (\dot{m}_{H_2})\ =\ \frac{cM_{H_2}I}{2F} \qquad \textbf{4-8}$$

$$Mass\ flow\ rate\ of\ Oxygen\ (\dot{m}_{O_2})\ =\ \frac{cM_{O_2}I}{4F} \qquad \textbf{4-9}$$

If the voltage of each cell in the stack is 'V_c', for a stack of 'c' cells, the electrical power output 'P_e' of the fuel cell is given by:

$$Power, P_e = V_c \times I \times c \qquad \textbf{4-10}$$

$$\textbf{So,}\ I = \frac{P_e}{V_c \times c} \qquad \textbf{4-11}$$

This equation can now be used to find the amount of oxygen or hydrogen used in the fuel cell in terms of moles per second, which can easily be converted to units of weight or volume.

- ***Oxygen and Air Flow***

Substituting for current in equations (4-8) from (4-11) above:

$$Mass\ flow\ rate\ of\ Oxygen;\ (\dot{m}_{O_2})\ =\ \frac{M_{O_2}P_e}{4V_cF} \qquad \textbf{4-12}$$

Substituting for the molar mass of oxygen gas (O_2) = 32x10^{-3} (*kg/mole*), and for the power output, number of cells and cell voltage from the table above:

$$Mass\ flow\ rate\ of\ Oxygen\ (\dot{m}_{O_2})\ =\ 1.38\times10^{-5}\ kg/s \qquad \textbf{4-13}$$

But; the molar proportion of Oxygen in atmospheric air is (≈ *0.21)*; hence the amount of air is nearly five fold the amount of oxygen needed, as follows:

$$Mass\ flow\ rate\ of\ Air\ (\dot{m}_{Air}) = \frac{1.38\times10^{-5}}{0.21} = 6.5\times10^{-5}\ kg/s \quad \textbf{4-14}$$

This is, of course, the exact amount of air needed, but in practice it has to be a little higher by a factor of stoichiometry which is used to ensure that an adequate amount of oxygen is available in the fuel cell.

To find the volumetric flow rate of air, the mass flow rate is divided by the density and multiplied by time to give the flow rate per hour; hence:

$$Volumetric\ flow\ rate\ of\ Air = \frac{6.5\times10^{-5}kg/s\times3600\ s/hour}{1.2\ kg/m^3} \approx 0.20\ m^3/hour \quad \textbf{4-15}$$

This gives the required amount of air to run a *100W* fuel cell module.

- ***Hydrogen Flow***

Following the same lines, substituting for current in equations (4.7) from (4.11) above:

$$Mass\ flow\ rate\ of\ Hydrogen\ (\dot{m}_{H_2}) = \frac{M_{H_2}P_e}{2V_cF} \quad \textbf{4-16}$$

Substituting for the molar mass of Hydrogen gas $(H_{2(g)}) = 2.02\times10^{-3}$ (*kg/mole*), and for the power output, number of cells and cell voltage from the table above:

$$Mass\ flow\ rate\ of\ Hydrogen\ (\dot{m}_{H_2}) = 1.74\times10^{-6}\ kg/s \quad \textbf{4-17}$$

Dividing by the density of hydrogen; 0.084 kg.m^{-3} and multiplying by 3600 to transform to a volumetric flow rate per hour gives:

$$Volumetric\ flow-rate\ of\ Hydrogen = \frac{1.74\times10^{-6}(kg/s)\times3600(s/hr)}{0.084(kg/m^3)} = 0.075\ m^3/hour \quad \textbf{4-18}$$

- ***Water Production***

Water is produced at the rate of one mole for every two electrons, so following the same lines as in equation (4.12):

$$Rate\ of\ water\ production\ (\dot{m}_{H_2O}) = \frac{M_{H_2O}P_e}{2V_cF} \qquad \textbf{4-19}$$

Substituting for the molecular mass of Water, $M_{H_2O} = 18.02\times10^{-3}$ $(kg.mole^{-1})$ and for the power output, number of cells and cell voltage from the table above:

$$\text{Rate of water production } (\dot{m}_{H_2O}) \approx 1.6\times10^{-5} \text{ kg/s} \qquad \textbf{4-20}$$

$$\text{Hourly rate of water production} = 0.056 \text{ kg/hour} \approx 0.056\ l/hour \qquad \textbf{4-21}$$

- ***Heat Production***

Heat production in the fuel cell depends on the load applied to the fuel cell which determines the flow rate of fuel and hence the electrical and thermal outputs of the fuel cell. Voltage of the fuel cell, as shown previously, is also a function of the fuel flow rate which determines the current.

It is possible here to calculate the maximum heat output of the fuel cell when it is operating at its full power output.

The efficiency of the fuel cell was derived in chapter three, and was found to be:

$$\varepsilon_{fc} = \mu\frac{V_{cell}}{1.38}\times100\% \qquad \textbf{4-22}$$

The cell voltage depends on the current and fuel flow rate, but for this calculation, the design point voltage of a single cell was assumed to be '*0.6 volts'*.

Hence, efficiency of the fuel cell, assuming a fuel utilisation efficiency of 100%, is:

$$\varepsilon_{fc} = \frac{0.6}{1.38} = 0.435 \qquad \textbf{4-23}$$

Hence;

$$Heat\ output\ of\ the\ fuel\ cell = (1-\varepsilon_{fc}) \times \dot{m}_{H_2} \times CV_{H_2} \quad \textbf{4-24}$$

Where 'CV_{H_2}' is the calorific value of hydrogen gas which is ($\approx 132 \times 10^6$ J/kg)

$$Heat\ output\ of\ the\ fuel\ cell\ = (1-0.435) \times 1.74 \times 10^{-6} \times 132 \times 10^6 = 130\ (W) \quad \textbf{4-25}$$

4.3.3. The Cooling System

Overheating of the fuel cell can lead to the evaporation of the water content of the membrane, consequently reducing its protonic conductivity. Unlike heat engines, which reject a great amount of their waste heat with the exhaust, all of the excess heat produced by the fuel cell has to be removed by the cooling system to maintain the fuel cell temperature at its optimum operating temperature. Furthermore, the temperature difference between the power-plant (which is the fuel cell) and the surroundings is much smaller when compared to heat engines, which makes heat rejection more difficult. In addition to this, the fuel cell power output and working life are greatly dependant on its operating temperature; so it is imperative to design an efficient cooling system for the fuel cell and to provide proper control of the system which should be coupled to the control system of the fuel cell as the amount of hear produced is a function of the output of the fuel cell. The control issues of the fuel cell are the subject matter of a parallel research work and will not be dealt with in the context of this thesis.

- ***Cooling Options***

  The available cooling options are as follows:

  1. *Evaporative air cooling*. In this method of cooling, the water product of the fuel cell is forced to evaporate carrying part of the heat output of the fuel cell with it, or collected and used to cool the inlet air used for cooling the fuel cell through evaporation.
  2. *Natural or forced air cooling*: air in this case is circulated in separate channels where it does not mix with the reactant air, and hence does not carry any water by-product with it. This is to ensure that the humidity of the membrane is retained. Excess water can be removed by increasing the

reactant air flow, but this has to be properly calculated and controlled to ensure that the air flow does not reduce the water content of the membrane.

3. *Water cooling*: this option is similar to air cooling, where cooling water will be flowing in cooling channels external to the gas distributors. Water cooling could be more efficient than air cooling because the specific capacity of water is more than that of air, hence less water will be circulated compared to air, but this increases the complexity of the system as more sealing and a circulation pump will be needed.
4. *Absorption cycle cooling*: in this case a separate absorption cycle will be installed, where a cooling gas such as ammonium will be used in an absorption cycle, this option is good for recovering part of the rejected heat of the fuel cell, as it can be used for cooling in an air-conditioning unit, or for heating in a heat pump.

For simplicity, the air cooling system will be considered for our application.

The thermal output and water product of the fuel cell are both generated at the cathode. At the same time, air is needed at the cathode for the cathodic reaction. It is very convenient to pump an extra amount of air at the cathode to remove the water product and a small amount of the excess heat at the same time, but the quality of the air should be controlled in such a way to maintain nearly 100 % relative humidity (*RH*) in the membrane. The remaining heat has to be removed utilising a stream of air in a separate channel, this channel is adjacent to the cathode side of the fuel cell.

In the present configuration, the cathodes of two cells are adjacent, hence the cooling channel can be placed in between each two cathodes in the fuel cell, this has the advantage of reducing the number of cooling channels and hence; the number of components needed to construct the fuel cell. The details of this design will be presented in this chapter.

In the following calculation, the amount of air required and the humidity of this air are calculated. The following table presents a summary of the inputs and outputs of the fuel cell calculated in the previous section:

Table 4-3 A summary of the inputs and outputs of the 100 *W* Fuel Cell Module

Basic Inputs and outputs	Value for the fuel cell stack module	Value /single cell	Unit
Air flow	6.5×10^{-5}	1.17×10^{-5}	*kg/s*
Volumetric air flow rate	*0.20*	*0.03*	m^3/hr
Hydrogen flow	1.74×10^{-6}	0.29×10^{-6}	*kg/s*
Water product	1.6×10^{-5}	0.27×10^{-5}	*kg/s*
Heat output	*130*	*21.7*	*W*

The excess heat of the fuel cell and the water product are both generated at the cathode, the water product will be removed by the reaction air together with an amount of heat which is needed to evaporate the water output.

The amount of heat consumed in evaporating the product water is:

$$Q_{wr} = \dot{m}_w L_w \qquad \textbf{4-26}$$

Where 'Q_{wr}'is the amount of heat needed for the removal of water, '$\dot{m}_w$' is the rate of production of water at the cathode, and 'L_w' is the latent heat of water which is *2.26 MJ/kg*.

Applying the equation to the present situation gives:

$$Q_{wr} = 1.6\times10^{-5}\ \text{kg/s}\times 2.26\times10^{6} J/kg = 36.16\ \text{W} \qquad \textbf{4-27}$$

Assuming the fuel cell is operated at full power, the heat remaining in the fuel cell is:

$$Q_{remain} = 130.0W - 36.16W = 93.84\ \text{W} \qquad \textbf{4-28}$$

This amount of heat is to be removed by the cooling fluid.

The two problems of cooling and maintenance of humidity in the membrane are inter-related, and have to be tackled together. The ideal case would be to use the reaction air in the fuel cell to remove the excess heat and the excess water product of the fuel cell at the same time, but the problem in this case is that the amount of air needed

for cooling is many times greater than the amount of air needed for the reaction; this air will carry with it the excess heat of the fuel cell, which will increase its capacity to carry more water from the membrane, in fact; the water carrying capacity of air flow will increase by a factor of five when it is heated from ambient temperature to 353K (80°C) which is the maximum operating temperature of the fuel cell.

- ***Configuration of the Cooling Channels***

The calculations for matching a proper flow rate of reaction air at a specific temperature and humidity ratio that would be able to carry the exact amount of water product and maintain the temperature of the fuel cell near the 353K (80 °C) were performed by the author. It was concluded that this cannot be achieved (unless operation was at lower temperatures < 303K (30 °C).

The solution to this problem is to use two separate channels for reaction air and coolant flow. The cooling channels could be open to the atmosphere from both ends, and a blower or fan is used to drive the required amount of air for cooling, or they can be closed and in this case they can be used for water or air cooling; this configuration has the following advantages:

- The cooling channels can be pressurised if a pump is used in the case of water cooling.
- Other fluids or mixtures can be used for cooling such as (anti-freeze solutions).
- They can be configured in a parallel flow or serpentine flow shape to guarantee a better distribution of temperature in the fuel cell. Modelling techniques such as CFD can be used to optimise the flow configuration.

In this work, air cooling through an open channel is considered and calculations are presented below. The temperature at the surface of the membrane electrode assembly, should not exceed 353K (80°C) to protect the membrane from damage due to glass transition which occurs at 353 – 393 K in the case of Nafion membranes.

- ***Heat Transfer Calculations***

According to studies performed by Khandelwal *et al.* [77], the temperature drop in the gas diffusion layers and catalyst layers was found to be less than (2°C) when Toray® Carbon Paper was used as the diffusion media at (1 A/cm^2) current density. Figure (4-6) below is the temperature profile in the fuel cell components for two different current densities of 0.1 and 1A/cm^2 with SIGRACET® and Toray® carbon paper diffusion media. For a 200 µm thick diffusion media, 5 wt.% PTFE content SIGRACET® has an almost 3–4°C drop in the diffusion media as compared to (1–2 °C) temperature drop in Toray® carbon paper for current density =1 A/cm^2 [77].

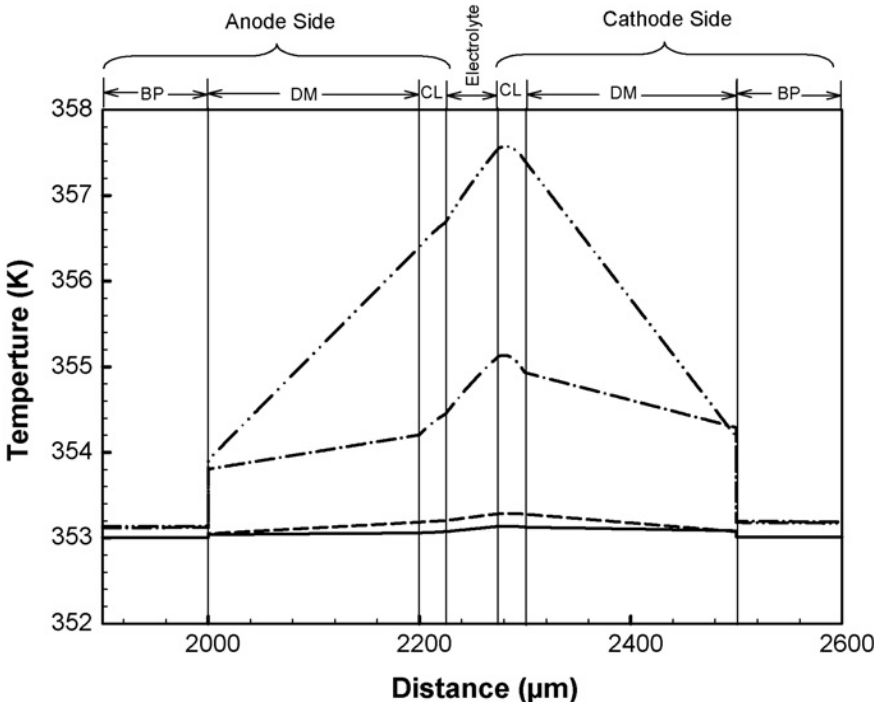

Figure 4-6 Estimated temperature drop in fuel cell components for current density *i* = 0.1 and 1.0 Acm^{-2} for Toray® carbon paper and SIGRACET® 5% PTFE as the diffusion media. (—) *i* =0.1 A/cm^2 (Toray), (– – –) *i* =1.0 A/cm^2 (Toray®), (– – –) *i* =0.1 A/cm^2 (SIGRACET®); (–· · –· · –) *i*=1.0 A/cm^2 (SIGRACET®). *CL*: Catalyst layer, *DM*: Diffusion media and *BP* is Bipolar Plate [77].

Furthermore, figure (4-6) indicates that an amount of heat will be transferred by conduction through the MEA to the anode side of the fuel cell, but this amount is much less than the amount of heat which is transferred to the cathode components due to the low thermal conductivity of the membrane which stands like a barrier between the anode and cathode sides.

In the present design a single cooling channel will provide cooling for two fuel cells at the same time, figure (4-7) represents the flow of heat in the cathode of one fuel cell. The temperature flow in the fuel cell components is represented by the profile line from *T1* to *T5*.

Heat transfer by conduction occurs in the stainless steel plates; *T1* to *T2* and *T3* to *T4,* while heat transfer by convection occurs in the air channels; *T2* to *T3* and *T4* to *T5*. An overall coefficient of heat transfer has to be determined to calculate the heat flux and the temperature gradient (*T5-T1*).

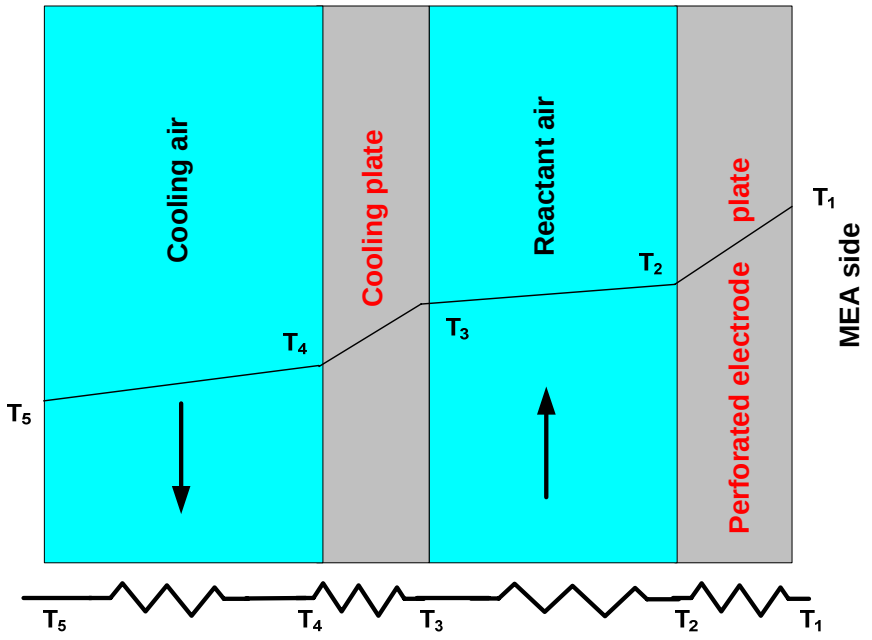

Figure 4-7 Schematic of the heat flux in the fuel cell cathode (Not to scale)

For *conduction through a solid surface*, the rate of heat flow is obtained from Fourier's law [78]:

$$\dot{Q} = kA\frac{\Delta T}{x} \qquad \textbf{4-29}$$

Where '*A'* is the cross-sectional surface area, 'ΔT' is the temperature difference between the two surfaces; '*x'* is the thickness of the medium and '*k'* is the thermal conductivity of the medium.

Applying this equation to the stainless steel plates, using the subscripts '*ss'* to denote the stainless steel, gives:

$$\Delta T = \frac{\dot{Q}x_{ss}}{kA} \qquad \textbf{4-30}$$

The coefficient of heat convection for air has to be evaluated using Newton's law for convection in a fluid:

$$\dot{Q} = h_p A(T_p - T_a) \qquad \textbf{4-31}$$

Where 'T_p' is the temperature of the plate; 'T_a' is the temperature of the air flow and 'h_p' is the heat transfer coefficient of the plate. Solving this equation for the temperature difference gives:

$$\Delta T = \frac{\dot{Q}}{h_p A} \qquad \textbf{4-32}$$

The heat transfer coefficient of the plate 'h_p' is related to *Nusselt number* by the equation:

$$h_p = \frac{k}{L}Nu \qquad \textbf{4-33}$$

Where '*k'* is the thermal conductivity of the fluid, air in this case, '*L'* is the length of the plate and '*Nu*' is *Nusselt Number* which can be given as an average by the following equation [78]:

$$Nu = 0.664 \times (\mathrm{Pr})^{1/3} \sqrt{\mathrm{Re}} \qquad \textbf{4-34}$$

This equation is applicable in the case of laminar flow only; where, '*Pr'* is *Prandtl number* for the fluid at the given temperature which can be looked up from tables; '*Re'* is *Reynold's number* for the flow which can be calculated from physical data and materials property tables.

An essential first step in the treatment of any convection problem is to determine whether the boundary layer is laminar or turbulent. Surface friction and the convection transfer rate depend strongly on which of these conditions exist [78]. Although it is desirable to have turbulent flow of the cooling air and reactant air in the fuel cell as this enhances the transfer of momentum, energy and species and improves mixing in the airstream due to the highly irregular velocity fluctuations, but the low flow rate of reactant air and the relatively small amount of heat flux in the fuel cell prevent the flow from reaching the critical Reynold's number at which transition occurs from laminar to turbulent. Thus, in all our calculations, the flow is assumed to be laminar.

In calculating boundary layer behaviour it is frequently reasonable to assume that transition begins at some location (*x)* from the leading edge of the plate. The critical Reynold's Number is the value of Re_x for which transition begins, and for flow over a flat plate, it is known that ($100{,}000 < Re_x < 3000{,}000$) depending on surface roughness and turbulence level of the free stream, a representative value of Reynold's number is ($Re_x = 500{,}000$) [77] which will be assumed in the present calculation.

From equations (4-33) and (4-34) the heat transfer coefficient for the convective flow of air can be estimated as follows:

$$h_p = 0.664 \times (\mathrm{Pr})^{1/3} \sqrt{\mathrm{Re}} \frac{k}{L} \qquad \textbf{4-35}$$

Using the proper values of the coefficients and numbers in the equation, the value of the heat transfer coefficient of the plate 'h_p' can be estimated as in table (4-4):

Table 4-4 Values of coefficients and calculated value of the convective heat transfer coefficient according to equation (4-35).

Pr	***Re***	***k [W/m.K]***	***L [m]***	***h_p [W/m2.K]***
0.71	500 000	0.024	0.090	1117

Assuming the temperature is constant along the channel, and considering an intermediate temperature of 323K (50°C) along the air channels. It is also assumed that the stainless steel plates are solid plates; hence, the overall heat transfer coefficient can be approximated.

Considering the overall temperature difference, denoted by the note subscript:

$$\Delta T_o = (T_1 - T_5) = (T_5 - T_4) + (T_4 - T_3) + (T_3 - T_2) + (T_2 - T_1) \quad \textbf{4-36}$$

Substituting for the temperature differences of each medium, using the subscripts (*ss)* for stainless steel plates, (*p)* for plate and (*a)* for air gives the following equations:

$$\Delta T_o = \frac{\dot{Q}}{A}\left\{\frac{x_{SS}}{k_{SS}} + \frac{1}{h_p} + \frac{x_{SS}}{k_{SS}} + \frac{1}{h_p}\right\} = \frac{2\dot{Q}}{A}\left\{\frac{x_{SS}}{k_{SS}} + \frac{1}{h_p}\right\} \quad \textbf{4-37}$$

Solving for the heat flow gives:

$$\dot{Q} = \frac{\Delta T_o A}{2\left\{\frac{x_{SS}}{k_{SS}} + \frac{1}{h_p}\right\}} \quad \textbf{4-38}$$

This expression compares to the general form of heat transfer equation:

$$\dot{Q} = \Delta T_o A U_o \quad \textbf{4-39}$$

Where 'U_o' is the overall heat transfer coefficient which can be expressed as:

$$U_o = \frac{1}{\left\{\frac{2x_{SS}}{k_{SS}} + \frac{2}{h_p}\right\}} \quad \textbf{4-40}$$

Substituting the following values for the constants in this expression the value of 'U_o' can be estimated as in table (4-5) as follows:

Table 4-5 Values of coefficients and resultant value for the calculation of the overall heat transfer coefficient according to equation (4-40)

$x_{SS}\,[m]$	$k_{SS}\,[W/m.K]$	$h_p\,[W/m^2.K]$	$U_o\,[W/m^2.K]$
0.55×10^{-3}	20	1117	541.85

To calculate the temperature of the cooling fluid we need to define the heat flux; '$Q^{"}$', in the fuel cell, which is the rate of heat transfer per unit area defined as:

$$Q^{"} = \frac{\dot{Q}}{A} \qquad \textbf{4-41}$$

Hence

$$Q^{"} = U_o \Delta T_o \qquad \textbf{4-42}$$

The amount of heat generated by a single fuel cell was calculated in equation (4-28). It is assumed that part of this heat will diffuse through the membrane to the anode side, as shown in figure (4-7) and a smaller amount will be conducted to the surrounding environment through the sides of the electrode plates and cooling plates. It is a fair assumption to consider one third of the heat produced by the fuel cell is conducted directly to the surroundings and the anode side, while two thirds are transferred to the cooling air through conduction and convection. Hence, the amount of heat to be removed by the cooling fluid is ≈ (62.56W).

Heat flux from equation (4-41) is

$$Q^{"} = \frac{\dot{Q}}{A} = \frac{62.56(W)}{45\times10^{-4}(m^2)} = 1.39\times10^{4}(W/m^2) \qquad \textbf{4-43}$$

Using equation (4-43) and the value of the overall heat transfer coefficient from table (4-3), the temperature gradient between the cooling air flow and the cathode side of the membrane can be calculated as follows:

$$\Delta T_o = \frac{Q^{"}}{U_o} = \frac{1.39\times10^4 (W/m^2)}{541.85(W/m^2.K)} = 25.66\ K \qquad \textbf{4-44}$$

Hence the temperature of air in the cooling channel is nearly 26°C less than the temperature at the surface of the membrane at the cathode side; hence, air temperature in the cooling channel is:

$$\textit{Air temperature in the cooling channel} = 80 - 26 = 54\ ^oC \qquad \textbf{4-45}$$

The amount of air required to remove the excess heat can now be calculated, assuming constant pressure conditions, the change in the specific enthalpy of dry air can be expressed as:

$$\Delta h_a = c_p \Delta T \qquad \textbf{4-46}$$

Where 'c_p' is the specific heat capacity of air at constant pressure (kJ/kg°C) and 'ΔT' is the temperature difference between the cooling air and the temperature in the cooling channel in (K).

From tables of physical properties, the specific heat capacity for air at room temperature; 'c_p' is *1.006 kJ/kg°C*, hence the amount of heat that can be carried by a certain amount of airflow per second, '*q'*, can be calculated using the following formula:

$$q = \dot{m} c_p \Delta T \qquad \textbf{4-47}$$

Where '$\dot{m}$' is the mass flow rate of the cooling air, which can be estimated as follows:

$$\dot{m} = \frac{q}{c_p \Delta T} = \frac{62.56(J/s)}{1006(J/kg.K)\times 24(K)} = 0.0026(kg/s) \qquad \textbf{4-48}$$

This is the air flow rate necessary for cooling a single fuel cell. For a module of 6 cells the air flow rate will be = *0.0155 kg/s*.

Hence;

$$Volumetric\ flow\ rate\ of\ Air\ = \frac{0.0155 kg/s}{1.2\ kg/m^3} \approx 0.013\ m^3/s \qquad \textbf{4-49}$$

Taking into consideration that *1 m^3/s of air is equivalent to 2118 ft^3/min (cfm);* the amount of air needed to cool the fuel cell module is *27.4 cfm*, which can be provided by an electric fan, such a fan will consume less than *2W* of the fuel cell power which is nearly 2% of the total power output.

4.4. Fuel Cell Design Details and Drawings

On the basis of the previously presented calculations and design specifications, the *100 W* fuel cell module has 6 cells which are operated in an individual manner, where each cell is supplied with hydrogen and reactant from the main manifold directly. The module plugs in place like a socket and can easily be removed if need arises for maintenance or replacement.

4.4.1. The MEA

The fuel cell is based on a 9.5 x 9.5 cm^2 Nafion® 117 membrane acquired from Ion Power Inc. The active area of the membrane is covered with 0.3 mg/cm^2 Platinum catalyst layer on each side; the active area of the membrane is 7.5 x 7.5 cm^2.

The active area is also covered with gas diffusion electrodes; Toray® paper GDL, of thickness 200μm on each side, the thickness of the membrane is 2 mil which is equivalent to 178μm, while the thickness of the catalyst layer on each side of the membrane is 100 μm, hence, making the total thickness of the membrane at the active area 0.778 mm.

The membrane is prepared as shown in the drawing figure (4-8) and has four holes at the corners spaced at 85 mm with a diameter of 3 mm each to facilitate assembly and proper positioning of the membrane with respect to other components.

4.4.2. The Electrodes

The membrane is embraced in between two perforated stainless steel electrodes, as shown in figure (4-9). The SS316 stainless steel is prefabricated in the meshed form, and cut to the right size and dimensions using a computerised laser cutting machine (Available at Coventry university workshop). In mass production, only the active area needs to be meshed while the rest is left solid. The non-active area of the membrane is sealed using 0.2 mm thick silicone rubber, which also has the guide pin holes in the same dimensions.

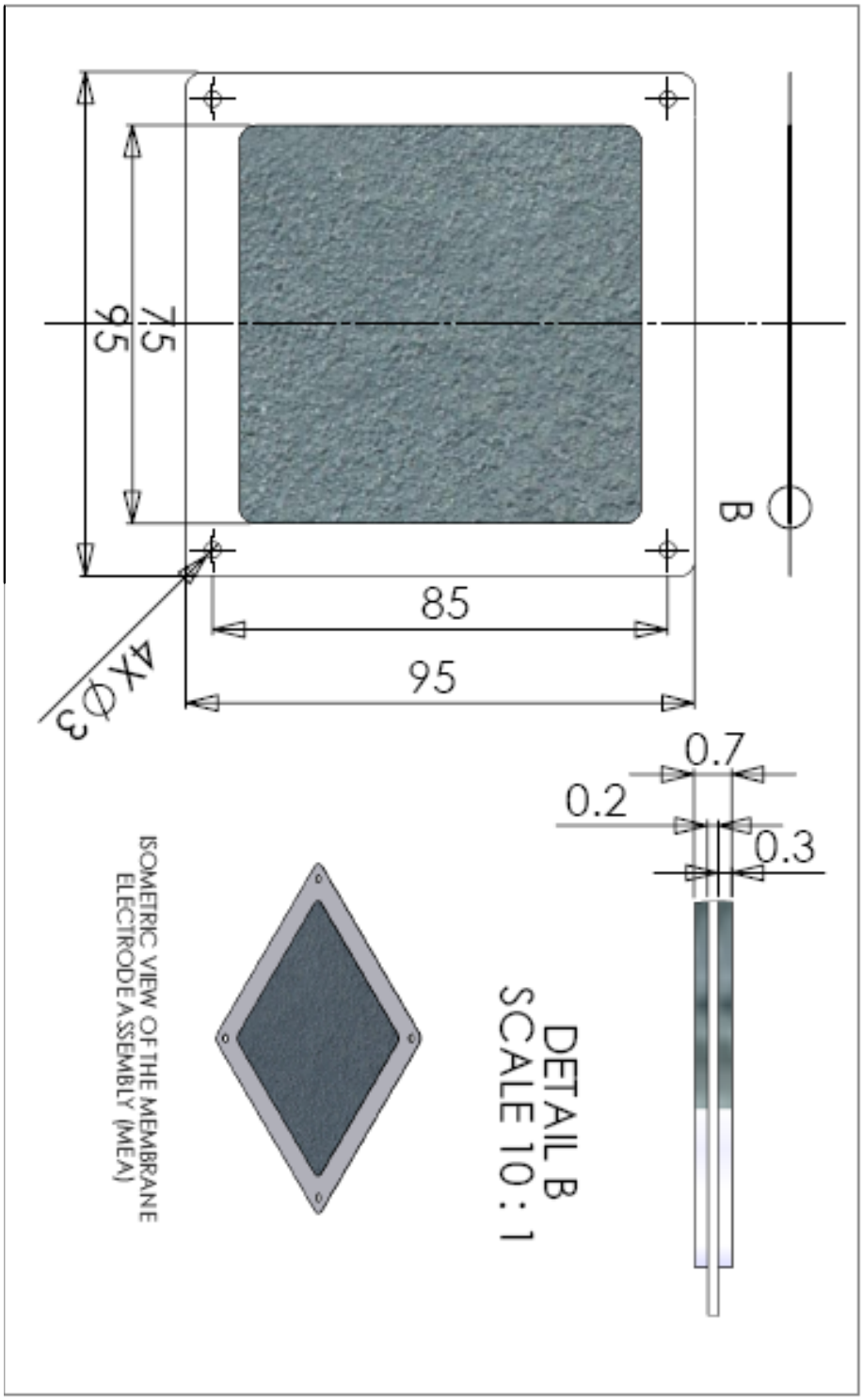

Figure 4-8 Drawing of the membrane electrode assembly (MEA)

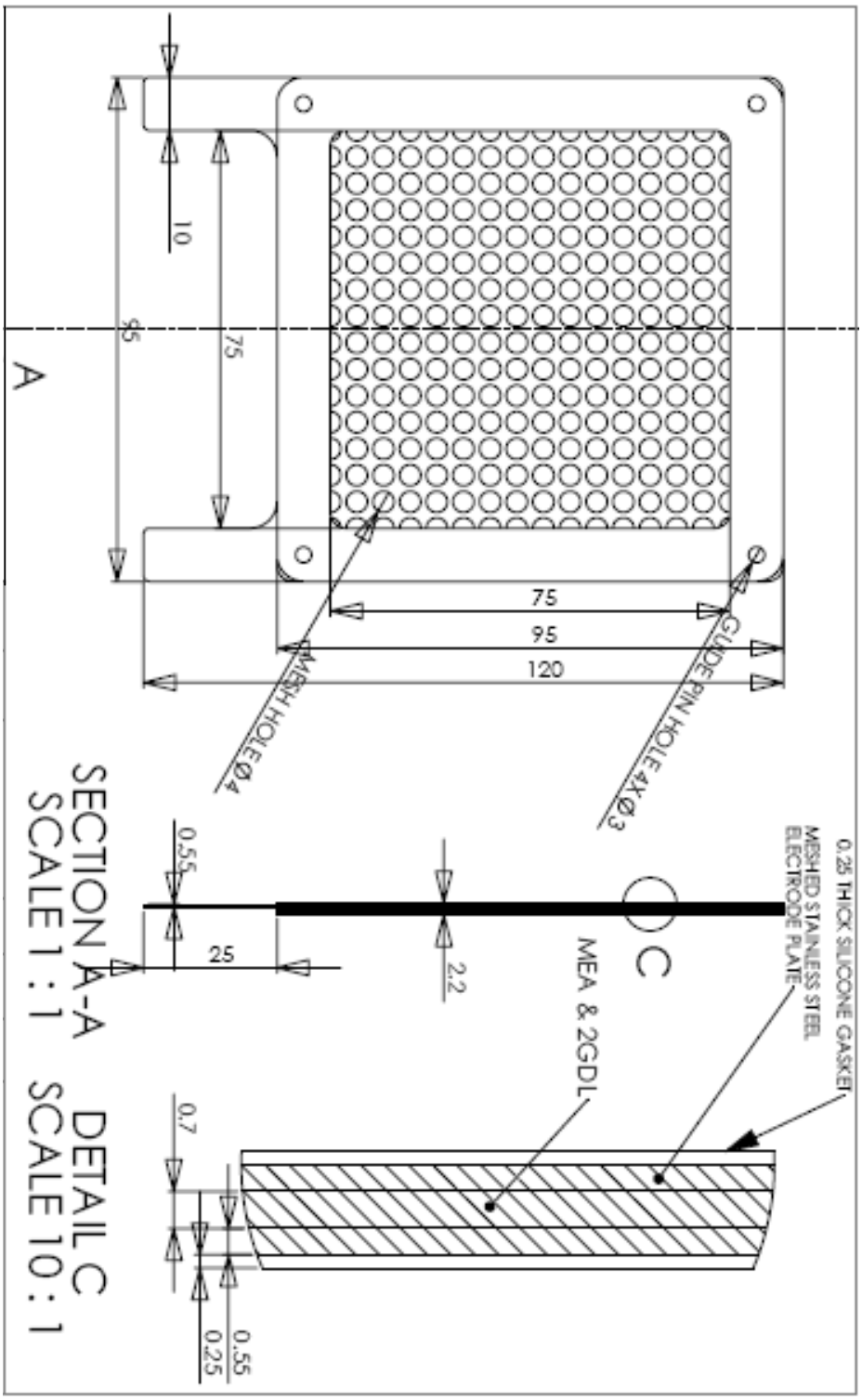

Figure 4-9 Membrane and stainless steel electrodes

4.4.3. The Trough (Gas Distributor)

One very important component in the proposed approach is the trough, which is the gas distributor. It is made of composite material, such as Polyurethane or any suitable composite, to be able to withstand temperatures up to the working temperature of the fuel cell.

As shown in figure (4-10), the trough is cut to the exact size of the membrane except for the gas inlet and outlet which are designed to tightly fit to the gas supply manifold when the fuel cell is plugged in place. The trough has a total of 8 M6 holes arranged at the corners and the middle of each side to facilitate tightening of the fuel cells in the stack module. Four M3 holes are equally spaced at the corners with the same location as on the membranes and electrode plates for the guide pins to facilitate easy assembly of the fuel cell module.

The gas ports are offset by 35 mm sideways to facilitate more efficient distribution of the reactant gases on the surface of the membrane. The trough is 4 mm thick; this dimension was chosen to provide enough thickness for the gas ports but at the same time without compromising the compactness of the fuel cell module.

The anode trough is exactly identical to the cathode trough, but only rotated by 180°. This simplifies the design and reduces the cost of manufacturing.

The electrodes and membrane assembly are sandwiched between two troughs to constitute a single fuel cell, as shown in the drawing, figure (4-11). If only one cell is required, then the external sides of the troughs can be sealed and blanked using two end covers, the end covers are shown in figure (4-12).

It is much better to use two fuel cells instead of one in the current arrangement, figure (4-13), because the same anode trough can be used to supply two membranes with hydrogen at the same time. The external sides of the fuel cell will be cathodes in this case, which makes it easier to cool the fuel cell as most of the heat output is generated at the cathode.

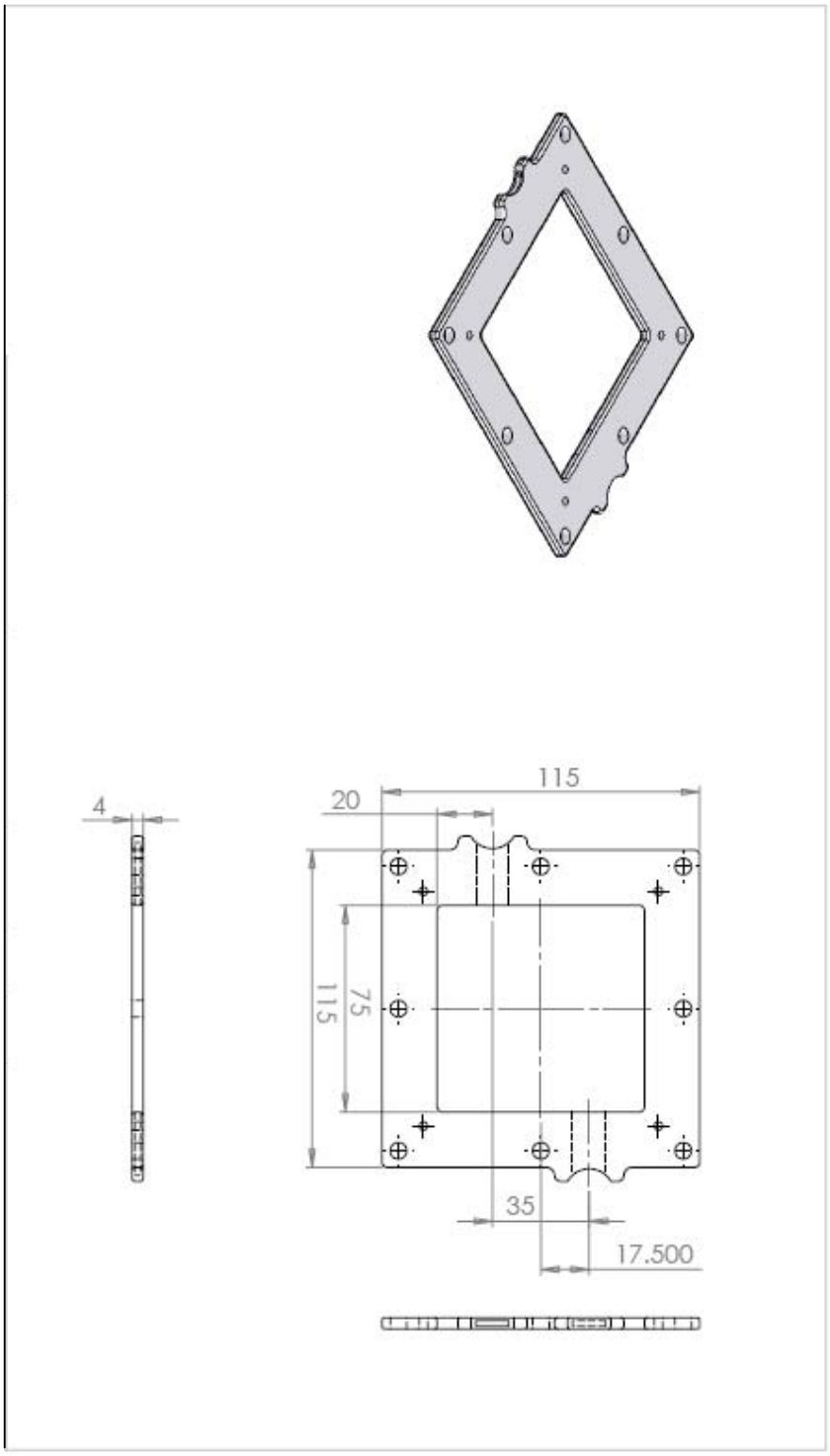

Figure 4-10 The trough or gas distributor

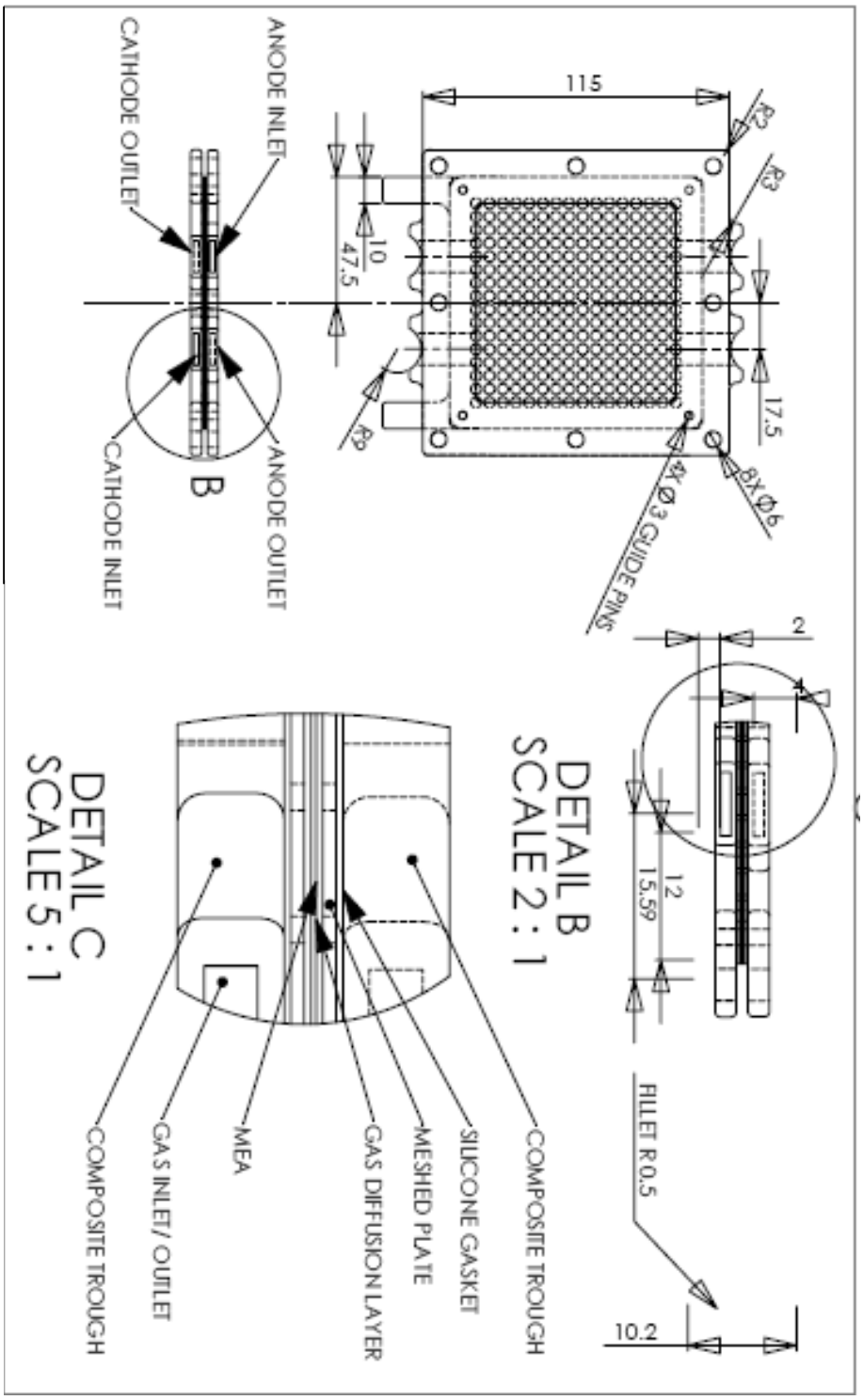

Figure 4-11 Single cell embraced in between two troughs

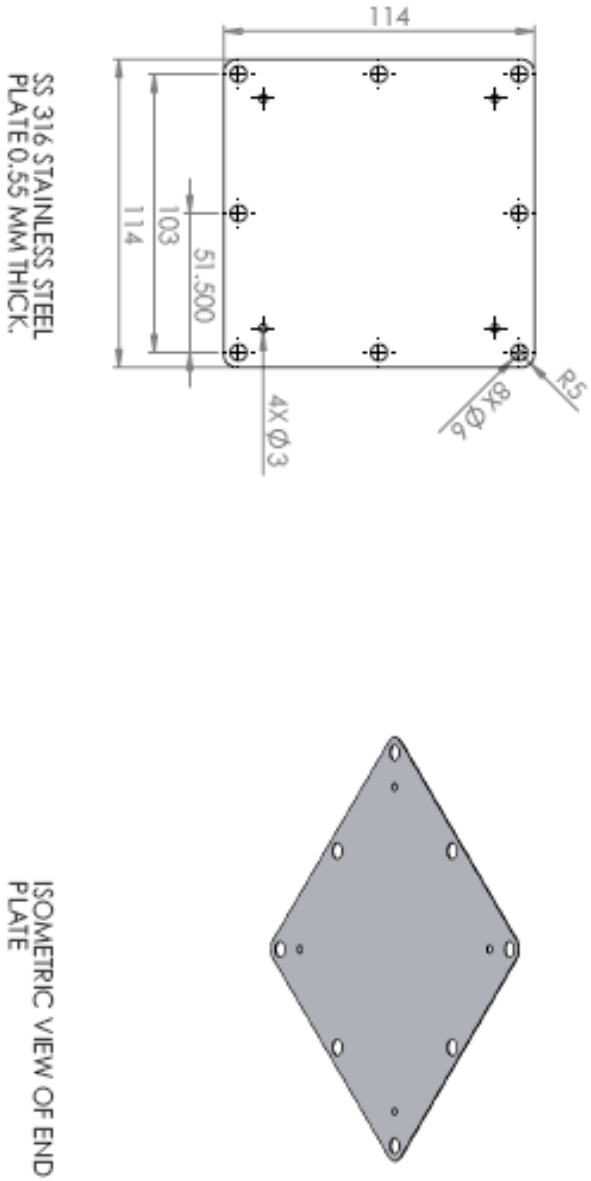

Figure 4-12 End Plate

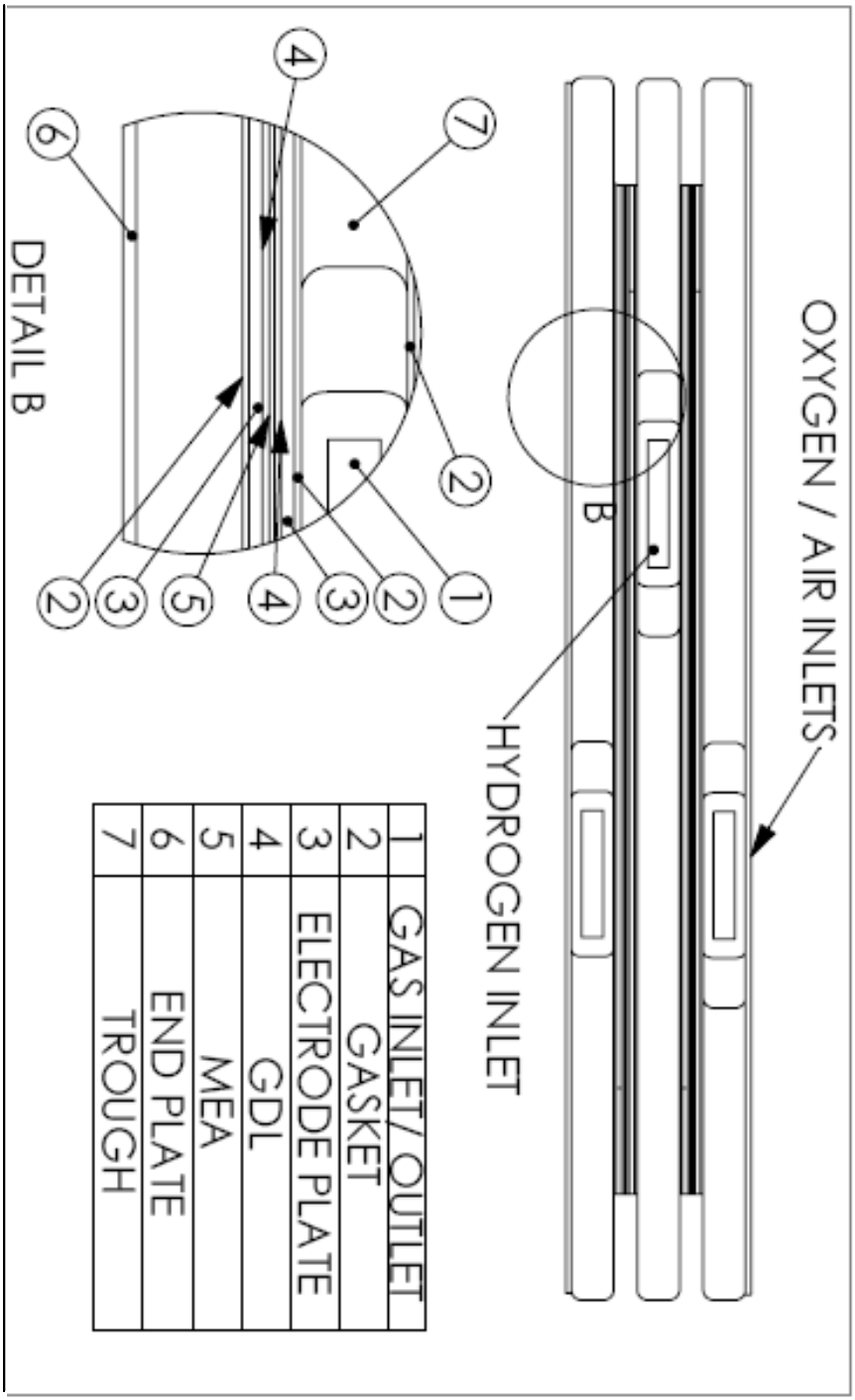

Figure 4-13 Two cell assembly, the middle trough supplies hydrogen to two membranes at the same time, the external sides of the two membranes are cathodes (Oxygen or Air sides)

4.4.4. The 6-Cell Module

The 2 cell/ 3 trough unit makes it easier to cool the fuel cells as the cathode sides constitute the outer sides of the fuel cell, which can be cooled either by ambient air or sealed and cooled in a closed air, water or refrigerant system. To build the 100 W module; three of the two cell units are needed, they are bolted together as one single unit, but separators are used to maintain a gap for coolant, shown in the drawing; figure (4-14). The gas ports are apparent in the drawing; there are more ports for oxidant than hydrogen as the hydrogen trough supplies two cells at the same time.

In the present design, the coolant is ambient air which is circulated using a blower selected in the light of the total size of the fuel cell stack. The scope and main focus of this thesis does not require the calculations for the specifications of the blower unit to be presented, but the amount of air needed for cooling has been presented earlier in this chapter. The fuel cell module is shown in figure (4-15).

The electrical connections of the fuel cell module and stack are made externally, when the module is plugged in place, the electrical poles connect to the circuit with other fuel cells, the connections are made in parallel or in series as required, this way the output of the fuel cell can be configured to the required load output.

The gas ports also fit in position to the gas supply and outlet manifolds, this arrangement more flexibility for easier maintenance and replacement of fuel cell modules.

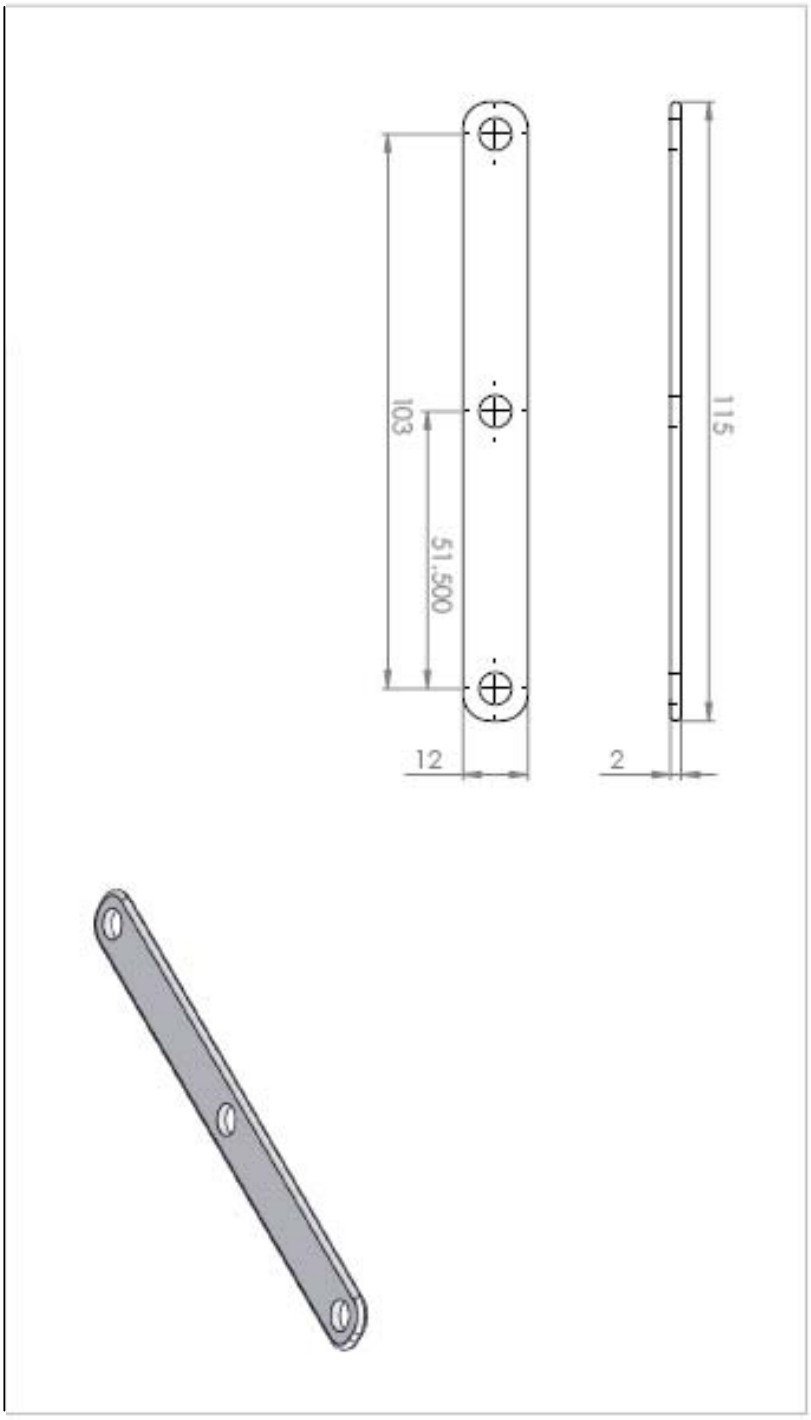

Figure 4-14 The separator which is used to separate two-cell units to allow for the flow of cooling air

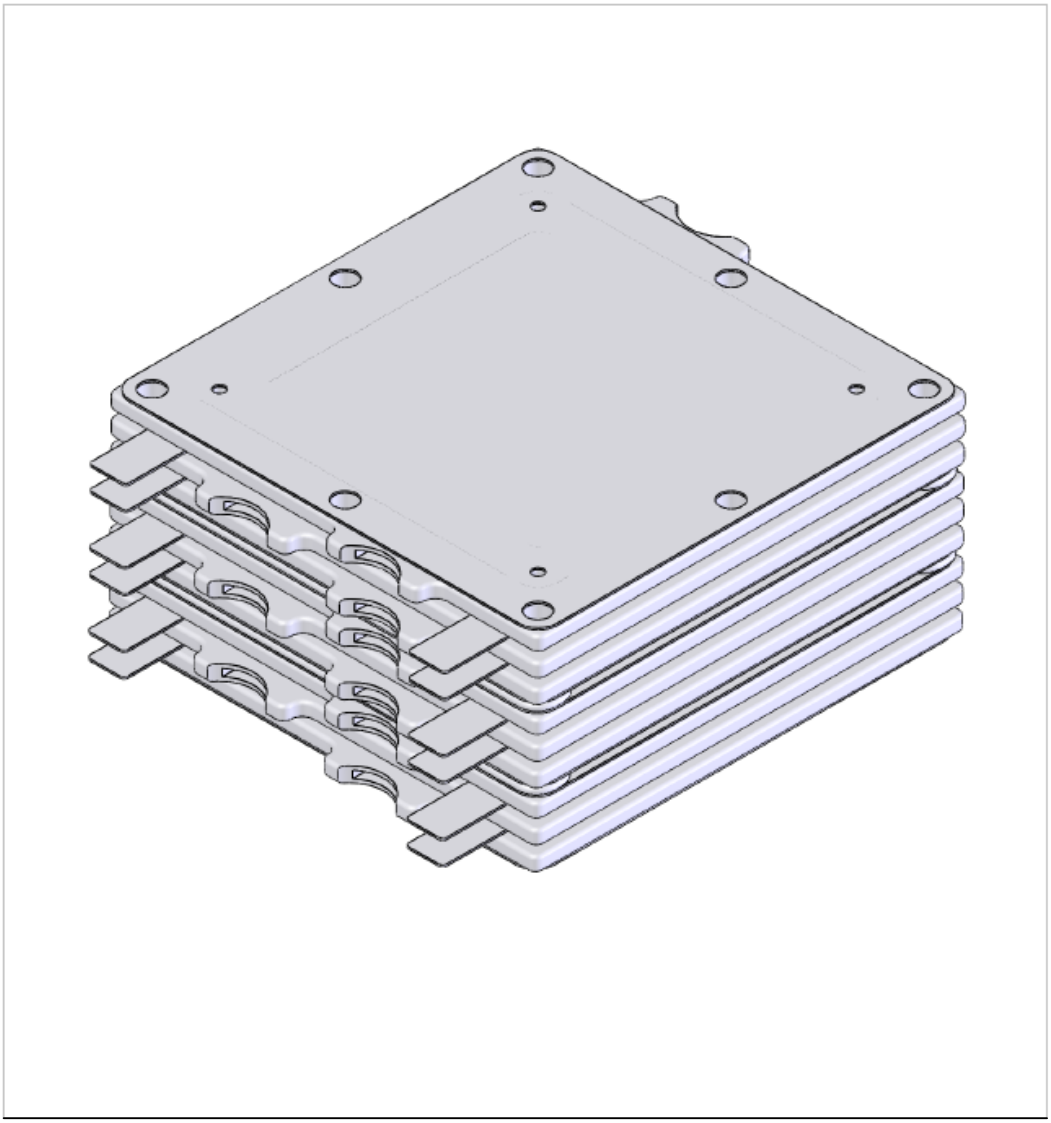

Figure 4-15 Complete fuel cell module, comprising 6 single cells, 9 troughs, 6 end plates and two cooling gaps, the electrical poles and gas ports can be seen in the drawing

4.5. SUMMARY

The main aim of this research project is to reduce the cost of production of PEM fuel cells through simplifying the design approach and following a design methodology in which common materials and production techniques are used instead of costly machining and exotic materials.

In this chapter; the full design and calculations for a *100W* fuel cell module based on meshed stainless steel electrode plates and gas distributors made of composite materials were presented. This module can constitute a building block in a larger fuel cell for stationary applications.

A novel architecture of the fuel cell is presented in which the anodes of each two cells are adjacent and the cathodes are distant to simplify cooling and reduce the number of components used in the fuel cell. Each cell in the module is operated individually which improves their performance, and findings of the theoretical and mathematical studies with regards to optimal gas distributor thickness, mesh type, gas flow directions and supply and exhaust hole locations are implemented in the proposed design.

The proposed design offers flexibility in cell configuration and output manipulation to suit the intended usage. It also offers flexibility in assembly and maintenance of the fuel cell.

Chapter 5 DESIGN OF EXPERIMENTS AND TESTING FACILITY

5.1. INTRODUCTION

To understand the physical behaviours and to improve the performances of fuel cells, multi disciplines and skills are needed such as: chemistry, electrochemistry, fluid mechanics, thermal, electrical and mechanical engineering. Advances in FC research are obtained by conducting a variety of investigations ranging from fundamental domain and material field with; for instance, the development of new catalysts and new electrolytes, to more application oriented works as the optimization of FC balance-of-plants to fulfil final operating conditions and requirements (e.g. load current cycles linked with dynamical mission profiles for vehicles) [79].

FC performances estimated at different scale levels, i.e. Materials, components, single cells, FC stacks and complete FC systems, are generally highly dependant on different physical phenomena from mixed domains. Fuel Cells are difficult to model due to their complex non-linear multivariate natures. A large number of input factors that contribute to the FC final output voltage could be mentioned. This can motivate Design of Experiment (DoE) approaches rather than or complementary to first-principles/mechanistic models [80]. However, the experimental set up for this work is not intended to merely find the best combination of variables for best performance, but the main aim is to optimise or control the inputs of the fuel cell under steady state conditions and to measure its outputs to evaluate its performance under a specific set of conditions.

5.2. OPERATING PARAMETERS

The parameters that influence the performance of the fuel cell can be grouped into three categories: Performance variables, geometric variables and operating conditions. The performance of the fuel cell depends on the geometric and operating conditions. However, it is not possible under real-life application of the fuel cell to vary the geometry of the fuel cell, which leaves the operating conditions as the only variables

changeable. Nevertheless, under laboratory conditions, the geometric variables can be changed, and various components of the fuel cell can be replaced to vary the geometry of the fuel cell. The main concerns of this work are: the fuel cell electrodes, flow field design and the Gas diffusion layers, which are all architectural components with different geometric variables. The operating conditions are not as important as these variables in the present case, however; they have to be measured to examine their influence on the fuel cell performance under certain geometric conditions.

Although there are many variables that can be considered, the approach considered in this work is simple. All measurements are performed under steady state conditions and the variables to be measured are the following:

Table 5-1 Variables to be measured and their ranges

VARIABLE	RANGE	UNIT
Current density	0-1500	mA/cm^2
Cell voltage	0- 1.2	*Volt*
Temperature	300-373	*Kelvin*
Pressure	1-3	*bar*
Relative humidity	0-100%	*Ratio*
Flow rate	0-10	cm^3/s

5.3. EXPERIMENTAL SET UP

One major problem in fuel cell operation, and particularly when testing a fuel cell stack, is the control of the humidity of the membrane, which should be maintained wet throughout the experiment. The issue of humidity is also relevant to the heating of the fuel cell and reactants whether heat added to the inputs to heat the fuel cell or heat output of the fuel cell as a result of the exothermal chemical reaction. As the temperature of the fuel cell and the temperature of the reactant gases increase, humidity

of the gases drops; because their capacity to carry water increases and more water has to be added to the gas streams to maintain their humidity level, figure (5-1) shows that the saturation vapour pressure increases rapidly as the temperature increases.

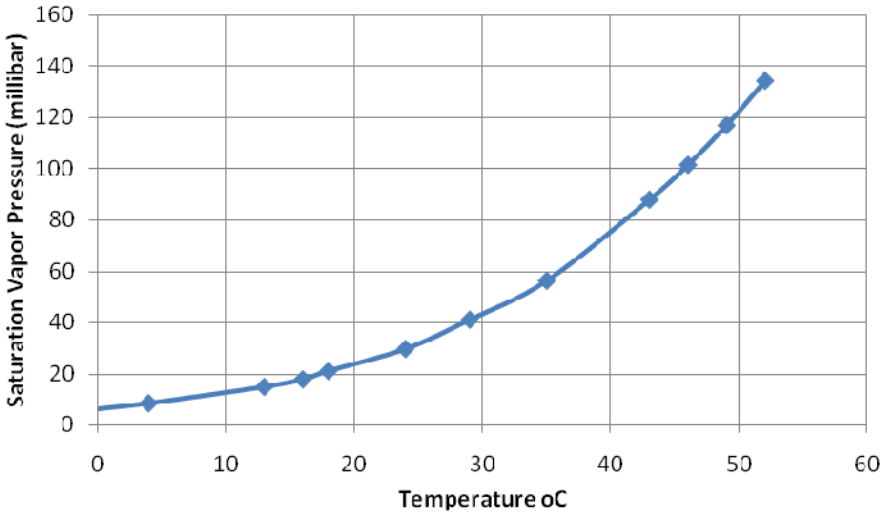

Figure 5-1 Saturation vapour pressure as a function of temperature

To maintain full humidification of the membrane, both gas streams at the cathode and anode have to be humidified. Water is transported to the cathode side from the anode through electro osmosis, while at the cathode, water is generated due to the reaction, but at the same time it is carried away with the excess gas stream and also transported back to the anode through capillary action. Hence, humidification is needed at both sides of the fuel cell and has to be controlled in such a way to prevent flooding of the fuel cell.

Another important problem is the measurement of the flow of gases. As flow is a function of temperature, the two measurements of flow and temperature have to be read simultaneously. Another important factor affecting the measurement of flow is the value of the flow measurement, which is very small especially in the case of a single fuel cell, and indeed, flow measurement was one of the major problems faced during performing the experiments.

In the light of these difficulties, the experimental rig is designed to perform three tasks:

1. To provide a controllable apparatus for the preparation of the gases for the fuel cell in terms of flow rate, temperature, pressure and humidity.
2. To measure the condition of the gases in terms of pressure, temperature, relative humidity and flow rate.
3. To measure the output conditions of the fuel cell such as; voltage and current outputs outlet flow rates and humidity of the gases at the outlet.

5.3.1. The Test Rig

The system comprises two functionally identical but independent gas flow circuits; one for the anode (Hydrogen) and one for the cathode (Oxygen or Air). Each circuit is sized to match the flow associated with each reactant. Each one of these circuits comprises measurement and control apparatus which will be described in due course. A schematic of the test rig is shown in figure (5.2) below:

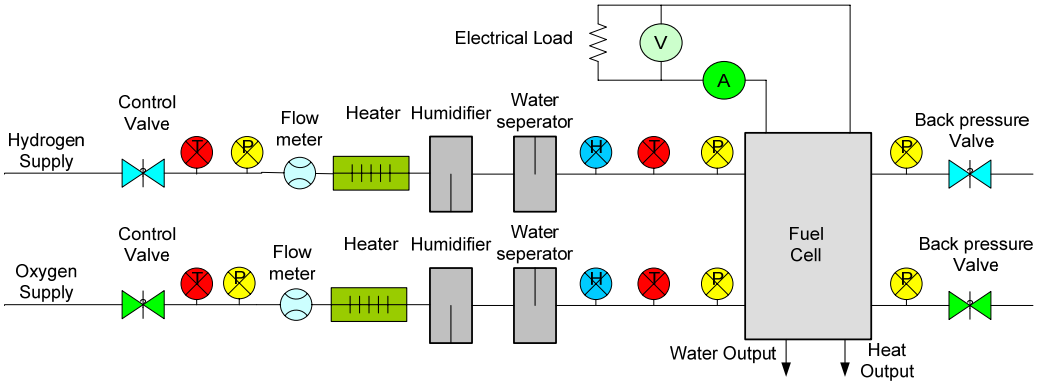

Figure 5-2 Schematic diagram of the experimental set up

The schematic diagram shows the various components of the test rig. Hydrogen which is supplied from a compressed gas cylinder enters at the hydrogen supply point

where the flow is controlled by the flow control valve. Temperature, pressure and volumetric flow rates of the gas are read at this stage to calculate the mass flow rate of the gas because it is a function of pressure and temperature.

The gas then enters a heating process where heat is added using a rope heater and a heating coil. The heat flux in the case of hydrogen is very slow to avoid combustion of the gas, both heat fluxes are controlled by *time percent controllers*.

The flow of gas is then routed to the humidifiers. In the case of hydrogen; the gas bubbles through distilled water in the humidifier as a continuous built-in feature, however, more moisture can be added to the flow when the ultrasonic vaporiser is on. In the case of oxygen/ air supply, the flow passes through the humidifier without bubbling and passes over the distilled water in the humidifier where it can carry a slight amount of moisture, but more moisture can be added when the vaporiser is on. Humidity, temperature and pressure of the flow are read at this point.

The gases are then directed to the fuel cell, where they react, and the excess gases are vented out through a back pressure valve to control the pressure of the cathode and anode. The fuel cell is also treated as a black box where only the external measurements are considered.

5.3.2. LabView® Application

A LabView® application which represents a virtual and a display unit of the test results was set up to aid in understanding the performance of the test facility and to model fuel cell performances under different conditions. Figure (5-3) below represents the front panel of the application, it shows the main measurements and measurement points. The front panel objects were controlled by a Visual Instrument (VI) block diagram.

The LabView® application can be used to demonstrate the mathematical model of the fuel cell, to display the experimental results acquired through the data acquisition system and to fit the experimental results to the mathematical model and predict the values of curve fitting parameters.

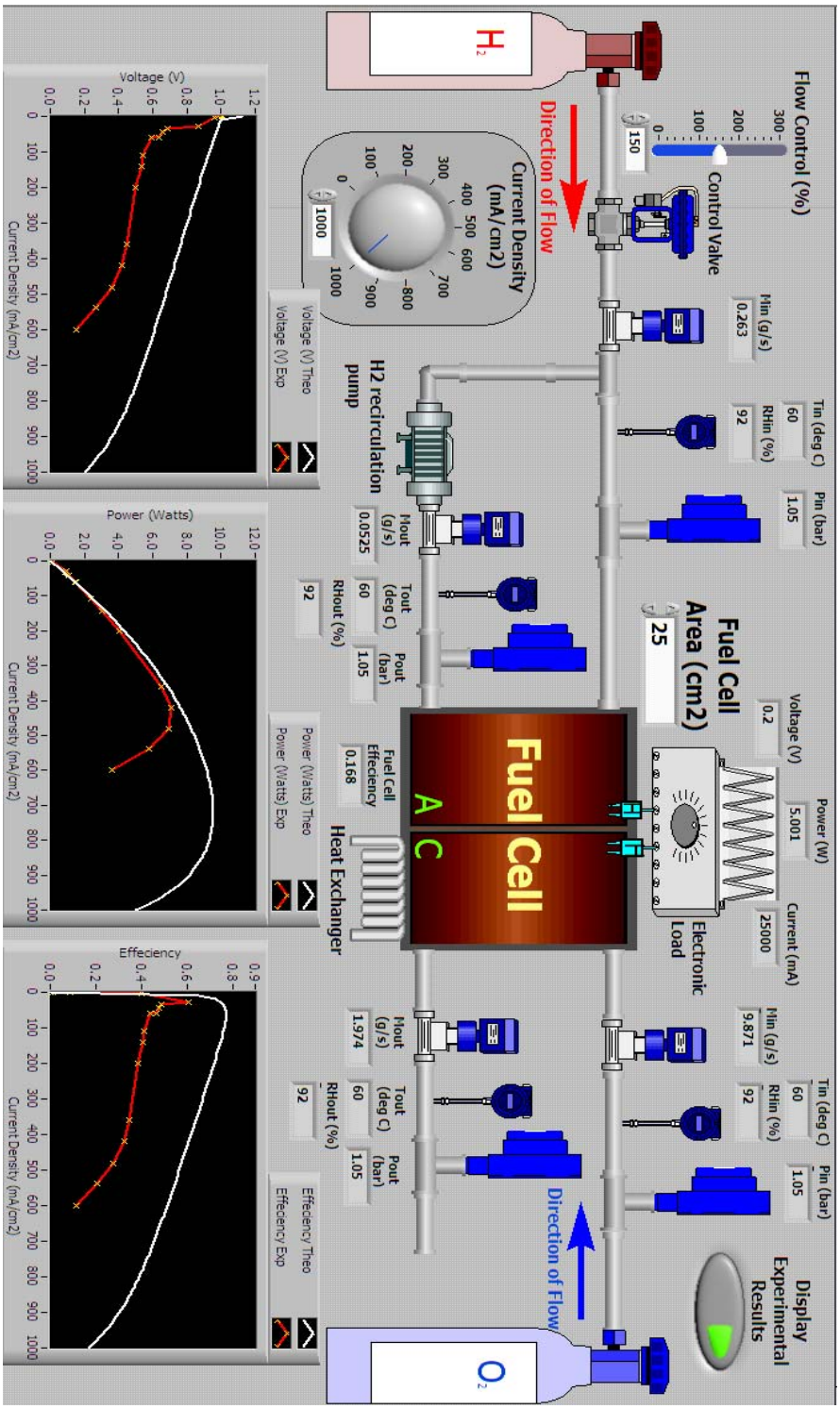

Figure 5-3 Front panel of the LabView application, mathematical model displayed in *White*, while experimental results are displayed in *Red* with an asterisk

The current density and cell active area are the two main variables on the front panel, while other parameters can be changed from the block diagram. A (% flow controller) is added to the application to control the stoichiometric ratio of the reactant gases. In this application both gases are supplied at the same stoichiometric ratio.

Exact values of flow rates for hydrogen and oxygen are calculated using the power output of the fuel cell according to equations (4-12) and (4-16) at the supply points, and then they are multiplied by the stoichiometric ratios.

The values of temperature, relative humidity and pressure, are entered as fixed numerical values at first hand because steady state measurements were used in the present experiments, however, this can be modified easily to read these values from the data logger.

At the exit from the fuel cell, the calculated amount of excess gas is calculated and displayed together with values of pressure, temperature and humidity. In the case of hydrogen, a recirculation pump to recover excess gases is shown, but this was not used on the actual test facility.

The value of open circuit voltage is input as a constant value calculated at 333K (60°C) and ambient pressure; as the experiments were mostly run under these conditions. The other constants in the model can be varied manually to obtain the best curve fit.

The LabView® application can be run to display the mathematical model only, or can display both mathematical and experimental results. A special control switch is provided on the control panel for this purpose, the experimental results are displayed in red. The mathematical equations and parameter values used in the mathematical model are shown in table (5-2) below:

Table 5-2 Mathematical equations and parameter values used in the LabView mathematical model

Parameter	Equation or value	Numerical values	Equation reference
Activation overvoltage	$\eta_{act} = b\log\left(\frac{i_c}{i_o}\right)$	*b= 0.200*	3-34
Tafel's coefficient	$b = -\frac{RT}{\alpha nF}$	*b= 0.200*	3-35
Ohmic overvoltage	$\eta_{ohmic} = r_i i$	r_i*=0.006*	3-42
Concentration overvoltage (empirical)	$\eta_{conc} = m\exp(ni)$	*m=2.11e-5* *n=0.009*	3-46
Mass flow rate of Oxygen	$Mass\ flow\ rate\ of\ Oxygen;\ (\dot{m}_{O_2}) = \frac{M_{O_2}P_e}{4V_cF}$	*Calculated by model*	4-12
Mass flow rate of Hydrogen	$Mass\ flow\ rate\ of\ Hydrogen\ (\dot{m}_{H_2}) = \frac{M_{H_2}P_e}{2V_cF}$	*Calculated by model*	4-16
Efficiency of the fuel cell	$\varepsilon = \frac{0.87 \times iV_{cell}}{(i+i_{\text{int}})E^o}$	*Calculated by model*	3-57
E (Open circuit voltage)	$E = 1.229 - \beta_2\left(T - T^o\right) + \varphi T\left\{\ln\left(P^*_{H_2}\right) + \frac{1}{2}\ln\left(P^*_{O_2}\right)\right\}$	*1.031*	3-26

For the mathematical model, the range of values for current density can be varied using the proper control, the values of current density are input into a for-loop in increments of *10 mA/cm*^{2}. This value goes into a formula node together with values of fuel cell area '*A*', open circuit voltage '*E*', Tafel's coefficient '*b*', resistance '*r*', and the concentration constant parameters '*n*' and '*m*'.

The mathematical equations for output voltage, total current output, power output, efficiency and mass flow rates of reactant gases are calculate in the formula node and their values forwarded to the proper displays. Figure (5-4) shows a view of the

block diagram for the mathematical model which is presented here as an example and is expected to help other researchers improve on the current programme to desing a more advanced data acquisition system for the fuel cell test station.

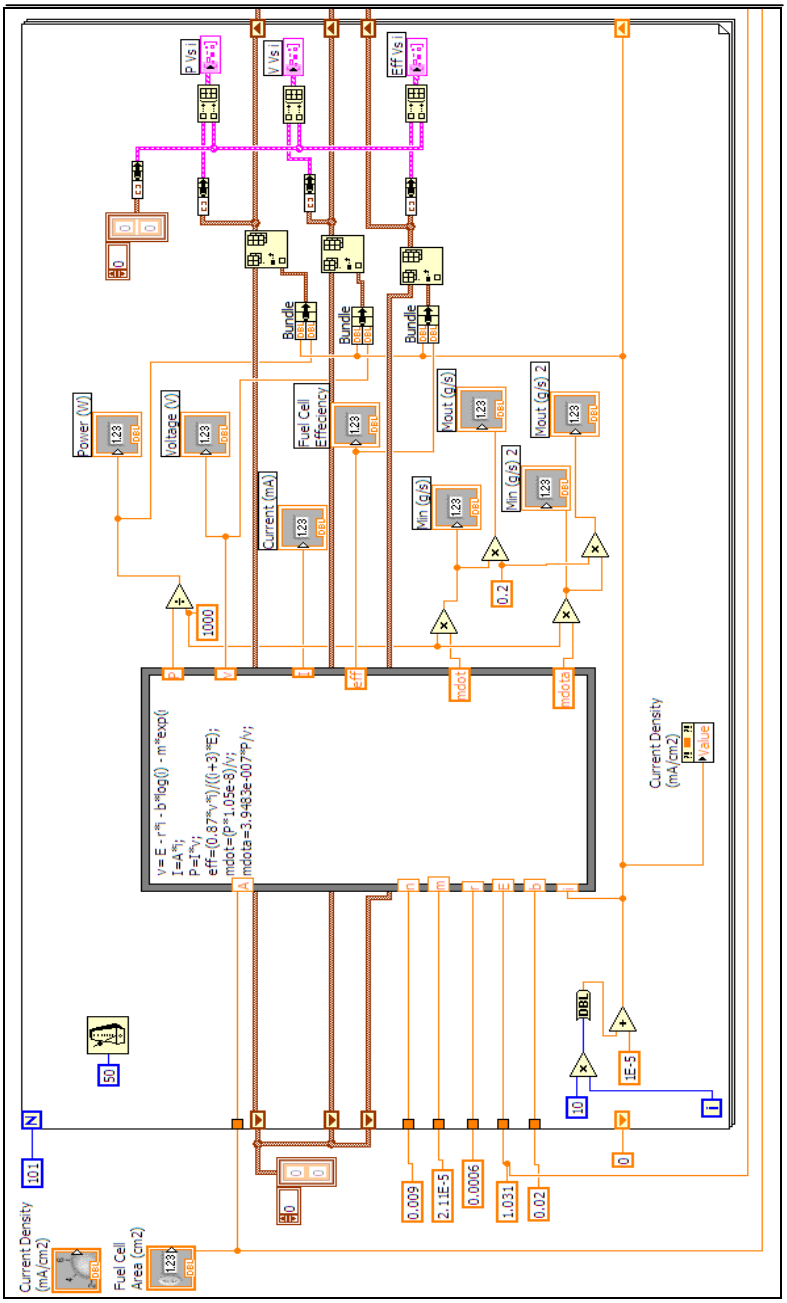

Figure 5-4 Block diagram for the mathematical model on LabView®.

The LabView application is ready to read and process values of all the readings on the control panel, however, in the experiments performed through this study, the experiments were performed under steady state conditions of ambient pressure and 333K (60°C) temperatures. The humidity was maintained at 92% at the inlets, and only the readings of voltage were read using the data logger. The value of the resistive load was varied and the current density was calculated using Ohm's law.

The acquired readings of voltage and the calculated values of current density were entered manually into two arrays *X (i) and Y (V)* on figure (5-5). The same formulae for power output and efficiency from the formula node in the mathematical model, figure (5-4) were used to calculate power output and fuel cell efficiency, but using measured values for current and voltage and then they were sent to the proper displays. Constant values of *3 mA/cm*^{2} and *0.87* on figure (5-5) represent the values of crossover current and thermal efficiency of the fuel cell respectively. The display of experimental results is controlled by a Boolean switch which operates through a case structure (True/ False) as shown in figure (5-5) below:

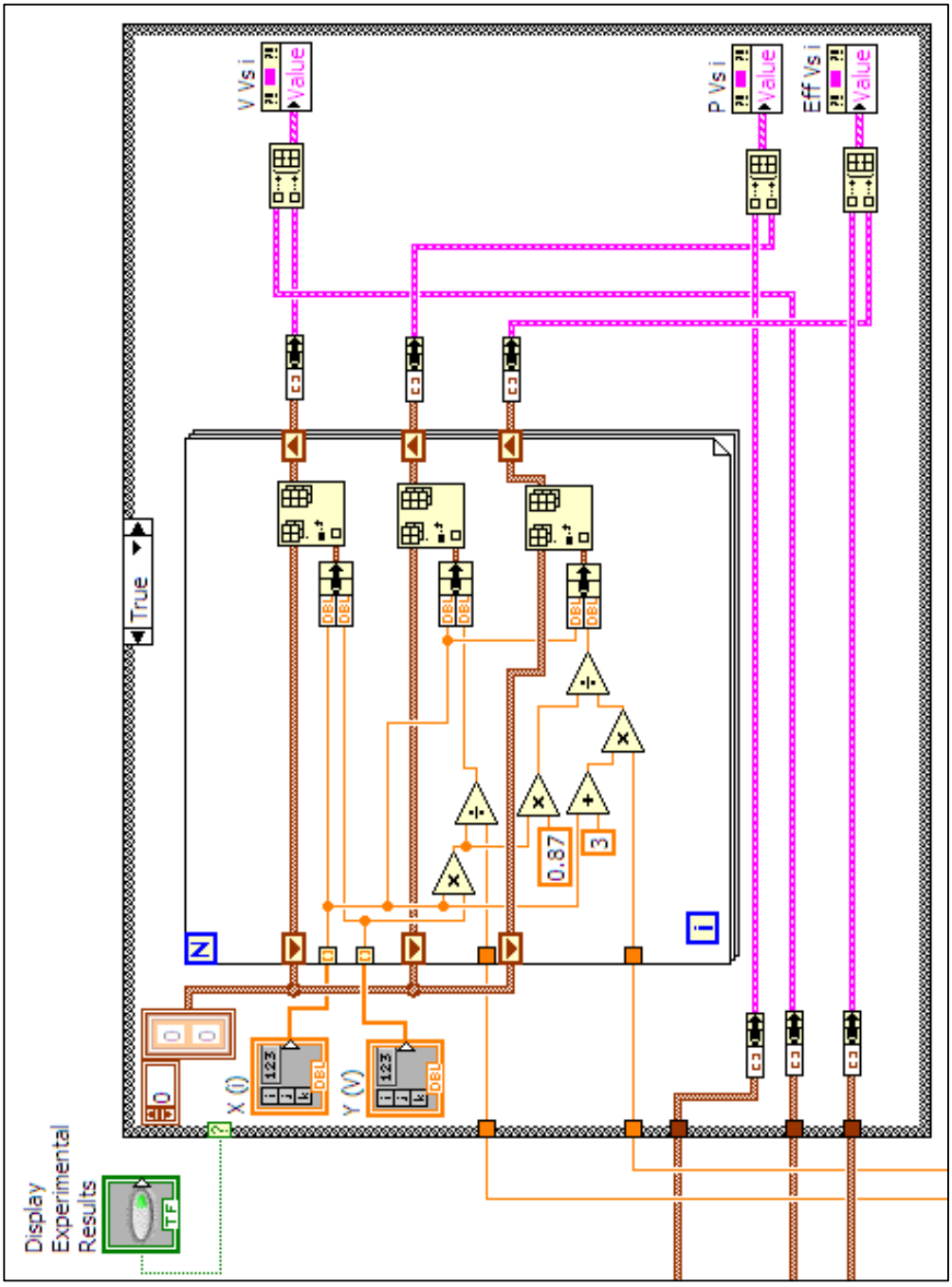

Figure 5-5 Block diagram for the display of experimental results using LabView®

5.4. SYSTEM COMPONENTS AND DESIGN

A brief description of the major components of the test rig is described here, further details are provided in Appendix C.

- ***Flow Measurement***

Two standard type floating ball flow meters were used for each of the reactant gases to measure the inflow and out-flow. The difference between the two measurements indicates the amount consumed by the fuel cell, including fuel cross over in the membrane. This type of flow meter is simple to use and not too expensive. Accuracy of the measurement is acceptable (in the range of <5%).

- ***Temperature Measurement***

A set of K-Type thermocouples were used to measure temperature at the following points:

1. Inlet gas temperature
2. Outlet gas temperature

The thermocouples were used together with a four-channel type-K thermocouple amplifier unit, designed to interface type-k thermocouples to data acquisition systems due to the fact that the thermocouple voltage is very low, usually in terms of a few millivolts, and was below the resolution of the data acquisition system.

The amplifier modifies the output voltage of the thermocouple to give a standard *10mV/°C* output for a type-k thermocouple input; hence the use of calibration charts was not necessary. Details of the thermocouples and the amplifier are given in Appendix C.

- ***Humidity Control and Measurement***

A stainless steel cylinder equipped with an ultrasonic vaporiser powered by 24 VDC and a water level float sensor are used as a humidification chamber. Gases pass through the chamber and carry water vapour as they go through. In the case of hydrogen, the gas stream is forced to bubble through the distilled water as a standard feature, while oxygen just passes through the chamber without bubbling. The ultrasonic

vaporisers are switched on via a switch on the control panel when more humidity is needed.

Humidity measurement is performed using an electronic sensor (HH-4000 Series Humidity sensor from RS components). The HH-4000 RH sensor is a laser trimmed, thermoset polymer capacitive sensing element with on-chip integrated signal conditioning. More details are provided in Appendix C.

- ***Pressure Measurement***

The test rig is equipped with pressure transducers type (Gems sensor series 2200) capable of measuring 1 to 5 atmospheric pressures, obtained from RS components for measuring the pressure of inlet and outlet gases for both hydrogen and oxygen.

Pressure control is achieved via check valves at the outlet ports of the fuel cell, and by adjusting the flow control valves on the cylinders. All the experiments were performed at atmospheric pressure, so this feature was not utilised during the experiments reported in this study, but the facility is available for future work.

- ***The Data Acquisition System***

The DAQ system comprises the data logger and the software, below is a brief description of both, but further details are presented in Appendix C.

  - **The Data Logger**

A USB based analogue and digital Input / Output unit for data logging, data acquisition, measurement and control applications; commercially known as (Labjack® U12) data logger was obtained from Audon Electronics (UK). The unit is facilitated with a wide range of data logging and oscilloscope software and examples for use with most programming and DAQ packages. The data logger is shown in figure (5-6) below.

  - **Data Acquisition Software**

The (Labjack® U12) data logger can be operated on LabView® as well as DaqFactory®, which is a new software package designed for scientists and engineers who need a low-cost but highly capable data acquisition/control package. It can acquire

data, control outputs, has user defined pages complete with a symbol library and has many other functions.

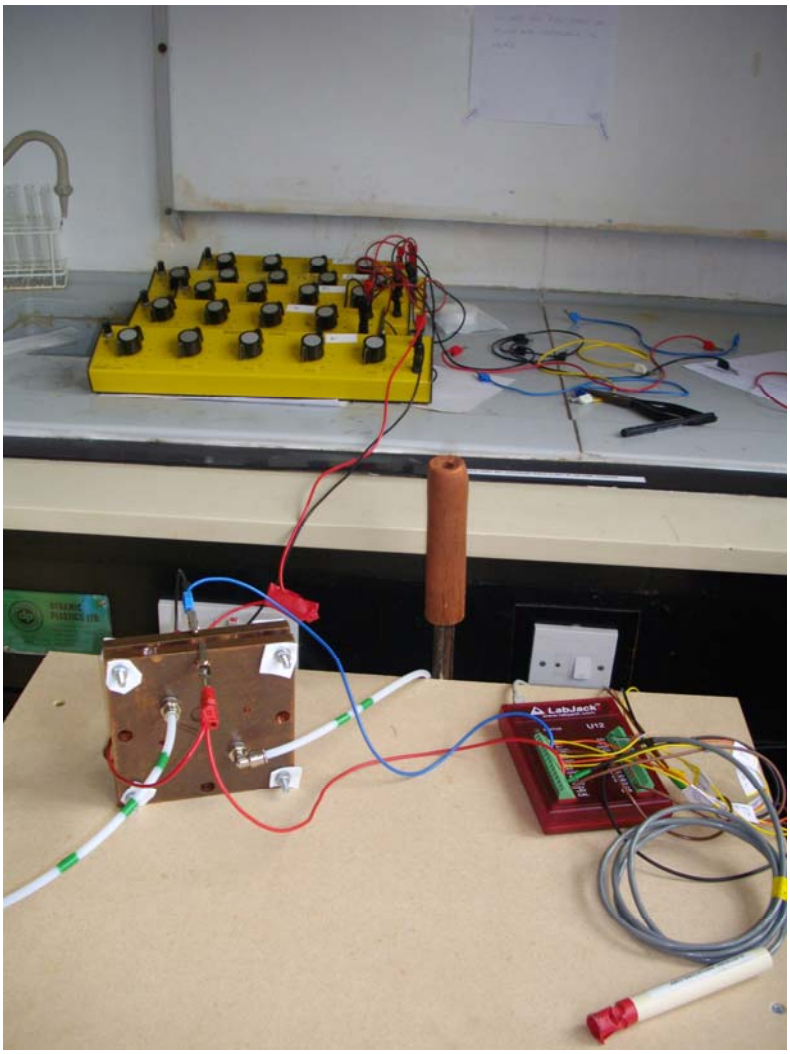

Figure 5-6 Fuel cell based on graphite plates under testing, Data logger and Load bank are shown in the picture. An external humidity and temperature sensor is used to test the quality of the gases at outlet for comparison and calibration.

- ***The Load Bank***

The fuel cell performance curve is a plot of voltage against current density. The current values were obtained by loading the fuel cell by connecting it to a variable resistance. As the resistance varies, the current and voltage values vary. The current is calculated using Ohm's law, and then divided by the cell area to obtain the current

density. The final values of current density and voltage are input manually into an array on LabView and polarisation; power output and efficiency curves are obtained.

A set of standard resistances were used to provide the load, figure (5-6). The resistances had to be connected in parallel to get resistances below 1 Ohm. Resistors with very low values such as; 0.01 and its multiples up to 1 Ohm were obtained from RS components. Appendix C presents more details on the measuring procedures and equipment.

- ***The Complete Unit***

To avoid confusion, the gas supply lines are distinguished with red ribbons for hydrogen and green ribbons for oxygen. Tests can be performed on top of the test rig, where a removable top has been designed to make the unit compact and versatile. The gas supply lines and fuel cell connections are shown in figure (5-7):

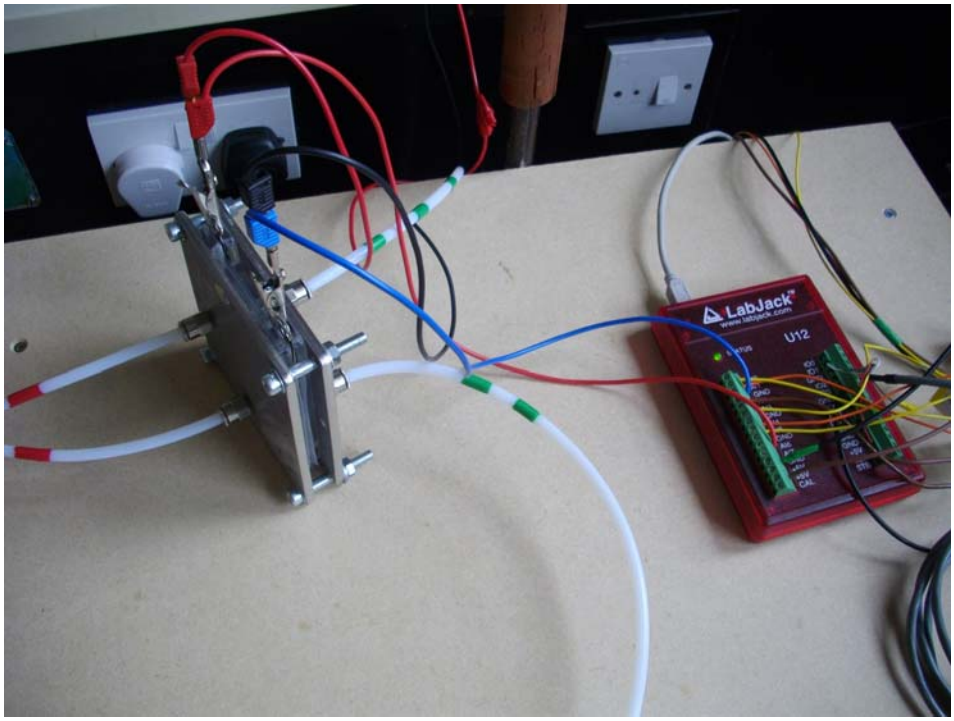

Figure 5-7 PEM fuel cell based on meshed SS316 electrode plates under testing. The LabJack U12 DAQ system is shown. Gas supply lines are marked with red ribbon for Hydrogen and green ribbon for air.

Figure (5-8) depicts the complete test facility. On top of the test rig; the hydrogen side of a graphite based fuel cell can be seen together with the data logger.

As indicated on the front panel of the rig, the left side is for hydrogen measurements, and the right side for air/ oxygen. The floating ball flow meters are shown, the fittings for the sensors are apparent at the bottom side of the front panel.

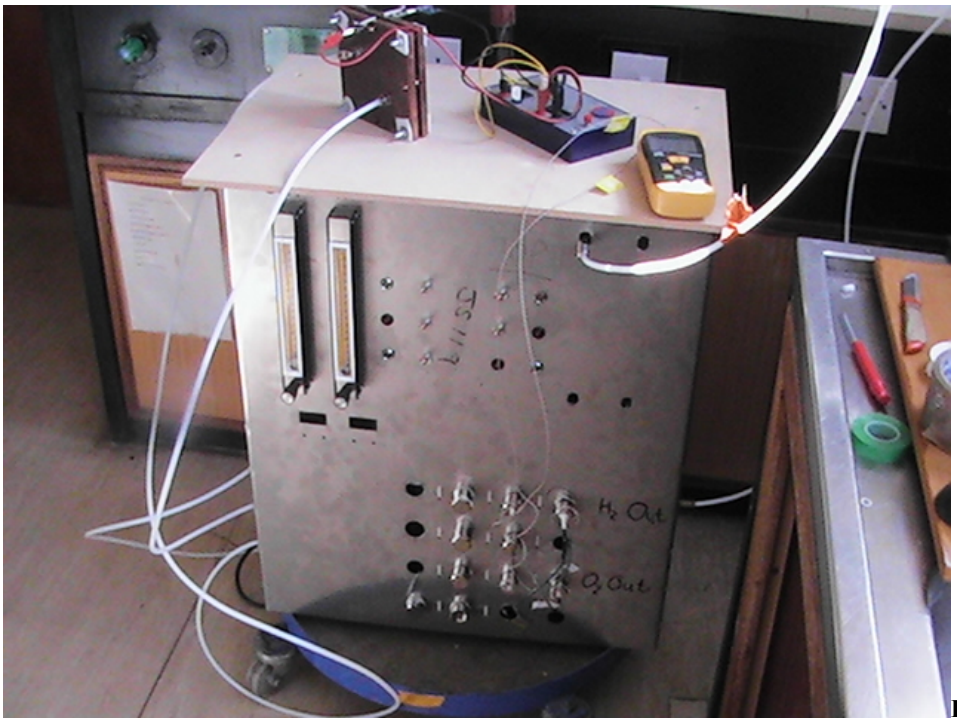

Figure 5-8 The test rig (under construction), a view from the front panel. A graphite-based fuel cell and a millimetre for measuring voltage and current appear on top of the rig.

The test facility in its final shape, together with schematic diagrams of the front panel with their identification are presented in Appendix C.

5.5. SUMMARY

The fuel cell test facility and gas conditioning system is a very important tool for fuel cell research. It enables the researcher to undertake stack performance testing, investigating new concepts in fuel cell technology and model validation and to perform experimental parametric studies on the fuel cell.

The test facility presented in this chapter was designed and produced as part of this research work, which added a considerable amount of knowledge and expertise. This facility was designed to measure and control the mass flow rates, relative humidity, pressure and temperature of the reactant gases. It could also measure the output voltage of the fuel cell. All measurements were performed using a data acquisition system.

The test rig was also equipped with safety precautions such as fire arrestors for the gas cylinders, a nitrogen purge facility and warning indicators for the level of water in the humidification system and for the heaters.

Chapter 6 RESULTS AND DISCUSSION

6.1. INTRODUCTION

The main aim of this research was the investigation of certain aspects of fuel cell technology, which is reckoned proprietary in nature with very limited data available in the open literature [15], in order to acquire this technology through hands-on experience.

The work led to a novel design of a modular proton exchange membrane fuel cell, the formulation of a computational 3D fuel cell model using CFD techniques and the design and fabrication of a test facility for performing practical tests on the fuel cell and using the acquired test data for the experimental validation of the computational model.

The fuel cell design was considered in chapter 4 where a 6-cell module was presented, but a two cell version was actually tested. For this purpose, a fuel cell test system equipped with a data acquisition system which is capable of conditioning the reactant gases for the fuel cell was built and used for acquiring the necessary data for this research and other fuel cell studies that are likely to be conducted in the future. The results are presented and discussed in this chapter.

6.2. ASSEMBLY OF A TWO CELL TEST UNIT AND INSTALLATION IN THE FUEL CELL TEST STATION

A 100 *W* fuel cell module is proposed in this study which is designed to constitute a building block in a larger fuel cell stack. The proposed fuel cell is based on 316SS stainless steel meshed plate as the electrodes. The novel aspects of this design approach are mainly in the configuration of the fuel cell stack; where the concept of bipolar plates is eliminated, and each fuel cell functions independently, as it has separate inlet and outlet ports for the reactant gases, furthermore, the electrical connections of the fuel cells are performed externally, which allows for parallel or series

connections, thus manipulating the voltage and current outputs of the fuel cell as desired.

A single-cell unit of the fuel cell module with an active area of (25 cm^2) was used as the test unit. Figure (6-1) shows an isometric drawing of a single cell fuel cell. The trough and meshed plate can be observed in the figures.

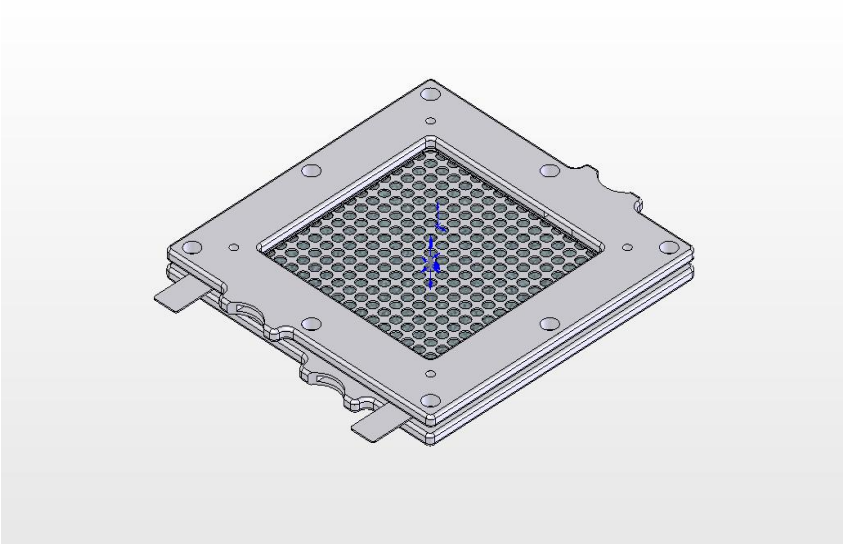

Figure 6-1 A SolidWorks® CAD isometric drawing of a single cell fuel cell, the trough, the meshed plate electrodes, inlet and outlet ports can be seen (Drawing to scale)

Figure (6-2) below shows an experimental single cell fuel cell in which the electrode plates are made of hexagonal mesh stainless steel. Reactant gases are supplied at the centre points of the trough sides.

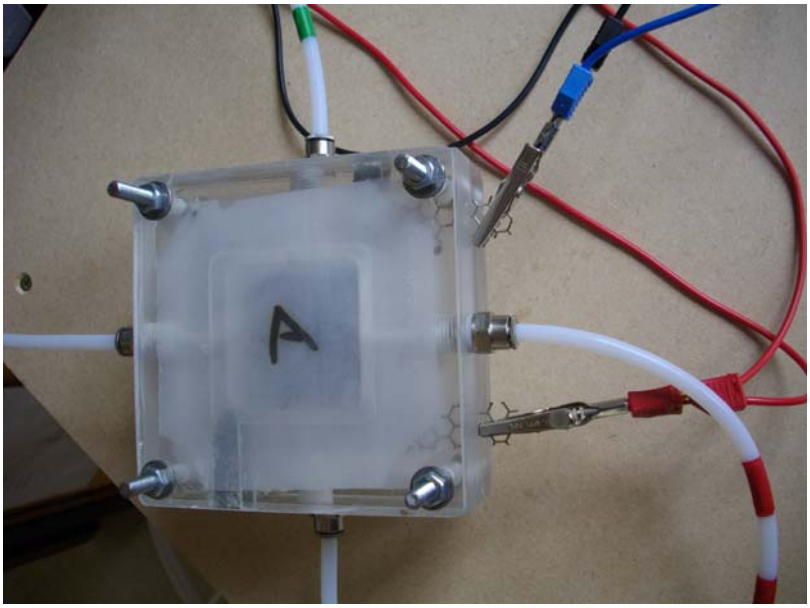

Figure 6-2 Actual experimental single cell fuel cell using Hexagonal type meshed SS 316 stainless steel electrode plates, the letter 'A' denotes the anode side of the fuel cell

The fuel cell was installed in the fuel cell test station described in chapter 5. Most of the testing was performed under atmospheric pressure conditions. Heating and humidification were applied; but were not considered major parameters due to the fact that the goal of the testing was to verify the design and study the effects of various geometries of the fuel cell under unified conditions, rather than measuring the influence of varying the operating conditions.

6.3. EXPERIMENTAL PROCEDURES

The fuel cell module was connected to the test unit and the data acquisition system. Humidification was applied to both anode and cathode sides of the fuel cell, the humidification at the anode side was provided in two ways:

- Passing the hydrogen gas in the humidification chamber through bubbling in distilled water, which is a built-in feature of the test unit.
- Operating the ultrasonic humidifier and heater to the humidification chamber.

In order to achieve the highest level of performance, the high purity reactant gases (Hydrogen and Air) were preheated to the desired temperature and then passed to

the fuel cell for a period of 1 hour in order; to remove air residues from the fuel cell channels, and to give the fuel cell enough time to reach the desired operating temperature.

The fuel cell was run open-ended, and hence the pressure in the fuel cell was atmospheric, but the flow rates of the hydrogen and air were fixed at fairly high stoichiometric ratios; 2 for hydrogen and 3 for air. The fuel cell was then connected to the variable resistive load and readings of voltage for various resistances were recorded by the data acquisition system. The current output of the fuel cell was calculated using Ohm's law as the resistance and voltage were both known values.

A standard technique was followed in recording the readings. The fuel cell was allowed a few minutes to stabilise at open circuit, and each time the resistive load was varied. A group of readings was logged to the data acquisition system each time the resistive load was changed. The average voltage reading was taken and recorded against the respective resistance value. A simple function of Ohm's law was used to calculate the current output.

6.3.1. Goals of the Experimental Study

The main aim of the experimental study was to generate sufficient data to:

- Verify the proposed fuel cell design through testing a single/ two cell fuel cell module of the proposed design under various geometric conditions.
- Study the effects of varying certain geometric conditions such as; electrode plate configuration, channel dimension and other parameters on the performance of the proposed fuel cell.
- To acquire experimental results that can be compared to the numerical model in order to validate it.
- To verify the design of the test facility and the data acquisition system.

6.3.2. Approach to the Testing Procedures

In the first set of experimental results, the polarisation curve for a 25 cm^2 fuel cell based on electrodes made of graphite and Nafion® 117 Membrane with (3 mg/cm^2 Pt/C) catalyst loading on each side was obtained through operating the fuel cell under specific operating conditions as described earlier and indicated below.

In the second set of experiments, different geometries of the fuel cell are compared under similar operating conditions. The electrode plates, which were made of untreated 316SS stainless steel meshed plates of different mesh dimensions and geometries, were compared and different thicknesses of the channel plates (troughs) were also compared to determine the optimum configuration of the fuel cell and to verify the fuel cell design which is proposed in this study.

6.4. Discussion of Experimental Results

6.4.1. Operating the Fuel Cell with Nafion® Membrane on Pure Oxygen

Initially the fuel cell was assembled with a Nafion® 117 membrane acquired from Ion Power plc., and one layer of Gas diffusion electrode (GDL Toray® Carbon Paper) using a 5mm hexagonal mesh electrode plate as the fuel cell electrodes. The fuel cell was operated on pure oxygen and hydrogen, initially the fuel cell indicated good performance and fairly high open circuit voltage (higher than 1 Volt), but soon the fuel cell indicated a short circuit and the voltage dropped to zero. This was an indication of an internal leakage. The fuel cell was disassembled and it was found that the membrane was defected at the oxygen inlet and along the flow direction.

This was attributed to the oxygen permeation across the membrane from the cathode side. The defect was more pronounced near the inlet of oxygen, which enhanced the penetration due to the impact of the gas stream with the membrane. This was ascribed to the exothermic nature of the hydrogen/oxygen reaction in the presence of the catalyst, hydrogen at the anode and oxygen crossing over reacted producing heat,

which caused the membrane to reach its melting point and hence producing the defect shown in figure (6-3)

This is also an indication that cross over through the membrane is considerable, but less harmful when the gases are diluted by mixing with an inert gas such as nitrogen. As a result of this experiment, operation on pure oxygen was avoided and not recommended, and operation on air was considered instead.

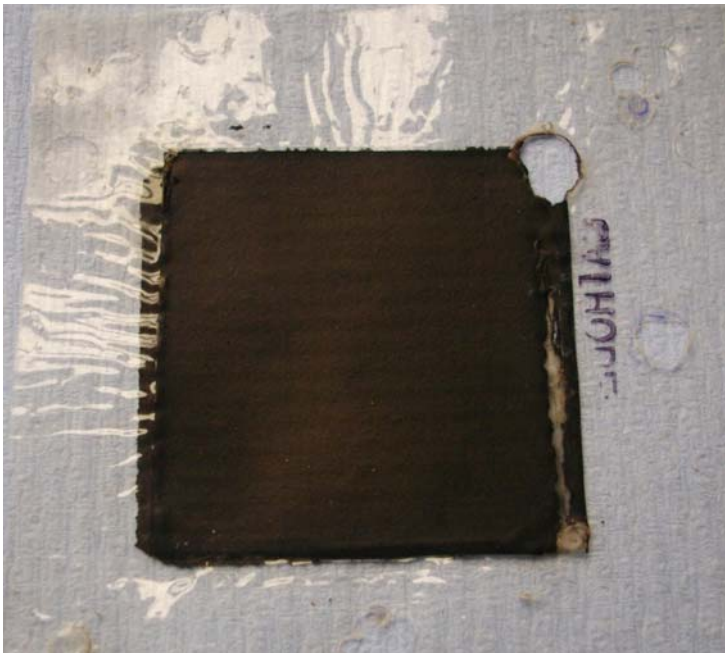

Figure 6-3 Nafion® 117 membrane used in fuel cell operated on pure oxygen and hydrogen using stainless steel meshed electrodes, damage of the membrane due to gas permeation at the oxygen inlet port can be observed at the top right corner of the active area

6.4.2. Effect of Assembly Pressure on Fuel Cell Operation

During the initial operation of the fuel cell on H_2/Air, the performance of the fuel cell was found to be qualitatively poor. Varying the operating parameters, such as operating temperature and pressure, did not result in any improvement in performance. The fuel cell was disassembled and it was observed that; because a gasket of a larger thickness than that of the Gas Diffusion Layers (GDLs), the membrane was not properly compressed (i.e. tightened) between the GDLs, figure (6-4). This resulted in poor contact between the membrane and other components of the fuel cell; namely the GDLs

and electrode plates which resulted in an increase in the *interfacial contact resistance* (ICR) between the steel and the carbon backing material.

This is similar to the effect observed by Wang and Turner [39] but that was attributed to the passive film formation on the electrode plates due to the oxidation of chromium under fuel cell chemical environment. However, both observations indicated high resistive losses in performance.

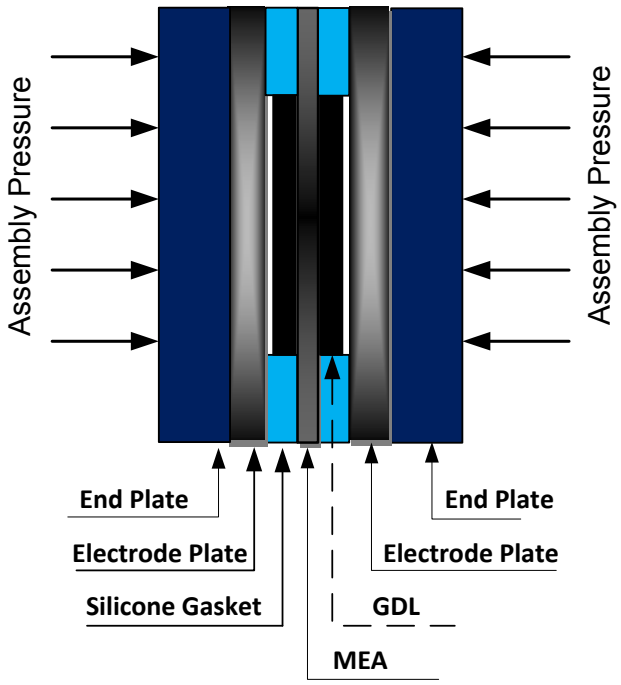

Figure 6-4 Schematic of the fuel cell to illustrate the poor contact between the Gas Diffusion Electrodes (GDL) and the electrode plates due to the fact that the thickness of the silicone gasket is larger than the thickness of the (GDL). Not to scale

When the membrane is properly hydrated, its dimensions increase due to swelling. Due to the fact that the membrane was not properly compacted between the electrode plates and GDLs, the active area of the membrane changed its geometry due to space availability. Only a small percentage of the total active area was in contact with the GDLs. Hence, contact between fuel cell components was poor. These reasons resulted in the reduction in the contact area between the membrane, the electrodes and GDLs and enhanced performance losses due to high electrical resistances. Figure (6-5 left) shows the actual shape of the membrane before swelling, while figure (6-5 right)

shows the membrane after it has been used in a fuel cell with low compression applied on the membrane.

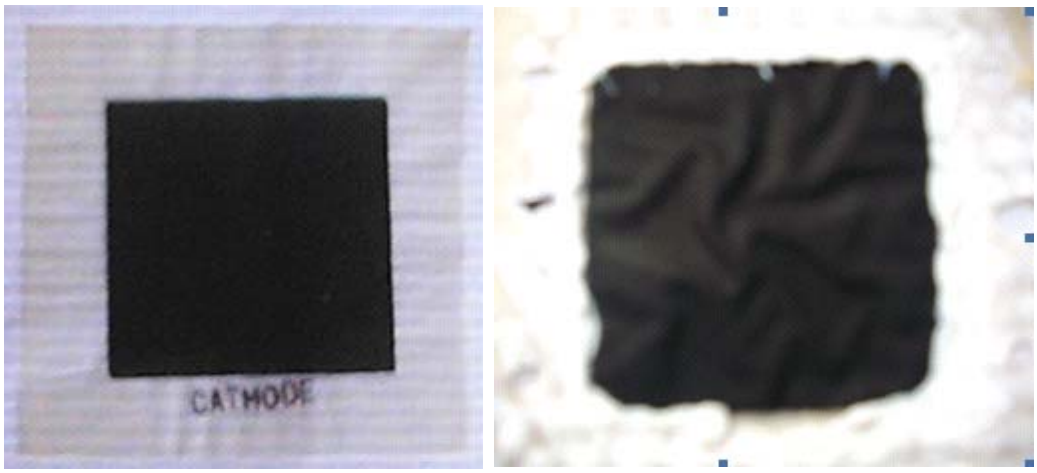

Membrane before swelling **Membrane after swelling**

Figure 6-5 Actual shape of 3 layer MEA based on Nafion® 117 and *3 mg/cm²* catalyst layers (*Left*) and shape of same membrane after application in a fuel cell with insufficient compaction torque (*Right*).

The polarization curves for the fuel cell with low stack compression and the case with proper stack compression are shown in figure (6-6).

A qualitative comparison between the two polarization curves indicates that operation with proper tightening improves the performance of the fuel cell and reduces the Ohmic losses. The activation voltage losses behaviour is almost similar between the two cases, the two curves start to separate at 50 A/cm^2, this is mainly attributed to the high electrical resistance between the cell components, especially between the gas diffusion layer and the electrodes on one hand, and the GDLs and the catalyst layers on the other hand. The open circuit voltage also decreases due to improper contact between fuel cell components because of the increase in electrical resistance which has an influence at all values of current density.

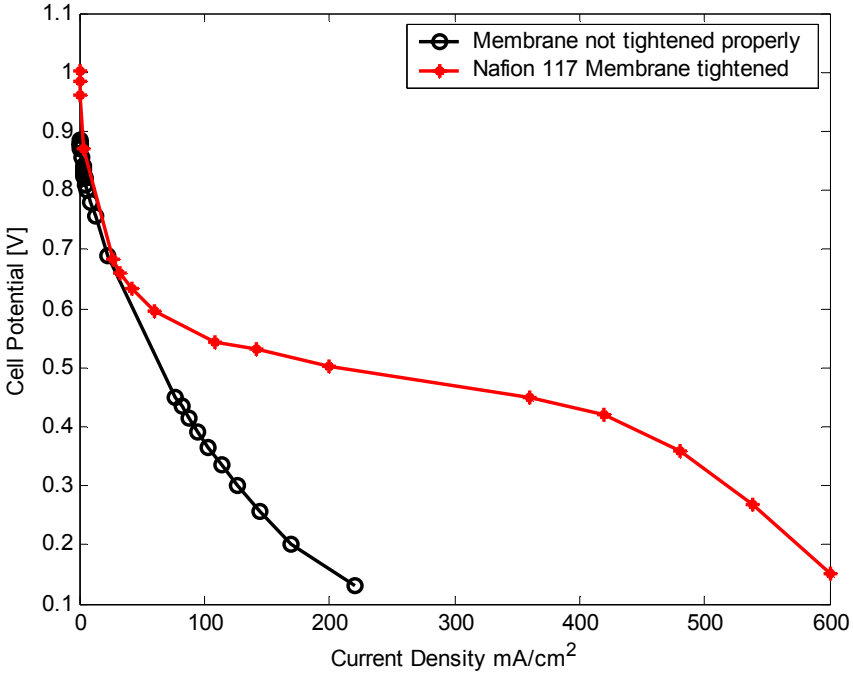

Figure 6-6 Performance of a properly compacted fuel cell as compared to a fuel cell with high contact resistances due to poor compression, both fuel cells are based on Nafion 117 and hexagon mesh 316SS stainless steel electrodes

Contact resistance occurs at all interfaces inside the fuel cell, the most important one being the interface between the bipolar plates and the gas diffusion layers, and its magnitude depends on various parameters such as the surface material, treatment of the surfaces and the applied stack pressure [20].

It has been shown in chapter (3) that the cell potential vs. current density data is represented by the formula:

$$V = E + \eta_{act+\text{int}} + \eta_{Ohmic+\text{int}} + \eta_{conc+\text{int}} \qquad \textbf{3-50}$$

Kim *et al.* presented an equation that models the polarization curve of the fuel cell as follows [69]:

$$E = E_r - b\log\frac{i}{i_o} - R_i i - m\exp(ni) \qquad \textbf{6-1}$$

'i_o' and 'b' are the Tafel parameters for oxygen reduction, 'R' represents the resistance, mainly Ohmic, which causes a linear variation of the cell potential with current density. The other contributions to 'R' are the charge transfer resistance of the hydrogen electrode reaction and mass transport resistances, predominantly at the oxygen electrode which are more so when air is used as the cathodic reactant [21].

The reversible cell potential for the given conditions is represented by 'E_r' and the three following terms describe the activation, Ohmic and concentration overpotentials respectively.

As discussed earlier in this write up, the first term can be recognized as the Tafel's equation that describes the activation overpotential, which is predominant at low current densities. The second term '$R_i i$' describes a linear drop-off, which is predominant in the intermediate current density region, where 'R_i' is the internal resistance caused by membrane and contact losses. The last term becomes predominant in the high current density region, and is used to match the drop-off towards the limiting current density.

- ***Open Circuit Voltage (OCV)***

The open circuit voltage is an indication of the electrochemical activity in the fuel cell and reflects the current exchange density for the oxygen reduction reactions. It is noted that the (OCV) in figure (6-6) is slightly higher when the membrane is properly compacted between the electrodes, as compared to the less compacted case. It is expected that as proper compaction increases the contact between the membrane, the *GDL* and the electrodes, it will also increase the activities of the reactant gases due to better catalytic activity in the membrane, hence increasing the exchange current density. This conclusion is derived from the definition of the open circuit voltage which is expressed by the Nernst equation (3-21):

$$E = E_o + \frac{RT}{nF} \ln \left\{ P^*_{H_2} \left(P^*_{O_2} \right)^{1/2} \right\} \qquad \textbf{3-21}$$

As discussed earlier, the main parameters affecting the *OCV* are mainly the partial pressures of the reactant gases and the operating temperature of the fuel cell. The

diffusion and distribution of the reactant gases in the fuel cell are affected by the geometry of the membrane and this results in reducing the exchange current density and hence reduction in the *OCV*.

- ***Activation Overvoltage***

Looking at the polarisation curve for the Nafion® membrane in figure (6-6), it is noted that the polarisation curve drops steeply due to activation overvoltage, the voltage drops by nearly 0.5 Volts within the first 100 mA/cm^2.

Activation losses are mainly considerable at the oxygen electrode, and they are the main loss of fuel cell efficiency. In the present case, it is expected to have more pronounced activation losses due to the fact that the fuel cell is operated at ambient pressure, and fairly low temperature, but the dramatic reduction in voltage due to activation losses is an indication of other reasons such as the roughness of the electrode plates which promotes the contact between the fuel cell components and provides a larger area for the chemical reaction.

The use of air as a reactant is also a reason for the increased activation overvoltage; another reason is attributed to the presence of impurities in the fuel cell and the composition of an oxidative layer on the surface of the stainless steel electrodes, being untreated, which might have an effect on the catalyst activity.

- ***Ohmic Losses***

The PEM fuel cell with higher compaction of the membrane shows better performance, qualitatively and quantitively, than the lower compaction membrane, mainly because of the considerably lower Ohmic losses in the fuel cell. The Ohmic losses include the electrical resistance to the flow of electrons in the fuel cell components as well as the protonic resistance to the flow of protons in the membrane.

The mathematical expression for the Ohmic losses was presented in chapter three and it was modelled using the formula:

$$\eta_{ohmic} = -i(R^{electronic} + R^{protonic}) \qquad \textbf{3-44}$$

This was simply represented as:

$$\eta_{ohmic} = R_i i \qquad \textbf{6-2}$$

Where 'R_i' represents the total resistance in (Ωcm^2), which causes the linear variation of the cell potential with current density. The other contributors to 'R_i' are the charge transfer resistance of the hydrogen electrode reaction and mass transport resistances, predominantly at the oxygen electrode which is more so when air is used as the cathode reactant [21].

The losses due to the contact resistance at the interface between the electrode plates and the GDLs is the main reason for this loss when the membrane is not properly compacted between the electrodes, this type of loss has not been considered as a specific reason for voltage losses in most of the modelling studies on fuel cells, but Berning *et al.* [20] incorporated this into their model assuming that the voltage loss due to contact resistance has an Ohmic nature, i.e.

$$\eta_{contact} = i r_{contact} \qquad \textbf{6-3}$$

Where '$r_{contact}$' is an assumed contact resistance in (Ωcm^2) that varies with the porosity of the gas diffusion layer and the contact area between the electrode plate and the gas diffusion layer.

The linear region in the properly fitted Nafion® membrane curve is quite smooth and allows for a wider range of operation. In this range; the voltage lies between 0.4 – 0.55V while the current density ranges between 100 – 400 mA/cm^2.

Both values of current density and voltage are rather low for practical applications, but we have to take into consideration the following factors:

- The fuel cell is operated at temperatures below 323K (50°C), which means that the performance of the fuel cell is lower than optimum. It is well known that higher temperatures promote the kinetics of the chemical reaction, thus increasing the value of the exchange current density; 'i_o', of the oxygen reduction reaction (ORR); and consequently reducing the activation losses at the cathode. However, in the case of PEM fuel cells utilising perfluorinated membranes, the water content in the membrane cannot be maintained at

temperatures higher than 373K (100°C), the optimum operating temperature being 343-353K (70 – 80 °C), otherwise, the membrane loses its protonic conductivity. This also has an effect on increasing the reference potential ' E^o ', although the Nernst equation shows a decrease in potential with the increase in temperature, but actual experiments indicate the contrary [17]. Operating at higher temperatures also improves the membrane conductivity, because a higher temperature leads to a higher diffusivity of the hydrogen protons in the electrolyte membrane, thereby reducing the membrane resistance[20], they also help in removing the product water from the fuel cell which improves the performance by allowing the gases to reach the electrodes more easily.

- The fuel cell in this study is operated at ambient pressure. The effect of pressure on the fuel cell was discussed in chapter 3 and it was shown that the performance is improved at higher pressures figure (3-4). However, there is a combined effect of pressure and temperature on the inlet gas composition. As shown by [20], the effect of temperature on the inlet gas composition is much stronger than at elevated pressures. At 353K (80°C) for atmospheric pressure, almost 50% molar of the incoming cathode side gas stream consists of water vapour, and only around 11 % is oxygen, this is shown in figure (6-7) below:

Figure 6-7 Molar inlet composition of the cathode side gas stream as a function of temperature and pressure [20]

- Using air as the oxidant gas reduces the concentration of oxygen on the cathode which reduces the performance of the fuel cell due to the reduced activity of oxygen. Achieving a good performance; high power density and high energy efficiency, with air at 1 atm. is a major challenge [21]. The results of this work confirm that this problem can be overcome only by the optimization of the structure and the composition of the electrodes.
- Another important factor is the use of untreated stainless steel as the electrode material. It has been discussed in chapter (2.3.1) that common stainless steels such as SS304 or SS316 could compose an oxidative layer under fuel cell environment which would increase the electrical resistance and decreases the output of the cell. While this surface oxide layer protects the metal and stops the corrosion from progressing further beneath the surface, it forms an electrically insulating interfacial layer [36]. This issue has to be investigated more thoroughly in future work.

- ***Concentration Losses***

Considering the figures again, it is noted that the Nafion membrane in the fuel cell design under consideration, curve with asterisk in figure (6-6), exhibits the pseudo-linear behaviour at currents up to 400 *mA/cm*), but above this current density the PEMFC shows a rapid drop in the cell voltage due to mass transport limitations, this is attributed to mass–transport rate of oxygen to the catalyst sites reaching a limit, represented by the third term in equation (6-1). The main reason for this phenomenon is the presence of liquid water in the cathode backing layer (GDL) which blocks the gas pores and limits the transport of oxygen and, hence, reduces the cathode and fuel cell performance.

6.4.3. Effect of Trough Dimensions and Flow Velocity

The effects of flow velocity were studied through the variation of the channel dimension. Results are shown in figure (6-8):

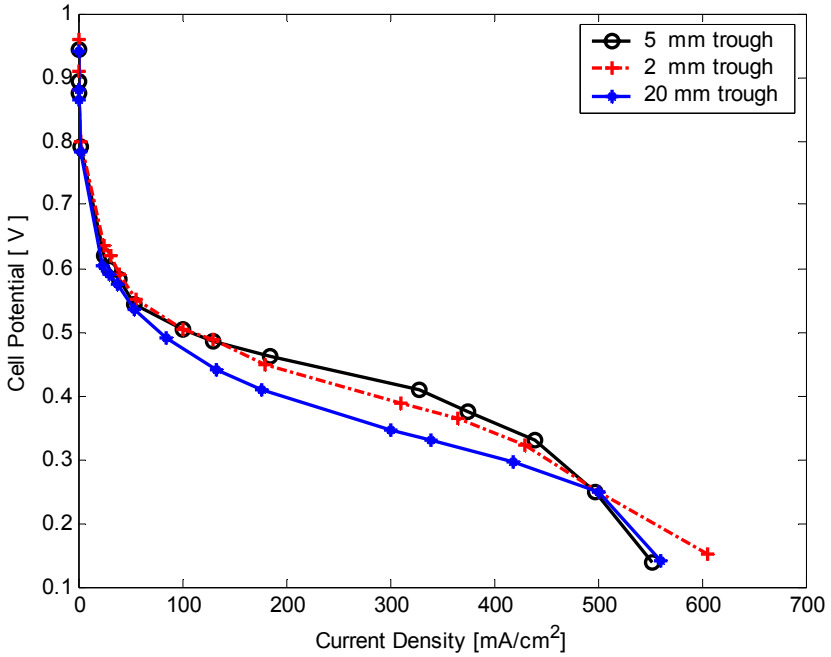

Figure 6-8 Comparison of fuel cell performances with various flow channel (trough) dimensions. Operating conditions: 333K and 91% RH on anode and cathode sides.

In the experiment; three different thicknesses of trough were used: 2 mm, 5 mm and 20 mm. The electrode plates were 5 mm hole diameter, 0.55 mm thick *SS316* meshed stainless steel plates. Hydrogen and air were used at fairly high stoichiometric ratios of 2 and 3 respectively. Same type of Nafion® 117 membrane and GDL were used.

Under the same flow conditions, the height of the trough determines the velocity of flow; thus the residence time of the reactant gases in the reaction chamber. This has a direct effect on the concentration of the reactant gases and water removal from the gas diffusion electrodes especially at the cathode.

As seen from figure (6-8), the slight variations in the open circuit voltage (*OCV)* for the three types of trough are less than 5% of the measurements, which are within the resolution of the experimental measurements. It was discussed in chapter (3.3.2) that the (*OCV)* does not depend on the geometric parameters of the fuel cell, but rather, it is an indication of the electrochemical activity of the species and represents the potential difference that exists between the electrode and the electrolyte; as the reaction produces an electron on the electrode at one potential and a positive ion, H^+ in the electrolyte at another potential.

Throughout the three experiments, the partial pressures of the reactant gases and the operating temperature of the fuel cell were maintained the same, as well as the same type of membrane which was Nafion® 117, hence it can be concluded that the trough dimension does not have any significant impact on the *OCV*.

As we proceed further along the *x*-axis, a dramatic drop in voltage due to activation losses is noticed. The activation overpotential is mainly due to the slow kinetics of the (ORR) at the cathode. The use of air as a reactant instead of pure oxygen increases the activation overvoltage. The presence of impurities in the fuel cell, the composition of an oxidative layer on the surface of the stainless steel electrode and the reduced catalyst activity result in the reduction of the exchange current density and hence; the high activation overpotential. In the present case, the oxidation of stainless steel and the relevant oxidation currents inside the fuel cell increase the losses due to activation.

It is noticed from the graph that the three curves follow the same path up to $50 mA/cm^2$ when the curve for the *20 mm* trough starts to display larger activation losses. Obviously, the velocity of flow in this trough is lowest, and the residence time of reactant gases is longest. This results in the reduction of the concentration of oxygen in the air stream passing through the reaction chamber due to the slow movement of the reactant air, and hence reduction in the partial pressure of oxygen at the cathode side, which reduces its activity and, in accordance to the Nernst equation, increases the activation overpotential.

The case at the hydrogen side is different because hydrogen was not diluted, but; in either case, the activation losses at the anode side are negligible when compared to those at the cathode side.

Upon observing the effects of the Ohmic overpotential, it is noticed that the three curves have fairly the same slope, a slight variation is observed in the case of the 5 mm trough, but this lies within the resolution of the experiment.

Concentration losses start to be observed beyond 400 mA/cm^2 in the cases of the *20 mm* and *5 mm* troughs, but they are less obvious in the case of the *2 mm* trough. This is mainly due to mass transport limitations caused by the presence of water condensate in the GDLs and membrane.

Water content in the membrane is determined by the balance between water production and three water transport processes: electro-osmotic drag of water, associated with proton migration through the membrane from the anode to the cathode side; back diffusion from the cathode; and diffusion of water to/from the oxidant/fuel gas streams. Without control, an imbalance between production and removal rates of water can occur. This results in either dehydration of the membrane, or flooding of the electrodes; both phenomena have a very detrimental effect on performance and fuel cells have to be carefully designed to avoid the occurrence of either phenomenon [20].

In the case of the *20 mm* trough, the velocity of flow is slower and not sufficient to carry as much water product of the fuel cell as the other configurations, hence; water accumulates in the gas diffusion layer at the cathode side and prevents air from reaching the active sites in the membrane, hence increasing the effect of concentration losses.

The *2 mm* trough shows a slightly better performance than the *20 mm* trough, but still not satisfactory for practical applications. The velocity of flow in this case is much higher than the *20 mm* trough which implies better water removal, due to this, the drop in voltage due to concentration losses is not observed in this case. The slight improvement in performance is attributed to the short residence time of the gases in the fuel cell as compared to the other trough configurations. The high velocity of flow prevents the gas from penetrating into the membrane and tends to push the gases

through the fuel cell along the surface of the membrane, hence; having an effect similar to the concentration phenomenon.

6.4.4. Effect of Mesh Configuration

The mesh type of the electrode plates has a significant effect on the performance of the fuel cell; this is due to the distribution of gases and the flow shape across the gas diffusion layer and the membrane. Through the experimental work, it was observed that the larger the mesh size, the better the operation of the fuel cell.

Figure (6-8) presents a comparison between three types of meshed stainless steel plates. The fuel cells were operated under the same operating conditions and using the same type of Nafion® membranes. The performance was also compared to a parallel channel graphite plate fuel cell. The performance of the stainless steel fuel cell is, from a qualitative point of view, lower than the graphite fuel cell, most likely due to the formation of an oxidative layer on the stainless steel under the acidic conditions of the fuel cell environment.

The activation part of the fuel cell characteristic curve is shown in figure (6-9), the sharp drop in voltage due to activation losses is obvious in the case of the meshed plates as compared to the graphite plate, the reasons for this drop were discussed elsewhere, but the point to observe here is that the larger the mesh holes, the less activation losses are observed. This can be attributed to the activity of the gases which is enhanced by more exposure of the GDL to the gas stream. The activation losses are more predominant on the air side of the fuel cell, and hence more exposure to air is necessary at this side.

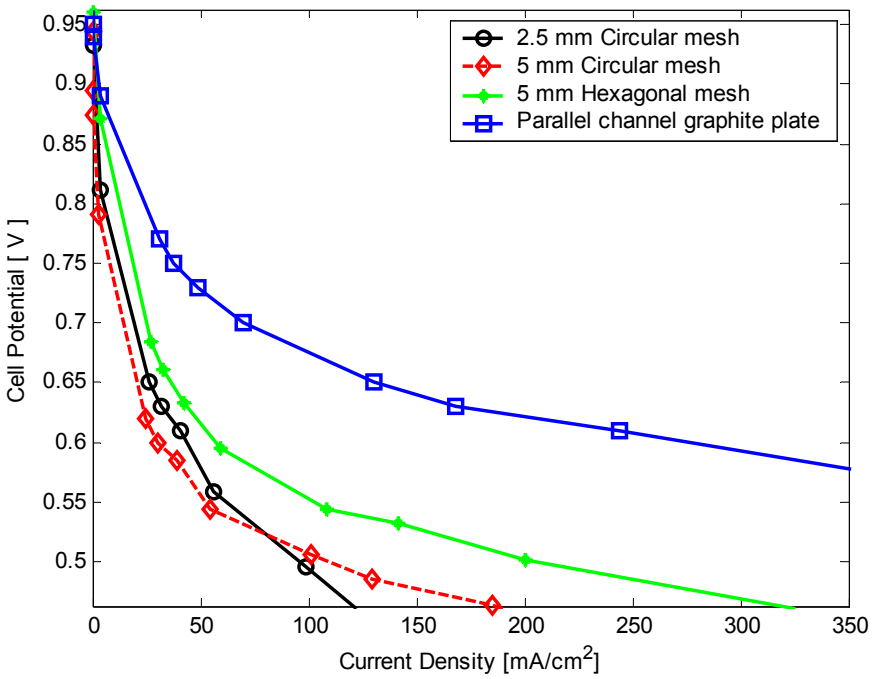

Figure 6-9 The activation region of the polarisation curves for various meshed stainless steel electrode fuel cells and one fuel cell based on parallel channel graphite plates as electrodes, all fuel cells were operated open ended at atmospheric pressure, Operating conditions at 92% RH, 373k and 20 mm trough thickness.

The linear portion of the three curves, as seen in figure (6-9) has almost the same slope as the graphite based fuel cell. This is an indication that the voltage losses due to resistances in the fuel cell are not more pronounced than those in the graphite plate fuel cell, but the poorer performance is mainly due to the initial shift of the curve to the low voltage region due to activation losses.

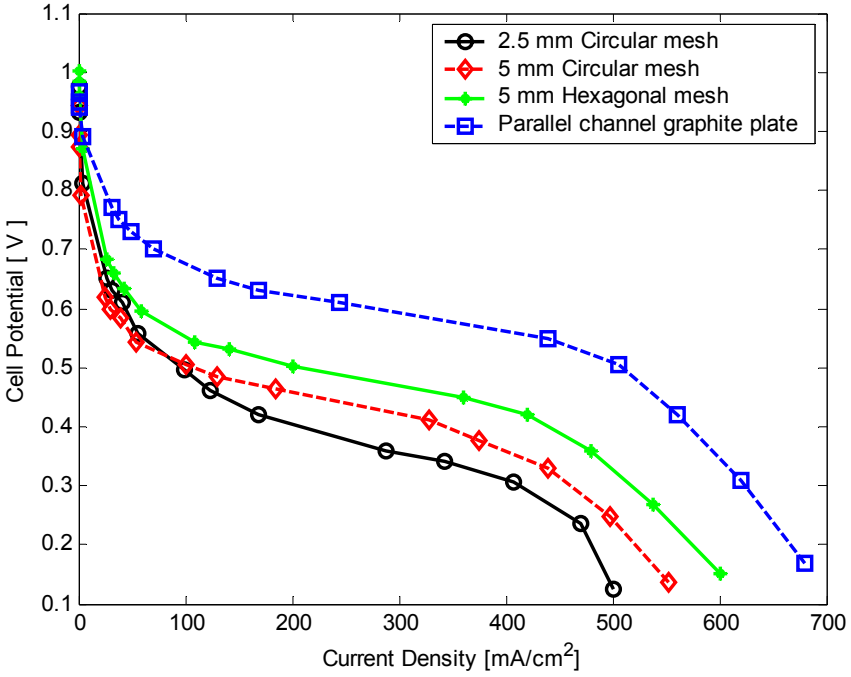

Figure 6-10 Polarisation curves for various meshed stainless steel electrode fuel cells and one fuel cell based on parallel channel graphite plates as electrodes, all fuel cells were operated open ended at atmospheric pressure, operating conditions at 92% RH and 373k and 20 mm trough thickness.

The stainless steel based fuel cells under investigation start to indicate concentration losses at nearly the same current density, which is around 400 mA/cm^2. Due to the fact that the three cells had the same trough dimensions, the flow velocity was similar, and hence the cells had similar water removal characteristics. Obviously, the more the GDL is exposed to the gas stream, the more water will be removed, and hence the less concentration effects will be observed. This is an additional advantage of the larger exposure area of the membrane and GDL, but has to be balanced with the mechanical support requirements of the membrane, which also reflect on the contact resistance of the fuel cell.

In the case of the graphite based fuel cell, concentration losses are observed at around 500 mA/cm^2, which are due to water condensation in the flow channels and GDLs. The performance of the graphite fuel cell is expected to be better than observed when operating at higher pressure and temperature.

6.4.5. Fuel Cell Efficiency

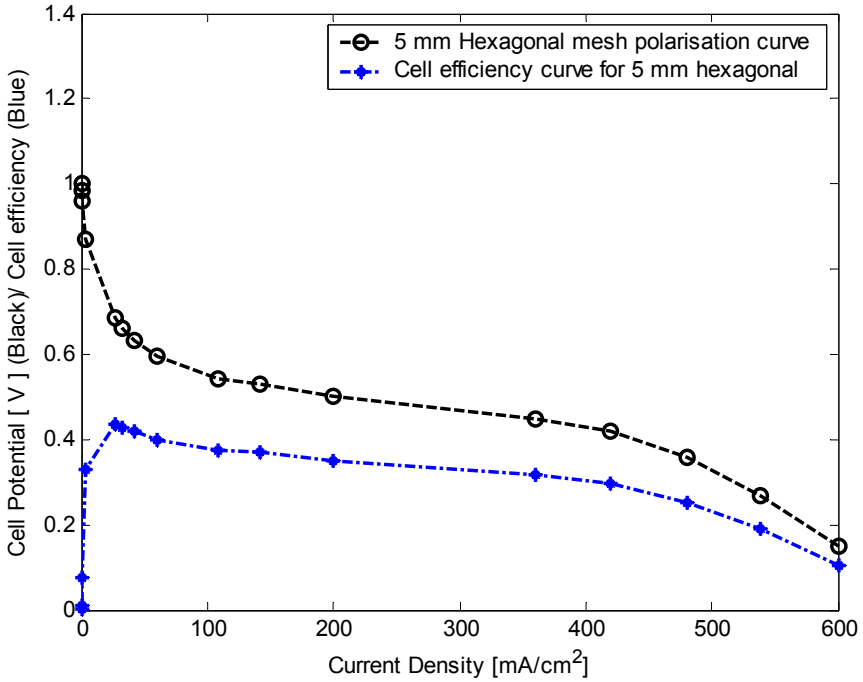

Figure 6-11 Polarisation and efficiency for a 316 SS stainless steel hexagonal meshed plate fuel cell. Operating conditions: 92% RH, 373K and 20mm trough thickness.

The efficiency of the hexagon mesh plate is presented in figure (6-11); it is observed that the best efficiency occurs at very low current densities, however, the practical operating range lies between *100 - 400 mA/cm*^{2}, with an efficiency of *25-30%*; which is in the same range as IC engines.

6.5. DEVELOPMENT OF A COMPUTATIONAL FUEL CELL MODEL

With the increased computational power of today's computers, more detailed simulations are possible. Thus, complex equations such as the Navier-Stokes equation can be solved in multiple dimensions, yielding accurate descriptions of such phenomena as heat and mass transfer and fluid and two-phase flow throughout the fuel cell.

The types of models that do this analysis are based on a finite-element framework and are termed Computational Fluid Dynamics (CFD) models. CFD models are widely available through commercial packages, some of which include an electrochemistry module. As mentioned earlier in the literature review, almost all of the CFD models are based on the Bernardi and Verbrugge model [56], in other words, the incorporated electrochemical effects stem from their equations, such as their kinetic source terms in the catalyst layers and the use of Schlogl's equation for water transport in the membrane [81].

Detailed experimental work to test and optimise the proposed fuel cell design was presented in the previous parts of this chapter. In this section, numerical studies based on CFD modelling will be carried out to test the validity of this technique and to optimize the performance of the fuel cell by varying different geometric parameters such as; meshed plate hole diameter, gas channel height (trough thickness), meshed-hole shape and location of inlet and outlet-holes and their diameters for air and fuel.

Flow direction of fuel at the anode side is taken opposite to that of the reactant gas at the cathode side. For numerical modelling; a three dimensional (3D) fully coupled numerical model was used, which resolved coupled transport phenomena of PEM fuel cell and accounted for voltage losses at the catalyst layer as well as convention and diffusion of different species in the channels and in the porous gas diffusion layer (GDL).

Figure (6-12) is a schematic overview of a 3D CAD model of the proposed PEM fuel cell design, where fuel cell domain is divided into seven layers: gas channels, perforated gas flow channels and gas diffusion layers for both anode and cathode and a sandwiched membrane electrode assembly comprising the membrane and catalyst layers

between both anode and cathode. Gas inlets and outlets are shown in the drawing where gas is supplied along the centre line of the trough from a vertical direction.

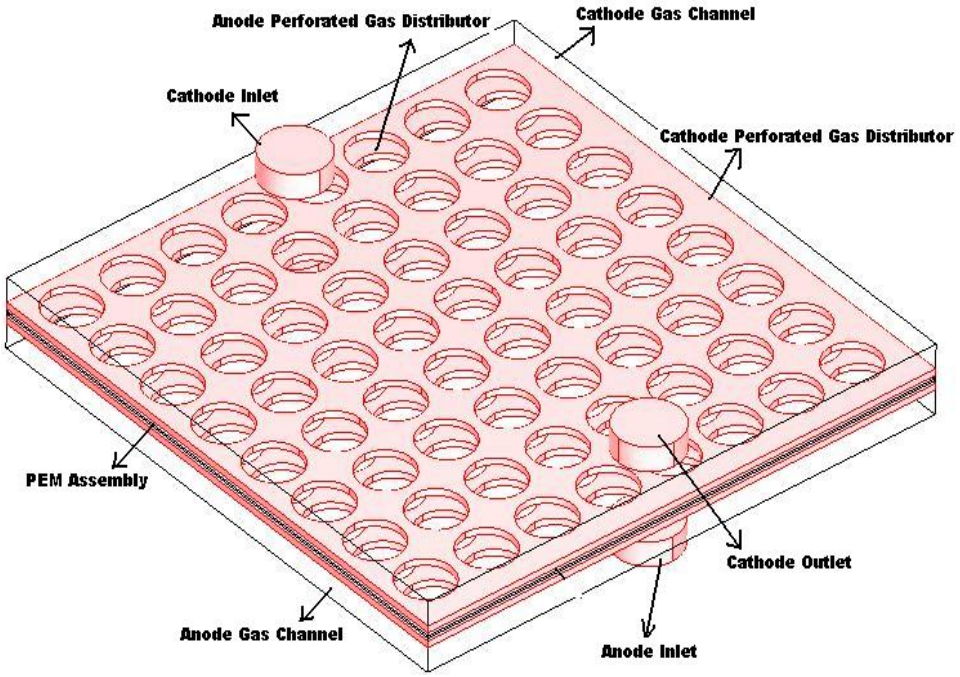

Figure 6-12: Schematic 3D CAD Model of the PEM fuel cell domain with perforated type gas flow channels

Physical and electrochemical phenomena that take place inside the PEM fuel cell are represented by the following mathematical model, where the analyses are based on the solution of conservation of mass, momentum, species and charge transport.

Flow characteristics in the gas channels, perforated gas flow channels and porous media are obtained by solving the following form of the steady state Navier-Stoke equation [82]:

$$\nabla.\mu(\nabla u + (\nabla u)^T) + \rho(u.\nabla)u + \nabla p = 0 \qquad \textbf{6-4}$$

Where ' μ ' is the viscosity (kg $m^{-1}s^{-1}$), ' u ' is the velocity vector (m s^{-1}), ' ρ ' is density (kg/m^3), 'p' is pressure (Pa) and 'T' is the temperature (K). The species balance is described by the divergence of mass flux through diffusion and convection, using the following steady state mass transport equation [63]:

$$\nabla\left[-\rho w_i \sum_{j=1}^{N} D_{ij}\left\{\frac{\nabla M}{M_j}\left(\nabla w_j + w_j \frac{\nabla M}{M}\right)+\left(x_j - w_j\right)\frac{\nabla p}{p}\right\}+ w_j \rho u\right]=0 \qquad \textbf{6-5}$$

Where subscripts '*i*' denotes oxygen at the cathode and hydrogen at the anode sides, while '*j*' is the water vapour in both cases, '*D'* is the diffusion coefficient (m^2/s), '*M'* is the molecular weight ($kg.mol^{-1}$), *'x'* is the mole fraction, '*w*' is the mass fraction and 'ρ' is the gas mixture density calculated by;

$$\rho = \frac{\sum x_i . Mw_i}{RT} p \qquad \textbf{6-6}$$

Diffusion coefficients of reactant species 'D_{ij}' in non porous media is calculated by the Maxwell Stefan diffusion equation, which accounts for coupling between multi species components and binary mass diffusion coefficients [63].

$$D_{ij} = \frac{T^{1.75}(1/M_i + 1/M_j)^{1/2}}{\rho((\sum_k V_{ki})^{1/3} + (\sum_k V_{kj})^{1/3})^2} \qquad \textbf{6-7}$$

In this equation '*T*' is the temperature in Kelvin, '*p*' is the pressure in atm, *'M_i'* is the molecular weight of species *'i'*, and *'V_{ki}'* is the atomic diffusion volume. Temperature variation plays an important role on flow behaviour in the gas channel which consequently affects the overall performance of the PEM fuel cell, therefore; to make such analysis more realistic, variation of temperature is taken into consideration by most of numerical modellers.

In order to account for the geometric constraints of the porous media, the diffusivities are corrected using the following Bruggemann correction formula [82, 83]:

$$D_{ij}^{eff} = D_{ij} \times \varepsilon^{1.5} \qquad \textbf{6-8}$$

Where 'D^{eff}' is the effective diffusion coefficient; that takes into account the additional drag by irregular shapes; and the actual length of the pores in the GDL, in comparison to a bundle of straight parallel capillaries with constant diameter. 'D_{ij}' is the diffusion coefficient and 'ε' stands for porosity of the GDL.

During the operation, the H^+ protons move from the anode to the cathode and pull water molecules with them, this is known as the electro-osmotic drag effect. Physically, the water transport rate through the membrane from anode to cathode by electro-osmotic drag is computed as:

$$\dot{m}_{H_2O} = \frac{n_d M_{H_2O}}{F} R_{cat} \qquad \textbf{6-9}$$

Where '$\dot{m}_{H_2O}$' is the water transport rate through the membrane from anode to cathode, 'M_{H_2O}' is the molecular weight of water in the gas mixture, *kg/kmol*, 'R_{cat}' is the *Volumetric current density*, (Am^{-3}) and 'n_d' is the drag coefficient and is proposed by Springer *et al*. [57] for Nafion membrane as follows:

$$n_d = \frac{2.5}{22}\lambda \qquad \textbf{6-10}$$

Where 'λ' is the membrane water content; expressed as the number of water molecules per ionic group (mol H_2O / mol SO_3^-) defined as[9]:

$$\lambda = \frac{n(H_2O)}{n(SO_3^-)} \qquad \textbf{6-11}$$

Where: $n(H_2O)$ is the H_2O mole number, $n(SO_3^-)$ the sulfonic group mole number, 'λ' *can be* calculated with:

$$\lambda = \frac{EW_m . c_w}{\rho_m . M_{H_2O}} \qquad \textbf{6-12}$$

Where 'ρ_m' is the dry membrane density and 'EW_m' is the equivalent molecular weight of the membrane.

Membrane water diffusivity 'D_w' and water concentration 'C_w' across the membrane are calculated by[20, 84]:

$$C_w = \frac{\rho_{m,dry}}{M_{m,dry}}\lambda \qquad \textbf{6-13}$$

$$D_w = D_\lambda \exp\left[2416\left(\frac{1}{303}-\frac{1}{T}\right)\right] \quad \textbf{6-14}$$

Where:

$D_\lambda = 10^{-10}$ $\lambda<2$

$D_\lambda = 10^{-10}(1+2(\lambda-2))$ $2 \le \lambda \le 3$

$D_\lambda = 10^{-10}(3-1.67(\lambda-3))$ $3 \le \lambda \le 4.5$

$D_\lambda = 1.25\times10^{-10}$ $\lambda > 4.5$

An electrical potential difference exists between the catalyst and electrolyte to drive the transfer current, keeping the electrochemical reaction continuous. The current passing through the catalyst layer can be decomposed into two parts; electrode potential at the anode and electrode potential at the cathode, which interact through electrochemical reactions. Current fluxes at the cathode boundary between the electrode and the membrane are calculated using the following current conservation form [85]:

$$n.\left(-\sigma_{s,eff}\nabla\phi_s\right) = i_c \quad \textbf{6-15}$$

$$n.\left(-\sigma_{m,eff}\nabla\phi_s\right) = -i_c \quad \textbf{6-16}$$

Where 'σ' is the effective conductivity and 'ϕ' is the potential. Subscripts '*s*' and '*m*' denote the gas distribution along the electrode and membrane respectively, while '*eff*' stands for the effective value. At the anode side this current flux is calculated by:

$$n.\left(-\sigma_{s,eff}\nabla\phi_s\right) = -i_a \quad \textbf{6-17}$$

$$n.\left(-\sigma_{m,eff}\nabla\phi_s\right) = i_a \quad \textbf{6-18}$$

To express the relation between the local transfer current densities '*j'*, the reactant concentrations 'C_i' and the phase potentials, the following form of Butler-Volmer equation is used [82]:

$$i_c = i_c^{ref}\left(\frac{C_{O_2}}{C_{O_2}^{ref}}\right)\left[\exp\left(\frac{\alpha_a F}{RT}\eta_{act,c}\right)-\exp\left(-\frac{\alpha_a F}{RT}\eta_{act,c}\right)\right] \quad \textbf{6-19}$$

$$i_a = i_a^{ref}\left(\frac{C_{H_2}}{C_{H_2}^{ref}}\right)^{\frac{1}{2}}\left[\exp\left(\frac{\alpha_a F}{RT}\eta_{act,a}\right) - \exp\left(-\frac{\alpha_a F}{RT}\eta_{act,a}\right)\right] \quad \textbf{6-20}$$

Where 'i_o' is the exchange current density, 'n' is the number of electrons per mole of reactant, 'η' is the local over-potential and 'R' is the universal gas constant. 'α' is the is the transfer coefficient, which is determined empirically to be between 0 and 1, subscripts 'c', 'a' stand for cathode and anode respectively.

The activation over potential 'η_{act}' at the cathode is calculated by [85]:

$$\eta_{act,c} = \phi_s - \phi_m - V_{oc} \quad \textbf{6-21}$$

And, from the Nernst law, the open circuit voltage (OCV); 'V_{oc}'is given by [85]:

$$V_{oc} = 0.2329 + 0.0025T \quad \textbf{6-22}$$

During these analyses; the catalyst layer is treated as a thin boundary interface, where sink and source terms for the reactants are implemented.

The consumption of reactant species and the production of water and heat are modelled as sink and source terms in the catalyst layers. The mass consumption rate of oxygen per unit volume is given by [86]:

$$S_{O2} = -\frac{M_{O2}}{4F} i_c \quad \textbf{6-23}$$

The production of water is modelled as a source term based on the local current density [86]:

$$S_{H2O} = \frac{M_{H2O}}{2F} i_c \quad \textbf{6-24}$$

At the anode catalyst layer, hydrogen is consumed to produce electrons and protons. The consumption of hydrogen is given by [86]:

$$S_{H2} = -\frac{M_{H2}}{2F} i_a \quad \textbf{6-25}$$

In this model, heat generation is assumed to be predominantly due to the electrochemical reactions, and Ohmic heating is not currently accounted for.

Furthermore, heat generation from the anode reaction is negligible compared to the cathode reaction, and hence only cathodic heat generation is considered [86]:

$$\dot{q} = \left[\frac{T(-\Delta s)}{n_e F} + \eta_{act} \right] i_c \qquad \textbf{6-26}$$

Where 'T' is the local temperature, 'Δs' is the entropy of the chemical reaction, 'n_e' is the number of electrons transferred per mole of hydrogen, 'η_{act}' is the activation overpotential and 'F' is Faraday's constant.

6.6. NUMERICAL SETUP

The above mentioned governing equations with their relative boundary conditions were solved using a commercial multi-physics numerical solver 'COMSOL version 3.4'. Convergence criterion is performed on each variable and the procedure is repeated until the convergence is obtained. All these numerical analyses were carried out considering the following assumptions:

a) Single Phase model as liquid is assumed in vapour form at operating conditions.

b) Isotropic and Homogenous electrodes and membranes.

c) Membrane impermeable for species in the gas phase.

d) Negligible contact resistance.

e) Negligible membrane swelling.

f) Catalyst layer assumed as a reactive boundary layer.

g) Steady state operation under fully humidified conditions is assumed.

h) The model assumes operation under ideal heat and water management ensuring the membrane remains fully humidified.

i) Both humidified air and hydrogen behave as ideal gases and since the characteristic Reynolds number in the gas channels are low; the flows there are assumed laminar.

j) Ohmic heating is neglected, as heat generation is assumed to be predominantly associated with the cathodic electrochemical reaction.

k) The potential drop in the electrode plate is negligible, since stainless steel is a good conductor.

For the numerical model, velocity, temperature and species mass fractions are specified as inlet boundary condition at both cathode and anode sides, while pressure and convective flux are specified as outlet boundary conditions. Continuous boundary is assumed between the gas channel and the perforated gas distributor open channels, while for the closed channels, wall is used as a boundary condition. At the diffusion layer/catalyst layer interface, there are phase changes between gaseous and dissolved species; therefore continuity is assumed at this interface. Solid phase potential is arbitrarily set to zero as a reference at the anode, while at the cathode; solid potential is set to ($E_{cell} - E_{rev}$) where ' E_{cell} ' is the desired cell potential and ' E_{rev} ' is the reversible cell potential.

6.7. MODEL VALIDATION

This section presents the numerical analyses in comparison with the experimental data to validate the performance of the proposed fuel cell design at various geometric conditions. The electrochemical properties and physical properties for various regions of the fuel cell together with the operating conditions are specified in table (6-1) below:

Table 6-1 Model parameters and physical properties of fuel cell components

Parameter	***Value***
Operating Temperature (*K*)	*333*
Inlet Pressure (*kPa*)	*100*
H_2, Air Flow Rate (*kg/sec*)	*1.57E-05*
Relative Humidity, Air	*70%*
Relative Humidity, H_2	*92%*
Oxygen/Nitrogen ratio in air	*0.21/0.79*
GDL and Catalyst Porosity	*0.5*
GDL and catalyst Permeability (m^2)	*1.76 e-11*
Exchange Current Density, Anode (A/m^2)	*1.00E04*
Exchange Current Density, Cathode (A/m^2)	*1.00E-03*
Concentration Parameter, Anode	*0.5*
Concentration Parameter, Cathode	*1*
Transfer Coefficient, Anode	*0.5*
Transfer Coefficient, Cathode	*0.5*
Membrane Ionic Conductivity (*S/m*)	*17.69*
GDL and Catalyst layer Conductivity (*S/m*)	*120*
Membrane Thickness (*m*)	*180 e-6*
GDL Thickness (*m*)	*200 e-6*
Perforated Plate Thickness (*m*)	*0.55 e-3*
Active Area of the PEM Fuel Cell (cm^2)	*25*

To validate this design concept, a comparison study was done with the results obtained form a conventional design fuel cell and the current design approach. A good comparison was found between experimental and numerical results obtained for the perforated design configuration, which validated the numerical model. A satisfactory performance comparison was found between results obtained from the conventional graphite-made parallel flow channels fuel cell and PEM fuel cell with perforated stainless steel flow channels.

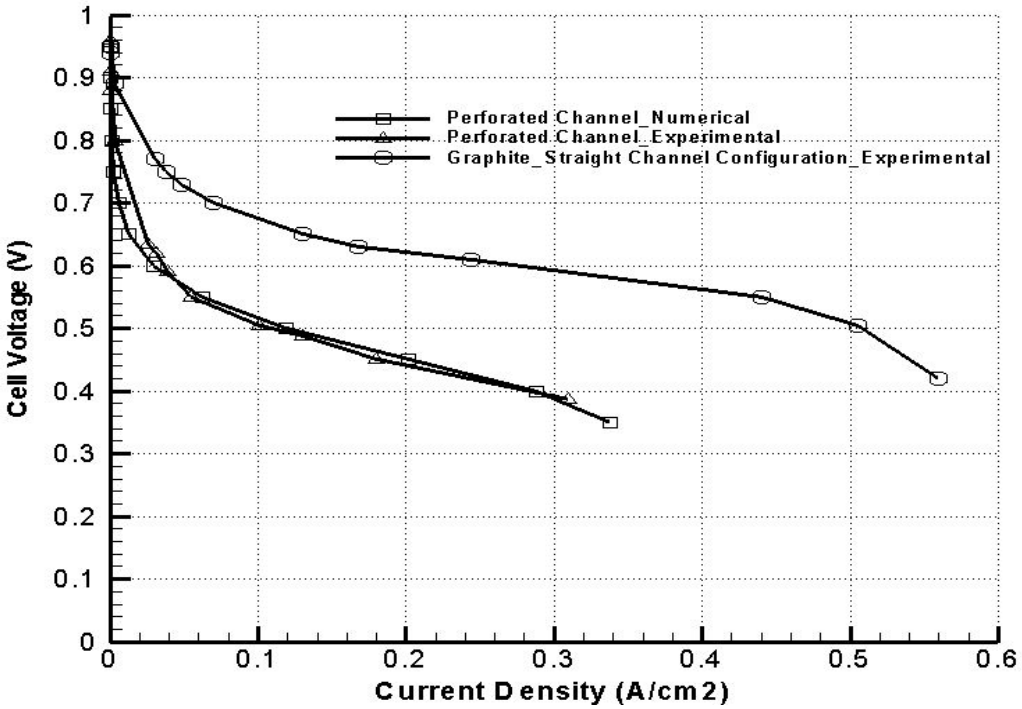

Figure 6-13: Comparison of PEM fuel cell performance polarization curves for Conventional parallel channel graphite gas distributor and perforated Stainless Steel gas distributor at T = 333K

For both these experimental models; Nafion® 117 membrane was used. As discussed earlier, although graphite is a suitable material for electrodes in PEM fuel cell, but on the other hand it's manufacturing and handling cost is considerably high as compared to stainless steel.

The low performance in the case of stainless steel; figure (6-13) is attributed to differences in material properties, particularly electrical conductivity and high fractional losses offered by the perforated holes.

Stainless steel is an alloy made up of 17% to 21% Chromium, 7.5% to 11.5% Nickel, 0.01% to 0.164% Carbon and 50% to 70% Iron. Apart from Carbon; these are transition metals[10] [87] which have their valence electrons, or the electrons they use to combine with other elements, present in more than one shell of the atom. This is the reason why they often exhibit several common oxidation states and consequently can react with the catalyst and reaction gases in the fuel cell. This reaction has a double effect: on one hand, it damages the performance of the fuel cell because an amount of catalyst and reactant gases will be consumed in the oxidation reaction, and on the other hand oxide layers are formed on the electrode plates which increase their electrical resistance hence increase Ohmic voltage losses in the fuel cell. This also has a dramatic effect on the exchange current density due to the side reactions taking place in the fuel cell and the reduced catalytic activity due to these reactions which explains the sharp activation losses at low current densities.

Another factor which is likely to have contributed to the performance losses in the fuel cell is the frictional loss due to flow past the perforated holes in the meshed

[10] The 38 elements in groups 3 through 12 of the periodic table are called "transition metals". As with all metals, the transition elements are both ductile and malleable, and conduct electricity and heat. The interesting thing about transition metals is that; their valence electrons, or the electrons they use to combine with other elements, are present in more than one shell. This is the reason why they often exhibit several common oxidation states. There are three noteworthy elements in the transition metals family. These elements are iron, cobalt, and nickel, and they are the only elements known to produce a magnetic field.

stainless steel electrodes. However, this factor can be controlled by certain geometric variations which can be discussed as a future investigation.

Keeping the material properties aside, further analyses were carried out to explore the performance of the current design approach by varying different geometric parameters in order to enhance and optimize its performance.

For this purpose; the distribution of reactant species and their potential impact on water management and current density in this particular design approach are taken into consideration. Figure (6-14) shows the distribution of oxygen and water mole fractions along the cathode catalyst layer at T = 333K and V = 0.4 Volt.

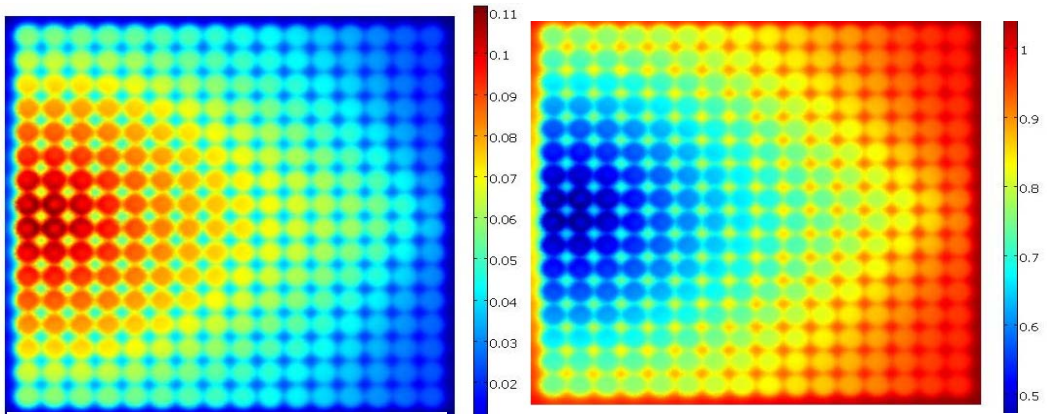

Oxygen mole fraction **Water mole fraction**

Figure 6-14: Distribution of oxygen and water mole fractions along the cathode catalyst layer at T = 333K, RH = 95% and V = 0.4V.

Results in figure (6-14) indicate a high value of oxygen mole fraction just below the cathode inlet, but at the corners and below the solid areas of the meshed plate; a considerably lower amount of oxygen is present, which could lead to potential water flooding in these areas. Moreover, the figure shows that reactant air is not covering the whole area of the fuel cell domain at the cathode side and is following the shortest possible path from inlet to outlet, which indicates that certain design changes can be undertaken to improve the distribution of reactant air to cover more surface area of the fuel cell domain.

The following sections present the numerical and experimental results on the effects of varying certain geometric parameters such as: perforation-hole diameter, shape, gas channel height and inlet and outlet-hole locations on the performance of the proposed PEM fuel cell design.

6.7.1. Effect of Trough Height Variation

Gas channel (trough) height of a PEM fuel cell is an important factor that could influence the behaviour of the reactant species in the fuel cell domain. Any change in gas channel height affects its boundary layer features, consequently changing the residence time of the reactant species and their distribution along the fuel cell domain. Increase in residence time improves the rate of diffusion of the species along the fuel cell domain.

Two different gas channel heights *2 mm* and *5 mm* were analysed to study the flow behaviour and its impact on the overall performance of the fuel cell. Figure (6-15) shows the results obtained from experimental and numerical studies at T = 333K:

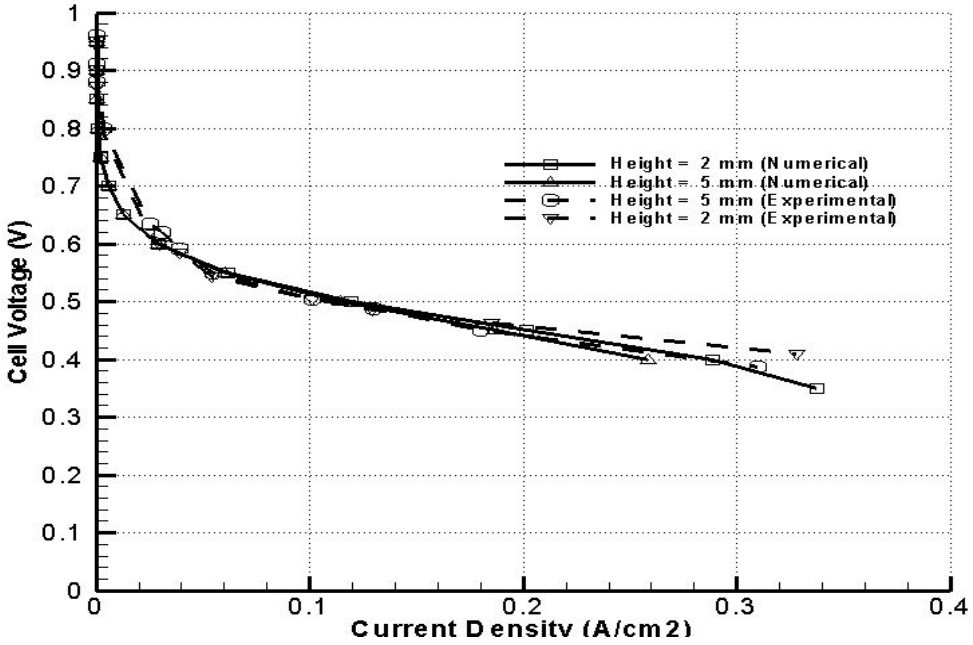

Figure 6-15: Effect of Gas channel height on the performance of the fuel cell, at T = 333K, RH = 95% and V = 0.4V. Comparison between experimental and numerical results.

From the figure above; it is observed that increasing the channel height slightly reduces the performance of the fuel cell. Such decrease in performance is attributed to the change in residence time of the reactant gases in the flow domain as a result of increasing the cross sectional area in the direction of flow. With the increase in gas channel height, the velocity of the gas flow decreases, hence the residence time of the gases increases, which is supposed to improve the performance of the fuel cell, however, this effect is counterbalanced by the decrease in the thickness of the boundary layer due to increasing the trough thickness, which results in a decrease in shear stresses and enhances the flow of the gases through the fuel cell. These flow interactions lead to an increase in convective flux and a reduction in diffusive flux of the reactant species.

The relatively low flow velocity and residence time in the case of the thicker trough deteriorate water removal from the fuel cell and lower its performance, while, on the other hand, reducing the trough thickness reduces the residence time of the reactant gases and reduces the amount of oxygen mole fraction along the cathode catalyst layer, thus leading to a change in the electrochemical reaction.

The activation losses in both cases are similar, which indicates that the flow characteristics do not have a direct impact on the activation overvoltages which were attributed predominantly to material characteristics. However, the overall analyses show that increasing the gas channel height slightly reduces the performance of this type of PEM fuel cell.

6.7.2. Effect of Varying Mesh Hole Diameter

To study the effect of perforated hole diameter variation; two different hole diameters *2.5 mm* and *5 mm* were taken into consideration. All the analyses were carried out assuming a constant channel height (trough thickness) of *5 mm*. Figure (6-15) above shows the current density distribution along the cathode catalyst layer for two different perforated type hole diameters.

Results demonstrate that increasing the meshed plate hole diameter increases the surface area of the PEM exposed to the reactant species along the fuel cell domain, which consequently increases the performance of the PEM fuel cell. Increase in mesh

hole diameter also reduces the frictional losses to flow through the holes which leads to an improved distribution of oxygen mole fraction along the cathode catalyst layer, thus resulting in improvement of the electrochemical reaction along the catalyst layer and, to a certain extent, reduction in water flooding.

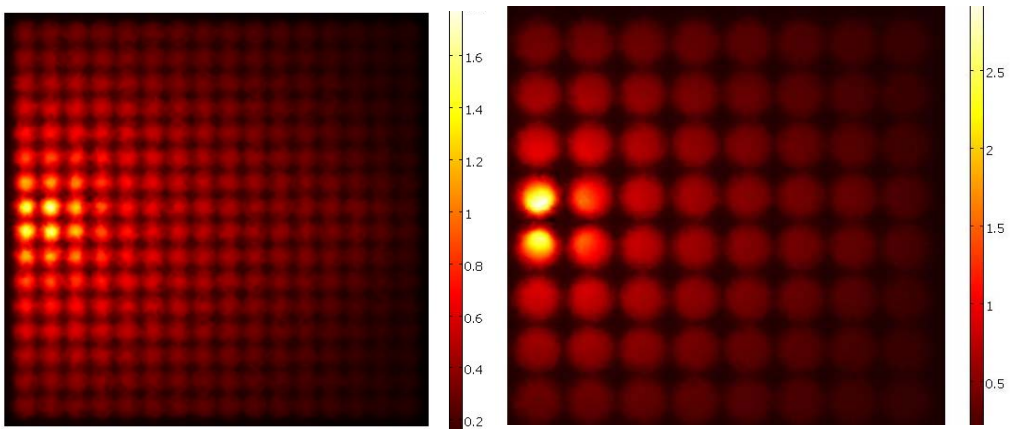

Hole diameter= 2.5 mm, Trough Height = 5mm **Hole diameter = 5 mm, Trough Height = 5 mm**

Figure 6-16: Effect of perforated holes diameter variation on current density distribution along the cathode catalyst layer, at V = 0. 4V, in both cases hole trough height = 5 mm.

A higher value of current density is obtained in the case of the *5 mm* diameter holes as compared to the *2.5 mm* diameter holes, this has a direct impact on the activation kinetics and should result in improving the activation overvoltage.

As an overall assessment, the results show that increasing the perforated hole diameter enhances the performance of this type of PEM fuel cells.

6.7.3. Effect of Varying Inlet Hole Diameter

During the above analyses, the outlet holes diameter was kept constant at *6mm*. In the following discussion, three different inlet hole diameters 6, 8 and 10 mm are analysed to see their impact on the overall performance of the fuel cell, while the outlet hole diameter is kept constant at *6 mm*.

Results confirm that with the increase of inlet hole diameter, a significant improvement in reactant species distribution along the fuel cell domain is observed. This improvement is attributed to the increase of the mass flow rate of reactant species at the inlet. During this study; outlet diameter is kept constant to increase the residence time of the flow in the fuel cell domain, so that a better diffusive concentration of reactant species can be obtained. For all these analyses perforated gas distributor with mesh hole diameter of 5 mm and gas channel height of 2 mm is taken into consideration.

Figure (6-17) illustrates the distribution of *Oxygen mole fraction* along the fuel cell domain at V = *0.5 Volts*. A more uniform gas distribution is obtained in the case of larger hole, with oxygen covering the full domain of the fuel cell, while in the case of the *6 mm* inlet hole, the remote corners seem to be poorly covered with the reactant gas.

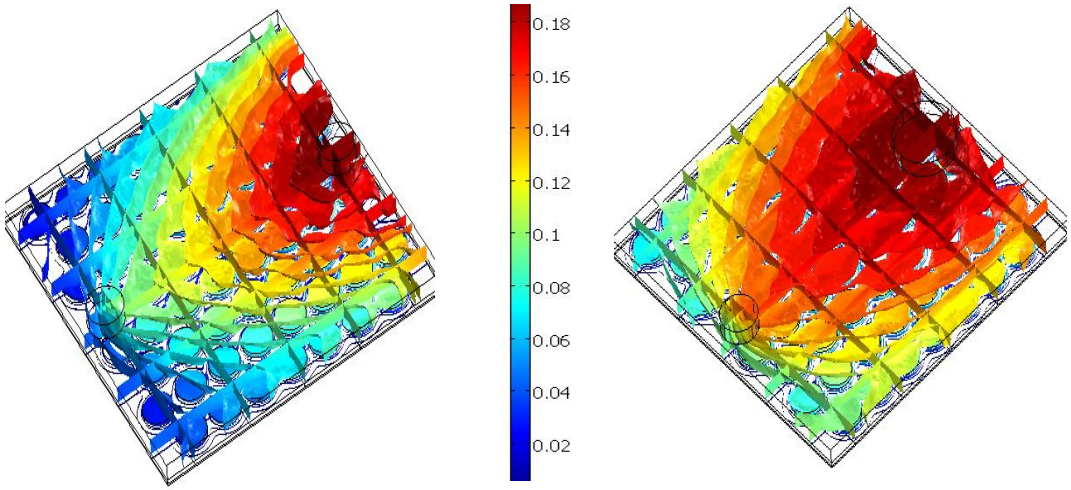

Inlet Diameter = 6 mm **Inlet Diameter = 10 mm**

Figure 6-17: Oxygen Mole fraction distribution along the cathode side of PEM fuel cell

The following figure (6-18) illustrates the distribution of *Water mole fraction* along the fuel cell domain at V = 0.5 Volts.

Water accumulation is observed at the remote corners in the case of the *6mm* hole, while much better water removal is achieved with the *10 mm* inlet hole.

Figure (6-18) clearly shows that increasing the inlet hole diameter improves the distribution of oxygen along the fuel cell domain, and simultaneously reduces the water flooding and improves the overall performance of the fuel cell.

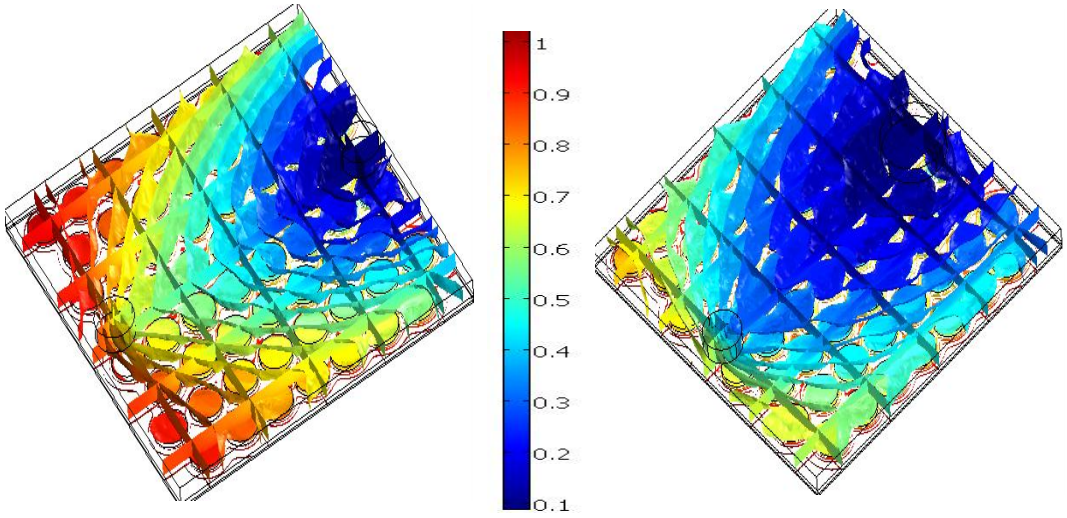

Inlet Diameter = 6 mm **Inlet Diameter = 10 mm**

Figure 6-18: Water Mole fraction distribution along the Cathode side of the PEM fuel cell

The effect of inlet hole diameter variation on the overall performance of the fuel cell is revealed in figure (6-19) below. It is observed that the activation overpotential is not significantly influenced by the change in the inlet hole diameter, which confirms again that the reaction kinetics are not dependant on flow characteristics.

A significant increase in Ohmic losses is observed as the inlet hole diameter reduces, this is attributed to frictional losses to the flow of reactant gases through the meshed plate holes and the low diffusivity of the plate as the meshed plate holes reduce in diameter. This is, in fact, contrary to expectations, as it is expected that the electrical resistance to the flow of electrons will increase as the meshed plate hole sizes increase, because the electrons will be transported through a larger distance in the GDL instead of the stainless steel plate, but it seems that this loss is compensated by the increase in the exposed area of the membrane to the reactant gases.

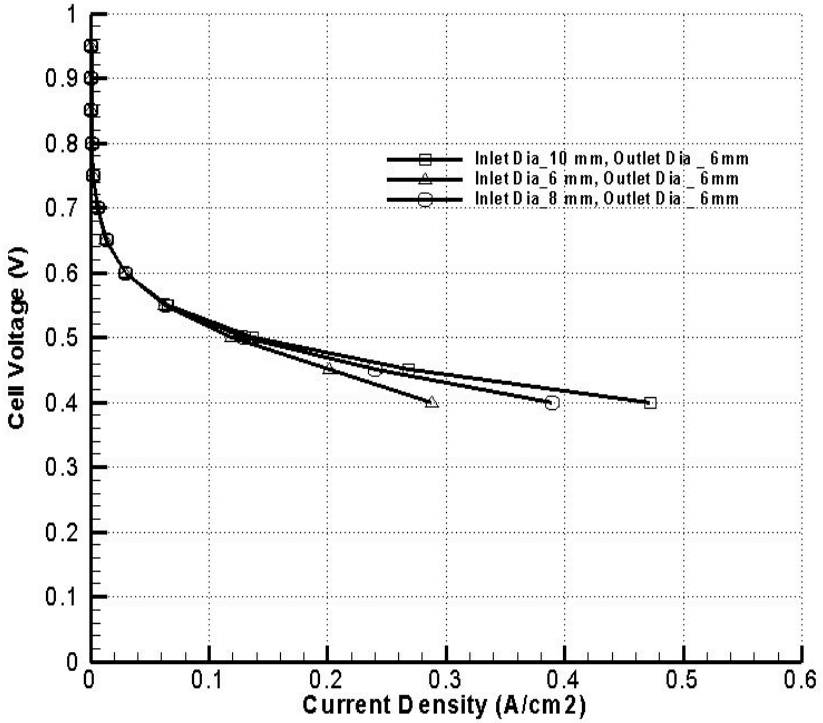

Figure 6-19: Effect of inlet hole diameter variation on the performance of PEM fuel cell, for perforated hole diameter = 5 mm and Trough height = 2 mm

6.7.4. Effect of Varying Gas Supply/Exit Port Location

The analyses presented earlier provided an insight of the effects of different geometric parameter variations on the overall performance of the fuel cell. For all these analyses; inlet and outlet holes for reactant gases (Air and Hydrogen) were assumed at the centre of the gas flow channel, the distance between the inlet and outlet ports are the shortest in this case. Analyses of flow behaviour in this case showed that the reactant species did not cover the maximum area of the fuel cell domain, as they followed the shortest possible path.

In this section, the effects of the locations of inlet and outlet holes on the overall performance of the fuel cell will be investigated. For this purpose two configurations were taken into consideration; in the first case both the inlet and outlet were assumed at the centres of the gas channel domains, while in the second case; they were diagonally opposed with counter- flows at the cathode and anode.

Figure (6-20) illustrates the oxygen mole fraction distribution at the cathode side of the fuel cell in both cases. It is observed that the distribution of the reactant gas is improved and is more uniform in the case of the diagonally opposed supply ports. Furthermore, water condensate is more likely to accumulate around the remote corners in the case of the centrally located holes due to the poor oxygen flow in these regions, which will result in an increase in concentration losses, as the gases will not be able to reach the reaction sites due to the presence of water.

Residence time of the gases is shorter in the case of centre holes, which has a negative influence on performance, but this is counterbalanced by the improvement in water removal due to the high velocity of flow as compared to the diagonally opposed supply ports.

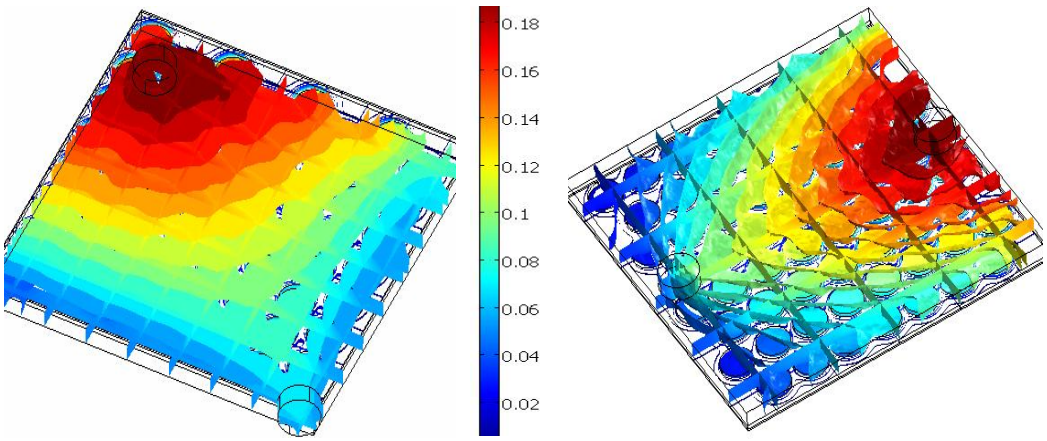

Diagonally opposed gas ports Centre-line gas ports

Figure 6-20: Effect of Inlet/Outlet hole locations on oxygen mole fraction distribution

Comparing the polarisation curves for both cases, figure (6-21), it is observed that the change in the supply port locations did not affect the activation and Ohmic regions of the polarisation curves. However, it is noted that the limiting current density tends to occur much earlier in the case of centre ports as compared to the diagonally opposed ports. This is attributed to the accumulation of water in the fuel cell domain in areas which are poorly covered with the flow of air especially in the case of the central supply port location. At this current density the performance of the fuel cell starts to

drop due to mass transfer limitations resulting from the presence of water in the fuel cell.

This is a very important point which was considered in the final design of the fuel cell so as to optimise the performance. The gas supply ports were offset from the centre of the active area in opposite directions, in the final design of the fuel cell presented earlier in chapter 4 of this report, so as to enhance better distribution of reactant gases.

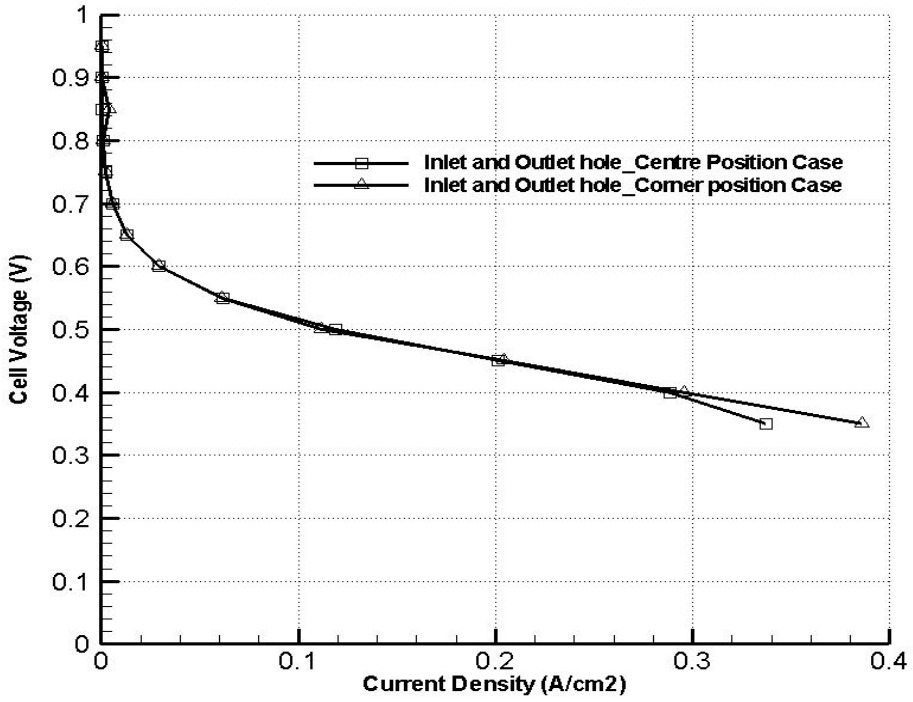

Figure 6-21: Effect of inlet and outlet holes locations on PEM fuel cell performance for perforated hole diameter = 5 mm, Trough height = 2 mm, Inlet and outlet diameter = 6 mm. concentration losses start to be observed at 0.3 A/ cm^2 current density in the case of the central holes.

6.8. COMPARISON OF FUEL CELL PERFORMANCE TO PUBLISHED FUEL CELL DATA

A detailed comparison with experimental results from the literature can only be made on a qualitative basis, since the exact operating conditions of the various experiments are not fully reported and it is quite certain that the design conditions are different.

In figure (6-22), experimentally obtained polarization curves by Kim *et al*. [69] are reproduced. The experiments were conducted with pure hydrogen at the anode side and air at the cathode side. It is fair to assume that the results were obtained from a fuel cell of a conventional design based on graphite plate electrodes and Nafion® membranes without detailed specifications.

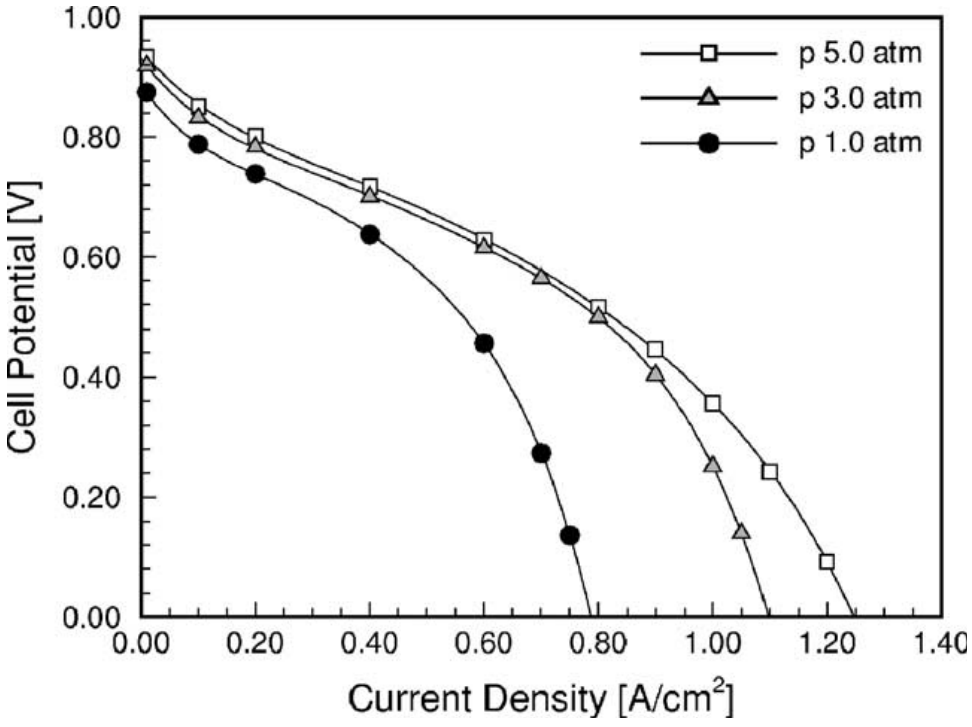

Figure 6-22 Experimentally obtained polarization curves for various cathode side pressures at a temperature of 343K and a stoichiometric flow ratio of (1.5). The experiments were conducted with pure hydrogen at the anode side and air at the cathode side, the exact details of the experiments such as the cell geometry are not known [20, 69]

Comparing the results presented earlier for the fuel cell design proposed in this study to the fuel cell performance reported by Kim *et al*.[69], the general behaviour of the two fuel cells is similar as far as the gradual decrease in performance with current density is concerned; the three regions of the fuel cell characteristic curves, namely; activation, Ohmic and concentration losses regions are observed in both cases.

The *OCV* in the case of the proposed fuel cell is higher than the one reported by Kim et al. It was discussed earlier that the open circuit voltage that is established at the platinum electrode in an oxygen containing environment has been shown to be a mixed potential. The mixed potential is set up due to the simultaneous occurrence of the oxygen reduction reaction (ORR) and the process of platinum oxidation. Impurity oxidation may also contribute to the observed OCV, which could have been the case in the published experimental results and resulted in reducing the *OCV* [67].

The activation overvoltage is not as sharp in the published results, the reasons for the sharp drop in potential due to activation has been discussed thoroughly elsewhere, and it is clear from this comparison that it is the major drawback in the proposed fuel cell performance.

However, qualitative agreement between the performance of the proposed fuel cell design and published experimental results indicates that the proposed design with the necessary improvement on the basis of optimization is feasible for industrial implementation.

Chapter 7 CONCLUSIONS AND RECOMMENDATIONS FOR FURTHER WORK

7.1. CONCLUSIONS

A novel fuel cell design with a new approach in design methodology has been presented in this work. Two major components of the fuel cell; namely; the electrode plates and the channel troughs have been redesigned and manufactured, together with a test apparatus and gas conditioning unit equipped with a data acquisition system to facilitate testing the performance of the new fuel cell design and to compare the performance to conventional fuel cell design and published fuel cell experimental data.

The theoretical background including a mathematical model of the fuel cell performance has been developed and used in a LabView® application to simulate fuel cell performances and to be used as a curve fitting model for the experimental results. The mathematical model was developed to perform a parametric study of fuel cell performance under various operating conditions such as temperature, pressure and reactant gas volume.

For the first time; the effects of irreversibilities on fuel cell behaviour is presented using a mathematical argument involving the polytropic index. Furthermore, a comprehensive formula for the efficiency of the fuel cell based on interpolated values of the main parameters affecting the performance of the fuel cell and incorporating the internal current effects which are usually ignored in most of the published work has been developed and presented in this thesis.

In order to optimise the proposed design, a computational modelling and simulation study using CFD techniques has been carried out to test the validity of this technique and to improve the performance of the fuel cell by varying different geometric parameters such as meshed plate hole diameter, shape, location of inlet and outlet-hole diameters for the reactant gases and gas channel (trough) height.

A three dimensional (3D) fully coupled numerical model was used, which resolved coupled transport phenomena of PEM fuel cell and accounted for voltage losses at the catalyst layer as well as convention and diffusion of different species in the channels and in the porous gas diffusion layer (GDL). The model was solved using a commercial multi-physics numerical solver 'COMSOL version 3.4'.

The results of the experiments and the numerical studies indicated the potential of the new fuel cell design for practical implementation, and for considerable reductions in fuel cell cost.

The following conclusions have been drawn through this exercise:

1. There is considerable potential for the improvement of the fuel cell design to reduce the cost and improve the performance through the use of common materials and design techniques.

2. The modular design presented in this thesis presents a simple fuel cell design which reduces the cost of production and compares to the performance of the state of the art fuel cells.

3. The trough size is an important design parameter as it reflects on the water management and gas distribution issues in the fuel cell operation. The *5 mm* trough proved to be more effective in maintaining good performance of the fuel cell due to its moderate flow velocity convenient for water management, and its suitability for maintaining high power density of the fuel cell.

4. The mesh size selection has to compromise between two major parameters: maximising the area of the membrane exposed to reactant gases so as to promote the reaction and enhance water removal from the fuel cell and to provide enough support and current collector along the surface of the membrane. The *5 mm* diameter hole meshed plate was found better than other meshed plates used in this study to satisfy both requirements; however, more investigations are required to find the best configuration of the electrode material.

5. The numerical modelling and simulation study revealed the following important findings:

- Increase in perforated hole diameter improves the performance of the fuel cell due to the increase in the effective surface area of the fuel cell covered by reactant species, which leads to an improvement in the electrochemical reaction and reduction in water flooding in the fuel cell domain.

- Increase in perforated holes diameter reduces the frictional losses to flow when passing through the perforated holes due to the reduction in side wall shear stress, which results in less friction to flow passing through the holes, and hence reduces Ohmic losses in the fuel cell.

- Increase in gas channel (trough) height affects the wall shear stresses in the gas channel domain and consequently affects the performance of the fuel cell. With the increase of gas channel height; the residence time of flow in the gas channel decreases which increases the convective flux and reduces the diffusive flux. Furthermore, it reduces the potential for water removal from the fuel cell and leads to a decrease in fuel cell performance.

- Increase in inlet holes diameter of PEM fuel cell increases the effective mass flow rate, which leads to an increase in fuel cell performance.

- Change in inlet/outlet holes location from centre to opposite corners with counter flow of reactant gases improves the reactant species distribution along the fuel cell domain and enhances water removal, thus effectively improves the performance of the fuel cell.

7.2. RECOMMENDATIONS FOR FURTHER WORK

The subject of this thesis 'Design and manufacturing of a (PEM) fuel cell' was an ambitious programme; as the intention originally was to design and manufacture a full scale 5kW (PEM) fuel cell for stationary application with the aim of acquiring the technology of making a full scale fuel cell including the polymer electrolyte, the catalyst layer, electrodes and gas distributors. The ultimate aim of the programme was to acquire the technology of making a fully working fuel cell and understanding the mechanism of performance loss and ways to decreasing these losses.

A good deal of work has been spent in the area of designing and synthesising a polymer electrolyte membrane based on polyimide materials and the synthesis of a platinum catalyst, but as the work progressed it became clear that the proposed programme was beyond the scope of this study because the membrane science is a complex issue by itself, and the work on the catalyst needs more resources and dedication.

In view of these limitations this research programme had to be modified without significantly altering its objective or scope. The emphasis was then shifted to the design and manufacturing of a *100W* modular fuel cell which can be used as a building block for a larger fuel cell stack for stationary applications; with focus on understanding the factors affecting the performance and reliability of the (PEM) fuel cell.

Therefore, it is felt that further research is still needed to carry the fuel cell research started in this thesis forward, the following suggestions point out areas of possible research:

1. The fuel cell electrodes chosen in this study were SS316 stainless steel meshed plates. The performance of the fuel cell did not compare to fuel cell results reported in the open literature. Further work has to be performed to improve the material used either by the use of different coating materials or by using different material alloys which can withstand the acidic environment of the fuel cell and maintain an electrical conductivity higher than the conductivity of graphite.
2. Understanding the physics of voltage losses in the fuel cell and the mechanisms which cause these losses to occur is very necessary to improve fuel cell performance. Hence, the use of advanced electrochemical techniques to determine the electrochemical behaviour of the fuel cell such as: cyclic voltammograms (*CV*) used to determine the active surface area of the membrane, and other electrochemical diagnostic tools are very important and recommended in further research work.

3. Fuel cell testing is very crucial in the development of fuel cells; hence special attention should be paid to the development of testing techniques and facilities. The fuel cell test unit built through this project offers a good base for fuel cell testing equipment and should be tackled as a dedicated project to develop a comprehensive test station. Special attention has to be paid to flow measurement as the potential users of the fuel cell would be interested to know the actual cost of using a fuel cell in terms of fuel input and power output.
4. The polyimide membrane offers a good candidate for fuel cell application. It has the potential to reduce cost and simplify the design of the fuel cell by operating at temperatures higher than 100°C. The work started in this research on the membrane did not reach a mature stage and more optimisation and characterisation work still needs to be done.
5. The numerical modelling and simulation study developed for present research and described in this thesis presents a good start for a more reliable and advanced simulation study of fuel cell performance.

References

1. Energy Information Administration, *World Marketed Energy Use by Fuel Type, 1980-2030 website :http://www.eia.doe.gov/oiaf/ieo/highlights.html.* [Cited 04.05.09] in *International Energy Annual* 2005.
2. Bhinder, F.S.*, et al.*, *Parametric Study of the Combined Fuel Cell-Gas Turbine Power Plant.* ASME Conference Proceedings, 2006. **2006** (42398): p. 703-711.
3. National Sunflower Association. *SUNFLOWER WEEK IN REVIEW*. 2009 [cited 18 May 2009]; Available from: www.sunflowernsa.com.
4. Hadjipaschalis, I., A. Poullikkas, and V. Efthimiou, *Overview of current and future energy storage technologies for electric power applications.* Renewable and Sustainable Energy Reviews, 2009. **13**(6-7): p. 1513-1522.
5. Nikam, V.V. and R.G. Reddy, *Copper alloy bipolar plates for polymer electrolyte membrane fuel cell.* Electrochimica Acta, 2006. **51**(28): p. 6338-6345.
6. S. Mandal, P.S., D. Roy, R. Chaudhari, M. Sastry, *A new method for the synthesis of hydrophobized, catalytically active Pt nanoparticles.* Chem. Commun., 2002. **24**: p. 3002-3003.
7. Wilson M. S., V.J.A., Gottesfeld Sh., *Low Platinum Loading Electrodes for Polymer Electrolyte Fuel Cells Fabricated Using Thermoplastic Ionomers.* Electrochemica Acta, 1995. **40**(3): p. 355-363.
8. Genies, C.*, et al.*, *Soluble sulfonated naphthalenic polyimides as materials for proton exchange membranes.* Polymer, 2001. **42**(2): p. 359-373.
9. Gunduz, N., *Synthesis and Characterization of Sulfonated Polyimides as Proton Exchange Membranes for Fuel Cells*. 2001, Virginia Polytechnic Institute and State University: Blacksburg. p. 311.
10. W.Grove, Philos.Mag., 1839. **3**(14): p. 127.
11. Hoogers, G., *Fuel Cell Technology Handbook*. 1 ed, ed. G. Hoogers. Vol. 1. 2003, London: CRC Press. 240.
12. Kordesch, K. and G. Simader, *Fuel cells and their applications*. 1996, Deerfield Beach, FL: VCH.
13. Fuel Cell Bus Club. 2008 [Cited 2008 14 May 2008]; Available from: http://www.fuel-cell-bus-club.com/index.php?module=pagesetter&func=viewpub&tid=1&pid=158.
14. The Register. *Fuel Cell Demonstrator Airplane*. 2008. UK.
15. Wang, L.*, et al.*, *A parametric study of PEM fuel cell performances.* International Journal of Hydrogen Energy, 2003. **28** (11): p. 1263-1272.
16. Balkin, A.R., *Modelling A 500w Polymer Electrolyte Membrane Fuel Cell*, in *Faculty of Engineering*. 2002, University of Technology: Sydney.

17. J. Larmine, A.D., *Fuel Cell Systems Explained*. 2 ed. Vol. 1. 2003, Chichester: John Wiley & Sons Ltd.

18. Kumar, A. and R.G. Reddy, *Effect of channel dimensions and shape in the flow-field distributor on the performance of polymer electrolyte membrane fuel cells.* Journal of Power Sources, 2003. **113** p. 11-18.

19. Janssen, G.J.M. and M.L.J. Overvelde, *Water transport in the proton-exchange-membrane fuel cell: measurements of the effective drag coefficient.* Journal of Power Sources, 2001. **101** (1): p. 117-125.

20. Berning, T. and N. Djilali, *Three-dimensional computational analysis of transport phenomena in a PEM fuel cell--a parametric study.* Journal of Power Sources, 2003. **124** (2): p. 440-452.

21. Wakizoe, M., O.A. Velev, and S. Srinivasan, *Analysis of proton exchange membrane fuel cell performance with alternate membranes.* Electrochimica Acta, 1995. **40** (3): p. 335-344.

22. efunda. [cited 18.05.09]; Available from: http://www.efunda.com/glossary/units/units--electric_conductivity--siemens_per_centimeter.cfm.

23. Savadogo, O., *Emerging membranes for electrochemical systems: Part II. High temperature composite membranes for polymer electrolyte fuel cell (PEFC) applications.* Journal of Power Sources, 2004. **127** (1-2): p. 135-161.

24. Faure S., *Sulphonated polyimides, membranes and fuel cell* 2001, Centre National de la Recherche Scientifique (Paris Cedex, FR): USA.

25. Mehta, V. and J.S. Cooper, *Review and analysis of PEM fuel cell design and manufacturing.* Journal of Power Sources, 2003. **114** (1): p. 32-53.

26. A. K. Shukla*, et al.*, *A 5 W liquid-feed solid polymer electrolyte direct methanol fuel cell stack with stainless steel.* Applied Electrochemistry, 1999. **29** p. 120-132.

27. E. Atonolini*, et al.*, *Physical and morphological characteristics and electrochemical behaviour in PEM fuel cells of PtRu/C catalysts.* J Solid State Electrochem, 2001. **5**: p. 131-140.

28. Mandal, S.*, et al.*, *A new method for the synthesis of hydrophobized, catalytically active Pt nanoparticles.* Chem. Commun., 2002. **24**: p. 3002-3003.

29. Zhang, Y.J.*, et al.*, *Synthesis and characterization of carbon black supported Pt-Ru alloy as a model catalyst for fuel cells.* Catalysis Today, 2004. **93-95**: p. 619-626.

30. Andreaus, B.*, et al.* (2003) *Investigation Of Gas Diffusion Layers Of Polymer Electrolyte Fuel Cells By X-Ray Tomographic Microscopy*. Paul Scherer Institute Scientific Report 2003 Volume VII **Volume**,

31. Wikipedia. [Cited 18.05.09]; Available from: http://en.wikipedia.org/wiki/Anisotropy.

32. Djilali, N. and B.R. Sivertsena, *Computational modelling of polymer electrolyte membrane (PEM) fuel cells: Challenges and opportunities.* Energy, 2007. **32**: p. 269-280.

33. Mathias, M.*, et al.*, *Diffusion media materials and characterisation*, in *Handbook of Fuel Cells – Fundamentals, Technology and Applications*, W. Vielstich, H.A. Gasteiger, and A. Lamm, Editors. 2003 John Wiley & Sons, Ltd.: London. p. 517-537.

34. Zhang, F.Y., S.G. Advani, and A.K. Prasad, *Performance of a metallic gas diffusion layer for PEM fuel cells.* Journal of Power Sources, 2008. **176** (1): p. 293-298.

35. Moreira, J.*, et al.*, *Dependence of PEM fuel cell performance on the configuration of the gas diffusion electrodes.* Journal of new material systems, 2002. **5**: p. 173-175

36. Li, X. and I. Sabir, *Review of bipolar plates in PEM fuel cells: Flow-field designs.* International Journal of Hydrogen Energy, 2005. **30** (4): p. 359 - 371.

37. Kumar, A. and R.G. Reddy, *Materials and design development for bipolar/end plates in fuel cells.* Journal of Power Sources,, 2004. **129** (1): p. 62-67.

38. Tawfik, H., Y. Hung, and D. Mahajan, *Metal bipolar plates for PEM fuel cell--A review.* Journal of Power Sources, 2007. **163** (2): p. 755-767.

39. Wang, H. and J.A. Turner, *Ferritic stainless steels as bipolar plate material for polymer electrolyte membrane fuel cells.* Journal of Power Sources, 2004. **128** (2): p. 193-200.

40. Wang, H., M.A. Sweikart, and J.A. Turner, *Stainless steel as bipolar plate material for polymer electrolyte membrane fuel cells.* Journal of Power Sources, 2003. **115** (2): p. 243-251.

41. T.V. Nguyen and M.W. Knobbe, *A liquid water management strategy for PEM fuel cell stacks,.* J. Power Sources, 2003. **114** p. 70-79.

42. Staschewski, D. and Z.M, *Hydrogen- Air PEMFC operation with extraordinarily low gas pressures and internal humidification, conception and experimental prototype stack.* International Journal of Hydrogen Energy, 1999. **24**: p. 543-548.

43. F.Liu*, et al.*, *Development of novel self humidifying composite membranes for fuel cells.* Journal of Power Sources 2003. **124** p. 81-89.

44. Murphy, O., G. Duncan, and D. Manko, *High power density proton exchange membrane fuel cells.* Journal of power sources, 1994. **47**: p. 353-368.

45. H.H. Voss*, et al.*, *Anode water removal: A water management and diagnostic technique for solid polymer fuel cells.* Electrochemica Acta, 1995. **40** (3): p. 321-328.

46. Mennola, T.*, et al.*, *Water balance in a free-breathing polymer electrolyte membrane fuel cell.* Journal of Applied Electrochemistry, 2004. **34** p. 31-36.

47. Santarelli, M.G. and M.F. Torchio, *Experimental analysis of the effects of the operating variables on the performance of a single PEMFC.* Energy Conversion and Management, 2007. **48** (1): p. 40-51.

48. Lin, P.-C., B.Y. Park, and M.J. Madou, *Development and characterization of a miniature PEM fuel cell stack with carbon bipolar plates.* Journal of Power Sources, 2008. **176** (1): p. 207-214.

49. Tori, C*., et al.*, *Advances in the development of a hydrogen/oxygen PEM fuel cell stack.* International Journal of Hydrogen Energy, 2008. **33** (13): p. 3588-3591.

50. Cheddie, D. and N. Munroe, *Review and comparison of approaches to proton exchange membrane fuel cell modelling.* Journal of power sources, 2005. **147** (1-2): p. 72-84.

51. Baschuk, J.J. and X. Li, *Modelling CO poisoning and O2 bleeding in a PEM fuel cell anode.* International Journal of Energy Research, 2003. **27**: p. 1095-1116.

52. J. Amphlett*, et al.*, *Performance Modelling of the Ballard Mark IV Solid Polymer Electrolyte Fuel Cell: I. Mechanistic Model Development.* J. Electrochem. Soc., 1995. **142** (1).

53. Mann, R.F*., et al.*, *Development and application of a generalised steady-state electrochemical model for a PEM fuel cell.* Journal of Power Sources, 2000. **86**(1-2): p. 173-180.

54. AL-Baghdadi, M.A.R.S. and H.A.K.S. AL-Janabi, *Optimization Study of Proton Exchange Membrane Fuel Cell Performance.* Turkish J. Eng. Env. Sci., 2005. **29**: p. 235-240.

55. Al-Baghdadi and M.A.R. Sadiq, *Modelling of proton exchange membrane fuel cell performance based on semi-empirical equations.* Renewable Energy, 2005. **30** (10): p. 1587-1599.

56. Bernardi, D.M. and M.W. Vebrunge, *A mathematical model of the solidpolymer electrolyte fuel cell.* J. Electrochem. Soc., 1992. **139** p. 2477-2491.

57. Springer, T.E. and S. Gottesfeld, *Polymer electrolyte fuel cell model.* J. Electrochem. Soc., 1991. **138** (8): p. 2334-2342.

58. Érdi, P. and J. Tóth, *Mathematical models of chemical reactions: theory and applications of deterministic and stochastic models*. 1989, Manchester Manchester University Press ND.

59. R Bradean, K Promislow , and B Wetton, *Transport phenomena in the porous cathode of a proton exchange membrane fuel cell,".* Numerical Heat Transfer, Part A,, 2002. **42** (2002): p. 121-138.

60. Gurau, V., H.L., and S. Kakac, *Two-dimensional model for proton exchange membrane fuel cells,.* AIChE J, 1998. **44** (11): p. 2410-2422.

61. Coppo, M., N.P. Siegel, and M.R.v. Spakovsky, *On the influence of temperature on PEM fuel cell operation.* Journal of Power Sources, 2006. **159** (1): p. 560-569.

62. Jung, C.-Y., C.-S. Lee, and S.-C. Yi, *Computational analysis of transport phenomena in proton exchange membrane for polymer electrolyte fuel cells.* Journal of Membrane Science, 2008. **309** (1-2): p. 1-6.

63. Wang, C.Y., *Fundamental Models of Fuel cell Engineering.* Chem. Rev., 2004. **104**: p. 4727-4766.

64. Bhinder, F.S., *Design Parameters of a Centripetal Gas Turbine in Non-Steady Flow*, in *Faculty of Engineering*. 1974, University of London: London. p. 319.

65. Berger, C., *Handbook of Fuel Cell Technology*. 1 ed. 1968, Englewood Cliffs, New Jersey: Printice-Hall, Inc. 607.

66. Williams, K.R., *An Introduction to Fuel Cells*. 1966, London: Elsevier Publishing company.

67. Parthasarathy, A*., et al.*, *Temperature Dependence of the Electrode Kinetics of Oxygen Reduction at the Platinum/Nafion[registered sign] Interface---A Microelectrode Investigation.* Journal of The Electrochemical Society, 1992. **139** (9): p. 2530-2537.

68. Hughes, E., *Electrical Technology*. 5th ed. 1981: Longman Group Ltd.

69. Kim, J*., et al.*, *Modelling of proton exchange membrane fuel cell performance with an empirical equation.* J. Electrochem. Soc., 1995. **142** (8): p. 2670-2674.

70. Bevers, D*., et al.*, *Simulation of a polymer electrolyte fuel cell electrode.* J. Appl. Electrochem, 1997 **27**: p. 1254-1264.

71. Nikam, V.V*., et al.*, *Corrosion resistant low temperature carburized SS 316 as bipolar plate material for PEMFC application.* Electrochimica Acta, 2008. **53** (6): p. 2743-2750.

72. Arthur D. Little, I., *Report to Department of Energy, Cost Analysis of Fuel Cell System for Transportation, Ref. No. 49739, SFAA No. DESC02-8EE50526,.* 2001.

73. Padhy, B.R. and R.G. Reddy, *Performance of DMFC with SS 316 bipolar/end plates.* Journal of Power Sources, 2006. **153** p. 125-129.

74. Williams, P.C. and S.R. Collins, *Mechanical design using low-temperature carburization.* JOM Journal of the Minerals, Metals and Materials Society, 2008. **60** (12): p. 27-30.

75. Open University, *T881 Manufacture Materials Design: Block 1: The design activity model*. 2001, Milton Keynes: The Open University.

76. Einsla, B.R., *High temperature polymers for proton exchange membrane fuel cells*, in *Macromolecular science and engineering*. 2005, Virginia Polytechnic Institute and state University: Blacksburg. p. 291.

77. Khandelwal, M. and M.M. Mench, *Direct measurement of through-plane thermal conductivity and contact resistance in fuel cell materials.* Journal of Power Sources, 2006. **161** (2): p. 1106-1115.

78. Incropera, F.P. and D.P.D. Witt, *Fundamentals of Heat and Mass Transfer*, ed. 3. 1990: John Wlley and Sons.

79. Gasteiger, H.A., J.E. Panels, and S.G. Yan, *Dependence of PEM fuel cell performance on catalyst loading.* Journal of Power Sources, 2004. **127** p. 162-171.

80. Wahdame, B*., et al.*, *Design of experiment techniques for fuel cell characterisation and development.* International Journal of Hydrogen Energy, 2008. **1** (14).

81. Weber, A.Z. and J. Newman, *Modeling Transport in Polymer-Electrolyte Fuel Cells.* Chem. Rev., 2004. **104**: p. 4679-4726.

82. Sadiq Al-Baghdadi, M.A.R. and H.A.K. Shahad Al-Janabi, *Parametric and optimization study of a PEM fuel cell performance using three-dimensional computational fluid dynamics model.* Renewable Energy, 2007. **32** (7): p. 1077-1101.

83. Chen, F., M.H. Chang, and C.F. Fang, *Analysis of Water Transport in a Five Layer Model of PEMFC.* jounal of Power source, 2007. **164**: p. 649-658.

84. Motupally, S., A.J. Becker, and J.W. Weidner, *Diffusion of water in Nafion 115 membranes.* J. Electrochem. Soc., 2000. **147** (9): p. 3171.

85. Guvelioglu, G.H. and H.G. Stenger, *Computational fluid dynamics modelling of polymer electrolyte membrane fuel cells.* Journal of Power Sources, 2005. **147**: p. 95-106.

86. Nguyen, P.T., T. Berning, and N. Djilali, *Computational model of a PEM fuel cell with serpentine gas flow channels.* Journal of Power Sources, 2004. **130**(1-2): p. 149-157.

87. http://www.chemicalelements.com/groups/transition.html. *Transition Metals*. 2009 [Cited 01.05.09].

88. Brady, J. and G. Humiston, *General Chemistry, Principles and Structure*. 3rd edition ed. 1982: John Wiley & Sons.

89. Winterbone, D.E., *Advanced Thermodynamics for Engineers*. 1997: Arnold Publishing.

90. Engineers Edge. *Instrumentation, Electrical, Electronic Control Sensing Devices*. 2009 [Cited 30. 04. 09]; Available from: http://www.engineersedge.com/instrumentation/instrumentation_table_content.htm.

91. Engineering Tool Box. *Flow meters*. [Cited 20.08.09]; Available from: http://www.engineeringtoolbox.com/flow-meters-d_493.html.

Bibliography

1. Baird*, et al.*, *Polymer electrolyte membrane fuel cells: opportunities for polymers and composites*. 2003: Virginia Tech. Plastics Engineering.
2. Berger, C., *Handbook of Fuel Cell Technology*. 1 ed. 1968, Englewood Cliffs, New Jersey: Printice-Hall, Inc. 607.
3. Brady, J. and G. Humiston, *General Chemistry, Principles and Structure*. 3rd edition ed. 1982: John Wiley & Sons.
4. Érdi, P. and J. Tóth, *Mathematical models of chemical reactions: theory and applications of deterministic and stochastic models*. 1989, Manchester Manchester University Press ND.
5. Hoogers, G., *Fuel Cell Technology Handbook*. 1 ed, ed. G. Hoogers. Vol. 1. 2003, London: CRC Press. 240.
6. Hughes, E., *Electrical Technology*. 5th ed. 1981: Longman Group Ltd.
7. Incropera, F.P. and D.P.D. Witt, *Fundamentals of Heat and Mass Transfer*, ed. 3. 1990: John Wlley and Sons.
8. J. Larmine, A.D., *Fuel Cell Systems Explained*. 2 ed. Vol. 1. 2003, Chichester: John Wiley & Sons Ltd.
9. Kordesch, K. and G. Simader, *Fuel cells and their applications*. 1996, Deerfield Beach, FL: VCH.
10. Mathias, M.*, et al.*, *Diffusion media materials and characterisation*, in *Handbook of Fuel Cells – Fundamentals, Technology and Applications*, W. Vielstich, H.A. Gasteiger, and A. Lamm, Editors. 2003 John Wiley & Sons, Ltd.: London. p. 517-537.
11. Vielstich, W., A. Lamm, and H. Gasteiger, *Handbook of fuel cells - fundamentals, technology and applications* Vol. 4. 2003: John Wiley & Sons.
12. Williams, K.R., *An Introduction to Fuel Cells*. 1966, London: Elsevier Publishing company.
13. Berlowitz, P.J. and C.P. Darnell, *Fuel Choices for Fuel Cell Powered Vehicles*. 2000, New York: Society of Automotive Engineers.
14. Blomen, L. and M. Mugerwa, *Fuel Cell Systems*. 1993: Plenum Press.
15. Liebhafsky, H.A. and E.J. Cairns, *Fuel Cells and Fuel Batteries, A guide to their Research and Development*. 1968, New York: John Wiley & Sons, Inc.

Appendix A: Thermodynamics of the Electrochemical Energy Conversion

Thermodynamics of the Electrochemical Energy Conversion

For a better understanding of the main factors influencing the fuel cell performance, it is necessary to understand the thermodynamics of the electrochemical energy conversion and the main factors involved in this process.

The main factor determining the performance of the fuel cell is the electrical work that can be obtained from the fuel cell. Hence, it is important to find the relationship between chemical energy content of the fuel that would be released as a result of an electrochemical reaction, in order to determine the maximum electrical energy that can be extracted from a chemical system.

- ***The Second Law of Thermodynamics***

The second law of thermodynamics provides us with a way of comparing the effects of the two driving forces involved in a spontaneous process, namely; changes in energy and changes in entropy.

One statement of the second law is that: "*In any spontaneous process there is always an increase in the entropy of the universe ($\Delta S_{total} \geq 0$); this increase takes into account entropy changes in both the system and its surroundings*":

$$\Delta S_{total} = \Delta S_{system} + \Delta S_{surroundings} \qquad \textbf{(A- 1)}$$

The entropy change that occurs in the surroundings is brought about by the heat added to the surroundings divided by the temperature at which it is transferred. For a process at constant Pressure (P) and temperature (T), the heat added to the surroundings is equal to the negative of the heat added to the system, which is given by 'ΔH_{system}'; thus:

$$Q_{surroundings} = - \Delta H_{system} \qquad \textbf{(A- 2)}$$

Where 'Q' is the *Heat added to the system*.

The entropy change for the surroundings is therefore:

$$\Delta S_{surroundings} = -\frac{\Delta H_{system}}{T} \quad \textbf{(A- 3)}$$

And the total entropy change is:

$$\Delta S_{total} = \Delta S_{system} - \frac{\Delta H_{system}}{T} \quad \textbf{(A- 4)}$$

Or

$$\Delta S_{total} = \frac{\left(T\Delta S_{system} - \Delta H_{system} \right)}{T} \quad \textbf{(A- 5)}$$

This can be rearranged to give:

$$T\Delta S_{total} = \left(T\Delta S_{system} - \Delta H_{system} \right) \quad \textbf{(A- 6)}$$

For a spontaneous change to take place, 'ΔS_{total}' must be a positive number (the second law of thermodynamics), whence, the product '$T\Delta S_{total}$' must also be positive. Thus, for a spontaneous change to take place, the expression **(**$\Delta H_{system} - T\Delta S_{system}$) must be *negative*.

At this point it is convenient to introduce the thermodynamic state function called the *Gibbs free energy (G)*, which is defined as:

$$G = H - TS \quad \textbf{(A- 7)}$$

For a change at constant temperature; '*T*' and Pressure '*P*', we write:

$$\Delta G_{T,P} = \Delta H - T\Delta S \quad \textbf{(A- 8)}$$

From this argument, we see that 'ΔG' must be less than zero for a *spontaneous* process *at constant temperature and pressure (STP)*. The above and the following equations are derived on the basis of this assumption; hence it is expected to find some departure of the measured values from the theoretical values when experimental work is carried out.

The Gibbs free energy represents a composite of the two factors contributing to spontaneity, 'ΔH' and 'ΔS'. For systems in which 'ΔH' is negative (*exothermic*

reactions in which heat is emitted) and 'ΔS' is positive, both factors favour spontaneity and the process will occur spontaneously at all temperatures. In this case; ($\Delta G_{T,P} \leq 0$), at constant temperature and pressure, with ($\Delta G_{T,P} = 0$) at equilibrium.

Physically interpreted, the Gibbs free energy of the system decreases during any spontaneous process at constant temperature and pressure, until equilibrium is achieved and the process can continue no further. The equation therefore allows us to calculate both the direction and the end point of a physical or chemical change within the system, but *it does not* tell us anything about the rate at which the change occurs.

Conversely, if 'ΔH' is positive (in the case of *endothermic* reactions in which heat is absorbed by the reaction) and 'ΔS' is negative (increase in order), 'ΔG' will always be positive and the change cannot occur spontaneously at any temperature.

In situations where 'ΔH' and 'ΔS' are both positive, or both negative, Equation (A-8) shows that temperature plays the determining role in controlling whether or not a reaction will take place. In the first case **(**ΔH and $\Delta S > 0$), $\Delta G_{T,P}$ will be negative only at high temperatures, where '$T\Delta S$'is greater in magnitude than 'ΔH'; as a consequence, the reaction will be spontaneous only at high temperatures.

When 'ΔH' and 'ΔS' are both negative **(**ΔH and $\Delta S < 0$); $\Delta G_{T,P}$ will be negative only at low temperatures [88].

- ***Equilibrium Potential (*** E^o ***)***

For an electrochemical reaction where '*n*' number of electrons participates in the reaction, the maximum electrical work obtained is related to equilibrium potential as follows:

$$Maximum\ electrical\ work = -nFE^o \qquad \textbf{(A- 9)}$$

Where;

'n' = number of electrons participating in the reaction of interest

'F' = Faraday's Constant (96, 473 J/Volts-mol)

E^o = Equilibrium potential (also called the reversible potential or theoretical *Open Circuit Potential* or *Open Circuit Voltage*, i.e. *OCP* or *OCV*).

The chemical energy of a system can be expressed in terms of several thermodynamic quantities including: *Enthalpy, Helmholtz free energy and Gibbs free energy,* the chemical energy of interest here is the *Gibbs free energy*. The *molar free energy change* of reaction in terms of Gibbs free energy is related to the maximum electrical work according to the following relationship:

$$\Delta g = -nFE^o \qquad \textbf{(A- 10)}$$

Where, ' Δg ' is *Gibbs free energy* change for the reaction defined on a (per mole) basis of one of the reactants.

It is important to emphasize that several forms of the Gibbs free energy for a given species exist, however, the most commonly used form is the *Gibbs free energy of formation* ' Δg_f '. As long as a consistent form of *Gibbs free energy* and the reference state are used, the numerical value of 'Δg' will be the same.

- ***Standard Equilibrium Potential (E_o^o):***

When the reactants and products exist in the standard states of unit activity at a given temperature, the equilibrium potential is referred to as standard equilibrium potential **(** E_o^o **)** and related to standard *Gibbs free change for the reaction* as follows [17]:

$$\Delta g_o = -nFE_o^o \qquad \textbf{(A- 11)}$$

In a fuel cell, the energy released is equal to the change in *Gibbs free energy of formation*; this is the arithmetic difference between the Gibbs free energy of the products and the Gibbs free energy of the inputs or reactants. It is convenient to consider these quantities in their "per mole" form, usually indicated by an $\left(^-\right)$ over the lower case letter. Considering the basic reaction for the hydrogen /oxygen fuel cell:

$$H_2 + \frac{1}{2}O_2 \rightarrow H_2O \qquad \textbf{(A- 12)}$$

The *product* is one mole of H_2O, and the *inputs* are one mole of 'H_2' and half a mole of 'O_2', hence

$$\Delta \bar{g}_f = \left(\bar{g}_f \right)_{H_2O} - \left(\bar{g}_f \right)_{H_2} - \frac{1}{2}\left(\bar{g}_f \right)_{O_2} \qquad \textbf{(A- 13)}$$

- ***Effect of Pressure and Temperature on the Equilibrium Potential,*** E^o

The pressure dependence of 'E^o' can be derived from basic thermodynamics by relating how the Gibbs free energy change for a given reaction varies with pressure [11].

Considering the equations for the internal energy of the system, together with *Gibbs and Helmholtz free energies* and enthalpy. The fundamental thermodynamic equations in this regard are:

- ***The Internal Energy***

The internal energy of a closed system during any physical or chemical process, from the first law of thermodynamics:

$$dU = dq + dw \qquad \textbf{(A- 14)}$$

Where dq is the heat added to the system, and dw the work done on the system, and according to the second law of thermodynamics:

$$dS \geq \frac{dq}{T} \qquad \textbf{(A- 15)}$$

Where; the inequality applies in the case of an *irreversible* system and the equality in the case of a *reversible* system.

In the general case, where the composition can change, it is useful to *decompose the work done on the system into two components*:

$$dw = -p_{\exp} dV + dw_e \qquad \textbf{(A- 16)}$$

Where ' $p_{\exp} dV$ ' is the *expansion work* associated with an incremental change in the system volume and ' dw_e 'is *the remaining work* done on the system by its surroundings, which could be written as:

$$dw_e = -\sum \mu_i dn_i \qquad \textbf{(A- 17)}$$

Where:

μ_i = *chemical potential* of component '*i*' and ' n_i ' = amount of component '*i*'.

The chemical potential terms will be omitted in the following analysis for simplicity, and equation (A-16) can be rewritten as:

$$dw = -p_{\exp} dV \qquad \textbf{(A- 18)}$$

Now, combining equation (A-14) with equations (A-15) and (A-18), the second law of thermodynamics for a reversible process can be written as:

$$TdS = dU + pdV \qquad \textbf{(A- 19)}$$

This can be rearranged to give a general expression for the internal energy as follows:

$$dU = TdS - pdV \qquad \textbf{(A- 20)}$$

- ***Gibbs free energy, where:***

$$G = H - TS \qquad \textbf{(A- 21)}$$

And its derivative with respect to '*S'* and '*T'* is:

$$dG = dH - TdS - SdT \qquad \textbf{(A- 22)}$$

- ***Helmholtz Free Energy:***

$$A = U - TS \qquad \textbf{(A- 23)}$$

And its derivative with respect to '*S'* and '*T'* is:

$$dA = dU - TdS - SdT \quad \textbf{(A- 24)}$$

- ***Enthalpy:***

$$H = U + pV \quad \textbf{(A- 25)}$$

And its derivative with respect to '*p'* and '*V'* is:

$$dH = dU + pdV + Vdp \quad \textbf{(A- 26)}$$

Now substituting equation (A-20) in (A-26) gives:

$$dH = TdS + Vdp \quad \textbf{(A- 27)}$$

And substituting equation (A-27) in (A-22) gives:

$$dG = Vdp - SdT \quad \textbf{(A- 28)}$$

For an ideal gas, if '*T'* is constant, the Gibbs energy at one pressure can be determined with respect to its value at a reference pressure.

To derive a relationship between the Gibbs function and pressure, the ideal gas equation of state is used, where:

$$PV = nRT \quad \textbf{(A- 29)}$$

For an isothermal process $(i,e : dT = 0)$, equation (A-28) becomes:

$$dG = Vdp \quad \textbf{(A- 30)}$$

Substituting the ideal gas equation (A-29) in equation (A-30):

$$dG = nRT\frac{dP}{P} \quad \textbf{(A- 31)}$$

Integrating from state *1* to state *2*:

$$\int_1^2 dG = nRT\int_1^2 \frac{dP}{P} \quad \textbf{(A- 32)}$$

Integrating to obtain the *Gibbs free energy change* for a change in pressure at constant temperature [89]:

$$G_2 - G_1 = nRT \ln\left(\frac{P_2}{P_1}\right) \qquad \textbf{(A- 33)}$$

If state *1* is replaced by a standard reference state, ' G_o ' and a reference pressure ' P_o ', the change in Gibbs energy is:

$$G_2 = G_o + nRT \ln\left(\frac{P_2}{P_o}\right) \qquad \textbf{(A- 34)}$$

Or, in the molar form (kJ/mol):

$$\bar{g}_2 = \bar{g}_o + RT \ln\left(\frac{P_2}{P_o}\right) \qquad \textbf{(A- 35)}$$

Equation (A-35) clearly shows the dependence of the Gibbs free energy on pressure and temperature. More light is shed on the dependence of Gibbs free energy on pressure and concentration when discussing the Nernst equation in chapter 3 of this thesis.

Appendix B: Matlab® Code for Plotting the Polarisation Curve

Matlab® Code for Plotting the Polarisation Curve

% Theoretical voltage of the fuel cell is given by *E=-delta g/2*F* (electrical work %done=C*harge *Voltage*) delta g for hydrogen oxidation where the product water is liquid at temperature 80^{o}C = -228.2 *kJ/mole*

% Activation voltage losses are given by the equation delta *V= %R*T/(2*alfa*F)*ln(i/i$_o$)*

% Voltage losses due to fuel cross over can be accounted for using the same equation %by adding *3 mA/cm^2 to i* [17]

% Ohmic losses are represented by V$_{Ohmic}$=*-i*r* (*r=3e-5 kOhm/cm^2* in this example).

% Concentration losses are represented by *V$_{conc}$=R*T/(2*F)*ln(1-i/i$_l$)* where *i$_l$* is the % %limiting current.

% Exchange current density *i$_o$*=50 *mA/cm^2* taken from (table 3.1 Larmine) [17] for platinum %electrode. In this programme the constant values are defined and graph is plotted for %Voltage vs. current density

F=96485; % Faradays Constant in Coulomb/mole

R=8.31; % Universal Gas constant in *J/K/Mole*

alfa=0.5; % Charge transfer coefficient, electrical energy harnessed in changing the rate %of the reaction

i$_o$=50; *i$_l$=2000*; % *mA/cm^2* the limiting current density

r=3e-5; % Resistances in the fuel cell in *kOhm/cm^2*

*E=1.03; T=353;i=10:50:2000; V$_{act}$ =-(R*T)/(2*alfa*F).*log((i+3)/i$_o$);*

*V$_{Ohmic}$=-(i+3)*r; V$_{conc}$=(R*T)/(2*F).*log(1-(i+3)/i$_l$); V=E+V$_{act}$+V$_{Ohmic}$+V$_{conc}$;*

plot(*i,V*,'r'); title('Polarisation Curve');

xlabel('Current Density [*mA/cm^2*]'); ylabel('Voltage [*Volt*]');

Appendix C: Major Components of the Test Facility

Major Components of the Test Facility

- ***Flow Measurement***

Measurements of flow of gases in the fuel cell are very important; as they give indication of the efficiency of the chemical reaction in the fuel cell and consequently enable the operator to calculate the actual efficiency of the fuel cell by comparing outputs to inputs.

As discussed elsewhere in this thesis, the amount of current flow in the fuel cell, in terms of electrons, is equal to the number of protons transferred across the membrane, which is equal to the amount of hydrogen molecules involved in the reaction (as a total number).

On the cathode side, the same argument applies to the number of oxygen molecules involved in the reaction except that the number of oxygen molecules is half that of hydrogen or electrons.

This argument is based on the assumption that hydrogen and oxygen do not pass through the membrane in their molecular form, and only hydrogen ions can go through. The amounts of hydrogen and oxygen required for the reaction have been calculated in molar, mass and volumetric quantities.

For the measurement of mass flow rate, the measurement of volumetric flow alone is not sufficient, as both gases: hydrogen and air can be assumed to be ideal, and the density, hence the volume, of the gas will change with changes in temperature and pressure, consequently, the measurement of these two variables is important wherever mass flow measurement is needed, and the mass flow rate is then calculated.

The amounts of reactant gases needed for *(100 W)* fuel cell module indicate that the flow measurement should be performed with great care as the amount of flow in terms of cubic centimetres is very low. When the fuel cell is operated in the closed end mode, i.e. when the hydrogen outlet is closed and only the amount of hydrogen needed for the reaction is consumed by the fuel cell, the amount of flow is very low.

The following options have been considered for the flow measurement:

- ***Orifice Flow Meter***

This type of flow meters operates on the principle of placing a restriction in the flow line to cause a differential pressure head. The differential pressure, which is caused by the head, is measured and converted to a flow measurement. The flow-path restriction, such as an orifice, causes a differential pressure across the orifice. This pressure differential is measured by a mercury manometer or a differential pressure detector. From this measurement, flow rate is determined from known physical laws [90].

The flow meter actually measures volume flow rate rather than mass flow rate. Mass flow rate is easily calculated or computed from volumetric flow rate by knowing or sensing temperature and/or pressure. Temperature and pressure affect the density of the fluid and, therefore, the mass of fluid flowing past a certain point. According to the universal gas equation, temperature and density are inversely proportional (hence temperature and volume are directly proportional as volume is the inverse of density), while pressure and density are directly proportional. These equations can be expressed as follows:

$$\dot{m} = \rho A v \qquad \textbf{(C- 1)}$$

Where '$\dot{m}$'is mass flow rate, 'A' is cross sectional area, 'ρ' the density of the fluid and 'v' velocity of flow. Substituting for density from the universal gas equation yields:

$$\dot{m} = \frac{P}{RT} A v \qquad \textbf{(C- 2)}$$

- ***Hot Wire Anemometer:***

The hot-wire anemometer consists of an electrically heated, fine platinum wire which is immersed into the flow. As the fluid velocity increases, the rate of heat flow from the heated wire to the flow stream increases. Thus, a cooling effect on the wire electrode occurs, causing its electrical resistance to change. In a constant-current anemometer, the fluid velocity is determined from a measurement of the resulting change in wire resistance. In a constant-resistance anemometer, fluid velocity is determined from the current needed to maintain a constant wire temperature and, thus, the resistance constant. Knowing the velocity of flow, density of the fluid and dimensions of the flow pipe, the volume of the gas can be calculated. [90].

- ***Variable Area (Floating Ball) Flow Meter***

The floating ball flow meter consists of a vertically oriented glass tube (or plastic) which is tapered with a larger end at the top, and a metering float which is free to move within the tube. Fluid flow causes the float to rise in the tube as the upward pressure differential and buoyancy of the fluid overcome the effect of gravity.

The float rises until the annular area between the float and tube increases sufficiently to allow a state of dynamic equilibrium between the upward differential pressure and buoyancy factors, and downward gravity factors. The height of the float is an indication of the flow rate. The tube can be calibrated and graduated in appropriate flow units. The accuracy of the flow meter may be as good as 1% of full scale rating [91].

This type of flow meter is simple to use and not too expensive, for the simplicity of the measurement; a standard type of floating ball flow meter was used. Accuracy of the measurement is acceptable (in the range of <5%). Two flow meters, acquired from (Audon Electronics, Nottingham, UK), were used for each of the reactant gases to measure the inflow and out-flow and find out the consumption of the fuel cell. The readings were very small and it was very difficult to sort out an accurate and acceptable value for the amount of fuel consumed by the fuel cell. The flow meters are shown in figure (C-1):

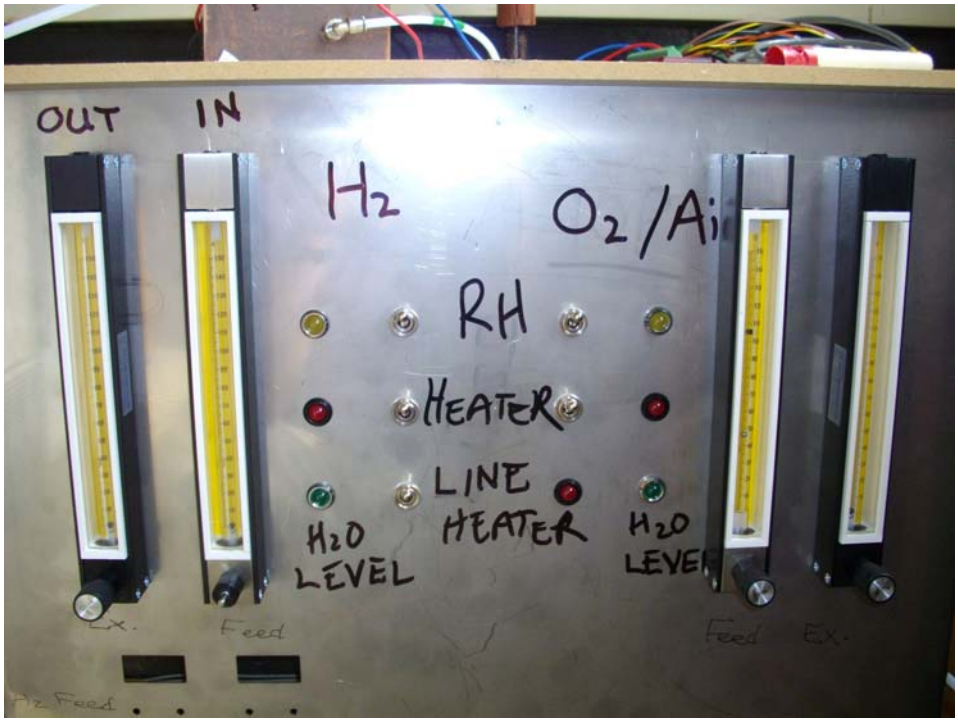

Figure *C- 1* Variable Area (Floating Ball) Flow Meters used for each of the reactant gases to measure the inflow and out-flow. The consumption of the fuel cell is calculated by subtraction.

- ***Temperature Measurement***

The importance of temperature measurement is to maintain a specific operating temperature during the experimental procedure to make sure that all experiments were performed under the same thermal conditions, and to make sure that a safe operating temperature has not been exceeded.

Another advantage of temperature measurements is to investigate the optimum temperature of operation of the fuel cell. The temperature dependence of the fuel cell performance was discussed in chapter three, and it was shown that higher temperatures promote the chemical reaction in the fuel cell; on the other hand, higher temperature can cause dehydration of the membrane and hence decrease the performance. Hence, temperature has to be monitored and controlled; at the same, time temperature measurement is necessary to calculate the mass flow rate of gases.

- ***The Thermocouple***

In this apparatus a set of *K-Type* thermocouples were used to measure temperature at the following points:

3. Inlet gas temperature
4. Outlet gas temperature

According to the principles of thermocouples, two dissimilar metals generate a DC current proportional to the temperature variation at the junction where the two metals are connected; calibration charts are available for the conversion of the millivolts readings to temperature.

A standard *K-Type* thermocouple wire was obtained from (RS components UK Ltd.), and cut to the required sizes; a bead of the two dissimilar wires was made using an arc welding apparatus and implanted in the flow of the gases, pipe fittings sealed with silicone were used for mounting the temperature, pressure and humidity probes in the flow of the gases as shown in figure (C-2) below:

Figure C- 2 Probe fitted to plug and sealed with silicone, the probe shown is an *HH-4000 RH* humidity sensor, but same technique was used for thermocouples.

The probe is mounted into a ½" plug through a (5 mm) hole and sealed with high temperature silicone; a Teflon disc is used to ensure proper sealing as shown in figure (C-3) which shows the components for mounting the humidity sensor.

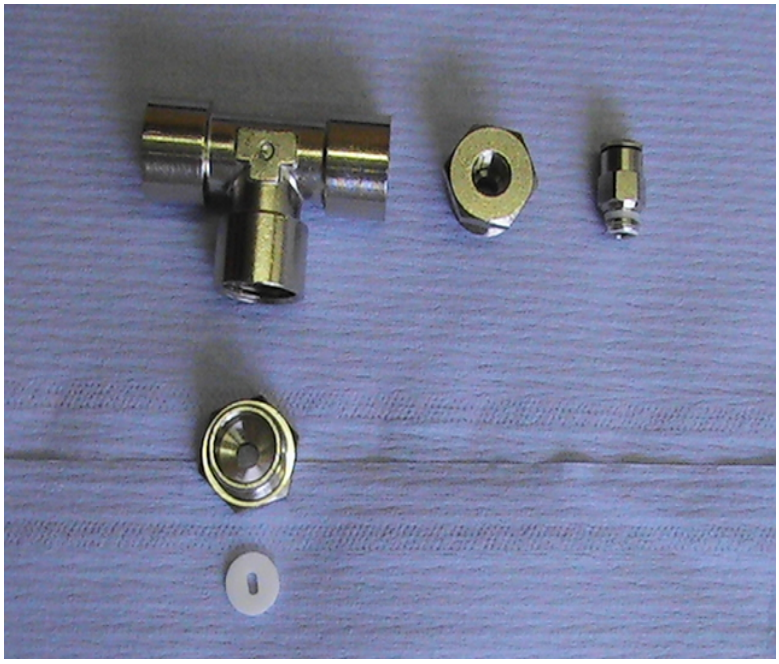

Figure C- 3 Fittings used in mounting test probes

- ***Thermocouple Amplifier***

The readings of the thermocouples were read using a data logging system together with a voltage amplifier designed to amplify the output voltage of the thermocouple. The resolution of the data logger was 12 *bit*, and the maximum voltage it could measure was *5 VDC*. The minimum voltage detected by the data logger is calculated as follows:

Resolution = 2^12 = 4096 **(C- 3)**

Voltage output of the data logger is 5 *VDC*, hence the voltage resolution is:

Minimum voltage detected = 5/4096 = 1.2 mVDC **(C- 4)**

But the output voltage of the *K- type* thermocouple = 0.039 *mV/°C* , hence it is much lower than the least voltage that can be detected by the data logger and it needs to be amplified about 30 times so that the data logger can detect it.

A thermocouple amplifier was obtained from (Audon Electronics, Nottingham, UK), which is *TCK-4*, a four-channel type-k thermocouple amplifier unit; designed to interface type-k thermocouples to data acquisition systems, figure (C-4). The *TCK-4* consists of 4 high-precision low-power instrumentation amplifiers. The gain of each amplifier is pre-set to give a standard *10mV/°C* output for a type-K thermocouple input. Thermocouple linearization is not included, so the output follows the non-linearity of a type-K thermocouple. The gain is set at a thermocouple input of 25°C.

Figure C- 4 TCK-4 type-k thermocouple amplifier unit from Audon electronics.

- ***Humidity Control and Measurement***

As discussed in chapters 3 and 4, humidity plays a major role in maintaining the proper performance of the fuel cell. The anode side of the membrane is prone to dry due to electro-osmotic drag of water to the cathode side, at the same time, water is being generated at the cathode side and if it is allowed to accumulate there it will block the path of gas to the membrane, this phenomenon is usually called flooding which gives the impression of an over-spill of water, but in fact a thin film of water on the cathode will cause blockage to the path of oxygen to the membrane.

This problem is combined with the thermal management in the fuel cell because as the gases heat up their capacity to carry water will increase, hence both gases have to be humidified initially to make sure that the level of humidity is maintained.

- ***Vapour Generator and Humidification Chamber***

An ultrasonic vaporiser powered by *24 VDC* is used to generate humidity in the flow streams of hydrogen and oxygen, figure (C-5).

Figure C- 5 Ultrasonic vaporiser

The vapour generator is immersed in distilled water at the bottom of a humidification chamber which is a stainless steel cylinder; figure (C-6). The humidification chamber is fitted with a water level sensor which is merely a float switch which lights a *24 VDC LED* light on the panel of the test rig, once the water level drops below the level of the floating switch, the electric circuit of the *LED* light opens and the light goes off to indicate low water level. The water level is topped up manually through a sealed hole in the chamber.

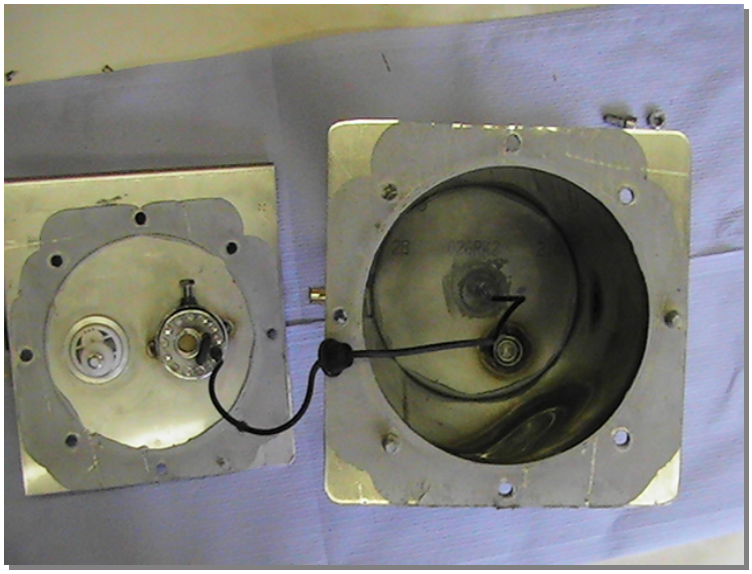

Figure C- 6 Humidification chamber, ultrasonic vaporiser and water level sensor

The same is applied to both hydrogen and oxygen humidification chambers, however, for the hydrogen circuit, a bubbling effect is added to the system, where the flow of hydrogen is allowed to pass through the distilled water, then carries away more moisture generated by the ultrasonic generator as it leaves the humidification chamber.

The humidification chambers are facilitated with rope heaters with a time percent temperature controller to provide the necessary heating. The gases are heated prior to entering the chambers in a main heater by passing through a copper coil with a rope heater controlled by a switch on the front panel of the test facility, the heater coil and the two humidification chambers are shown in figure (C-7).under construction, one time percent controller of the heaters is shown in the picture (far left).

Figure C- 7 The two humidification chambers and the main heater under construction, insulation and time percent controller of the heater are shown in the picture (far left)

The amount of water carried by the stream of gas depends on temperature, as the water carrying capacity is a function of temperature; hence the gases have to be heated to increase their ability to carry the required *%RH*.

Figure (C-8) is a top view of the test facility, the main heating coil, the two humidification chambers; the thermocouple amplifier (on the right) and part of the electrical wiring are shown in the picture.

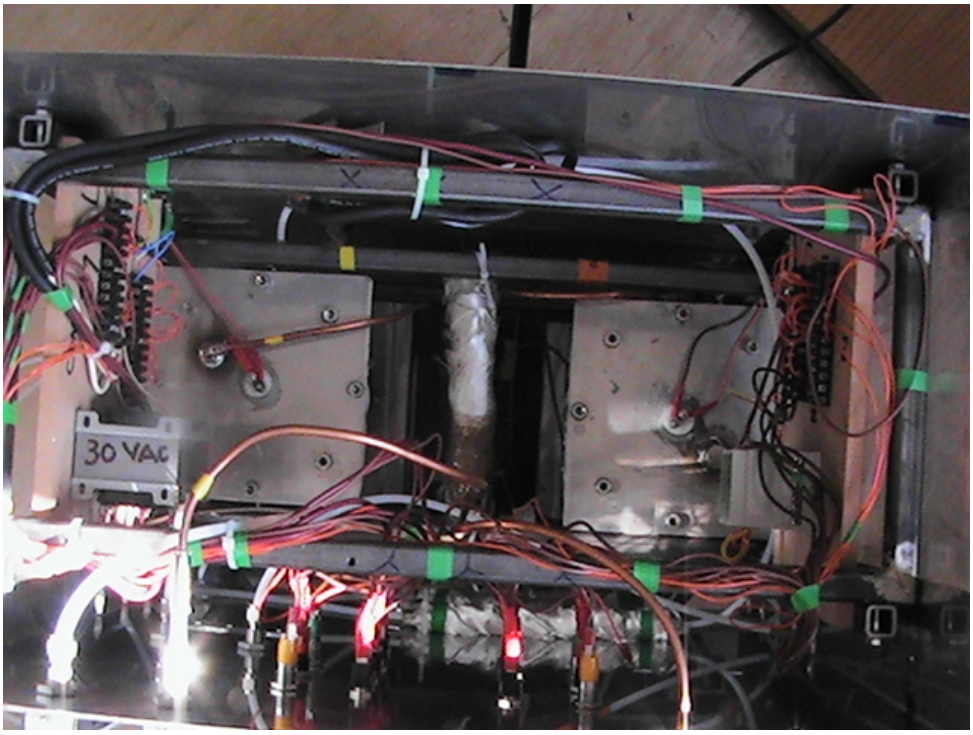

Figure C- 8 Top view of the test facility, the main heating coil, the two humidification chambers, the thermocouple amplifier (on the right) and part of the electrical wiring are shown in the picture.

- ***Humidity Sensor***

Humidity measurement is done using an electronic sensor (HH-4000 Series Humidity sensor from RS components UK Ltd.). The *HH-4000 RH* sensor is a laser trimmed, thermoset polymer capacitive sensing element with on-chip integrated signal conditioning. The sensing element's multilayer construction provides excellent resistance to most application hazards such as wetting, dust, dirt and common environmental chemicals. The sensor was shown in figure (C-2).

The sensor gives a linear output voltage as compared to %RH variations, highly accurate, fast response time and it covers a good range of humidity from *0 to 100% RH* between temperatures of 0 to 50°C as shown by figure (C-9) below:

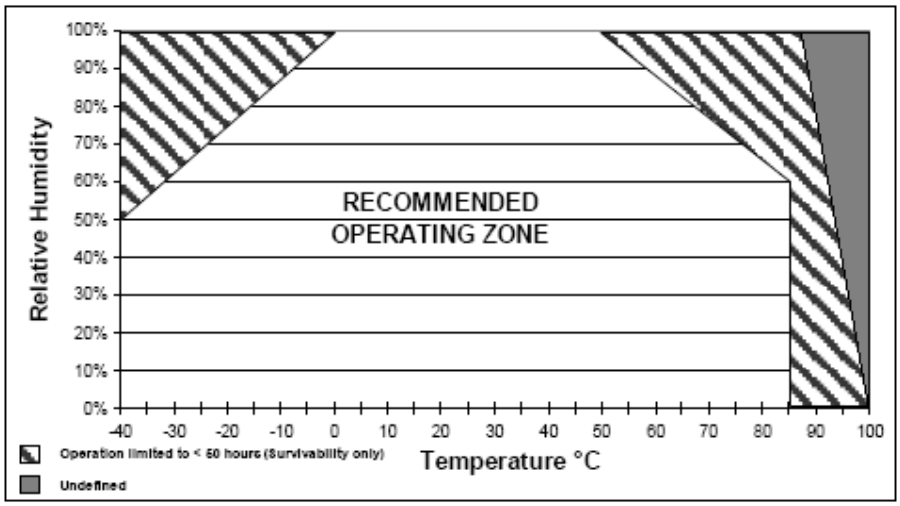

Figure C- 9 Recommended operating zone of humidity sensor (RS Components UK)

The humidity measurement above 333K (60°C) should be tackled with care. As seen from the graph, the higher values of relative humidity above 60°C are not covered by the range of the sensor accurately.

The response of the *RH* sensor is linear with comparison to the %RH. And can be modelled using the following equation for a first order fit, where 'V_{supply}' is the DC voltage supplied by the data logger which is *5VDC:*

$$V_{out} = V_{supply}(0.0062(sensorRH) + 0.16) \quad \textbf{(C- 5)}$$

The linear response of the *RH* sensor is represented by the first order fit curve shown below in figure (C-10).

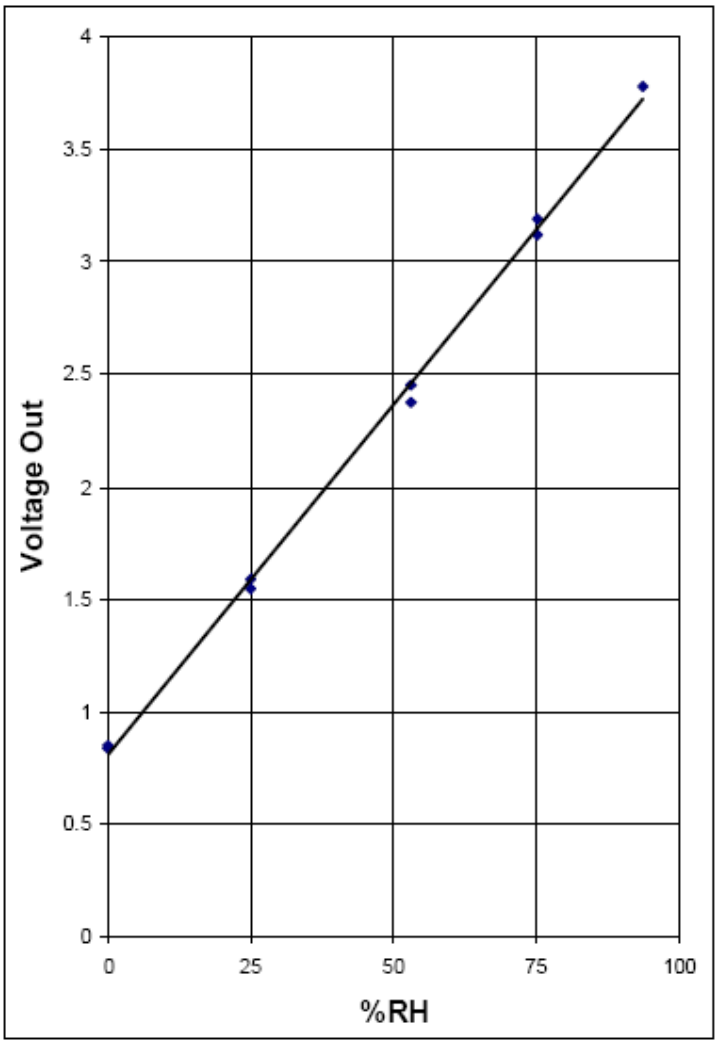

Figure C- 10 Typical best fit straight line for the humidity sensor

The humidity sensor was fitted to the fluid flow pipe by the same technique used with the thermocouple. Control of humidity is obtained manually by switching on and off the humidifier, but the bubbling of hydrogen through distilled water is part of the flow and cannot be controlled.

- ***Pressure Measurement***

The importance of pressure was discussed earlier in chapter 3, it was concluded that pressure improves the performance of the fuel cell but not very significantly. The performance improvement gained by pressurisation is overweighed by the cost of pressurising and structural modifications to the fuel cell design so that it can withstand pressure. However, pressure measurement is important to decide the density of the gases and their flow rate.

A pressure transducer type (Gems sensor series 2200) obtained from (RS components UK Ltd.) is used to measure pressure. Pressure sensing is performed using a diaphragm which deflects as a result of the difference in pressure between its two sides. The pressure measured is the gauge pressure which is pressure in the system with relevance to atmospheric pressure.[11] The range of the transducer is 1to 5 Atm. The transducers were obtained from RS components UK Ltd., they have the following specifications:

1. Accuracy: 0.25% of full scale
2. Thermal error: 1.5% of full scale.
3. Supply voltage: 10 VDC
4. Output: 4-20mA

[11] The term *Absolute* is used where the reference pressure is vacuum, *Gauge*, where the reference pressure is atmospheric pressure; or *Differential*, where the reference pressure is a certain value of pressure other than vacuum or atmospheric, in this case the sensor has two ports for the measurement of two different pressures.

- ***Gas Flow Lines***

Humidity, pressure and temperature measurements were read using the transducers and fittings described above. The probes were fitted along the inlet and outlet lines. Figure (C-11) shows the fittings on the front panel of the test facility.

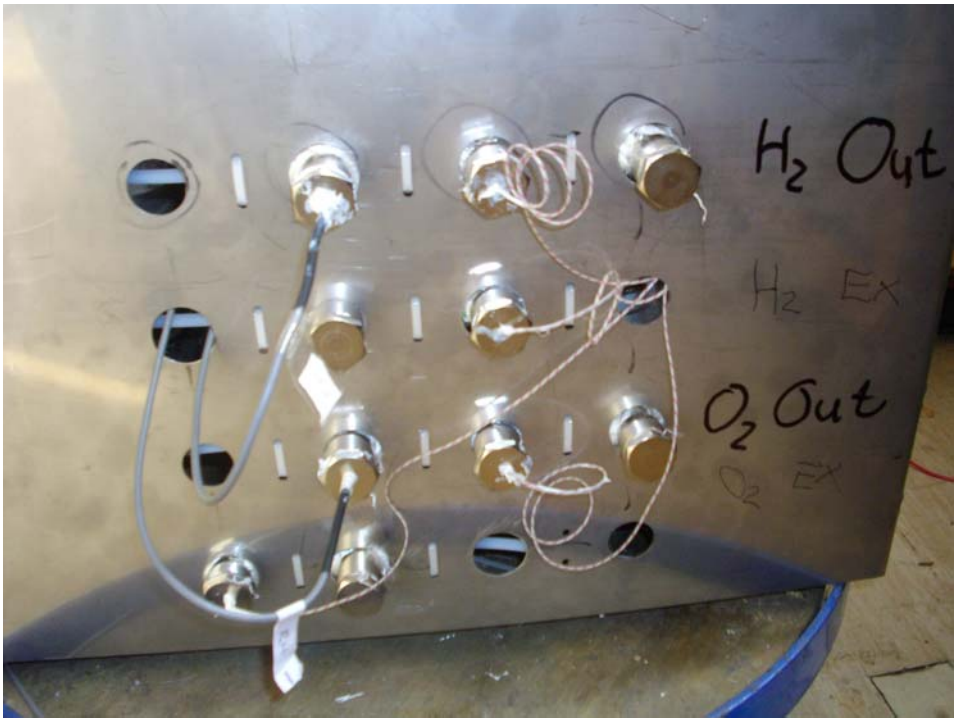

Figure C- 11 Measurement points for pressure, temperature and humidity along the inlet and outlet gas supplies, the pressure transducers are not fitted.

- ***The Complete Test Unit***

The components described above were assembled in the test rig with a front panel equipped with control switches and indicator/ warning LED lights to give the operator information on important functions such as the operation of the heaters and the water level in the humidifiers. The complete test rig is shown in figure (C-12) below. A schematic of the front panel and a list of components on the front panel are shown in figure (C-13) and table (C-1) respectively.

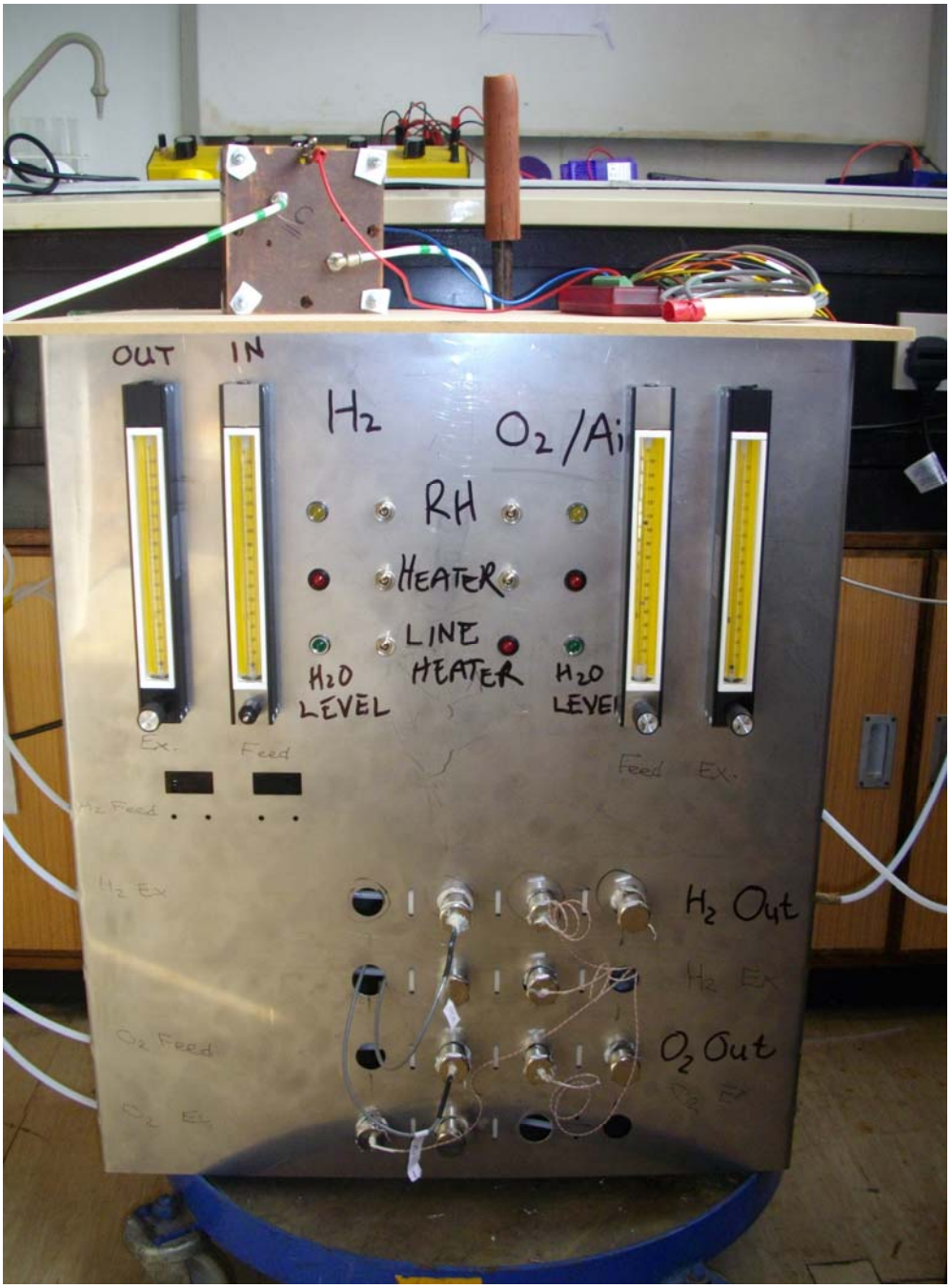

Figure C- 12 The complete fuel cell test facility and gas conditioning unit

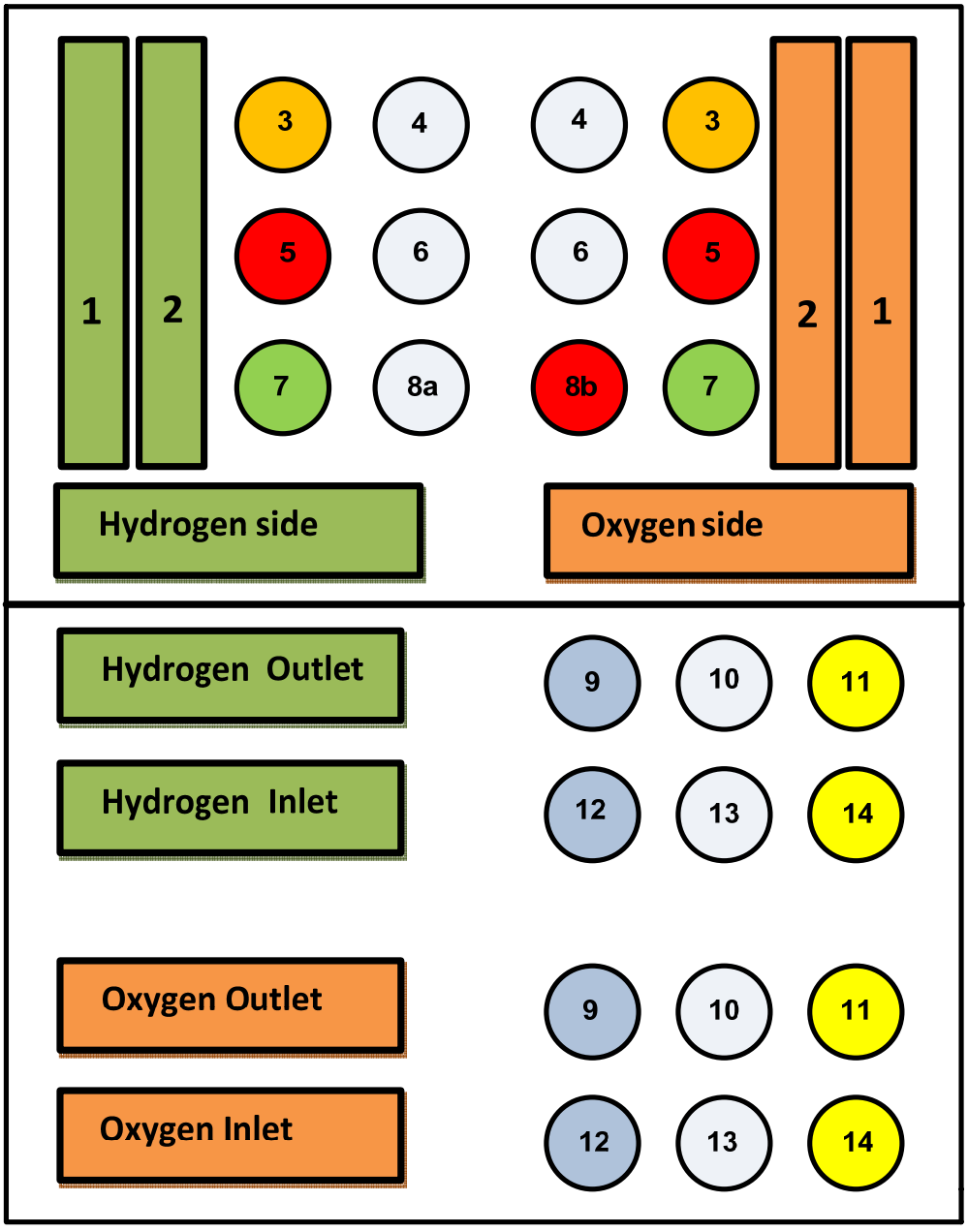

Figure C- 13 Schematic of the front panel with identification numbers

Table C- 1 A list of the controls and indicators and their identification numbers:

Control Number	Parameter or indicator	*Unit*
1	Inlet gas flow meter	m^3/s
2	Outlet gas flow meter	m^3/s
3	Humidifier indicator	m^3/s
4	Humidifier switch	m^3/s
5	Humidifier Heater Indicator	*On/ Off*
6	Humidifier heater switch	*On/ Off*
7	Water level indicator	*On/ Off*
8a	Line heater switch	*On/ Off*
8b	Line heater indicator	*On/ Off*
9	Inlet gas thermocouple	*°C*
10	Inlet gas Pressure sensor	*bar*
11	Inlet gas Humidity sensor	*%RH*
12	Outlet gas thermocouple	*°C*
13	Outlet gas Pressure sensor	*bar*
14	Outlet gas Humidity sensor	*%RH*

- ***The Data Acquisition System***

As mentioned previously, the aim of the experiment is to obtain performance data of the designed fuel cell and to compare its performance to a standard type fuel cell. Due to the fact that measurements are performed under steady state conditions, the only need was for a gas conditioning unit that can vary the temperature and relative humidity of the reactant gases and provide some safety precautions for the handling of oxygen and hydrogen.

Hence, the first attempt was to design a gas handling unit with analogue controls to monitor the pressure, temperature and relative humidity of the gases. The unit was built and used at the initial stages of this research, but then the need appeared to use data acquisition systems so that more data can be collected and analysed. The first test facility is shown in figure (C-14) below: the unit comprised the following sub systems:

1. Two gas flow systems one for oxygen or air and one for hydrogen,
2. A nitrogen gas purge system with a kill switch to stop the flow of reactant gases through two normally open solenoids
3. A heating system comprising a heat exchanger and a water heating unit with a temperature controller to control the temperature of the reactant gases.
4. A humidifier and humidification chamber on each gas system. A distilled water tank controlled by normally closed solenoids and water level switches to provide water to the humidification chambers when the water level goes down.
5. A water separator with a water level switch to separate water particles from the gases prior to entering the fuel cell.
6. Small Hydrogen, air and nitrogen cylinders together with fire arrestors and gas regulators are accommodated within the unit.

7. A ventury tube was used to re-circulate excess hydrogen from the outlet side back to the inlet side of the fuel cell, but due to the low flow rate this was not efficient for use.
8. Pressure and temperature gauges for the inlet and outlet gases together with indicator lamps and control valves.

Figure C- 14 Gas handling unit with analogue controls, first attempt to design and build a test facility for fuel cells for this research project.

As the work on the project progressed, the need arose for more efficient data acquisition system, the data acquisition system was used in the experiment to handle and record a larger number of variables. A Labjack® U12 acquired from (Audon Electronics, Nottingham, UK) was used as a data logger together with a thermocouple amplifier for reading the temperature measurements of a set of K- Type thermocouples.

- ***The Data Logger***

A (Labjack® U12) data logger was obtained from (Audon Electronics, Nottingham, UK), it is a USB based analogue and digital I/O unit for data logging, data acquisition, measurement and control applications. Supplied with a wide range of data logging, oscilloscope software and examples for use with most programming and DAQ packages; figure (C-15):

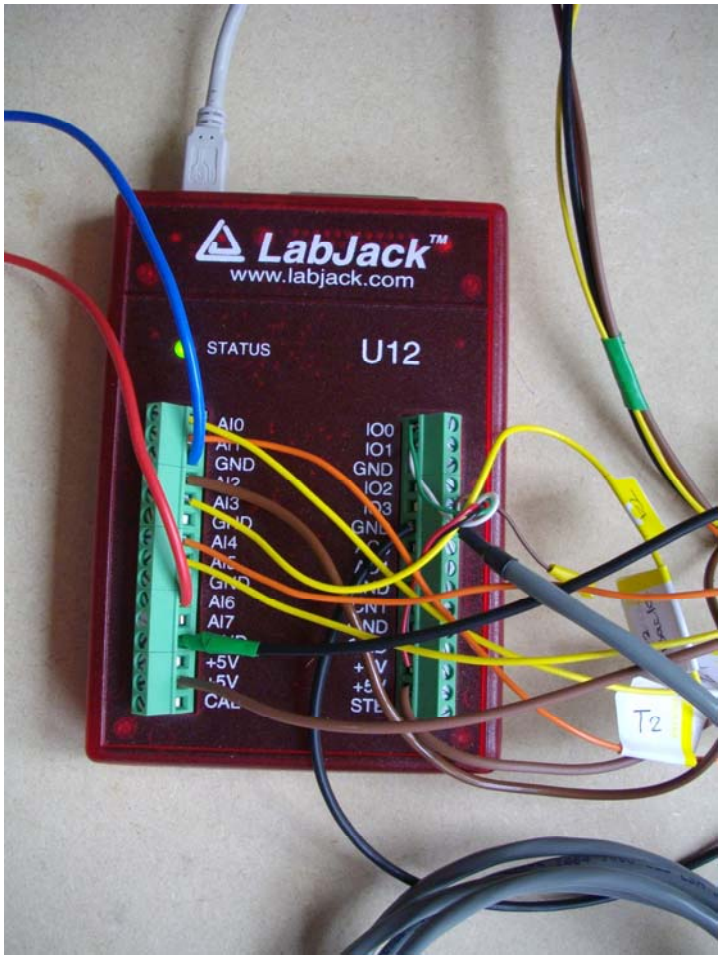

Figure C- 15 Labjack® U12 data logger, a USB based analogue and digital I/O unit for data logging, data acquisition, measurement and control applications.

The (Labjack® U12) has 8 screw terminals for analogue input signals (AI0-AI7). These can be configured individually as 8 single-ended channels, 4 differential channels, or combinations in between. Each input has a ±10 volt input range with 12-bit

resolution. Differential channels can make use of the low noise precision PGA to provide gains up to 20, giving an effective resolution greater than 16-bits.

The (Labjack® U12) has 2 screw terminals for analogue output signals (AO0 & AO1). Each analogue output can be set to a voltage between 0 and the supply voltage (+5 volts nominal) with 10-bits of resolution. The analogue outputs are controlled in command/response mode at up to 50 Hz per channel.

The data logger has the following specifications:

- 8 Single-Ended, 4 Differential 12-Bit Analogue Inputs
- ±10 Volt Analogue Input Range
- PGA with Gains of 1, 2, 4, 5, 8, 10, 16, or 20 V/V
- Up to 8k Samples/Sec (Burst) or 1.2k Samples/Second (Stream).
- 2 Analogue Outputs
- 20 Digital I/O (Up to 50 Hz per I/O)
- 32-Bit Counter
- Watchdog Timer Function
- Easy to Use Plug-and-Play USB Device
- No Power Supply Needed

- ***Data acquisition software***

The data logger can be operated on LabView® as well as DaqFactory® which is a new software package designed for scientists and engineers who need a low-cost but highly capable data acquisition/control package. It can acquire data, control outputs, has user defined pages complete with a symbol library, has alarm and PID control functions and has in-built data analysis capabilities. A copy of DaqFactory® express was provided with the (Labjack® U12), which was used for the data acquisition of readings. However, a LabView® application has been written for use with the DAQ system and presented in chapter 5 but most of the numerical data was acquired using the DaqFactory ® software as shown in figure (C-16).

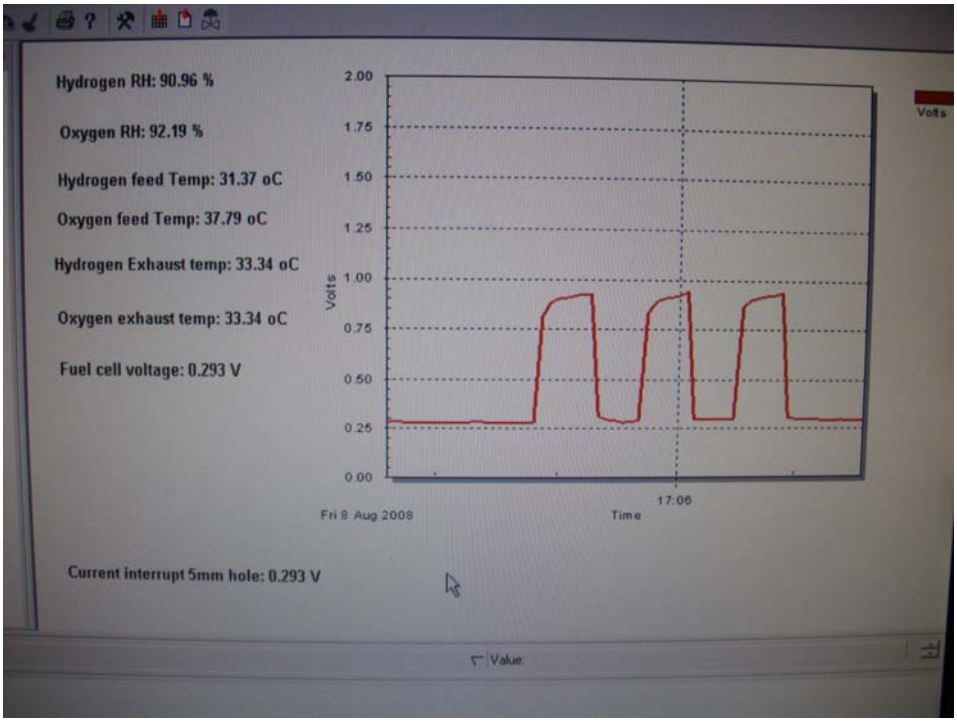

Figure C- 16 Computer screen of the data acquisition system software; Daqfactory, showing the output voltage of the fuel cell on the scope, the voltage increases and decreases as the current is interrupted. Temperature and humidity readings are on the left hand side.

- ***The Load Bank***

A set of standard resistances were used to provide the load. The resistances had to be connected in parallel to get resistances less than 1 *Ohm*. Below is the set up connected to the resistances and to the various sensors through the data logger, together with an experimental fuel cell figure (C-17):

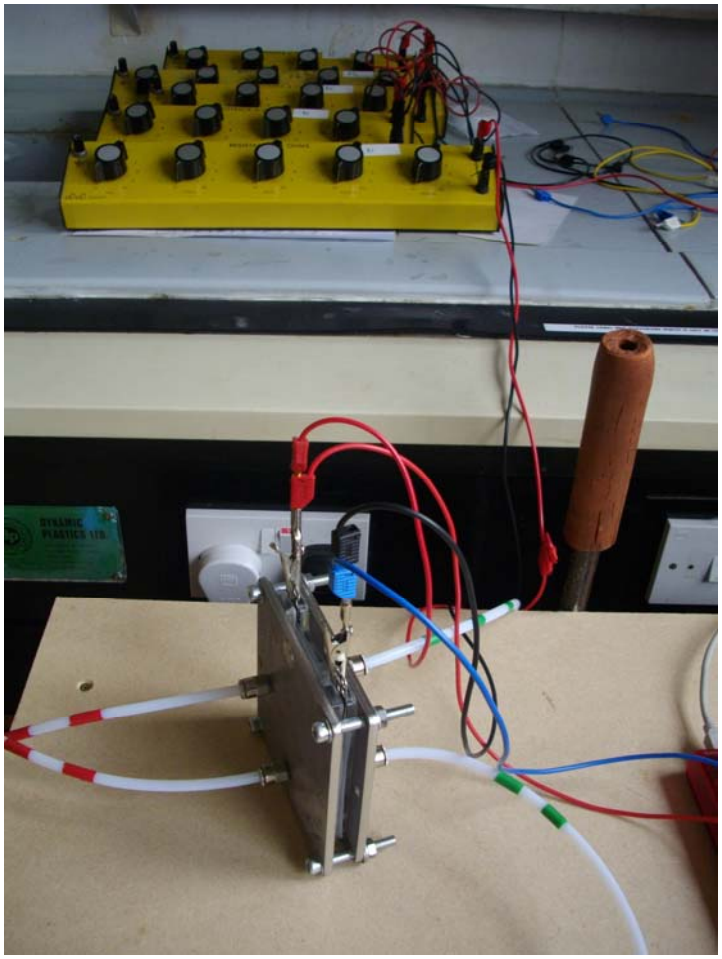

Figure C- 17 An experimental fuel cell connected to a resistive load.

- ***Safety Precautions***

Due to the fact that hydrogen is hazardous especially when used under high temperatures in the presence of oxygen and catalyst materials, the danger of hydrogen combustion and explosion remains present. The following procedures and equipment were used and observed throughout all experiments:

a. A full risk assessment was performed before undertaking any experiments.

b. All experiments were performed in a fume cupboard with proper alarms and ventilation.

c. Fire arrestors were used on oxidant and hydrogen cylinders, a fire arrestor is shown in figure (C-18) below.

d. Proper precautions were taken when turning on or off hydrogen and air cylinders and they were normally double checked before and after each experiment.

e. Hydrogen was turned off at its source each time the fuel cell was stopped.

f. Personal protective equipment such as goggles and gloves were used during experiments.

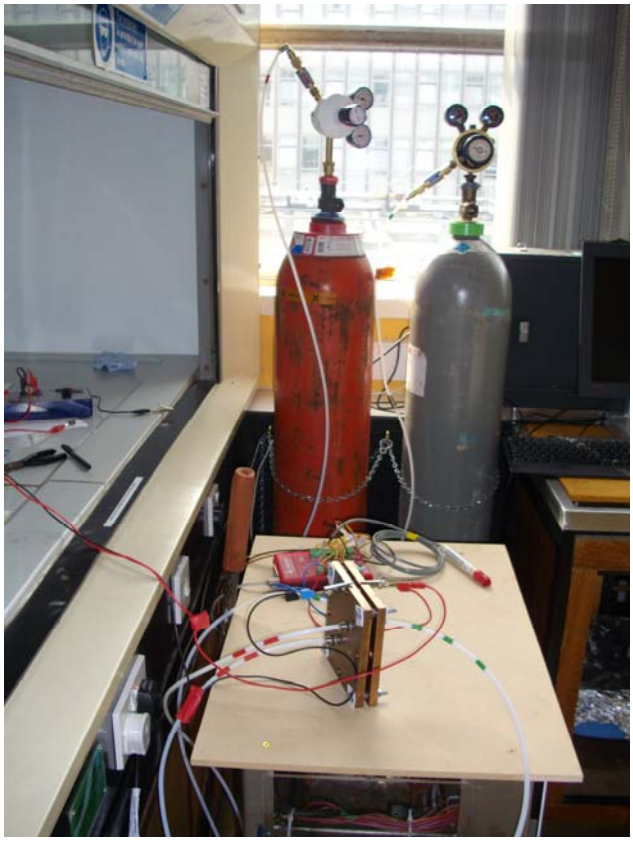

Figure C- 18 The complete experimental set up. fire arrestor are shown on Hydrogen (Red) and Air (Grey) cylinders, the fume cupboard is on the left hand side where the fuel cell was operated test rig and data logger are also shown.

Blank Page

END